Investigation of the mechanism of long term deformation of peat subgrade under embankment loading

by

Mohan Prasad Acharya

A thesis submitted in partial fulfillment of the requirements for the degree of

Doctor of Philosophy

In Geotechnical Engineering

Department of Civil and Environmental Engineering
University of Alberta

Abstract

Peat, the fragmented remains of vegetation is highly compressible foundation material. Road and railway embankments built on top of peat subgrades are associated with instability and long-term settlement. This thesis presents the results of the research work that included the field measurements, laboratory testing, and theoretical analysis to investigate the mechanism of development of pore pressure and long-term settlement in these peat subgrades.

Pore pressure generation was studied based on the measurement of pore pressure, deformation, and temperature in peat subgrade at a field site over three years. The laboratory tests included an incubation of peat specimens at room temperature and measurement of pore pressure generation in four peat specimens while varying temperature between 2 to 20°C. The results identified the decomposition of peat to form gas and the effect of gas bubbles in the development of pore pressure. The variation in pore pressure in peat subgrade during summer and winter months was found to be due to the thermal expansion and contraction of gas bubbles.

To investigate the movement of the gas through peat, laboratory isotropic consolidation tests were conducted on five peat and six cellulose foam specimens. The result of the laboratory tests and the theoretical analysis indicated that the gas bubbles move through the pore constrictions towards the drainage boundary, where they restrict the flow of water, this results in an increase of pore pressure towards an upper limit or *escape pressure*, ultimately causing an expulsion of gas bubbles. This expulsion of bubbles results in a rapid drop in pore pressure as measured in the field site and volume change within the specimen. A correlation developed between the pore pressure drop and the corresponding volume change within the peat specimens was extrapolated to estimate the settlement of peat subgrade due to the gas expulsion.

The mechanism of long-term settlement in peat was investigated by means of triaxial drained and undrained creep tests in nine peat specimens. The

development of strain and strain rate under variable stress states are presented. The uniqueness of the stress, strain, and strain rate at different stress states was analysed and the creep isotaches representing this uniqueness is presented. Further, the applicability of creep equations developed for normally consolidated clays to define the development of creep in fibrous peat, are discussed.

The result of this research identified that multiple mechanisms, including the creep deformation under constant embankment loading and the deformation due to the seasonal temperature driven rise in pore pressure, and expulsion of gases out of peat boundary are involved in the long term settlement of peaty foundation. The deformation is found to be predominantly volumetric with lateral deformation less than 25% of vertical deformation.

Preface

This dissertation is presented in the "paper-format" style. Chapters 3, and 4 have been accepted to publish in different journals as explained below. Chapter 3 of this thesis has been accepted in August 2015 as: Acharya M. P., Hendry, M. T. and Martin, C. D. 2015. Thermally induced pore pressure in peat beneath a railway embankment. International Journal of Geotechnical Engineering. I was responsible for all work reported in the manuscript, including field installation, design of the experimental program, implementation of the experiments, review of the literature, analysis and discussion of the results and writing of the text. As supervisors, Dr. M. T. Hendry and Dr. C.D. Martin reviewed all parts of the work.

Chapter 4 has been accepted in September 2015 as: Acharya M. P., Hendry, M. T. and Martin, C. D. 2015. Effect of gas bubbles on pore pressure response in peat beneath an embankment. Canadian geotechnical journal. I was responsible for the field measurement laboratory experiment and data analysis as well as manuscript composition. As supervisors, Dr. M. T. Hendry and Dr. C.D. Martin reviewed all parts of the work.

Acknowledgement

I am immensely grateful to both of my supervisors. Dr. Michael Hendry patiently helped me in every step of my research work and guided me to the outcome. Dr. Derek Martin provided me a great opportunity and his insight into the subjects covered in this thesis was invaluable towards the outcome of this research.

The completion of this thesis would not have been possible without the support and help of various organizations and people. This research was made possible through funding provided by the Natural Sciences and Engineering Research Council of Canada (NSERC), Canadian Pacific Railway, Canadian National Railway, and Transport Canada. I owe special thanks to Tom Edwards for his personal support and involvement with this project. Tom spent a lot of his time to make our site installations a success.

I am also grateful for the immense support of a number of people in the department. Special thanks go to my colleagues, most of them dear friends, who accompanied me during my fieldwork innumerable times. I will remember the technical and non-technical discussions with them over the years. Thanks also to Christine Hereygers who was there to help me in the lab whenever I needed help.

I cannot finish without highlighting the never-ending support from my family who were always beside me in pursuing my unending education. This work is dedicated to my parents whose hard work in supporting my education encouraged me to accomplish this goal and gave me the strength I needed throughout my work.

Table of Contents

List of Figures

List of Tables

1 Chapter 1: Introduction

Peat and highly organic soils are common throughout the world, from tropical regions to cold climates. These soils primarily consist of the fragmental remains of vegetation in various stages of decomposition in the presence of excessive moisture (MacFarlane, 1969; Hobbs, 1986). The fabric of peat varies from a fibrous mat to a structure-less mud (Landva, 2007) with a water content ranging from 500 to 2000% and a density almost equal to that of water (Hobbs, 1986). Due to the presence of excessive moisture and the cellular structure of the fibres, peat is characterized by high compressibility and a high rate of creep (Landva and La Rochelle, 1983). Embankments constructed on peat deposits are associated with instability and continuing settlement for many decades (Buisman, 1936; Weber, 1969; Landva, 2007). Despite many years of study and work experience, peat is still poorly understood and a difficult foundation material.

Peatland extends from east to west in northern Canada, covering about 18% of total area of Canada and more than 50% of Northern Alberta. Large stretches of major Canadian railways (Canadian National Railway, CN and Canadian Pacific Railway, CP) pass through these peat and marshy lands. The 440-km long CN Edmonton to Fort McMurray railway line (CN's Lac La Biche Subdivision) in Alberta has nearly one third of its embankment constructed over peat deposits. These embankments have been characterized as having excessive settlement that poses a risk of derailment and is associated with huge maintenance costs. The performance of such embankments over peat has become a more critical concern as the number of engineering projects built within peat-covered areas is increasing as resource and infrastructure development continues to expand in northern Canada.

This research program is the continuation of a study initiated following recommendations by the Transportation Safety Board (TSB, 2008) that the response of peat subgrade underlying railway embankments should be investigated. This program included full-scale field monitoring of a railway embankment, sampling, laboratory investigation, and theoretical explanation.

The goal of the overall research program was to develop an understanding of the mechanism of long-term settlement and pore pressure development within peat subgrades beneath embankments and to discuss the implications of this understanding such that it can be used to develop future remedial measures.

This research program focused on improving our understanding of the mechanisms associated with the long-term settlement behaviour of peat subgrade underlying railway embankments by: i) developing and implementing a field measurement program to measure the behaviour of in situ peat beneath a full-scale railway embankment, ii) developing an understanding of mechanisms related to the evolution of pore water pressure in peat subgrades, and iii) developing and conducting a laboratory testing program to characterize the long-term deformation behaviour of peat.

1.1 Description of problem

The Canadian railway embankments constructed over peatland at the beginning of the 20th century followed the methods described in MacKenzie (1902); specifically, embankments crossing soft deposits should be made as light as possible, using turf, peat, sawdust, or cinders. Many embankments were built directly on the top of the peat surface, referred as "Floating Fills" (MacFarlane, 1969). A typical cross-section of a railway embankment constructed over peat consists of a 1 to 2 m thick layer of ballast and sub ballast floated on a timber-corduroy log-raft, fascines, or wire mesh, etc. Below this is a layer of peaty organic material usually underlain by a deposit of soft silty-clay. These embankments had a low initial cost but are associated with large continuous settlement that requires extensive maintenance to achieve serviceability of the railway tracks (MacFarlane, 1969).

Over the last century, the axle loads of Canadian trains have tripled, and trains have become more frequent, faster, and longer (TSB, 2008; Hendry, 2011). Canadian railways are continuously maintaining and upgrading the railway network to meet the requirements of higher axle loads, increased traffic volume,

increased speed, and higher standards. The maintenance of railway lines over peat remains problematic as the structures continue to deform and settle. The stability of these peat foundations was questioned after the failure of an embankment and derailment of trains near Lévis, Quebec in 1999 and 2004 (Konrad et al., 2007; TSB, 2008).

Previous studies report continuous settlement and anomalies in the development of pore pressure in both laboratory specimens and beneath earth structures and test embankments (Ripley and Leonoff, 1961; MacFarlane, 1965; Forest, 1967; Lefebvre et al., 1984; Rowe et al., 1984; Edil and Simon-Gilles, 1986; Landva, 2007). The observed pore pressure anomalies have included: i) slower response of pore pressure development with the application of load (MacFarlane, 1965); ii) the existence of residual pore pressure long after the end of primary consolidation (MacFarlane, 1965; Lefebvre et al., 1984; Rowe et al., 1984); and iii) the build-up and dissipation of excess pore pressures relatively independent of depth below ground surface (Forest, 1967). The mechanism of such settlement and pore pressure generation has not yet been fully explained.

The study that resulted following recommendations of the TSB (2008) has included the instrumentation of several sites to understand the response of peat foundations subjected to heavy axle loads (Hendry, 2011; Hendry et al., 2013). Even though settlement was continuously observed in the embankments overlying peat subgrade, the study did not find a direct correlation between train load and deformation. This demonstrated that the mechanism of embankment settling is long term in nature and should be studied and treated separately. This finding as well as increasing maintenance costs of embankments overlying peat subgrades suggests that it is necessary to study and develop a more fundamental understanding of the long-term settlement of peat subgrades.

1.2 Description of study site

This study aims to achieve an understanding of the mechanism of long-term settlement and pore pressure generation in peat subgrade by in situ measurement

of deformation and pore pressure combined with laboratory tests. A railway embankment over peat was instrumented and peat samples were collected for laboratory testing. The site selected for investigation was provided by CN and was selected based on the history of maintenance issues and as the site of new construction. This site is located near milepost[1] (MP) 263.5 of the Lac La Biche (formerly Waterways) subdivision, near the town of Anzac, Alberta (Fig. 1.1). This railway line was originally constructed between 1916 and 1918 (Lester, 2005) as part of the Northern Alberta Railway. This subdivision runs from the mainline, near Edmonton, to Fort McMurray, Alberta (Figure 1.1). CN has recently reacquired the Lac La Biche to Fort McMurray section of the Lac La Biche subdivision from the short-haul operator, Athabasca Northern Railway and Lakeland and Waterways Railway. Extensive maintenance and upgrading of the track and embankment continue to the present day.

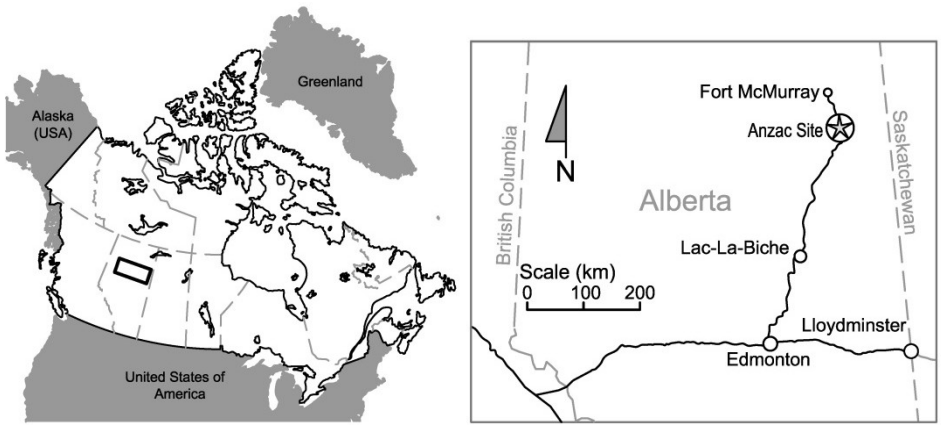

Figure 1.1. Location of the CN site in Alberta included in this study

Fig. 1.2 presents a lithological and aerial map of the site. The site is located in a large area of peatlands. The study site is the southern approach of the bridge at

[1] Locations along Canadian railway track are described using milepost markers and the units of 'miles'. Though not SI units, this is the standard for the industry and is accepted and used by government regulators such as the Transportation Safety Board and Transport Canada. This standard was used within this thesis to describe the location of the study sites to ensure that these sites can be readily found.

MP 263.5 (Fig. 1.2b). This bridge crosses a very soft section of peat that drains to the lake to the east. The original bridge was built in 1961. The alignment of the rail line was changed after the construction of a new bridge in 2008.

The old embankment, on the eastern side of the current railway track, is acting as a toe berm for the new embankment. It was observed that the embankment was not stable, probably due to the lack of support on the west side of the embankment. To limit this instability, a berm is proposed to be built. A 0.5 m thick granular fill was added in late 2010 to act as the foundation of the future toe berm.

In addition to this site, two more sites were investigated as a part of this research as an opportunity to monitor the response of peat subgrades. The first site is located 650 m north of the site at MP 263.5 (Fig. 1.2b). The second site is located at MP 3.87 of CN's Lévis subdivision, Lévis, Quebec. Only field data from MP 263.5, Anzac, Alberta are included in this study.

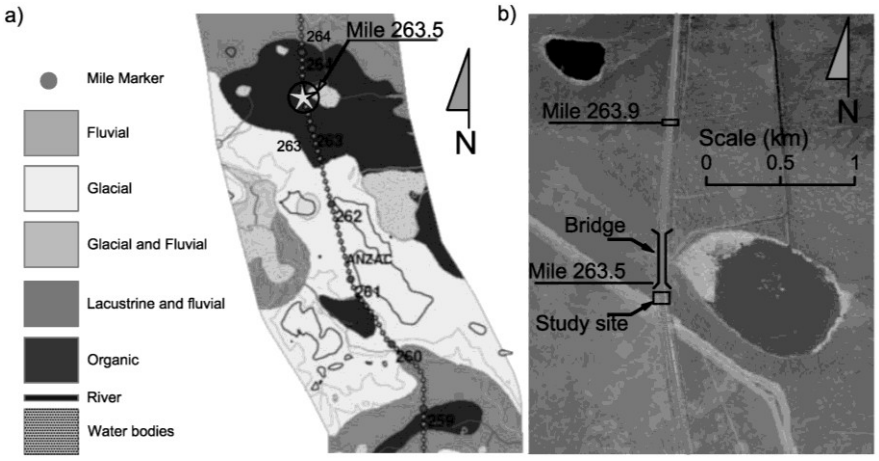

Figure. 1.2. a) Lithological map near MP 263.5 (from Klohn Crippen Berger, 2013), and b) Aerial photograph of the Anzac site peat bog crossing.

1.3 Research objectives

The global objectives of this research are to develop an understanding of the mechanisms that govern the long-term deformation and pore pressure generation

in peat that can be used to describe the long-term settlement of peat subgrade beneath embankments and earthworks and to determine the implication of these mechanisms on the stability of these structures. The main discussion will focus on the investigation of long-term deformation, the mechanism of development of anomalous pore pressure in peat subgrade, and deformation associated with this pore pressure behaviour in peat subgrade based on the behaviour observed in both the field and laboratory. The understanding gained from this study will be a basis for the development of future remedial methods and a viscoplastic model for peat.

The specific objectives of the research are:

I) To conduct field instrumentation and laboratory testing of peat samples to determine the mechanism of the generation of anomalous pore water pressure that has been observed within peat subgrade. The anomalous pore pressure behaviour includes variation of pore pressure, the existence of pore pressure for a long time after the construction of embankments, and the development of pore pressure independent of depth.

II) To analyse the effect of the anomalous pore pressure behaviour on the deformation of subgrade and to quantify this deformation.

III) To conduct laboratory testing of peat samples to determine the mechanical response of peat to the long-term application of multiple stress increments under various stress states.

IV) To evaluate the mechanism of development of volumetric and deviatoric creep strain under variable stress states based on the understanding of creep strain development from normally consolidated clay.

V) To develop expressions to define the development of volumetric and shear creep rate in peat based on laboratory triaxial creep test results and the expressions previously developed for normally consolidated mineral soils.

1.4 Scope and Methodology

The scope of this study included field investigations, laboratory tests, and a theoretical description of the mechanism of development of anomalous pore pressure and the development of creep strain. The following steps were carried out to achieve the research objectives.

- Instruments were installed to monitor the in situ vertical and horizontal deformation, pore water pressure developed under constant embankment loading, and temperature at different depths beneath the embankments and peat subgrade. The instruments included strain gauge and vibrating wire piezometers, vibrating wire settlement gauges, an extensometer, and ShapeAccelArrays.

- The field measurements showed a correlation between the measured pore pressure and the temperature in peat subgrade. To simulate the pore pressure variation in field peat subgrade during summer and winter, temperature controlled undrained compression tests were conducted on Shelby tube peat specimens collected from the same peat subgrade. Temperatures were incrementally increased and decreased in four peat specimens from 2 to 20°C in increments of 1.5 to 2 °C while cell pressures were kept constant. Peat was incubated at room temperature and in an anaerobic environment to demonstrate the decomposition of peat and the generation of gases.

- To study the mechanism responsible for the cyclic rise and sharp drops in pore pressure measured in the field, isotropic consolidation tests were conducted on Shelby tube peat and on cellulose foam specimens. In total, five Shelby tube peat specimens and six cellulose foam specimens were tested at confining pressures varying between 80 and 272 kPa. The cellulose foam specimens were tested to simulate the peat as they have highly permeable open cell structure that can hold water 1000 to 2000% of their weight. A mathematical analysis was done to calculate the pore

pressure needed to expel the gas bubbles through the small pore constrictions at the drainage boundary.

- Long-term laboratory compression tests on remoulded and Shelby tube peat specimens were conducted to understand the time-dependent compression behaviour of peat under constant deviatoric and isotropic stress for variable stress states. The tests included long-term triaxial drained and untrained compression tests as well as isotropic compression tests. The drained and undrained traiaxial tests were conducted to measure the time-dependent volumetric strain and deviatoric strain as well as the strain rate. In total, three Shelby tube specimens and two remoulded peat specimens were subjected to drained compression, and two Shelby tube and two remoulded peat specimens were subjected to undrained compression. Each specimen was subjected to several deviatoric and isotropic stress increments. The duration of the tests varied from four to seventeen weeks. Two remoulded peat specimens were subjected to one-dimensional consolidation tests to compare the strain with triaxial strain.

1.5 Overview of thesis

This thesis has been prepared in a paper-based format. The thesis consists of seven chapters including this first introductory chapter. Chapter Two presents the necessary literature review for this study.

Chapter Three (Manuscript #1) presents the instrumentation for the in situ measurement of pore pressure, vertical deformation, and temperature at different depths in the peat subgrade beneath the embankment. The results of pore pressure measurement from two different types of piezometers are presented to show the seasonal variation in pore pressure, including the rise in pore pressure observed during the summer. This pore pressure variation is correlated to the temperature measured at the same location within the peat subgrade. The laboratory incubation of peat specimens under anaerobic conditions demonstrated the decomposition of peat and generation of gasses. In addition, the measured

increase in pore pressure during incremental increases in temperature on peat specimens showed that the seasonal variation of pore pressure in peat subgrade is related to a volume change in the gas bubbles existing in the peat matrix. The gradual increase in pore pressure in peat subgrade during the summer months was due to both the generation and thermal expansion of gas.

Chapter Four (Manuscript #2) presents pore pressure measurements from the field along with the results of laboratory isotropic consolidation tests conducted on peat and cellulose foam specimens to describe the mechanism of the sharp drop in pore pressure following thermal expansion of the gases in the peat subgrade. The transient pore pressure behaviour was found to be related to the movement and drainage of gas bubbles out of a drainage boundary. The gradual rise in pore pressure was necessary to reach an *"escape pressure"* that was sufficient to push the gas bubbles through the pore constrictions.

Chapter Five (Manuscript #3) presents a quantification of settlement in peat subgrade due to the periodic expulsion of gas bubbles. The results from the isotropic consolidation tests on peat described in Chapter Four are used to derive a correlation between the magnitude of the pore pressure drops and corresponding volume changes. This correlation is extrapolated to estimate the settlement associated with the expulsion of gas bubbles in peat subgrade.

Chapter Six (Manuscript #4) presents the creep behaviour of both intact and remoulded peat specimens tested with long-term drained and undrained triaxial tests. The drained triaxial tests were conducted to measure the combined volumetric and shear creep strain and undrained tests were conducted to measure the shear creep strain. The development of volumetric, axial, undrained axial strains, and strain rate during drained and undrained creep tests under variable stress states are presented. The uniqueness of the stress-strain and strain rate at different stress states and loading durations was analysed and the creep isotaches representing this uniqueness are presented. Further, the applicability of creep rate expressions developed for normally consolidated clay are discussed and applied

to define the development of creep strain in fibrous peat under various stress state.

Chapters Seven provides conclusions and recommendations.

1.6 References

Buisman, A. S. K. 1936. Results of long-duration settlement tests. Proceedings, 1st International Conference SMFE, vol. 1, Cambridge, MA.

Edil, T. B., Simon-Gilles D. A. 1986. Settlement of embankments on peat: two Case Histories. In Proceedings, Advances in Peatlands Engineering, Carleton University, Ottawa: 147-154.

Forest, J. B. 1967. Field studies of the consolidation response of peat. Report 344, National Research Council of Canada, Division of Building Research Ottawa.

Hendry, M. T. 2011. The geomechanical behaviour of peat foundations below rail-track structures. PhD Thesis, University of Saskatchewan, Saskatoon, Canada: 1 254

Hendry, M. T., Martin, C. D and Barbour, S. L. 2013. The measurement and analysis of the cyclic response of railway embankments and underlying soft peat foundations to heavy axle loads. *Canadian Geotechnical Journal,* 50(5): 467-415.

Hobbs, N. B. 1986. Mire morphology and the properties and behaviour of some British and foreign peats. *Quarterly Journal of Engineering Geology, London*, 19: 7-80.

Klohn Crippen Berger, 2013. CN's Lac La Biche rail lines upgrade report, Edmonton, Canada.

Konrad J., Grenier S. and Garnier P. 2007. Influence of repeated heavy axle loading on peat bearing capacity. Proceedings of Ottawa Geo2007: 1551-1558.

Landva, A. O. 2007. Characterization of Escuminac peat and construction on peatland. In Characterization and Engineering Properties of Natural Soils. Edited by T.S Tan, K. K. Phoon, D. W. Hight and S. Leroueil. Taylor and Francis Group, London, 2135-2189.

Landva, A. O. and La Rochelle, P. 1983. Compressibility and shear characteristics of Radforth peats. In STP 820, P.M. Jarrett (Ed.), ASTM Committee D-18 Symposium, Toronto, Canada: 157-191.

Lefebvre, G., Langlois, P., Lupien, C. and Lavallée, J. G. 1984. Laboratory testing and in situ behaviour of peat as embankment foundation. *Canadian Geotechnical Journal*, 21(2): 322-337.

Lester, G. 2005. Atlas of Alberta Railways. University of Alberta Press, Edmonton, Canada. Available on-line at http://railways.library.ualberta.ca/ [Accessed May 12, 2015].

MacFarlane, I. C. 1969. Muskeg Engineering Handbook. University of Toronto Press, Toronto,

MacFarlane, I. C. 1965. The consolidation of peat: A literature review. National Research Council of Canada Division of Building Research Ottawa, NRC: 8-393.

MacKenzie, W. B. 1902. Notes on railway work. Lecture given to the Engineering Society of the University of New Brunswick, October 1902, Constitution and Lectures: 1902-1904.

Ripley, C. F., and Leonoff, C. E. 1961. Embankment settlement behaviour on deep peat. Proceedings, 7th Muskeg Research Conference. NRC of Canada, Technical Memo, 71: 185-204.

Rowe, R. K., MacLean, M. D., and Barsvary, A. K. 1984. The observed behaviour of a geotextile-reinforced embankment constructed on peat. *Canadian Geotechnical Journal*, 21(2): 289-304

Transportation Safety Board of Canada (TSB), 2008. Railway Investigation Report R04Q0040. Cat. No. TU3-6/04-2E, ISBN 978-0-662-47573-6

Weber W. G. 1969. Performance of embankments constructed over peat. *Journal of the Soil Mechanics and Foundations Division*, 95(1): 53-76

2 Chapter 2: Literature Review

2.1 Distribution and formation of peat

Peatland or muskeg refers to any system of plants, water, and underlying peat, irrespective of origin, nature, stage of development, or size. Peat itself consists of the remains of dead vegetation in various stages of decomposition (MacFarlane, 1969). Peat accumulates and peatland will form wherever the conditions are suitable, irrespective of altitude or latitude. Peatlands are common in comparatively cold and wet parts of the world (Hobbs, 1986). Most peatlands are located near the Equator (between 20° south and 20° north) and between 50° to 70° north. Canada has more peatlands than any other country, covering 18% of its land area, primarily in the north (Hobbs, 1986) (Figure 2.1a). More than 50% of Northern Alberta is covered by peatland (Figure 2.1b).

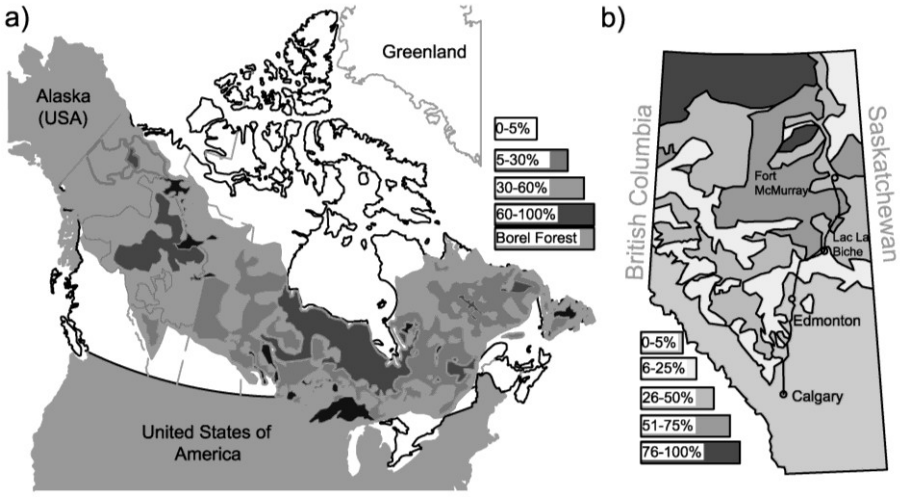

Figure 2.1. Map showing distribution of peatlands within a) Canada, and b) Alberta, with high concentrations in northern areas (after Tarnokai et al., 2002; Turchenek and Pigot, 1988).

Peat forms in both raised and depressed terrain. Peat in elevated terrain, where precipitation exceeds evaporation, forms as raised bogs. Peat known as fenlands develops in drier continental types of climates in lowlands and poorly drained depressions. The latter is more common in the interior of Canada (Hendry, 2011).

The morphological differences between these two peats arise from the circumstances surrounding their formation and the plant types constituting the peat. The differences extend to the structure, fabric, humification, and proportion of mineral material, factors that have a considerable influence on the peat's plasticity, permeability, compressibility, and strength.

The conditions under which peat will begin to accumulate are determined primarily by climate, topography, hydrology, and geology. The geology controls the chemistry and concentration of nutrients in the water entering the peatland in the basin and affects the diversity of vegetation. Peatland development is a long and very slow process (Hobbs, 1986). During this process, peatland will pass through three separate morphological stages, each with its specific plant communities producing characteristic peat with distinctive geotechnical properties. These stages, which are determined by the hydrological state (Hobbs, 1986) of the peatland, are the:

1) Rheotrophic stage, during which the peatland develops in mobile water in lakes, basins, and valleys. Nutrients are supplied by stream flow, runoff, and ground water. The resulting landscape is marsh-like and referred to as fen.
2) Transitional stage, in which the peatland changes by virtue of upward growth. This stage relies to an increasing extent on precipitation because water fluctuation provides the necessary nutrition.
3) Ombrotrophic stage, in which the peatland, having grown beyond the maximum physical limits of the ground water, relies solely on direct precipitation for its water supply above the ground water level. There is a nutrient deficiency and the peat acts as a reservoir, holding water above the ground water level.

These various stages in the normal hydroseral development from shallow open water to raised bogs are presented in Fig. 2.2.

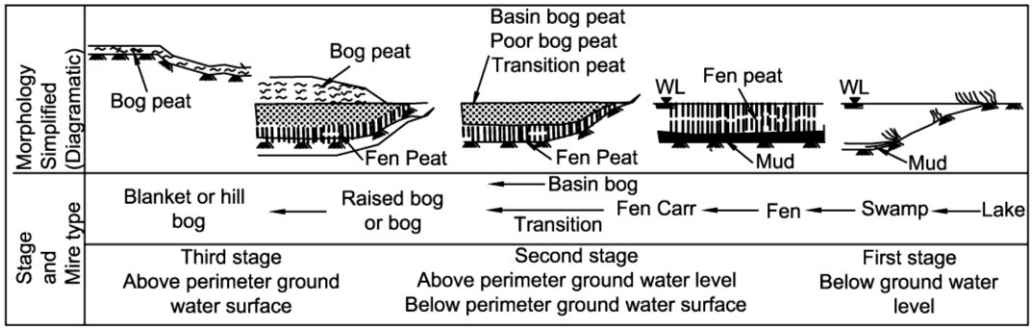

Figure 2.2. Stages of peat development and morphology of peatlands (after Hobbs, 1986).

2.2 Decomposition of peat

The accumulation and decomposition of peat is a continuous process (Hobbs, 1986). Gases are generated during the decomposition of plant material. Aerobic decomposition is one type of oxidation and the end products are carbon (CO_2) and water. Below the top layer and below the ground water table, anaerobic conditions exist, the rate of decomposition is slower, and the by-products are methane (CH_4), ammonia (NH_3), and sulphides (H_2S) (MacFarlane, 1965; Forest, 1967; Hobbs, 1986; Beckwith and Baird, 2001). The availability of nitrogen, the acidity of the soil, and the ambient temperature are the basic factors governing the rate of decay. Higher temperature and pH accelerate microbial degradation (Hobbs, 1986). The degradation of peat in an anaerobic environment and at a temperature as low as 5 °C has been reported (Hulzen et al., 1999; Van Winden et al., 2012). Temperatures above 5 °C can result in an accelerated degradation of peat (Van Winden et al., 2012). Peat heated in the presence of water undergoes autohydrolysis, which results in solubilisation of fibrous material and enhances the degradation process (Leger et al., 1987). Increasing the temperature (>25 °C) causes the peat to swell because the water molecules penetrate into the high molecular weight structure of the organic matter (Lishtvan, 1982).

The intensity of the humification process is neither uniform nor general throughout the peat, because certain parts of the plants are more resistant to degradation than others (Landva and Pheeney, 1980). The loss of organic matter

and the change in the chemical state during humification is accompanied by a breakdown of cellulose within the leaves, stems, and roots of the plants, with the soft inner cell walls being attacked first. The physical and engineering properties of peat are closely related to the state of humification (Hobbs, 1986)

The decay of peat has been shown to contribute to the settlement process. Waldwell et al. (1982) studied the long-term compressibility behavior of an organic soil and found that the total settlement is more than 50% greater in those samples with enough nutrients to promote decomposition than it is for those which are nutrient deficient. The compressibility of organic soil is influenced by decomposition in two ways: (1) by the volume loss associated with the microbial metabolism, and 2) by the increase in organic matter compressibility as the organic structure loses its integrity.

2.3 Profile of peat

The form of peat in any deposit will vary with depth. The acrotelm is the upper 10 to 60 cm of a peat formation, defined as the aerobic zone, and typically consists of plant or forest litter. This fibrous peat layer is the product of dense vegetation at the later stages of peat formation (bog peat) and is much younger than the catotelm that extends to the base of the peatland. This lower layer is often of most concern in geotechnical engineering, as it forms the majority of the peat. The catotelm, mostly amorphous peat, results from a greater degree of biochemical decomposition and mechanical breakdown of the plant remains. This layer is more compressible than the fibrous peat, but retains a similar physical and mechanical behaviour (Edil and Wang, 2000).

2.4 Classification of peat

Peat can vary from a light-colored mass of leaves, stems, and roots of considerable tensile strength to a dark brown or black jelly-like mass, with various stages and mixtures in between (Hobbs, 1986). Fig. 2.3 presents a picture of highly fibrous peat from Northern Canada and highly humified peat from central Africa. Historically, there have been two methods used to classify peat in

Canada: the Radforth classification system and the von Post classification system. The Radforth system is based on visible structure with the engineering properties estimated from this structure. The Radforth system is derived from a long experience with Canadian peat, and has been adopted only in Canada (Hobbs, 1986).

Figure 2.3. Left: highly fibrous peat from Northern Alberta; Right: highly humified peat from central Africa (after Lewis, 2014)

The von Post system is a more extensive classification method and forms the basis for the American Society for Testing and Materials (ASTM) standards for the classification and testing of peat and peaty organic soils (ASTM D4427). The von Post system is a testable classification of the physical properties of peat, some of which have shown strong correlation to engineering properties. These physical properties include the extent of humification (decay of plant mater) (ASTM D5715), the predominant plant, the fibre content (ASTM D1997), and the presence of wood and shrub remains. Other ASTM standards used in the classification include bulk unit weight/density (ASTM D4531), water content (ASTM D2974), specific gravity (ASTM D854), pH (ASTM D2976), and Atterberg limits (ASTM D4318). ASTM D2980 classification is based on absorption capacity and water holding capacity. Peat is classified as extremely, highly, moderately, or slightly absorbent. This classification, also called

functional classification, has been used to predict the repeatability of behavior after loading.

2.5 Engineering properties of peat

Peat exhibits traits and correlations between engineering properties and classification properties that are similar to mineral (particulate) soils, but values for these properties differ greatly from those of soils (Hobbs, 1986). One example of this is the strength of peat, which is remarkably high given its exceptionally high water content. Peat also demonstrates a high degree of variability spatially as well as between different formations within a single peatland (Landva and La Rochelle, 1983; Hobbs, 1986; Elsayed, 2003). The Muskeg Engineering Handbook (MacFarlane, 1969) provides a highly detailed study of the engineering properties of Canadian peat. Ajlouni (2000) and Mesri and Ajlouni (2007) summarize most of the engineering behavior of the peat and describe the consequences with respect to compressibility characteristics.

2.6 Water content in peat

The most striking characteristic of peat is its ability to hold water while possessing significant shear strength. Gravimetric water content, defined as the ratio of the mass of water to the mass of solids, often ranges from 200% to as high as 2,000% (Hobbs, 1986). This accounts for a void ratio as high as 30. Landva and Pheeney (1980) give an overview of microscopic thin walls of Canadian sphagnum peat and the possibility of those walls holding water. Three states or categories of retention are recognized by Dalton (1954), MacFarlane and Radforth (1964), and Hayward and Clymo (1982): i) inter-particle water held within the voids between fibres (macro voids); ii) intra-particle water held by the voids within fibres (micro voids); and iii) adsorbed water. The bulk of water is held as intra-particle and inter-particle water but the proportion of each and the total quantity depend chiefly upon the structure and morphology of the various plants present and on the degree of humification. Fibrous peats (low humification) have a hollow cellular structure largely full of water and have higher total water content than granular amorphous peats. The presence of

mineral soil clearly reduces the volume of inter-particle water in granular peats. The amount of intra-particle water generally exceeds the inter-particle water (2:1) in fibrous peats (Ohira, 1977; Landva and Pheeney, 1980; Landva, 2007), with the proportion decreasing with increasing humification as the cellular structure is destroyed. The thickness and rigidity of the adsorbed water zone is governed by the cation exchange ability of the tissue and the chemistry of the water containing the nutrient supply; the higher the cation exchange ability, the stronger the adsorption complex and the greater the inter-particle adherence (Hobbs, 1986).

2.7 Bulk density and gas content

The bulk density of peat is low and variable and is related to the organic content, water content, degree of saturation, and void ratio. Hobbs (1986) has shown that for both granular (fen) and fibrous peat with a high water content (>600%), the water content and specific gravity have little effect on the bulk density; the major influence is the degree of saturation and gas content. Due to the presence of gas, peats are generally under-saturated and often floating on water when the water content exceeds 500%. Below this limit, the bulk density exceeds that of water even if under-saturated (Hobbs, 1986). Measurements of the degree of saturation of high organic soils have shown that the volumetric gas content commonly ranges from 5 to 10% in Irish sphagnum peat (Hanrahan, 1954; Hobbs, 1986), 5 to 12% in Canadian peat (Lea and Brawner, 1963; Landva, 2007), and up to 15% in Dutch peats (Han and Kruse, 2007). The average degree of saturation in peats having gas volumes up to 15% varies from 0.85 to 1.0 (Hobbs, 1986).

2.8 Organic content and specific gravity

The organic content of peat consists of pure, ash free, vegetable matter and any residual organic compounds from the process of decomposition, in addition to extraneous mineral matter (soil). Peat that is free from extraneous material may have an organic content of more than 98%. Transitional peats may have an organic content of about 80% (Hobbs, 1986). The organic content determines the water holding capacity of the peat. In general, higher organic content is related to higher water content but the water content and the manner in which the water is

held are influenced by the state of the organic matter, i.e., the degree of decomposition (Landva, 2007).

Results reported in the literature show that the specific gravity of peat is variable and depends upon the amount of organic material present, and thus is directly related to the degree of humification (Ajouni, 2000). Most of the living plant tissues that contribute to the formation of peat have a specific gravity less than that of water. The fibers and other tissues, cellulose, lignin, and other substances in the peat are heavier than water. Lignin substances have an average specific gravity of 1.4 and cellulose has an average specific gravity of 1.5 (Davis, 1997). For an organic content of 75% or greater, the specific gravity varies between 1.3 and 1.8 but values as low as 1.1 have been reported (Lechowicz et al., 1996).

2.9 Permeability

The great variability in peat particles and their arrangement results in a wide range in permeability. The factors that affect peat permeability include botanical composition, degree of humification, bulk density, fibre content, mineral content, presence of gas, void ratio or porosity, and surface loading (MacFarlane, 1969; Lishtvan, 1981; Lefebvre et al., 1984; Hobbs, 1986). Hogan et al. (2006) undertook field-based measurements of the hydraulic properties of a Boreal Fen consisting of non-Sphagnum mosses and found values of hydraulic conductivity as high as 9.0×10^{-3} m/s near the surface, decreasing to 10^{-6} to 10^{-5} m/s below a depth of 2 m.

Hobbs (1986) summarized data for vertical permeability of undisturbed fibrous peats specimens from all around the world. Fibrous peats are the upper bound of permeability, on the order of 10^{-4} m/s. Highly humified peats form the lower bound of permeability, as low as 10^{-9} m/s, which is the same order of magnitude as that of calcium montmorillonite. The wide range of permeability amounting to some three orders of magnitude is not entirely due to the physical variability of peat, but also to the different natural void ratios from which peat specimens are consolidated. Hobbs (1986) found the variability in permeability in one site

embraces that of five different geological and climatic regions and concluded that peatlands of similar morphology may be expected to show intense local variation but broadly similar permeability.

A large reduction of the permeability with the increase of consolidation pressure in remoulded and undisturbed peat has been reported (Lea and Browner, 1963; Adams, 1965; Hobbs, 1986). For geotechnical purposes, the permeability must therefore be measured as a function of applied pressure or preferably as a function of porosity (Landva et al., 1986). Under compression, the fibres and particles of the peat get closer together and the adsorbed water layers tend to coalesce, therefore reducing the dimensions and increasing the length of the free water channels (Hobbs, 1986). Under constant load, the initial permeability of peat is generally high, and because peat contains a fairly significant amount of gas, substantial immediate settlement occurs after loading. After the immediate settlement, the organic structure will creep continuously, with the pore pressure and permeability remaining almost constant (Landva, 2007). The presence of gas does not necessarily affect the permeability of peat when gas is present within the stems (Landva and Pheeney, 1980)

Peat is reported to be hydraulically anisotropic with horizontal permeability generally greater than vertical permeability. The variation of permeability is considerable for fresh peat but fairly uniform for highly humified peat. Vertical and horizontal permeability ratios ranging from 1 to 7.5 have been reported (Colley, 1950; Kogure et al., 1986). In fibrous peat, this anisotropy accounts for the horizontal layout of peat fibres.

2.10 Consolidation and compression behaviour of peat

The consolidation behaviour of peat has been the subject of numerous investigations, in particular since the 1960s (Marfarlane, 1965; Wilson et al., 1965; Barden, 1968; Berry and Poskit, 1972; Landva and La Rochelle, 1983; Lan, 1992). The coefficients of primary and secondary consolidation (C_c and C_α) derived from odometer tests are used to quantify the consolidation and long-term

settlement under constant loading. Measured field settlements are often larger than those predicted from laboratory testing results (Samson and Rochelle, 1972; Landva and La Rochelle, 1983). This discrepancy has been attributed to the variability of peat, changes in loading condition, the three-dimensional nature of creep, and the tendency of C_c and C_α to increase with time.

The consolidation in peat is described as a continuous process that includes a sequential dissipation of pore pressure together with the destruction of the cellular structure (Adam, 1965; Barden, 1969; Berry and Poskit, 1972, Landva and La Rochelle). The primary consolidation of peat includes the expulsion of water due to dissipation of pore pressure and the simultaneous rearrangement of the peat particles and structure. Following initial consolidation, volume change continues in a creep-like process as the peat structure continues to undergo rearrangement and water is expelled almost exclusively from the micropores in the organic structures (Hobbs, 1986). Secondary consolidation is sometimes associated with a finite value of pore pressure developed as a result of the creep process or from what remains in some poorly connected cavities; i.e., micropores (De Jong and Virujit, 1965; Barden, 1969). More recent observations in peat show that, because of the large openings in the intact cells and the completely open framework, the expulsion of the micro and macro pore water takes place simultaneously (Landva, 2007). Thus, the assumption of secondary compression due solely to the drainage of micropores is potentially misleading.

2.10.1 Compression models for peat

Peat particles are reinforced by cells and baffle walls (Landva and Pheeney, 1980). These cells and baffle walls work as a frame and lend shape, strength, and resilience to the peat fabric (Fig. 2.4). Short-term and small-strain compression is predominantly elastic as the peat contains at least 10% gas (Landva and La Rochelle, 1983). The elastic behaviour is demonstrated by instant compression and a complete rebound once the load is removed. However, an extended application of load results in non-reversible compression due to the flattening of the open cell and baffle wall structure (Briaud, 1974). This destruction of peat

structures is reported to occur primarily during the secondary compression under a relatively higher load (Samson and La Rochelle, 1972).

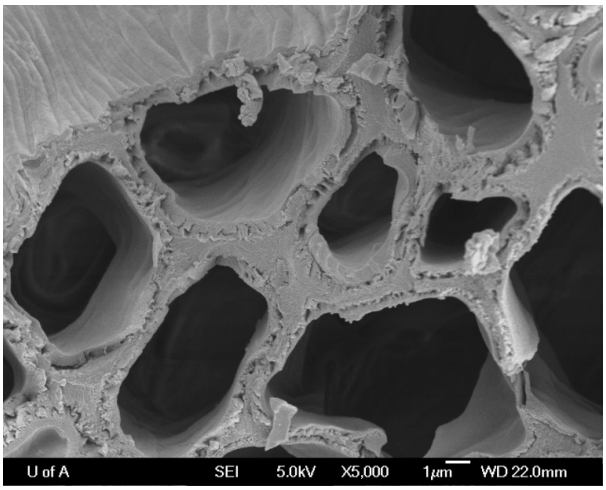

Figure 2.4. Scanning electron micrographs of peat samples from Anzac, Alberta

The consolidation process is thus a combination of primary consolidation in an ideal elastic soil and secondary compression that results from structural creep. The rate of creep increases with organic content as the cell structure is degraded. The rate of secondary compression will exceed the rate of primary consolidation with a decrease in the permeability of the material (Landva and La Rochelle, 1983). This increased rate of secondary compression results in a deviation from the characteristic S-curve shape in the time-compression curves for peat; the curve could be gentler or, depending on the creep rate, the tail of the curve may continue without deflection from the rest of the curve, may disappear, or may be reversed (Landva, 1980). An example of this is presented in Fig. 2.5, where a Type I curve follows Terzaghi's theory with an S-shaped curve and represents inorganic soils; a Type II curve shows rapid development of primary consolidation followed by secondary consolidation, but does not vary linearly with time (on a log scale); a Type III (a) curve shows no discontinuity between primary and secondary consolidation; and a Type III (b) curve shows the development of a secondary curve in the reverse direction.

The consolidation of peat involves a relatively complex physical process that does not follow Terzhaghi's theory of consolidation for the following reasons (Hobbs 1986): 1) large axial strains indicate a moving boundary, 2) large decreases in the permeability of the peat occur with large volumetric strains, 3) the volume change is not linear with pressure, and 4) pore water and solid fibres are compressible if gas is present. Thus, the terminology used for the consolidation of mineral soils, such as primary consolidation for the initial phase and secondary compression for the creep-like behaviour, are used with caution for peat. The boundary between these two phases is often only distinguishable from pore pressure measurements (Hobbs, 1986; Mesri and Ajlouni, 2007).

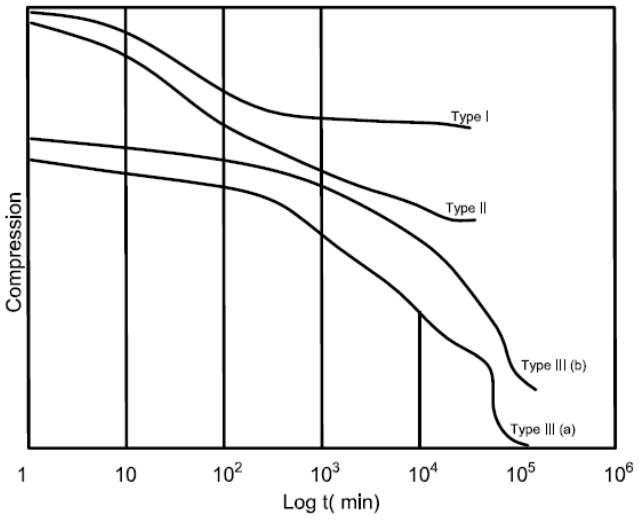

Figure 2.5. Time compression curve based on data from consolidation tests (after Leonards and Girault, 1961).

The primary consolidation of peat occurs rapidly due to its initial high hydraulic conductivity, and lasts for weeks or months. However, published field and laboratory findings have shown that the secondary deformation of peat is significantly larger than the primary deformation and can continue for many decades (Macfarlane 1965; Weber, 1969; Mesri et al., 1997; Gunaratne et al., 1998). Due to the higher rates of deformation and longer timespan, secondary

compression accounts for more than 60% of the total settlement (MacFarlane, 1965; Elsayed, 2003).

Many of the alternative models proposed for complex consolidation processes in clay and silt are the result of modifications made to Terzaghi's theory of consolidation. These models have incorporated changes in permeability and compressibility during consolidation, time-related compressibility during and after the primary consolidation phase, and the effect of self-weight. Consolidation models for peats have been developed considering the primary and secondary consolidation as a single continuous process without a discontinuity in between (Type III, Fig. 2.5), and with the majority of the strain being the result of secondary compression. The models used to describe both the primary consolidation and secondary compression of saturated clay and peat observed during one-dimensional odometer testing are rheological models. Within these models, the primary consolidation is governed by the dissipation of pore water pressure and the secondary compression is defined as creep under constant effective stress. Some of the models that have been developed for peat are as follows:

1. Barden (1965, 1968) proposed a simple rheological model for an element of saturated clay and solved for one-dimensional consolidation. The creep is defined by Ostwald's power law and a creep equation proposed by Wu et al. (1966).
2. Berry and Poskit (1972) proposed separate rheological models for consolidation of amorphous and fibrous peats. These models considered large strain, the variation of the void ratio with effective stress, the variation of permeability with the void ratio, and time-dependent compressibility. Creep is defined in terms of the void ratio as a function of both time and the magnitude of the applied stress. The creep functions used were those proposed by Murayama and Shibata (1964) and Wu et al. (1966). The creep considered is solely volumetric and the model is formulated and solved for the case of one-dimensional consolidation.

3. Lan (1992) proposed a one-dimensional consolidation model of peat based on a constant rate of strain and a constant rate of stress from laboratory test results. His basic assumption for the constitutive relationship was that there exists a unique relationship between effective consolidation pressure (σ'_v) and the rate of change of the void ratio ($\dot{e}$), similar to that developed for clays (Leroueil et al., 1985). This uniqueness implies that, at the same σ'_v and $\dot{e}$, the void ratio (e) should be unique and independent of the loading path and time duration of the pressure increment.
4. Den Haan (1996) presented a model for the calculation of the deformation of non-brittle soft clays and peat. Natural strain (ε_H), the integral of the ratio of change in specific volume to the final specific volume, is used instead of linear strain. Den Haan (1996) found the linear relationship between the effective vertical compression ($ln\ \sigma'_v$) and natural strain (ε_H), or the logarithm of specific volume ($log\ v$), to define the virgin compression line for many soils. During the secondary compression, the rate of volume change is calculated as the sum of the rate of compression resulting from a stress increase, plus the creep rate, where the creep rate is constant during and after the primary stage. The creep rate is derived from the linear relationship between ε_H and intrinsic time ($\tau = t - t_r$), where t is the linear time and t_r is the time shift resulting from the logarithmic transformation of time.

The main difference between these constitutive models is in the expression of creep as a function of time. All of these models are developed from one-dimensional consolidation tests, as most of the published long-term peat compression results and analysis are from one-dimensional consolidation. Efforts to study the long-term deformation under triaxial loading conditions are rare. The majority of the deformation in peat is assumed to be volumetric but to the best of author's knowledge there has not been any testing to quantify the amount of long-term volumetric and deviatoric strain. Thus, there is a deficit in the

understanding of the mechanism of development of deformation at different stress states and for different stress paths.

2.10.2 Time-dependent compression (creep) in soil and peat

Creep is the development of time-dependent plastic strain under a constant application of stress. In inorganic soils, this plastic straining occurs due to continuous rearrangement of particles. This rearrangement of particles is an ongoing process occurring both under constant effective stress and during the dissipation of pore water (Wood, 1990). For peat, creep has been attributed to the breakdown of cell structure and the dissipation of intracellular water, in addition to particle rearrangement (Adams, 1965; Barden, 1968; Berry and Poskit, 1972; Landva and La Rochelle, 1983).

The main objective of creep theories is to determine the stress, strain, and time relationship. Several creep theories have been developed to describe creep behaviour in different materials because of the complexity and the large number of factors that influence the creep phenomenon. These theories differ first in the equations of state correlating stress, strain, and time, and second in how to these equations describe creep phenomena. Three main approaches including the fundamental approach, the rheological approach, and the phenomenological approach have been developed to describe creep deformation.

The fundamental approach considers creep behaviour at the particle interaction level. In this approach, creep or secondary compression is assumed to be the result of either time-dependent stress transfer from viscous adsorbed water to the grain-to-grain contacts (Terzaghi, 1931) or as a time-dependent distortion of energy barriers or forces that keep particles in equilibrium due to applied stress (rate process theory: Murayama and Shibata, 1964; Christensen and Wu, 1964; Wu et al., 1966). De Jong and Virujit (1965) proposed the third approach that models the soil pores as compressible cavities with interconnected channels. The model was called the cavity channel network and was used to simulate primary and secondary consolidation. Channels of high conductivity allow the dissipation

of excess pore pressure from the cavities during primary consolidation. However, the excess pore pressure in some cavities remains greater than zero because of the low conductivity of the connecting channels. The slow dissipation of this excess pore pressure gives rise to secondary consolidation.

Amorphous granular peat may behave similarly to a clay soil, but fibrous peat has an open structure with the interstices filled with a secondary structural arrangement of non-woody fine fibrous elements (MacFarlane and Radforth, 1964). Adams (1965) and Wilson et al. (1965) introduced the concept of a cavity channel network in peat assuming the existence of two levels of voids (macro and micro). Fig. 2.6 is the simplified model proposed by Barden (1969) to represent this mechanism, where the dashpot provides the time-dependent compression of the microstructure when loaded by effective stress. It is impossible to deduce the precise laws governing the dashpot because the detailed drainage properties of the packets of micro voids are unknown. No further work has been done to quantify this mechanism.

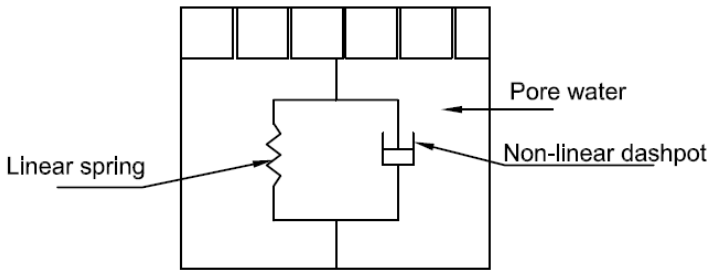

Figure 2.6. Model of saturated clay / peat under compression (after Barden, 1969).

The fundamental models are dependent on micromechanical properties and are difficult to apply because the model parameters are not interpreted in terms of macromechanical properties such as stress, strain, and time. The majority of recent studies on the time-dependent behaviour of soils have excluded the fundamental models (Liingaard et al., 2004).

Rheological models describe uniaxial conditions and model the stress, strain and strain rate behaviour of soil with a group of springs, linear and non-linear dashpots, and sliders. The dashpots and sliders represent the time behaviour of soil. Springs account for the linear elastic soil behaviour and are expressed in terms of Young's modulus (E) or the bulk modulus (K). The dashpot characteristics are chosen in accordance with rate process theory. The differences among the various rheological models are in the arrangement of their different components. The rheological models developed by Murayama and Shibata (1961), Christensen and Wu (1964), and De Jong (1968) are some of the widely applied rheological representations of the time-dependent behaviour of soil. Rheological models, however, need many parameters to characterize the stress, strain, and strain rate behaviour and approximation of complex mechanisms in the governing equations in order to model the true, time-dependent behaviour as depicted by other verified models (Singh and Mitchell, 1968).

The phenomenological approach uses the results of laboratory testing to develop an empirical equation to define the creep of the soil. Although this approach does not utilize theoretical procedures, its simplicity and wide application in many lab tests renders it the most practical. Singh and Mitchell (1968) developed a three-parameter phenomenological equation based on a wide range of laboratory tests on many clay types with different stress histories. This equation has been widely used to define deviatoric creep in developed visco-plastic modelling frameworks for clays (Borza and Kavazanjian, 1985; Morsy et al., 1995). The secondary compression equation from Taylor (1948) is widely used to define volumetric creep behaviour (Yin et al., 2002; Kelln et al., 2008).

Compression models for peat described in Section 1.6.1 combine the rheological and phenomenological approaches to describe the primary and secondary consolidation settlement in peat. Creep tests on peat conducted in a triaxial stress state, which may represent the three-dimensional nature of the consolidation of peat foundations beneath embankments, are not common in the literature. Thus, creep testing of peat in a triaxial stress state and the development of expressions

to define the development of volumetric and deviatoric creep rates must be undertaken to understand the long-term settlement mechanisms of peat subgrades under loading.

2.11 Pore pressure generation in peat

The development of pore pressure within peat that has been observed in both laboratory specimens and field measurements is reported to vary widely. This may be one of the reasons why pore water pressure measurements in peat are rarely reported. MacFarlane (1965) reported a slower response of pore pressure development to the application of load and the existence of residual pore pressure after the end of primary consolidation. Forest (1967) noted that the build-up and dissipation of excess pore pressures are relatively independent of depth below ground surface, and that the amount measured is in excess of the magnitude of vertical stress calculated using elastic theory.

The measured pore pressure developed in peat subgrade due to moving trains (Konrad et al., 2007; Hendry et al., 2013) is found to be cyclic and constant under repeated applications of axle loads. The measured residual pore pressures were small and predominantly elastic, undrained, and recoverable (Hendry et al., 2013). The distributions of cyclic pore pressures, however, were not consistent with depth (Fig. 2.7). Hendry et al. (2013) reported an increase in pore pressure with depth and Konrad et al. (2007) found that the greatest increase in pore pressure was near the middle of the peat layer.

Wong et al. (2006) found that the measured pore pressure on peat layers near piping holes below the rail load were cyclic and short lived but much higher than the elevation head, and thus responsible for the pumping of peat to the surface, producing piping holes. The measured in situ pore pressures were inconsistent with the elastic analysis. The developed pore pressure was lower or higher depending on how far the piezometers were located from the piping hole.

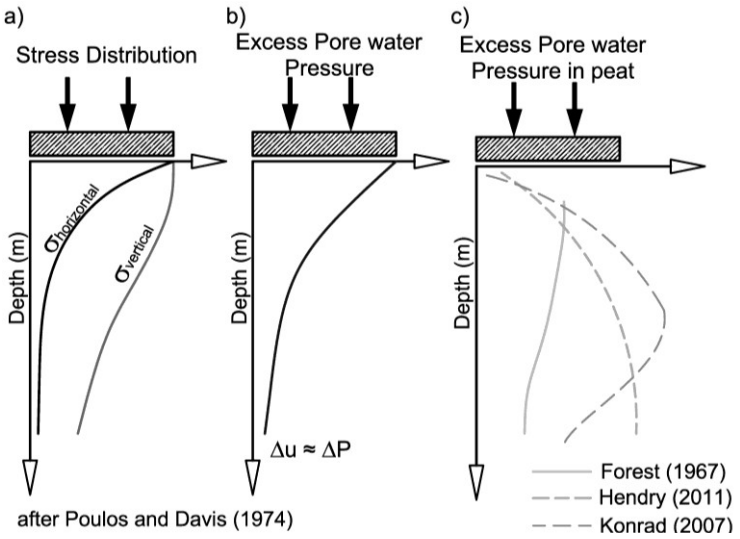

Figure 2.7. Elastic distribution of a) stress, b) pore pressure, and c) measured pore pressure in peat.

Hendry et al. (2012) reported the anisotropic generation of pore pressure based on laboratory undrained triaxial tests. The amount of anisotropy was reported to be related to the ratio of horizontal stiffness and vertical stiffness of the peat specimen tested as well as the amount of vertical strain and effective confining pressure. Tension resisted by peat fibres was proposed to be responsible for the anisotropic stiffness and anisotropic pore water pressure.

In general, the development of pore water pressure on peat under a dynamic train load and on an undrained triaxial test in a peat specimen is mostly uniform though different from that estimated based on elastic theory (Konrad et al., 2007; Hendry et al., 2013). Under static field load tests and consolidation tests, the excess pore water pressures in peat are mostly irregular. These irregular pore pressure behaviours have never been studied with respect to the mechanism of their development and their effect on the settlement mechanism of peat subgrade, and further study is thus necessary. The study of this erratic pore water pressure behaviour observed in a peat foundation might help to better understand the mechanism of long-term settlement in the peat subgrade.

2.12 Long-term response of peat foundation

The long-term settlement and pore pressure response in peat beneath earth structures have been previously monitored (Ripley et al., 1961; Landva and La Rochelle, 1983; Lefebvre et al., 1984; Rowe et al., 1984; and Edil et al., 1986). Landva (2007) presented the results of many field and laboratory compression test results on Escuminac peat. These studies have shown that: 1) the total settlement of fills on any one peat deposit varies widely even if the applied load, depth, and type of peat are the same; 2) the rate of settlement of fills on peat is largely unpredictable based on laboratory or field testing, including test fills; 3) the commonly used linear relationship between settlement and the logarithm of time does not provide a reasonable fit to the measured settlement under fill; and 4) the magnitude of the compression of the peat varies considerably with depth despite only small variations in water content and the degree of humification. This fourth observation is hypothesised to be responsible for the discrepancy often found between settlement predictions and observed settlement. Landva et al. (2007) attribute this discrepancy to the heterogeneity of the peat. In natural conditions, the peat is a heterogenic mass of unequal density and strength. Even with increasing depth, this heterogeneity does not reduce sharply because the specific gravity and, consequently, the available overburden weight are quite low (Hobbs, 1986; Landva et al., 1986). In this context, it is difficult to obtain comparative results from laboratory tests of natural peat. But because peat is highly compressible, heterogeneity should decrease with increasing confining pressure (Landva et al., 1986).

Fig. 2.8 and Fig. 2.9 present two examples of pore pressure and settlement measurements below test embankments that were monitored for three years and one year, respectively. Both of these examples show large deformations and the existence of excess pore pressure for long periods of time after the placement of fill. Fig. 2.9 shows some rise and drop in pore water pressure in peat even when the fill level was constant and lasted for several weeks. Such rises and drops in pore water pressure are also observed during the measurement of pore water

pressure in peat subgrades underlying railway embankments (Wong et al., 2006; Konrad et al., 2007). Several analyses based on one-dimensional consolidation tests have been presented to estimate the long-term settlement and pore pressure developed in fibrous peat (Barden, 1968; Mesri et al., 1997). However, the results of these studies have not fully described the mechanism of the existence of long-term excess pore pressure and the settlement of peat foundations underlying embankments and earth structures.

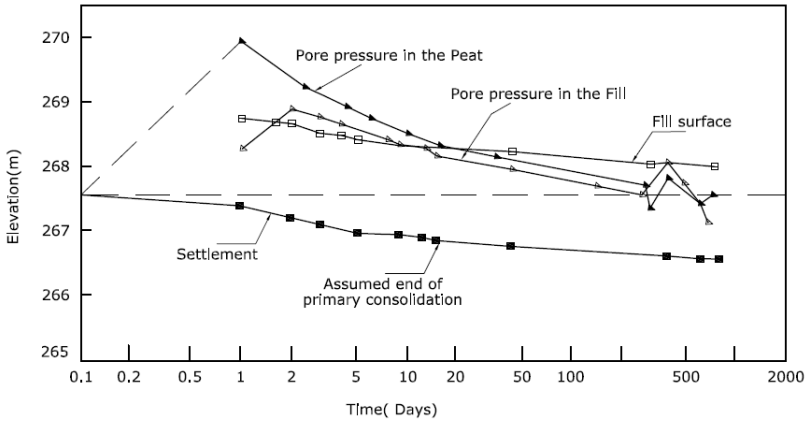

Figure 2.8. Settlement and pore pressure generation corresponding to fill placement in James Bay Territory in Quebec (after Lefebvre et al., 1984).

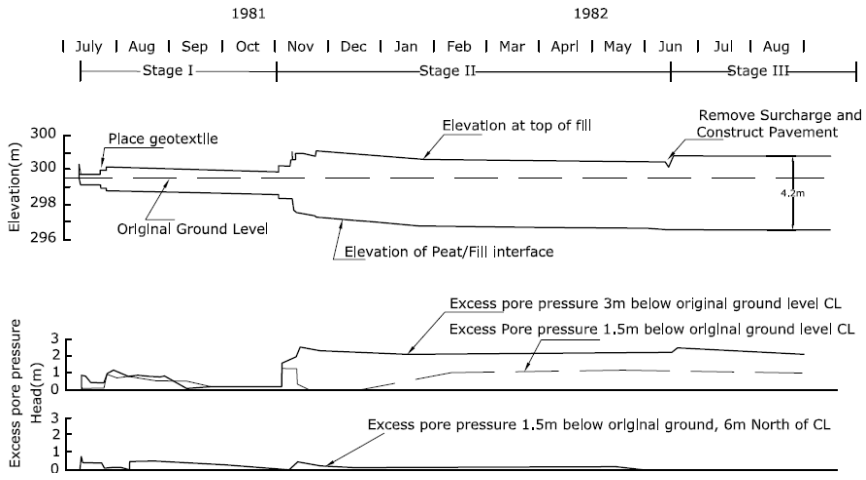

Figure 2.9. Settlement and pore pressure generation corresponding to fill placement in Ontario, Canada (after Rowe et al., 1984).

Large deformation of peat beneath test fills has been observed (Weber, 1969; Landva et al., 1984; Rowe et al., 1984). For more than three years, Landva and La Rochelle (1983) recorded the settlement of a 7 m-thick test fill over peat that was 7.4 m thick. The strain that was calculated to have occurred within the peat subgrade was more than 80%. Landva and La Rochelle (1983) estimated that two-thirds of this settlement would have occurred under laterally confined conditions (attributed to volumetric strain), and that the remaining third would have been the result of shear deformation (deviatoric strain).

Settlement under embankments due to volume change can be very large for peat due to its high water content (Hanrahan, 1954). Settlement under embankments not associated with volume change is the result of lateral "creep", or deviatoric strain, which is the result of ongoing shearing. Peat subgrades under embankments are especially susceptible to the shearing type of creep due to the low submerged density of the peat (Hanrahan, 1954). For a structure built upon peat, the component of the resulting settlement that occurred at confining pressures greater than 30 kPa was reported to be a result of deviatoric shear strain within the peat (Landva and La Rochele, 1983; Landva, 2007). The portion of shear deformation increases with increasing confining pressures above 30 kPa.

From laboratory tests on Sherman Island peat and observations on the performance of a levee constructed over the same peat, Wehling et al. (2003) suggested that shearing of the peat during construction of the levee might have resulted in the development of residual shear strength, which led to continual lateral spreading and strength reduction in the peat. Edil et al. (1986) used an inclinometer to monitor lateral deformation of embankments constructed over peat deposits that were 3 to 4 m thick. They reported that, in spite of a large vertical strain (20%), there was no significant lateral deformation for the one-year period after the construction of the embankments. This finding contradicts the conclusion of other studies (Landva and Rochele, 1983; Landva, 2007; Wehling et al., 2003), which reported that one-third of the vertical deformation might be related to shear deformation. It is still not clear whether embankments

spread laterally with the lateral deformation of peat. It is necessary to monitor both vertical and lateral deformations to understand the settlement mechanism in the peat subgrade.

2.13 The nature of gassy soils

In unsaturated soils near the ground surface, pore gas (mostly air) is continuous, connected to the surface, and has a uniform atmospheric pressure (Thomas, 1987). In soils with a high degree of saturation, i.e., greater than 0.85, such as sea bed soils, gas exists in the form of discrete bubbles within a continuous pore fluid (Barden, 1974; Nageswaran, 1983). Under these conditions, the gases are predominantly static and trapped within the soil skeleton. Such soils are often referred to as gassy soils (Nageswaran, 1983). Soils with a large amount of gas dissolved in pore fluid because of a higher solubility of gas within the pore fluid (e.g., CO_2 in water or CH_4 in oil) are also defined as gassy soils (Sobkowicz and Morgenstern, 1984). Fig. 2.10 presents the idealised structure of soil with discrete gas bubbles within the soil matrix. Gas within coarse soils, such as sands, displaces the pore water or exists as isolated bubbles, leaving the overall structure unchanged (Fig. 2.10a). In soft, fine-grained soils, gas is able to distort the saturated soil matrix and produce bubbles that are large compared to the soil particles and water-filled voids (Fig. 2.10b).

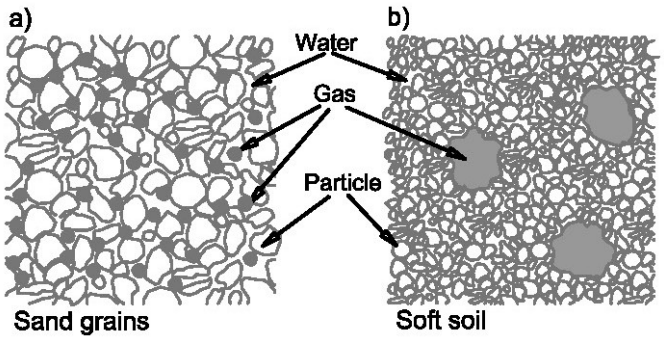

Figure 2.10: Structure of sand and soft soil containing gas bubbles (after Wheeler et al., 1988).

The volumetric gas content in peat commonly varies between 5 and 15%. This percent of gas is similar to the average degree of saturation in peat, reported to vary from 0.85 to 1.0 (Hobbs, 1986). There appear to be parallels in the behaviour of peat and gassy soils. Due to the presence of flexible fibres and openly jointed cells filled with water, gas bubbles in peat are expected to distort the fibres and structure of peat mass similar to the way that they distort soft soils. In addition, the broken structure of peat fibres and high permeability will allow the movement and coalescence of gas bubbles.

The size of the gas voids is a function of the volume of gas and the stiffness and strength of the soil (Sills et al., 1991). Gas and water in soil maintain a stable equilibrium condition at atmospheric temperature and pressure. The variation of external pressure or temperature causes the gas bubbles to move into larger void spaces to reduce the pressure and merge with one another and attain a more stable condition (Barden, 1974). If the gas bubbles are unable to move when the external pressure increases, the bubbles may collapse and disperse, resulting in a sudden drop in pore pressure (Schuurman, 1966; Teunissen, 1982; Sills et al., 1991).

Results from laboratory testing conducted on gassy soils are characterized by their inconsistency and are thus difficult to interpret. Consolidation tests on soft sea-bed gassy soils have shown no unique relationship between the void ratio and consolidation stress due to a significant variation in pore pressure (Nageswaran, 1983; Wheeler, 1986; Thomas, 1987). The gas volume does not change significantly even after drainage of pore fluid from the specimen, and gas pressure followed the total stress profile rather than consolidation stress (Thomas 1987). Sobkowicz and Morgenstern (1987) presented the variation in pore water pressure in gassy soil under constant volume and stress conditions; Fig. 2.11 shows the gradual build-up of pore pressure in an undrained isotropic compression test on dense Ottawa sand mixed with carbon dioxide-saturated water following the decrease in cell pressure. This pore pressure behaviour is explained by an exsolution of carbon dioxide gas from liquid, which attains an

equilibrium condition near the liquid gas saturation pressure. The liquid gas saturation pressure for carbon dioxide and water was 510 kPa. Wong and Maini (2008) presented a mechanistic model for the kinetics of gas bubble growth due to solute diffusion in supersaturated oil liquid. Wong and Maini (2008) reported that the bubble sizes could be estimated indirectly from the pore pressure response and the liquid (oil) gas saturation pressure was 3.45 MPa.

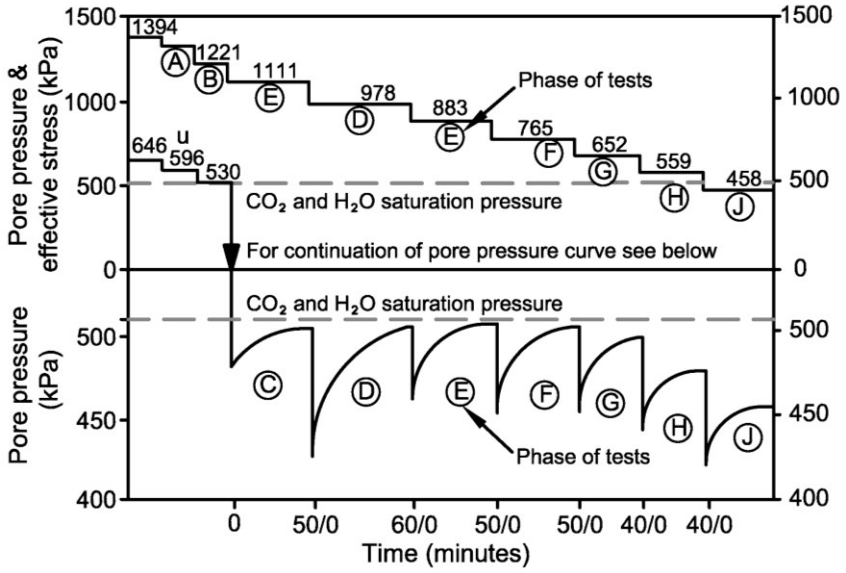

Figure 2.11. Pressure rise due to the exsolution of gas during undrained tests (after Sobkowicz and Morgenstorn, 1982).

3 Chapter 3: Thermally induced pore pressure response in peat beneath a railway embankment

3.1 Contribution of the Ph.D. candidate

All work reported in this chapter, including field installation, design of the experimental program, implementation of the experiments, review of the literature, analysis and discussion of the results and writing of the text, has been carried out by the Ph.D. candidate. As supervisors, Dr. M. T. Hendry and Dr. C.D. Martin reviewed all parts of the work. This chapter has been published with the following citation:

Acharya M. P., Hendry, M. T. and Martin, C. D. 2015. Thermally induced pore pressure in peat beneath a railway embankment. International Journal of Geotechnical, in press, online:
http://www.maneyonline.com/doi/abs/10.1179/1939787915Y.0000000022

3.2 Abstract

This paper presents the results of a study investigating the behaviour of peat subgrade beneath a railway embankment. Instrumentation was installed to measure the temperature, pore water pressure, and vertical settlement at different depths within peat strata over a three-year period. The pore pressures within the peat subgrade were observed to increase significantly during the warmer months (>10 kPa) and strongly correlated to the seasonal changes in temperature. However, no clear correlation was found between pore pressure and settlement. Gas bubbles coming out of saturated peat layer beside the embankment suggest that pore pressure could be associated with the expansion of gas bubbles within the peat. To confirm this hypothesis, laboratory tests were conducted. Peat specimens, kept at room temperature and in an anaerobic environment, demonstrated the potential of the degradation of peat and the generation of gas. Further peat specimens were placed within a triaxial cell at a constant confining pressure, while the temperature was incrementally increased. Measurements showed that a 30 kPa increase in pore pressure corresponded to a 10°C increase

in temperature. The results of this investigation presented the existence of gas in peat subgrade due to decomposition, and its effect on pore pressure generation.

3.3 Introduction

Peat's organic composition, variability in properties, low modulus, and potential for large volumetric strains have posed challenges for the construction of structures upon it (Stanek and Worley, 1983; Landva, 2007; Long and Boylan, 2013). The settlement and failure of railway and road embankments constructed on peat subgrade has been the subject of frequent study. Some of the recent studies include those published by Konrad et al., 2007; Hendry et al., 2013; and Long and Boylan, 2013, from Canada, Canada and Ireland respectively. In Canada, the performance of railway embankments constructed on peat subgrade has become a critical concern due to the ongoing settlement and recent embankment failure, and has highlighted the necessity to understand the behaviour of peat subgrade (Konrad et al., 2007).

The instrumentation of a railway embankment and peat subgrade in Northern Alberta, Canada, was carried out to monitor the long-term behaviour of the embankment structure and underlying peat. This instrumentation resulted in the measurement of anomalous increases in pore pressures within the peat strata. These increases in pore pressure showed a strong correlation to seasonal fluctuations in temperature, with significant increases in pore pressure of more than 10 kPa during the summer months. This increase in pore pressure occurred for three consecutive summers. Unexpected pore pressure responses in peat foundations have been reported in the literature. These responses have pressures that are higher or lower than the applied vertical stress (MacFarlane, 1965; Forest, 1967); they show increased pore pressure response at greater depths below embankment structures under heavy axle loads (Konrad et al., 2007; Hendry et al., 2013). There are no publications in the literature showing measurements of seasonal variations of pore pressure in peat foundations.

In the field site, the seasonal nature of the pore pressures, and the field observations of gas bubbling to the water ponded beside the embankment during the warmer months, resulted in the hypothesis that this pore pressure increase was due to thermal expansion of gas bubbles within the peat. Previous work has documented the generation of gases from the decomposition of peat (Macfarlane, 1965; Hobbs, 1986; Hulzen et al., 1999; Van Winden et al., 2012). These gases predominantly include carbon dioxide (CO_2) and methane (CH_4), with lesser amounts of nitrogen (N_2) and hydrogen sulphide (H_2S) (MacFarlane, 1965; Forest, 1967; Hobbs, 1986).

This study is novel because it has found that gas exists in the peat subgrade beneath railway embankments, and that the gas affects the seasonal generation of significant pore pressure, which has never been accounted for in published geotechnical works. This paper describes the study in two parts. The first part of the paper presents the field measurement of pore pressure, temperature, settlement, and the correlations between pore pressure and temperature. The second part consists of laboratory tests on peat specimens to show that gas is generated from the decomposition of submerged peat under anaerobic condition; and to reproduce the pore pressure response that increases with the temperature when gases expand while the peat is confined within a triaxial cell.

3.4 Description of the site

Long stretches of the Canadian railway network, especially in the northern regions of the country, have been constructed over thick peat deposits. In Alberta, the railway line between Edmonton and Fort McMurray, known as the Lac la Biche subdivision (LLBS), is estimated to have more than 120 km of embankment constructed over peat formations. The study site is located on the LLBS near mile post (MP) 263.5, near the town of Anzac, where the railroad crosses a large expanse of peat bog (Fig. 3.1). At the site, the air temperature ranges from maximum values exceeding +30°C in summer, to minimum values below -20°C during winter. A ground investigation was conducted at this site in May 2011. The site investigation showed that the embankment consists of 2 to 3

m of granular material (including ballast and subballast) overlying an undisturbed peat layer that is approximately 2.6 to 3.5 m thick (Figs. 3.2a and 3.2b). Underlying the peat is an unoxidized medium plastic silt containing traces of sand and gravel. The silt layer is extended below the depth of investigation (11.0 m from the top of the embankment). The alignment of this track section was shifted westward in 2008 due to the construction of a new bridge. Additional granular fill (0.5 m thick) was added to the west side of the embankment in November 2010 (Fig. 3.2a).

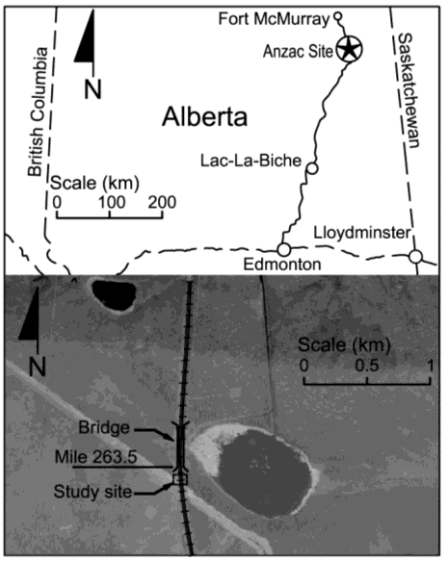

Figure 3.1. Locations of the Lac la Biche subdivision and the field site at Anzac near MP 263.5

The peat samples retrieved from the site investigations were tested to quantify the water content and the fibre content as per the American Society for Testing Materials (ASTM) standards D2974 (ASTM 2007) and D1997 (ASTM 2008). The water content and fibre content within the peat were found to decrease with depth, with mean values of 580% and 67%, respectively. The peat was found to have a coarse fibrous texture and a yellow-brown colour. The degree of humification was determined to be insignificant, with the plant structures within the peat appearing to be intact. The peat was observed to have finer fibres and a more homogeneous consistency with increasing depth.

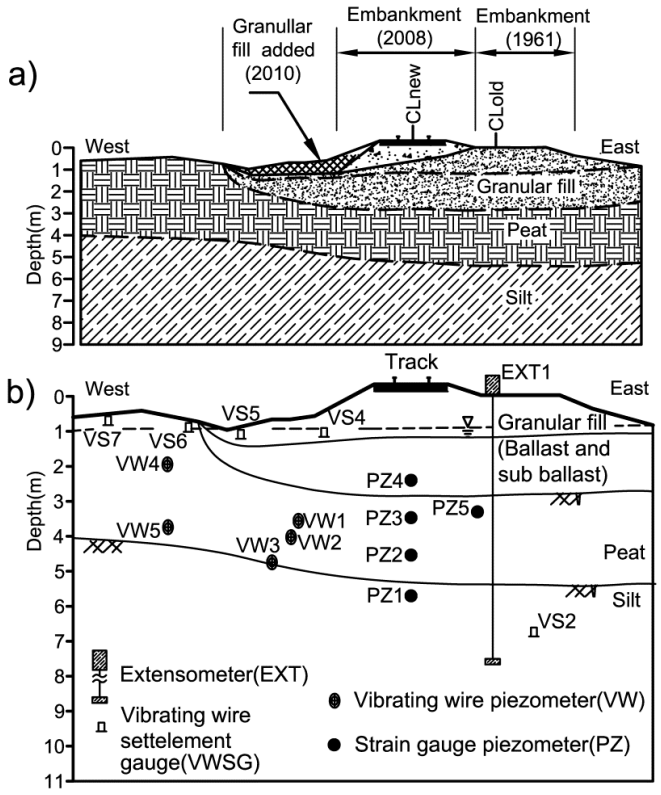

Figure 3.2. Summary of a) the stratigraphy, embankment geometry and history of construction at the field site, and b) the instrumentation installed at the field site.

3.5 Instrumentation

The instrumentation installed at MP 263.5 consisted of five strain-gauge piezometers (SGP), five vibrating wire piezometers (VWP), five vibrating wire settlement gauges (VWSG), and one extensometer (Fig. 3.2b). Measurements were logged every two hours for three years. The SGPs (RST model SGP-730-PI) and VWPs (RST model VW2100-0.35-DPC) were installed to measure pore pressure. The VWSGs (RST model SSVW105) and extensometer were installed to measure vertical settlement. The temperatures were recorded by both the VWPs and VWSGs, which require temperature to adjust their calibration. The temperature measurements have an accuracy of ±0.1°C. The thermistor attached to the data logger measured the near-surface temperature.

Four of the SGPs (PZ4, PZ3, PZ2 and PZ5) were installed under the centreline of the track at depths of 2.70, 3.80, 4.80 and 5.80 m, and one additional SGP (PZ5) was installed on the east side of the track at a depth of 3.40 m below the ground surface (Fig. 3.2b). Three of the VWPs (VW1, VW2 and VW3) were installed respectively at depths of 2.9, 3.5 and 4.4 m below the granular fill, and the two remaining VWPs (VW4 and VW5) were installed below the unloaded peat at depths of 1.50 and 3.20 m on the west side of the granular fill.

Two of the VWSGs (VS4 and VS5) were installed at 0.5 m below the top of the granular fill. Two more VWSGs (VS6 and VS7) were installed at 0.3 m below the unloaded peat to the west of the granular fill. The fifth, and final, VWSG (VS2) was installed in the deep silt layer at a depth of 7.0 m on the east side of track. One extensometer (EXT1) was also installed on the east side of the track to supplement settlement measurement.

All piezometers were push-in piezometers, and during installation these were pushed approximately 0.5 m beyond the base of the borehole. Before the installation of the piezometers and the VWSGs, the wires were marked at 0.1 m intervals to read the depths of the instruments after installation. The accuracy of the piezometer depths is estimated to be ± 5 cm. A Total Station was used to measure the elevations of the top of all of the boreholes to a common datum on a bridge just north of the site.

3.5.1 Measured pore pressures within the peat subgrade

Fig. 3.3 presents the pore pressures measured over the course of this study by the SGPs and VWPs beneath the embankment and granular fills. The piezometers installed in the silt (PZ1) and at the bottom of the peat (VW3) measured a relatively constant pore pressure with small seasonal variations. The pore pressure measured by PZ1 is consistent with the groundwater table observed in the boreholes when the instruments were being installed and in the constant water pool beside the embankment during the spring and summer (Figs. 3.3a). Thus, the pressure measured by PZ1 is solely due to hydrostatic pressure, and the near

constant pressure is an indication that the ground water table does not vary significantly.

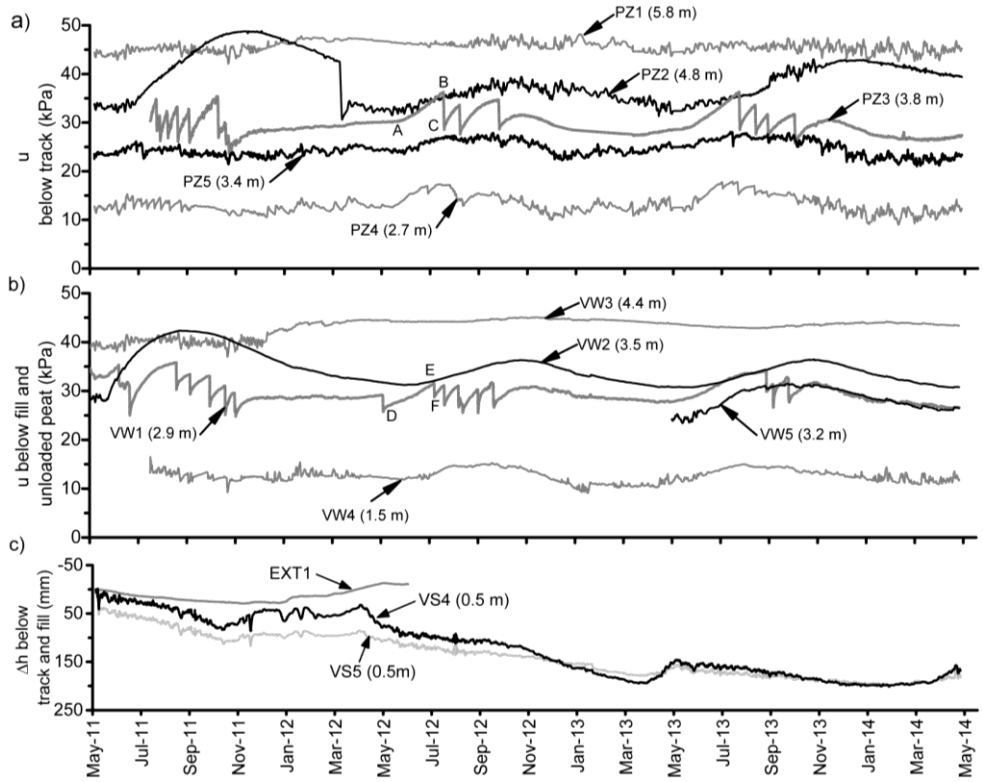

Figure 3.3. The measured a) pore pressures (u) beneath the centre of the track, b) pore pressure (u) beneath the granular fill, and c) vertical settlement (Δh) beneath the track and fill. Depths mentioned are relative to the respective ground surfaces.

The piezometers installed at the mid peat level (PZ2 and VW2) measured an increase in pore pressure that corresponded to increased temperatures. The maximum measured rises in pore pressure (above hydrostatic) during the late summer/autumn of 2011 were 12 and 15 kPa for VW2 and PZ2, respectively. Lesser seasonal increases in pore pressure occurred during the warmer months of 2012 and 2013; 5.8 and 6 kPa for VW2 and 4 and 8.2 kPa for PZ2. As the increased pore pressure response during summer has now been measured with both SGPs and VWPs, the authors have a high degree of confidence that this is a real phenomenon.

The piezometers installed in the top peat layer (PZ3 and VW1) measured significant increases in pore pressure during the summer and autumn months, accompanied by sharp drops in pore pressure (Figs. 3.3a and 3.3b). Beneath the embankment, the rise in pore pressure prior to the drop was similar in magnitude (>11 kPa) for the three successive summers of 2011, 2012 and 2013. Beneath the granular fill, the rise in pore pressure prior to the drop was 11, 8 and 9 kPa for the three successive summers of 2011, 2012 and 2013, respectively. The SGPs, installed at the bottom of the subballast beneath the track (PZ4) and at the top of the peat layer below the old alignment (PZ5), recorded relatively modest increases in pore pressure during the summers (Figs. 3.3a and 3.3b).

VW4 and VW5, which were installed below the unloaded peat surface, showed a significant increase in pore pressure (4 and 5 kPa) during the summer and autumn of 2012 and 2013 (Fig. 3.3b). The pore pressure recorded by VW5 during the summer was less than the pore pressure measured by the piezometer installed at the same elevation below the granular fill (VW1). Both piezometers (VW1 and VW5) recorded the same pore pressure during the winter.

Fig. 3.4 presents the measured pore pressure variation and calculated hydrostatic pore pressure plotted with depths. The plotted lines shown in Fig. 3.4 are for different times. Those times are denoted by the letters A through F and shown in Fig. 3.3. At the top peat layer (PZ3) the rise in pore pressure reached 12.5 kPa before dropping down to 3.2 kPa (Fig. 3.4a). At the top peat layer beneath the fill (VW1), the pore pressure increased to 9.0 kPa before dropping down to 4 kPa (Fig. 3.4b). The increases in pore pressure at the middle of the peat layer (VW2, PZ2) lagged behind the increases in pore pressure at the top peat layer (VW1, PZ3) and are not reflected in Fig. 3.4.

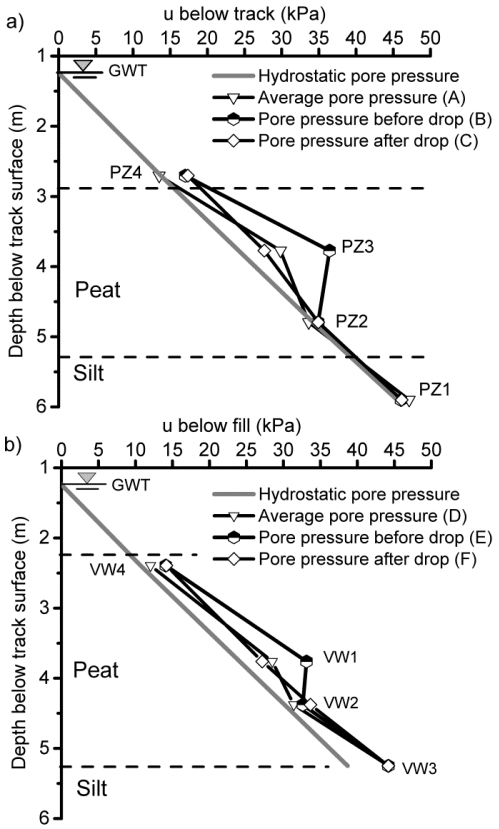

Figure 3.4. The measured pore pressures (u) in 2012 plotted with depth at times corresponding to the letters A to F shown in Fig. 3.3 a) beneath the centre of the track, and b) beneath the granular fill. The depths plotted are relative to the track surface (top of the sleeper).

3.5.2 Measured vertical settlement of the peat and embankment

Two VWSGs, VS4 and VS5, and one extensometer, EXT1, recorded the gradual settlement and seasonal upward movement of embankment, fill and peat subgrade throughout the monitoring period (Fig 3.3c). In general, the settlement gradually accelerated in the early spring and achieved a constant rate in the summer before the upward movement started in the fall. Because the VWSGs are near to the ground surface, they are affected by weather changes and snowfall. The extensometer, EXT1, did not function after the first winter. The total settlement recorded by EXT1 between May and October 2011 was 28 mm. The average annual settlement recorded by the two VWSGs, VS4 and VS5, was 92

mm, 64 mm and 25 mm in 2011, 2012 and 2013 respectively. This shows that the maximum settlement occurred in the first summer (2011) after the granular fill was placed in November 2010.

3.5.3 Temperature measurements

Fig. 3.5 presents the corresponding temperatures and pore pressure from below the embankment and fill at different depths. Fig. 3.6 presents the temperatures and pore pressures measured by two VWPs, and one VWSG, beneath the surface of the unloaded peat (Fig. 3.2). Fig. 3.7 shows the variation of temperatures at different depths below the track surface between July 2011 and January 2012. As expected, the response to the changes in the surface temperature decreases with increasing depth.

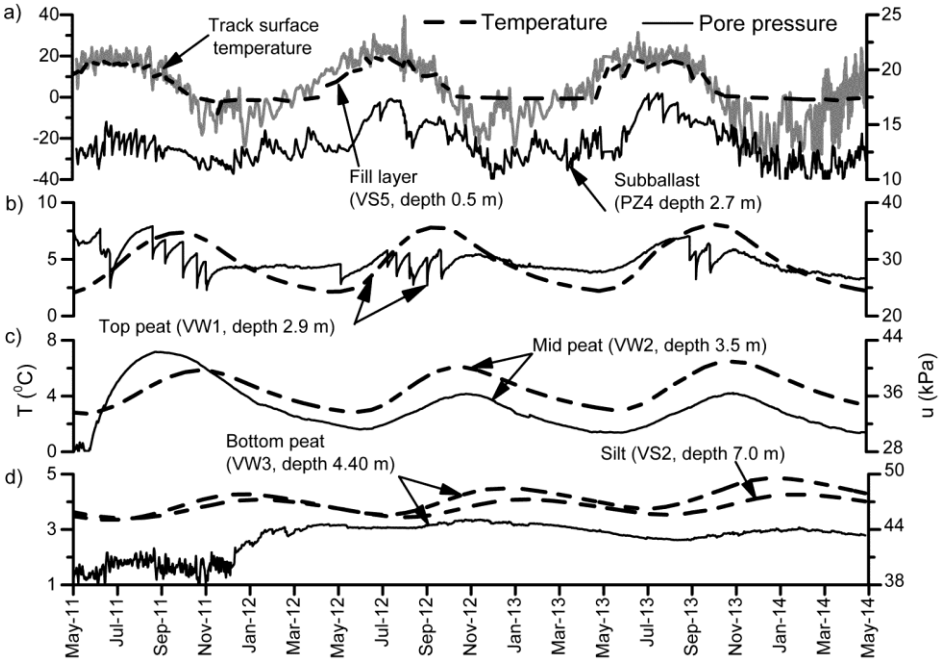

Figure 3.5. The measured temperature (T) and pore pressure (u) below the embankment at a) the ground and subballast layer, b) top peat, c) mid peat, and d) bottom peat and silt layers. Depths mentioned are relative to the respective ground surfaces.

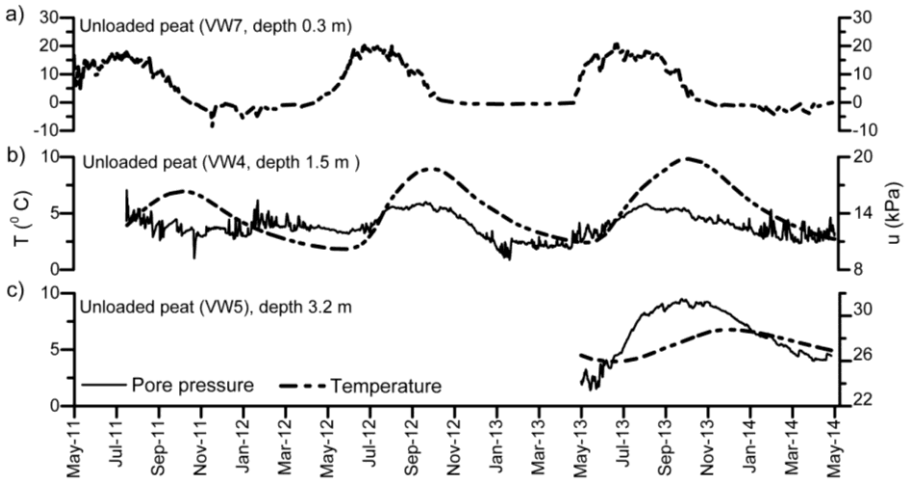

Figure 3.6. The measured temperature (T) and pore pressure (u) beneath the unloaded peat surface at a) 0.3 m; b) 1.5 m; and c) 3.2 m. Depths mentioned are below the surface of unloaded peat.

The temperature near the surface of the embankment (Fig. 3.5a) ranged from 30°C, during the summer to -20°C during the winter (October to May). At 0.5 m beneath the fill surface, the temperature ranged from a high of 20°C in mid-July to a low of -3°C in mid-February. The temperature was below 0°C between the end of October and the end of April. The temperatures ranged from 2 to 8°C near the top peat layer, from 2.7 to 6.5°C at the middle of the peat layer (3.5 m depth) and from 3.4 to 4.8°C at the base of the peat (4.4 m depth) (Figs. 3.5b, 3.5c and 3.5d). Deeper within the silt layer, at a depth of 7.0 m, the temperature variation was 0.7°C, ranging between 3.5 and 4.2°C (Fig. 3.5d).

In the unloaded peat, the variation of temperature ranged from 1.8 to 9.8 °C at a depth of 1.5 m (VW4) and between 3.5 and 6.8°C at a depth of 3.2 m (VW5) respectively. These values recorded by VW5 are less than the temperature range measured by VW1 at the same elevation below the embankment (Figs. 3.5b and 3.6b).

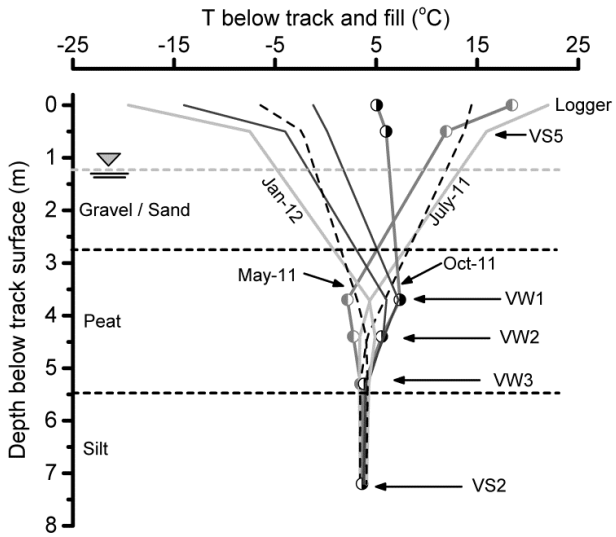

Figure 3.7. Cyclic variation of temperature (T) at different depths below the track surface between July 2011 and January 2012. Depths plotted except for VS5 are relative to the track surface (top of the sleeper).

There is a temporal delay in the temperature change with depth and a variation between temperatures beneath the embankment, fill and in unloaded peat (Figs. 3.5, 3.6 and 3.7). As the track surface starts to freeze, the middle of the peat layer is still warming. The upper portion of the peat reaches its peak temperature in October, while the base of the peat is at its minimum temperature. The time lag between the peak of track surface temperature and peak middle peat layer temperature is more than four months. The peak temperature in the silt layer lagged two and half months behind the peak mid-peat level temperature. Below the unloaded peat, the peak temperature lagged well behind the peak temperature at the same elevation below the embankment. This is a result of the lower thermal conductivity and higher thermal capacity of peat compared to that for ballast and subballast.

3.5.4 Discussion of field measurements

Both Figs. 3.5 and 3.6 present the pore pressure measured at the corresponding peat layers and the temperature measured at those depths. A correlation between the measured pore pressures and temperature is readily evident. The pore

pressures at the bottom of subballast, and at the top and in the middle of the peat layer, followed a cyclic rise and fall in temperature. The relationship between the temperature and pore pressure held true with the exception in in the summer of 2011, the first summer after the granular fill was placed. In the summer of 2011 the rate of increase in pore pressure at the top and middle peat layer was higher than the rate of increase in temperature, and the peak temperature lagged behind the peak pore pressure (Figs. 3.5b and 3.5c). The amount of increase in pore pressure was also higher compared to the increase in pore pressure in the following two summers.

The pore pressure within the unloaded peat also correlated to the rise in temperature, although the peak temperature lagged behind the pore pressure. The peak pore pressure occurred at almost the same time as the peak pore pressure at the same depth below the embankment (Figs. 3.5b and 3.6c). The top and middle of the peat layer below the fill had higher temperatures and corresponding rises in pore pressure than that at the same elevation below the unloaded peat.

Fig. 3.8 presents the plot between the rise in pore pressure above hydrostatic (Δu) and the observed increase from minimum to maximum temperature (T) during the summer of 2012. The Δu - T plots for the top and middle of the peat layer are linear and parallel to each other, indicating a constant rise in pore pressure for the same increase in temperature at different time periods. Beneath the unloaded peat there was a smaller increase in pore pressure corresponding to same temperature increase.

Unlike the temperature, the vertical settlement beneath the track and fill didn't correlate with the pore pressure (Fig. 3.3). On average, the settlement started in the early spring (April to May), while the pore pressure at the top and middle peat layer was still decreasing. The pore pressure at the top and mid-peat layer started to increase in early summer (June to July) and reached its maximum in the fall (October to November), while the track surface was freezing. In the summer of 2013, the pore pressure in the peat layer beneath the fill and track increased

until it was almost equal to that in the summer of 2012, whereas the vertical settlement measured beneath the fill was only one-third of that measured in 2012. Moreover, a significant increase in pore pressure occurred in the unloaded peat to the west of the fill material. This increase in pore pressure occurred in the absence of external stress.

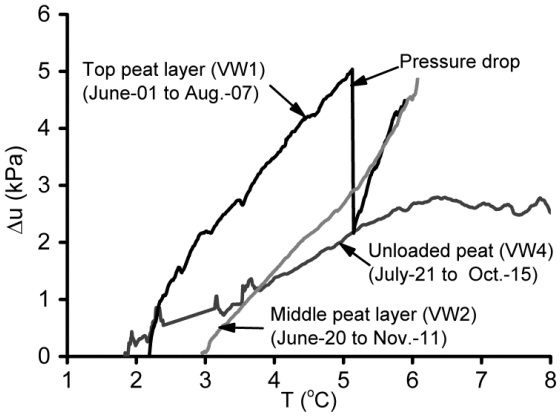

Figure 3.8. The increase in pore pressure above hydrostatic pore pressure (Δu) versus the temperature (T) measured at the same locations during the summer of 2012.

The correlation between pore pressure and temperature, and the lack of correlation between pore pressure and settlement, suggests that the gradual build-up of pore pressure is not associated with the additional stress applied and deformation (compression or shearing) of the peat subgrade. Thus the build-up of pore pressure must be the result of the gradual volume change in pore fluid within the peat matrix. This rise in pore pressure is hypothesized to be due to the expansion of gas bubbles in the peat matrix with increasing temperature. This hypothesis is further supported by two phenomena. One is that the maximum rise in pore pressure occurred at the top of the peat beneath the embankment where the largest increase in temperature was measured. The other is that the pore pressure in the top and middle layers increased at the same rate as the temperature (Fig. 3.8). The top peat layer, which is near to the ground water table, has been reported to have maximum organic decomposition and generation

of CO_2 and CH_4 (Beer et al., 2007). Further evidence of the generation of gas was observed by the flow of gas bubbles up to the water surface of the submerged section of the granular fill between June and September in 2012 and 2013.

There are logical explanations for why pore pressure rose more significantly in the summer of 2011 and why it rose almost constantly in the summers of 2012 and 2013 at the top and mid-peat levels. Both situations suggest that the pore pressure in the summer of 2011 was the combined response of additional stress due to the placement of fill and the pore pressure resulting from the thermal expansion of gas bubbles. The rise in pore pressure measured below the fill and embankment in the summers of 2012 and 2013 was due to the thermal expansion of gas bubbles.

3.6 Laboratory testing

The following laboratory testing was conducted on Shelby tube samples that were collected from beneath the centreline of the embankment at depths between 2.6 and 5.0 m. The tube samples were sealed and stored in a moisture-controlled room with a constant temperature of 1.5°C until they were tested.

3.6.1 The generation of gas due to the decomposition of peat

This testing of the Shelby tube samples, from the site, was conducted to confirm the decomposition and generation of gases within an anaerobic environment. Three peat specimens, each consisting of 100 g of peat mixed in 200 mL of water, were incubated in air-tight glass flasks for 100 days at 22 ±2°C, and the amount and type of gases generated were monitored. The generation of CO_2 and CH_4 was monitored by a portable gas detector equipped with an infrared sensor to measure CO_2 and CH_4. The measured concentration of the gasses was relative to the concentration of corresponding gases in the laboratory space. The increase in the concentration of CO_2 and CH_4 during the incubation is presented in Figs. 3.9a and 3.9b. The concentration of CO_2 gradually increased from the beginning, but the concentration of CH_4 remained low for four weeks before it began to increase exponentially. The results of these tests show the generation of gas from

peat specimens within an anaerobic environment. The degradation of peat in an anaerobic laboratory environment and at temperatures as low as 5°C has been reported (Hulzen et al., 1999; Van Winden et al., 2012). Studies have shown that temperatures above 5°C can accelerate the degradation of peat (Van Winden et al., 2012).

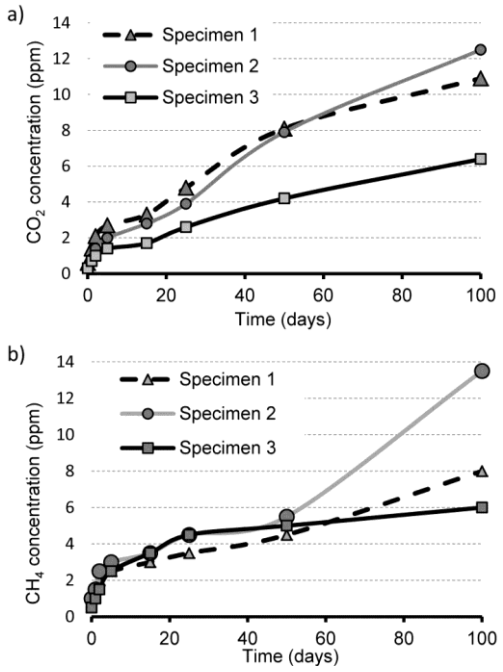

Figure 3.9. Measured generation of a) carbon dioxide, and b) methane, from field site peat samples incubated at room temperature.

3.6.2 The pore pressure generation with a change in temperature

The purpose of this laboratory testing was to determine if it was possible to reproduce the pore pressure generation in peat due to temperature variation. The four peat specimens used in this testing were cut from a Shelby tube. Shelby tube samples have been used to study the drained and undrained compression behaviour of peat (Hendry et al. 2012; Long and Boylan, 2013). These Shelby tube samples were extruded and trimmed into specimens with diameters of 72 ±2 mm and lengths 160 ±10 mm to allow for mounting into a triaxial testing apparatus. Specimens including large root or wood remnants were rejected. Table 3.1 presents the physical properties of specimens used for tests.

Table 3.1. Summary of physical properties of peat specimens including the initial water content (w_0), the initial density (ρ_0), initial void ratio (e_0), the preconsolidation pressure (p'_0), volumetric strain at the end of consolidation (ε_{vp}), and the water content at the end of test (w_f).

Specimen type	Specimen ID	Diameter (mm)	w_0 (%)	ρ_0 (g/cm^3)	e_0	p'_0 (kPa)	ε_{vp} (%)	w_f (%)
Intact	A	69.2	543	0.91	11.7			521
	B	72.1	509	1.002	9.9			479
	C	69.5	665	0.92	14	20	5.60	559
	D	71.11	583	0.98	11.5	20	4.89	543

All of the specimens were saturated with the application of backpressure. The Skempton B value was calculated and found to be greater than 0.97 for all tests. As the results of the testing show, these specimens do have a gas phase and were not entirely saturated. However, the purpose of this process was to remove most of the air that had entered the sample during sampling and preparation to be more representative of in situ conditions.

Two peat specimens (specimens A and B) were subjected to temperature change after the saturation. Two more specimens were consolidated with an isotropic effective stress (p') of 20 kPa, generated with total confining stresses (p) of 100 and 150 kPa (specimens C and D, respectively) before the temperature change was applied. Both of the consolidated specimens underwent a 6 to 7% volume change in a 24-hour period.

The temperature within the triaxial cell and specimens was controlled by a heating fluid which was circulated through a copper coil placed around the peat specimens (Fig. 3.10). The temperature within the cell and specimen was increased by increments of 1.5 to 2°C up to 20°C. Each temperature increase was held for 24 hours to allow enough time to attain uniform temperature inside the peat specimen.

The cell pressure was maintained at 100 kPa for two specimens (specimens A and C) and 150 kPa for the other two specimens (specimens B and D). The pore pressure inside each specimen was measured using a pressure transducer (accuracy of ±0.08% of the measured value). The outflow of water from each specimen during saturation and isotropic consolidation was measured using an ISCO pump (accuracy of ±0.5% of set point). This pump was also used to apply confining pressure and to measure the inflow of water into the cell, outside of the peat specimen, while the volume of the peat specimen decreased due to the compression of gas bubbles.

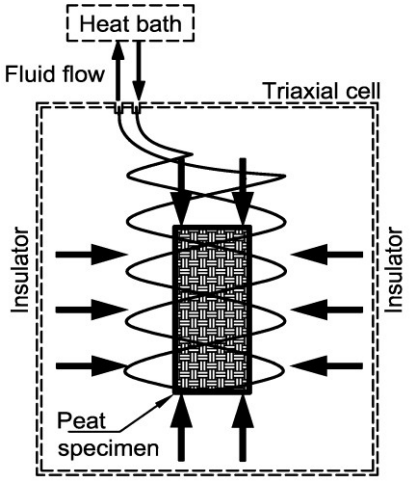

Figure 3.10. Schematic diagram of peat specimen heated inside triaxial cell under constant cell pressure.

Figs. 3.11 and 3.12 present the pore pressure change and volumetric strain measured within the peat specimens subjected to incremental increases in temperature. Figs. 3.11a and 3.11b present the change in pore pressure and volumetric strain in specimens A and B subjected to temperature variations. Figs. 3.12a and 3.12b present the pore pressure and volumetric strain corresponding to temperature increases on specimens C and D.

Increases in pore pressure were observed for several days within the two unconsolidated specimens (specimens A and B), with rapid decreases in pressure

as the temperature was increased above 12°C. The volume of both specimens decreased linearly from the beginning of the tests. In specimen A the volumetric strain exceeded 7.0% when the temperature reached 12°C. The pore pressure decreased slightly in the beginning and rapidly increased after the temperature reached 5°C. Between 5°C and 12°C the pore pressure increased linearly to more than 30 kPa above the initial pore pressure, while the volume of the specimen decreased by 5% (undrained). After the peak pore pressure, the peat specimens expanded by 2%, followed by a rapid decrease in pore pressure.

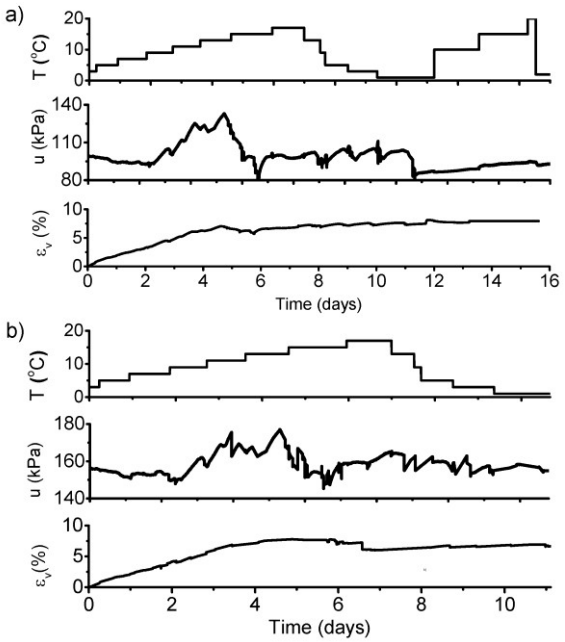

Figure 3.11. Plots of step increases in temperature (T), the generation of pore pressure (u), and volumetric strain (ε_v) on peat specimens in a) specimen A, and b) specimen B.

The two consolidated specimens (specimens C and D) showed slight increases in pore pressure with the increase in temperature. This includes a few transient rises and falls of pore pressure that occurred within an hour (Figs. 3.12a and 3.12b). This is due to the thermal expansion of the few isolated gas bubbles remaining within the peat specimen. The volume of both of these consolidated peat specimens decreased by less than 2.5%.

The testing showed that the pore pressures could be increased with increases in temperature while the specimens were undrained at constant confining pressures. The significant volume change and increase in pore pressure in the unconsolidated peat specimens, and the small volume change and transient pore pressure increase in the consolidated specimens while increasing the temperature by the same amount, showed that the increase in pore pressure is solely due to the thermal expansion of gas bubbles.

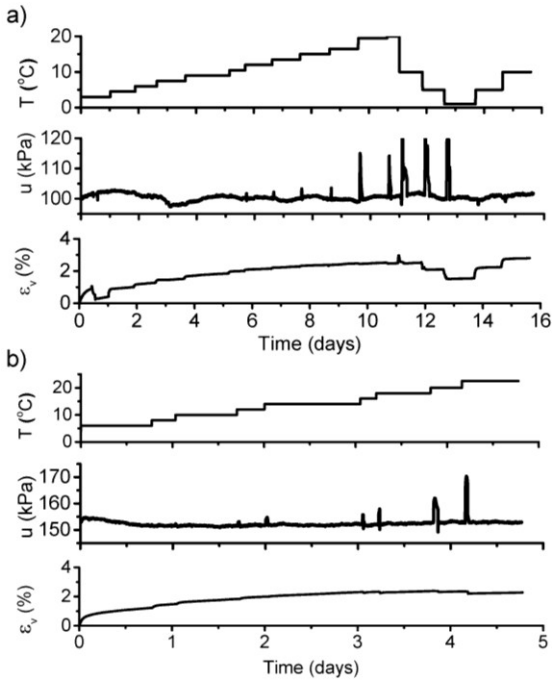

Figure 3.12. Plots of step increases in temperature (T), the generation of pore pressure (u), and volumetric strain (ε_v) in a) specimen C, and b) specimen D.

The correlation between the linear increase in pore pressure and decrease in the volume of specimen with increasing temperature (Fig. 3.11a) was used to estimate the gas volume in the peat specimen in the early testing stages. The decrease in the volume of the specimen was assumed to be solely due to gas compression. From the combined gas law, and using the pore pressure and the decrease in the specimen volume at 7, 9 and 11 °C, the gas volume in the peat specimen at a temperature of 7°C was calculated to be 9 ±2% of the total volume

of specimen tested. This is consistent with the range of 5 and 15% which has been found in other studies (Hanrahan, 1954; Lea and Brawner, 1963; Landva and La Rochelle, 1983; Hobbs, 1986; Fechner-Levy and Hemond, 1996; Den Haan and Kruse, 2006).

3.7 Discussion

The field measurement showed the rise in pore pressure at the peat subgrade, which doesnot correlate with the deformation. The laboratory tests showed i) the generation of gases due to the anaerobic decomposition of peat, and ii) the increase in pore pressure in peat specimens while increasing the temperature of specimens confined within a triaxial cell at constant isotropic pressure. Thus, the developed pore pressures are not due to the compression, distortion or change in volume of the peat matrix due to application of external pressure. This proved the hypothesis that increases in pore pressure in peat subgrade occur when gas bubbles in the peat pores expand due to increase in temperature while confined under the embankment loading. The decrease in pore pressure in the peat subgrade during the winter is related to the contraction of gas bubbles.

The increase in pore pressure in laboratory peat specimens (>30 kPa) is significantly larger than the maximum increases in pore pressure in the field (11 kPa). This is related to compression of gas (decrease in volume) under higher confining pressure (100 kPa) in laboratory tests. Even in the field, the increased pore pressures were higher beneath the embankment and the fill than beneath the unloaded peat corresponding to the same temperature increase (Fig. 3.8). The smaller increase in pore pressure measured beneath the unloaded peat accounts for the expansion of gas bubbles and the consequently the peat matrix at unconfined condition.

The existence of gas bubbles is the necessary requirement for the seasonal variation of pore pressure. Laboratory tests described above estimated the gas content equal to 9 ±2% of the volume of the peat samples collected from beneath the railway embankment. There is little literature on field measurements of the

decomposition of peat and the concentrations of gas underlying engineering structures (Landva et al., 1986). However, there have been studies about the decomposition of peat in the field, the effect of temperature on the decomposition, and the concentration of gas bubbles below the ground water table at different depths beneath the natural peat surface (Fechner-Levy and Hemond, 1996; Clymo and Bryant 2008). The rate of decomposition of peat decreases along with the decrease in oxygen and temperature at greater depths. Beneath an unloaded natural peat, the concentration of CO_2 and CH_4 has been reported to be linearly increased with depth near to the ground water table and it remains almost constant below this depth (Clymo and Bryant 2008). As the peat exists at a shallow depth, most of these gases are stored in gas bubbles (Hobbs 1986; Fechner-Levy and Hemond, 1996). The same amount of increase in pore pressure measured at different depths beneath the embankment corresponding to the same temperature increase also suggests an equal concentration of gas beneath the embankment.

This study showed the decomposition of peat and the existence of gas bubbles beneath the railway embankment under the ground water table. These gas bubbles exist within multiple layers of peat fibres or in the form of discrete bubbles due to the higher degree of saturation (Barden, 1974; Hobbs, 1986). These gas bubbles expand or contract depending on the variation of temperature or space and can significantly alter the compression mechanism of peat. The increase in pore pressure is capable of driving fluid flow out of the peat matrix, starting the consolidation of peat. During the fluid flow, gas bubbles should pass through the pores constriction that's why the fluid flow cannot be continuous. The sharp decreases in pore pressure recorded in the field site are hypothesized to be due to this intermittent flow of gas bubbles out of the peat boundary. However, this gaseous nature of peat is rarely considered within the geotechnical literature. During laboratory tests, peat is often considered as fully saturated or saturated with very high backpressure (Mesri and Ajlouni, 2007; Hendry et al., 2012; Long and Boylan, 2013).

3.8 Conclusion

The field measurement of temperature and pore pressure on a peat subgrade of a railway embankment and laboratory testing demonstrated the presence of gas within the peat subgrade and its effect on the pore pressure generation beneath the railway embankments.

The field measurement of pore pressure at the peat subgrade showed a seasonal increase in pore pressure in excess of hydrostatic well after the placement of additional weight or within unloaded peat away from the embankment. The pore pressures are not the result of a total stress change but strongly correlated to the temperature measured at the same location. Beneath the embankment, the maximum increase in pore pressure was more than 11 kPa at the top of the peat layer, corresponding to a temperature increase of 6°C. This increase in pore pressure is due to the thermal expansion of gas bubbles in the peat subgrade.

The results of the laboratory tests showed the decomposition of peat and generation of significant amounts of CO_2 and CH_4. Further, the placement of peat specimens at constant pressure while increasing the temperature showed that the thermal expansion of gases within peat specimens generates excess pore pressure. In unconsolidated peat specimens, the increase in pore pressure of 30 kPa resulted from a 10°C increase in temperature, and was accompanied by 7% decreases in the volume of the specimens. The gases in the tested peat specimens are estimated to account for 9 ±2% of the total volume of the specimen. This value lies within the range of gas volume reported for the peat around the globe. The implication of this study is that the in situ fibrous peat consists of a substantial amount of gas bubbles which can significantly alter the compression behaviour of peat from that of the saturated inorganic soil.

3.9 Acknowledgements

The authors would like to acknowledge the Canadian National Railway (CN), especially Tom Edwards, for providing both the project and funding. This research was made possible through the Railway Ground Hazard Research

Program, which is funded by the Natural Sciences and Engineering Research Council of Canada, Canadian Pacific Railway, and CN.

3.10 References

ASTM D1997-91 (2008), Standard Test Method for Laboratory Determination of the Fiber Content of Peat Samples by Dry Mass. ASTM International, West Conshohocken, PA, 2008, www.astm.org

ASTM D2974-07, Standard Test Methods for Moisture, Ash, and Organic Matter of Peat and Other Organic Soils. ASTM International, West Conshohocken, PA, 2007, www.astm.org

Barden, L. 1974. Consolidation of clays compacted dry and wet of optimum water content. *Géotechnique*, 24(4): 605-625.

Beer J. and Blodau C. 2007. Transport and thermodynamics constrain below ground carbon turnover in a northern peatland. *Geochimica et Cosmochimica Acta,* 71: 2989-3002.

Clymo R. S. and Bryant C. L. 2008. Diffusion and mass flow of dissolved carbon dioxide, methane, and dissolved organic carbon in a 7-m deep raised peat bog. *Geochimica et Cosmochimica Acta* 72: 2048-2066.

Den Haan, E. J. and Kruse, G. A. M. 2007. Characterisation and engineering properties of Dutch peats. Proceedings of the second international workshop on Characterisation and Engineering, Properties of Natural Soils, (eds. K . K . Phoon, D . W. Hight, S. Leroueil, and T. S. Tan), Singapore, Taylor & Francis: 2101-2133.

Forest, J. B. 1967. Field studies of the consolidation response of peat, in Report 344, Ottawa, National Research Council of Canada. Division of Building Research.

Fechner-Levy, E. J., Hemond, H. F. 1996. Trapped methane volume and potential effects on methane ebullition in a northern peatland. *Limnology and Oceanography*, 41(7): 1375-1383.

Hanrahan, E. T. 1954. An investigation of some physical properties of peat. *Géotechnique*, 4(3): 108-123.

Hendry M. T., Martin, C. D. and Barbour, S. L. 2013. The measurement and analysis of the cyclic response of railway embankments and underlying soft peat foundations to heavy axle loads. *Canadian Geotechnical Journal,* 50(5): 415-467.

Hendry, M. T., Sharma, J. S., Martin, C. D. and Barbour, S. L. 2012. Effect of fibre content and structure on anisotropic elastic stiffness and shear strength of peat. *Canadian Geotechnical Journal*, 49(4): 403-415.

Hobbs, N. B. 1986. Mire morphology and the properties and behaviour of some British and foreign peats. *Quarterly Journal of Engineering Geology and Hydrogeology*, 19(1): 7-80.

Hulzen, J. B. V., Segers, R., Bodegom, P. M. V. and Le, P. A. 1999. Temperature effects on soil methane production: an explanation for observed variability. *Soil Biology and Biochemistry*, 31: 1919–1929.

Konrad, J., Grenier, S. and Garnier, P. 2007. Influence of repeated heavy axle loading on peat bearing capacity. Proceedings of Ottawa Geo2007: 1551-1558.

Landva, A. O. 2007. Characterization of Escuminac peat and construction on peatland. Proceedings of the second international workshop on Characterisation and Engineering Properties of Natural Soils, (ed. K. K. Phoon, D. W. Hight, S. Leroueil, and T. S. Tan), Singapore, Taylor and Francis: 2135-2191.

Landva, A. O., Clark, J. I., Crooks, J. H. A. and Burwash, W. J. 1986. Degradation of peats and organic soils under engineered structures - A

preliminary study. Proceedings of Advances in Peatlands Engineering, Ottawa: 110 -115.

Lea, N. D. and Brawner, C. O. 1963. Highway design and construction over peat deposits in lower British Columbia. *Highway Research Board*, Rec. 7, Washington, DC.: 1-33.

Long, M. and Boylan, N. 2013. Predictions of settlement in peat soils. *Quarterly Journal of Engineering Geology and Hydrogeology*, 46(3): 303-322.

MacFarlane, I.C. 1965. The consolidation of peat: A literature review. National Research Council of Canada Division of Building Research Ottawa, NRC, 8: 393.

Mesri, G. and Ajlouni, M. A. 2007. Engineering properties of fibrous peat. *Canadian Geotechnical Journal*, 133(7).

Stanek, W. and Worley, I. A. 1983. A terminology of virgin peat and peatlands. Proceedings, international Symposium on Peat Utilization, Bemidji, USA: 75-104

Van Winden J. F., Reichart G. J., McNamara N. P., Benthien A. and Damste´ J. S. S. 2012. Temperature - induced increase in methane release from peat bogs: A mesocosm experiment. *PLoS ONE 7(6)*

4 Chapter 4: Effect of gas bubbles on pore pressure response in peat beneath an embankment

4.1 Contribution of the Ph.D. candidate

All work reported in this chapter, including field installation, design of the experimental program, implementation of the experiments, review of the literature, development of the theoretical framework, analysis and discussion of the results and writing of the text, has been carried out by the Ph.D. candidate. As supervisors, Dr. M. T. Hendry and Dr. C.D. Martin reviewed all parts of the work. This chapter will be published with the following citation:

Acharya M. P., Hendry, M. T. and Martin, C. D. 2015. Effect of gas bubbles on pore pressure response in peat beneath an embankment, Canadian geotechnical journal, in press.

4.2 Abstract

This paper presents the pore pressure behaviour observed within peat beneath a newly constructed embankment. Piezometers installed at different depths beneath the structure showed episodic increases in pore pressure, above hydrostatic pressure, followed by a rapid pore pressure decrease. It was postulated that this fluctuation in pore pressure was due to the movement and expulsion of gases within the peat. An investigation was conducted in the laboratory to replicate this pore pressure response. The results of this investigation indicate that the gas bubbles move through the channelled network of voids towards the drainage boundary, where they restrict the flow of water which results in the increase of pore pressure towards an upper limit or *escape pressure*, ultimately causing an expulsion of gas bubbles. This expulsion of bubbles results in a rapid drop in pore pressure and volume change within the specimen. Further isotropic consolidation tests were conducted on specimens of cellulose foam to show that this behaviour is due to the movement of gas bubbles through interconnected voids and channels. The implications of the volume change associated with this pore pressure behaviour are discussed.

4.3 Introduction

Peat consists of a fibrous material consisting fragments of long stem, leaves, and peat fibres, and a decomposed amorphous material (Landva, 2007). The amorphous peats result from a greater degree of biochemical decomposition and mechanical breakdown of the plant remains. The microscopic examination of sphagnum peat had shown that the fibrous peat consists of 85 to 90 % leaves and 10 to 15% of stem and fibres (Landva and Pheeney, 1980). These stem and leaves are made of layers of open jointed porous cells of size varying 10 to 30 μm. This cellular structure of peat is capable of holding water as much as 2000 % by its weight. This water is considered to be distributed in inter-particle and intra-particle voids (Adams, 1965; Hayward and Clymo, 1982). Due to this high water content and porous structure peat foundation are highly compressible. The amorphous peat is likely to have lower void ratios and lower compressibility, than the fibrous peat, but maintains a similar physical and mechanical behaviour (Edil and Wang, 2000). In addition, the vegetative structures of peat continuously decompose and produce gases including carbon dioxide and methane (MacFarlane, 1965; Hobbs, 1986; Acharya et al. 2014). Compared to the fibrous peat the finer peat, having lower organic content and acidic nature has low rate of decomposition (Hobbs, 1986).

While many previous studies have focused on the characterization and classification (Landva and Pheeney, 1980; Landva, 2007), the field and laboratory measurement of deformation (Weber, 1969; Lefebvre et al., 1984; Landva et al, 2007), and laboratory measurement of strength of peat (Edil and Wang, 2000; Hendry et al. 2012). Far fewer publications have attempted an analysis of the complexities of pore pressure generation within peat foundations (Weber, 1969; Lefebvre et al., 1984).

Ongoing investigations into the behaviour and performance of railway embankments on peat in Quebec and Alberta have been reported in Konrad et al. (2007), Hendry et al. (2013), and Acharya et al. (2014). Using the same type of instrumentation, these investigations have identified a pore pressure response that

appears to be unique to some peat formations investigated. Hendry et al. (2013) presented the measured pore pressure and deformation under the moving train load. Acharya et al. (2014) presented the pore pressure and temperature measured continuously for three years in peat subgrade beneath a railway embankment in Northern Alberta. The measured pore pressure response has shown an episodic increase followed by rapid decreases in pore pressure, while in Southern Quebec it has not. A similar behaviour of pore pressure has been discussed in an undrained test of sand mixed with gas (Sobkowicz & Morgenstern, 1984 & 1987) and in consolidation tests conducted on gassy seabed soil (Sills et al 1991). Research presented in Acharya et al. (2014) showed that these pore pressure increases are a result of the presence of gas, and that the rises are correlated to temperature. This paper is focused on the mechanism of the expulsion of gas bubbles out of the varying sizes of voids (inter-particle) through the smaller pore constrictions that results in the rapid drops in pressure, and the magnitude of pressures drops. Previous studies have differentiated between inter and intra-particle peat voids (Adams, 1965; Berry and Poskit, 1972). However, as the pore pressure measurements presented within this paper are from inter-particle voids, and recent studies suggest that the highly porous structure of both the inter and intra-particle voids drain simultaneously (Landva and Pheeney, 1980; Landva, 2007), this paper does not separate the intra-particle and intra to inter-particle processes.

Further analysis of the field data and additional laboratory testing examine how the mobility of the gas through the void network of the peat contributes to this behaviour, and the implication for the performance of structures.

4.4 Field investigations and monitoring

The study site from which the field measurements and samples were collected is located in Alberta, on the Canadian National Railway's (CN) Lac La Biche subdivision (between Fort McMurray and Edmonton). The embankment structure near mile post (MP) 263.5 is complex. The alignment of this section of the track was shifted in 2008 due to the construction of a new bridge and the granular fill

was added in late 2010 to the western side of the embankment (Fig. 4.1). The field investigation showed that the embankment consists of 2 m to 3 m of granular fill on top of a 2.6 m to 3.5 m thick layer of peat (Fig. 4.1). Underlying the peat is an unoxidized medium plastic silt containing traces of sand and gravel.

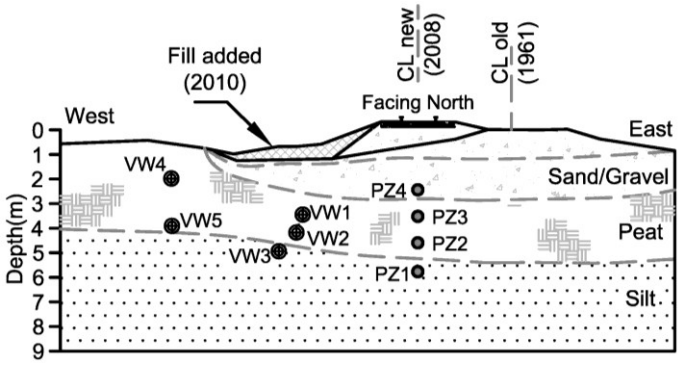

Figure 4.1. Summary of the instrumentation installed and the stratigraphy, embankment geometry and history of construction near MP 263.5 at Anzac, Alberta.

The water content and fibre content of intact peat were determined from samples retrieved during site investigations, and were determined using American Society for Testing Materials (ASTM) standards D2974 (ASTM, 2007) and D1997 (ASTM, 2008). The water content of the peat varies with depth, and ranges from 800 % near the top to 400 % at the base. The fibre content of the peat also varies with depth, ranging from 90 % at the top to 42 % at the base. The peat at this site has a course fibrous texture and is yellow-brown in colour. The degree of humification was insignificant, with the plant structures within the peat appearing to be intact.

4.4.1 Measured pore pressure response

The pore pressures at the site were measured with four strain gauge piezometers (SGPs) and five vibrating wire piezometers (VWPs) installed at the site (Fig. 4.1). The four SGPs were installed under the centreline of the track at depths of 2.7 m, 3.85 m, 4.80 m and 5.9 m. Three of the VWPs were installed at depths of 2.9 m, 3.5 m and 4.1 m below the fill, and the two remaining VWPs were

installed at depths of 1.45 m and 3.2 m below the unloaded peat on the west side of the granular fill. The SGPs (model SGP-730-PI) have a working range of up to 350 kPa and an accuracy of ± 0.1 % of the measured pressure. The VWPs (model VW2100-0.35-DPC) have a working range of up to 350 kPa and an accuracy of ± 0.1 % of the measured pressure and ± 0.1 ^{o}C of the measured temperature.

Fig. 4.2a presents the pore pressures measured by the SGPs, and Fig. 4.2b presents the pore pressure measured by the VWPs. The piezometers installed in the silt (PZ1 and VW3) both measured a nearly constant pore pressure, with some slight seasonal variations presumed to be a result of seasonal changes in hydrostatic pressure. Both the VWPs and SGPs installed within the peat layer show an increase in pore pressure during summer and autumn. The maximum rise in pore pressure of 14 kPa and 15 kPa above hydrostatic pressure was recorded in late summer and autumn of 2011 by VW2 and PZ2, respectively. Similar rises in pore pressure, to a lesser magnitude, occurred during 2012 and 2013.

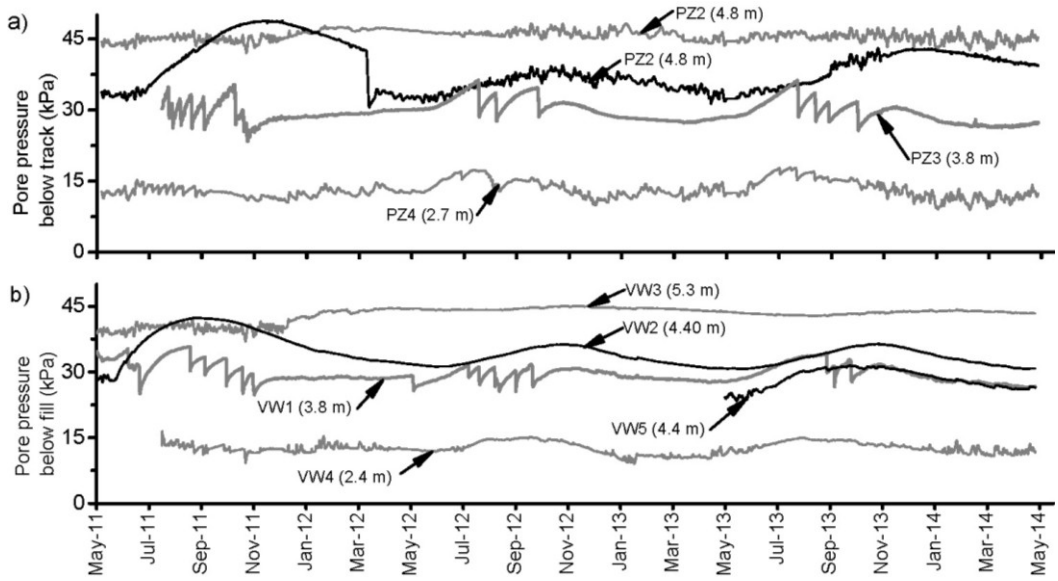

Figure 4.2. Plot showing the measured change in pore pressure within the peat measured (a) beneath the centre of the track, and (b) beneath the granular fill added in 2010.

Two of the piezometers installed near the top of the peat layer (PZ3 and VW1) recorded a series of gradual rises and rapid drops in pore pressure during the study period from 2011 to 2013. The pore pressure response was measured for all three years that this site has been monitored. The magnitude of increased pore pressure (peak value above the hydrostatic pressure, Δu) before the rapid drop ranges from 6 kPa to 12.1 kPa below the track and 5.5 kPa to 11.7 kPa below the fill, respectively. Below the track, Δu varied slightly during the study period. Δu was at its maximum at the beginning of the pore pressure rise-and-drop cycle during the summer and autumn of 2011, 2012 and 2013. The average values ranged between 8.0 kPa and 9.0 kPa. Below the fill, Δu was highest at the beginning of the summer of 2011 (11.7 kPa) and considerably decreased in the same year (5.5 kPa). During the following two summers, Δu remained relatively constant. The average values of Δu before the drop were between 6.5 kPa and 7.5 kPa. Figs. 4.3a and 4.3b respectively present the Δu recorded by PZ3 and VW1 before the rapid drop in pore pressure during the summer of 2011. Typically, successive peaks appear to decrease over the course of a season.

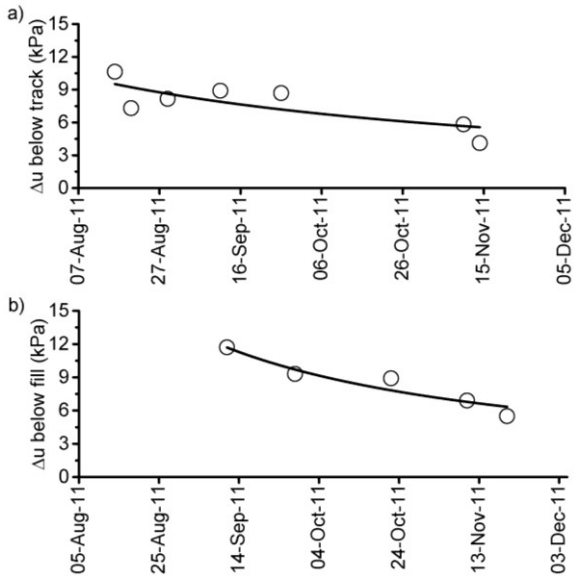

Figure 4.3. Plot showing the amount of pore pressure generated in excess of the hydrostatic pressure (Δu) measured before the sharp drop (a) below the centre of the track, and (b) below the granular fill.

The piezometer installed at 3.5 m below the unloaded peat surface (VW5), at a similar elevation as VW1, showed a significant increase in pore pressure during the summer and autumn of 2013 (Fig. 4.2b). However, no sharp drops in pore pressure are recorded. Both of these piezometers recorded the same magnitude of pore pressure during the winter months.

4.4.2 Discussion of pore pressure response

Both the VWPs and SGPs installed within peat have shown considerable increases in pore pressure during the summer and autumn months (Figs. 4.2a, 4.2b). This increase in pore pressure occurs because the gas bubbles present within peat undergo thermal expansion with the increase in temperature in corresponding peat layers (Acharya et al., 2014).

There is a spatial distribution of observed pore pressure variation. These seasonal pore pressure variations within the peat are highest directly under the embankment structure (VW1, VW2, PZ2 and PZ3), with the high pore pressure in the upper portion of the peat layer punctuated with three to five rapid drops (VW1 and PZ3). The increase in pore pressure (Δu) was highest beneath the fill in the summer of 2011, the first summer after the placement of the fill (Fig. 4.3b). During the same period, Δu below the embankment varied only slightly. It appears that Δu may decrease with the consolidation of peat strata below the fill.

This increase and the sharp drop in pore pressure response were observed in the field by both SGPs and VWPs for three consecutive years. Thus, the authors conducted laboratory tests to try to replicate this behaviour and understand the mechanism and implications.

4.5 Pore pressure response in laboratory tests

The purpose of this laboratory testing was: (1) to measure the pore water pressure and volume change behaviour of peat during isotropic consolidation tests and to determine the mechanism by which the pore pressures are generated; and (2) to determine if pore-pressure response in peat could be replicated using a simple

cellulose foam, to see if this behaviour is a result of the movement of gas through a network of voids.

4.5.1 Isotropic consolidation of peat specimens

Triaxial specimens were cut from Shelby tube samples collected during the site investigation at MP 263.5. The samples were collected from beneath the centre line of the embankment at depths between 2.60 m and 5.0 m. The samples were extruded to result in specimens with diameters of 72 ± 2 mm and were trimmed to a length of 160 ± 10 mm. The specimens were then subjected to isotropic consolidation pressure to observe their pore pressure and volume change behaviour under drained conditions.

The specimens were saturated through applying a backpressure of 75 kPa before each of the isotropic consolidation tests. The Skempton *B* value was checked and found to be greater than 0.97 for all of the tests conducted. The isotropic consolidation of the each of the specimens was conducted at constant cell pressure and backpressure. However, the effective confining pressure (*p'*) varied with the dissipation of pore pressure during the period of consolidation. For the six specimens tested, the *p'* values ranged between 10 kPa and 40 kPa and were generated with a total confining pressure (*p*) of 80 kPa to 230 kPa and the applied back pressure of 70 kPa to 190 kPa. The *p'* range was selected to represent the range of effective mean pressure found in the peat layer between 2.6 m to 5.0 m beneath the track level. The total pressure range was used to study the effect of the total pressure on the pore pressure behaviour of peat. The pore pressure inside the specimen was measured using a pressure transducer with an accuracy of 0.08 % of the measured pressure. During both the saturation and isotropic consolidation components of the testing, the flow of water was measured by a Teledyne ISCO 500D syringe pump with an accuracy of 0.5 % of the set point. All of the tests were conducted at a temperature of 22 ± 2 °C.

The measured behaviour of the peat during the isotropic consolidation tests is shown in Fig. 4.4. Fig. 4.4a presents the measured volumetric strain with time

and Fig. 4.4b presents the measured pore pressure with time. The pore pressure of the tested specimens gradually increased over several hours and then rapidly dropped within minutes. These drops in pore pressure were accompanied by rapid volume change (Figs. 4.4).

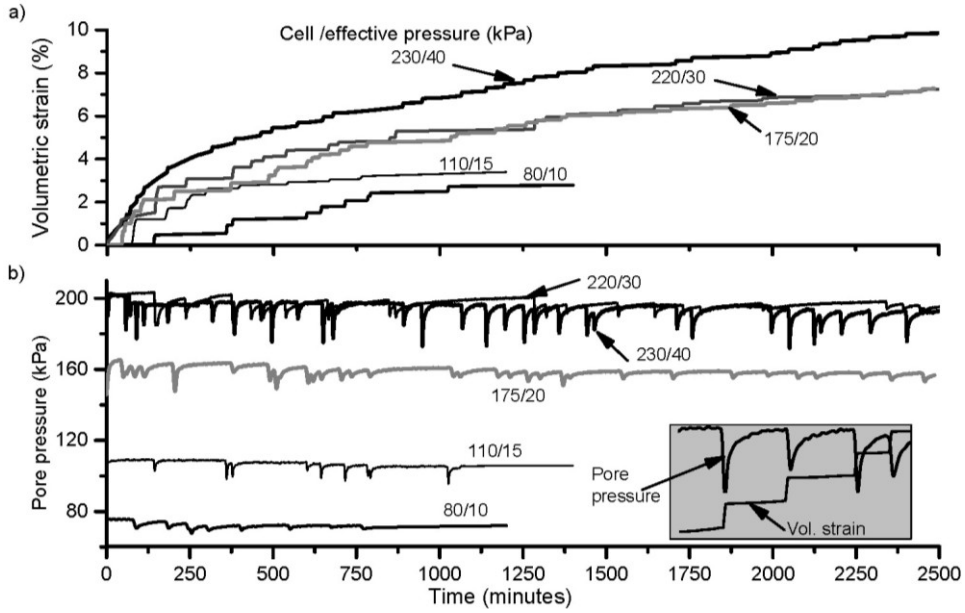

Figure 4.4. Presentation of the results from the isotropic consolidation tests on peat specimens showing (a) the volumetric strain versus time, and (b) the pore pressure versus time. The inset graph shows the pore pressure drops and instant volume changes plotted with time.

The magnitude, frequency and number of pressure drops varied with the applied confining pressure, with greater and more frequent drops at higher confining pressures (Fig. 4.4b). The average time interval between pore pressure drops ( ) for specimens tested at total confining pressures of 230 kPa (40 kPa effective) and 80 kPa (10 kPa effective) was 66 and 95 minutes, respectively (Fig. 4.5a). Similarly, the average magnitude of drop in pore pressure (was 7.9 kPa and 3.08 kPa, respectively (Fig. 4.5b). The time interval and magnitude of pressure drops were correlated to both the *p'* and *p,* though with a notably stronger correlation with *p* (Fig. 4.4b). This is consistent with the findings of Thomas

(1987), that the generation of pore pressure is correlated to total pressure applied for soil containing gas bubbles.

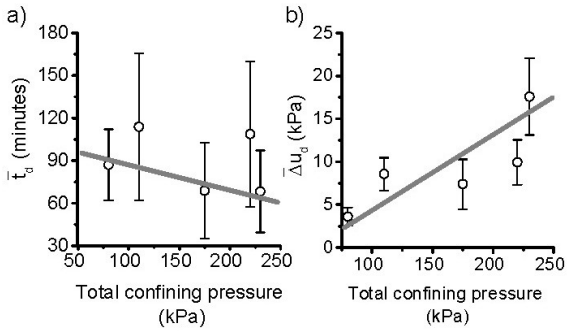

Figure 4.5. Plot of (a) the average time between drops ( ), and (b) the average magnitude of pore pressure drops ( ) with total confining pressure.

Fig. 4.6a presents the peak pore pressures (Δu_p) at which the rapid drops occurred and Fig. 4.6b plots the magnitude of drop in pore pressure (Δu_d) against consolidation time. The Δu_p varied with confining pressure and was highest for the specimen tested at 230 kPa total (40 kPa effective) confining pressure. The Δu_p ranged from 3 kPa to 16 kPa. Both Δu_p and Δu_d decreased with consolidation time (Figs. 4.6a, 4.6b). These plots show a high degree of variability, but appear to be best represented by logarithmic functions. Fig. 4.6c presents the time between two subsequent pore pressure drops (t_d) for all of the tests. There is a high degree of variability, and there appears to be a weak correlation between t_d and the amount of time that the specimens were allowed to consolidate. The correlation showed that t_d increases with consolidation time. In the later stage of the tests, the pore pressure attained a stable value and the rise and drop in pore pressure became negligible.

The initial volume change was correlated to the magnitude of Δu_d (Figs. 4.4a, 4.4b) with larger values of Δu_d resulting in higher volumetric strain. The volumetric strains better correlated with the effective confining pressure. With the exception of the specimen tested at an effective pressure of 10 kPa, the measured volumetric strain had shown that higher strain corresponded to higher

effective confining pressures (Fig. 4.4a). The cumulative volumetric strain that resulted from all of the drops in pore pressure ranged between 7 % and 10 % of the peat specimen volume. These values roughly represent the volumetric gas content inside the peat specimens and are in the range of the volumetric gas content of peat found in the literature (Hanrahan, 1954; Lea and Brawner, 1963; Hobbs, 1986; Den Haan and Kruse, 2007). Just after the drop in pore pressure, the specimen sustained a maximum *p'*. The *p'* decreased with the gradual build-up of pore pressure; when the pore pressure reached another peak value (Δu_p), the *p'* was at its smallest value. Consequently, the volume change between the pressure drops was negligible (Figs. 4.4a, 4.8a).

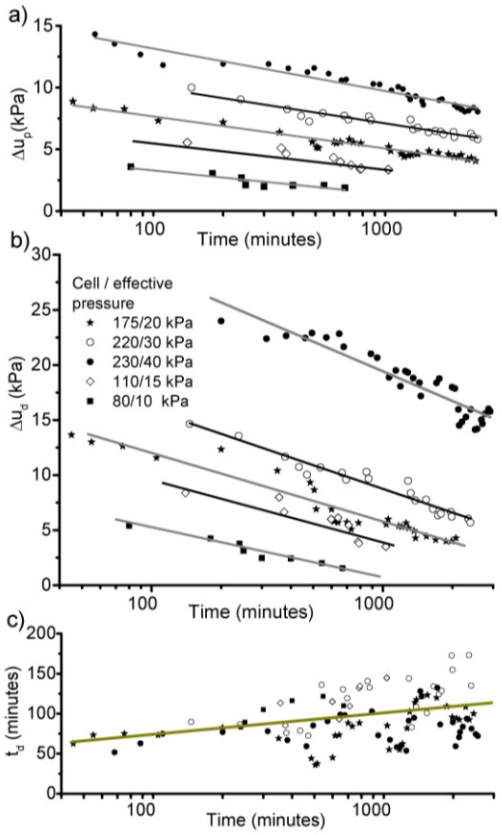

Figure 4.6. Results from the isotropic consolidation tests on peat specimens: (a) the magnitude of the peaks of pore pressure preceding the drops (Δ_{up}) versus time, (b) the magnitude of the pore pressure drop (Δ_{ud}) versus time, and (c) the time between the pore pressure drops (t_d) in all tests.

The isotropic consolidation tests were able to reproduce the gradual rise and sharp drops in pore pressure recorded by the field piezometers. The series of pore pressure build-up after each rapid drop is similar to the pore pressure build-up shown by Sobkowicz and Morgenstern (1987). The current experiment, however, significantly differs from Sobkowicz and Morgenstern's experiment in a number of ways: (1) the cell pressure used in this study (< 230 kPa) was far smaller than the gas saturation pressure; (2) the drops and built-up pore pressure occurred at constant cell pressure; and (3) the build-up of pore pressure occurred under drained conditions.

Both the field and laboratory data showed that the additional pore pressure (Δu and Δu_p) needed to result in the rapid pore pressure drop and that the magnitude of drop in pore pressure (Δu_d) decreased with consolidation time. Thus, it can be inferred that the variation in pore pressure is related to the variation in pore fluid volume in the pore spaces.

4.5.2 Laboratory testing of cellulose foam specimens

To confirm that the observed pore pressure behaviour in peat is due to the movement of gas and fluids through a channelled void network in peat structures, isotropic consolidation tests were replicated with specimens made of open cell cellulose foam. The interconnected open cell structure of the cellulose foam is such that when it is submerged in water it can hold a considerable amount of gas and develop a gravimetric water content of 1000 % to 2000 %. Because of these open cell networks, water can easily flow through the entire structure.

Six foam specimens, each with a length of 76 ± 2 mm and a diameter of 38 ± 2 mm, were trimmed from a single block of cellulose foam (Fig. 4.7). These specimens were immersed in water and allowed to saturate. Both the dry and wet masses of the specimens were recorded, and the resulting water contents ranged from 1390 % to 1520 %, which occupied 80 % of the total volume of the wet specimen. The volume of the dry foam material was measured by immersing the specimen in a graduated cylinder filled with water and was found to be 20 ± 2

cm^3, which corresponded to 15 % of the total volume of the soaked foam specimen. The remaining volume, 5 % of total volume of the wet foam specimens, consisted of air voids.

Figure 4.7. Photograph of the cellulose foam specimens used for the isotropic compression tests.

The wet foam specimens were subjected to the same isotropic consolidation testing as the peat specimens. These tests were conducted at *p'* values ranging from 20 kPa to 72 kPa. The *p'* values were generated with cell pressures (*p*) ranging from 195 kPa to 272 kPa, and the applied backpressures ranged from 175 kPa to 200 kPa. Several unsuccessful trials were attempted, as significant volumes of water and air tended to drain immediately after opening the drainage valve. The results of the successful tests are presented in Fig. 4.8. Fig. 4.8a presents the measured volume of water drained out of the specimen with time, and Fig. 4.8b presents the pore pressure with time. Two out of six specimens showed a gradual increase in pore pressure that occurred over hours. This increase in pore pressure was punctuated rapid drops in pore pressure and volume. The remaining four tests demonstrated large drops in pore pressure and volume change at the beginning of the consolidation tests, and both pore pressure and volume change remained constant after that. The peak pore pressure before the drops ranged from 2 kPa to 4 kPa.

The difficulty in maintaining the water content while mounting the specimens resulted in poor repeatability. It also limited the analysis of the results. However,

the pore pressure response of the peat was at least partially repeatable using this material. Thus, this behaviour is not unique to the compression of peat, but it is rather a transient behaviour due to the movement of gas bubbles through connected voids.

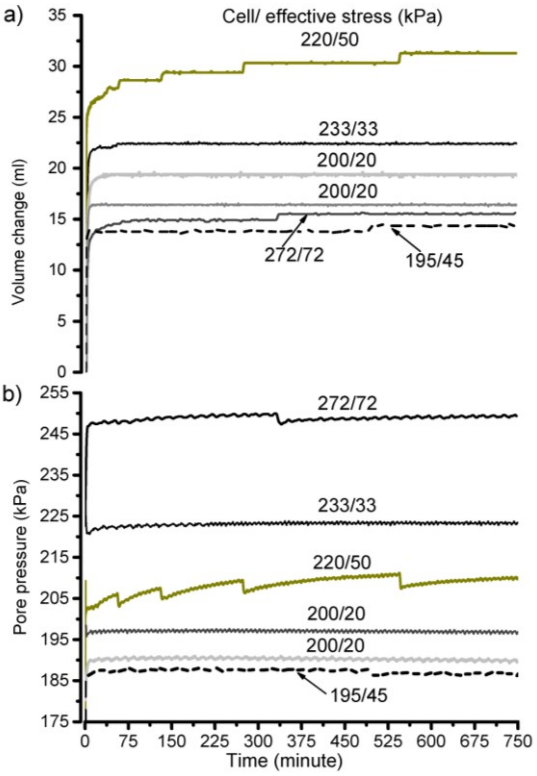

Figure 4.8. Results from isotropic consolidation tests of foam specimens show (a) the volume change versus time, and (b) the pore pressure versus time.

4.5.3 Discussion of laboratory results

The build-up and sharp drop in pore pressure is hypothesised as a three-step process including: (1) the exfiltration of gas bubbles out of the micro voids within the peat fibres to the pore space between the peat fibres and the accumulation of the gas near the drainage boundary of the peat specimen, (2) the build-up of pressure inside the peat specimen to a peak value (Δu and Δu_p), and (3) the rapid expulsion of a volume of gas. The amount of instant volume change includes both water and air released from the specimens.

The state of gas bubbles within the soil matrix is a function of the amount of the gas, the soil stiffness and the confining pressure (Sills et al., 1991). In soils having a higher degree of saturation, these gas bubbles exist as discrete bubbles (Barden 1974; Thomas 1987). The increase of pressure, as a result of an increase of total stress or temperature, causes the gas bubbles to move into larger voids and to merge to attain a more stable condition (Barden, 1974). Due to the flexible nature of peat structure, the gas bubbles are expected to distort the structure to accommodate an increase in volume. The idealised structure of peat with gas bubbles is shown in Fig.4.9a.

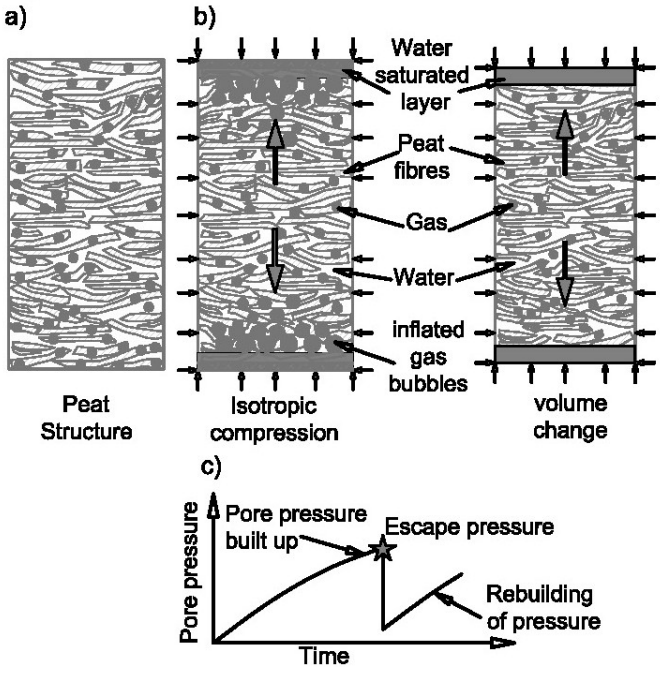

Figure 4.9. (a) Idealised structure of peat containing gas bubbles, (b) idealised mechanism during isotropic drained compression, and (c) rise and drop in pore pressure representing the mechanism shown in (b).

Within the peat specimen, the pressure of the water and the gas obtains equilibrium and governs the volume of the gas. The relationship between gas pressure (u_g), water pressure (u_w), surface tension (T) and the radius of the gas bubble (R) is expressed in Eq. 4.1, and illustrated in Fig. 4.10a (Wheeler, 1988).

— . ---------- [4.1]

During the isotropic consolidation the gas bubbles are pushed towards the drainage boundary. The gas was observed to accumulate at this boundary until the pressure within the specimen reached an *escape pressure* high enough to force it through the filter paper and porous stone (Fig. 4.9b). This escape of the gas from the specimens was accompanied by a sharp drop in volume and pore pressure (Figs. 4.4b, 4.9b, 4.9c). This reoccurred with cyclic pressure build-up and the expulsion of gas bubbles (Figs. 4.9c).

The basis for an *escape pressure* is that for a gas bubble to move through a constriction requires a pressure great enough to overcome the surface tension of the water (Gardescu, 1930). This process of the movement of gas bubbles from the peat is illustrated in Fig. 4.10b. Additional pore pressure is needed to push the gas bubbles from the voids in the peat through voids in the filter paper and porous stone. These voids range from between 5 μm to 10 μm (Fig. 4.10). Gardescu (1930) expressed the peak pore pressure needed to push a bubble through a small pore space as:

— —). ---------- [4.2]

where, u_w is the water pressure at the two ends of the escaping gas bubbles (Fig. 4.10b); u_{we} is the escape pressure; R_1 and R_2 are the radius of air bubbles in the peat specimens and at the pores within the porous stone, respectively; and, T is the surface tension. From Eq. 4.2, the range of 14 to 3 kPa *escape pressure* corresponds to a transition of gas bubbles, with diameters ranging from 200 to 6 μm, into the filter paper and porous stone (Fig. 4.11). For comparison, the diameter of a sphagnum cell varies between 15 μm and 30 μm, and the average size of a sphagnum stem can range from 20 μm to 500 μm (Landva and Pheeney, 1980).

This decrease of u_{we} with the decrease in bubble size is consistent with the test results presented in Fig. 4.6a, where the peaks of pore pressure preceding the drops (Δu_p) decreased with consolidation time. The magnitudes of u_{we} are similar to the increase in pore pressure recorded at the study site (Δu) and peaks measured in laboratory tests (Δu_p). The *escape pressure* gradually decreased with time, suggesting gradual dissipation of pore water pressure and, consequently, the gas pressure. The magnitude of the pore pressure drop (Δu_d), which indicates the size of the gas bubbles, also decreased with time. The observation of this pore pressure response at this site, and not other sites, may be in part due to the coarse nature of this peat.

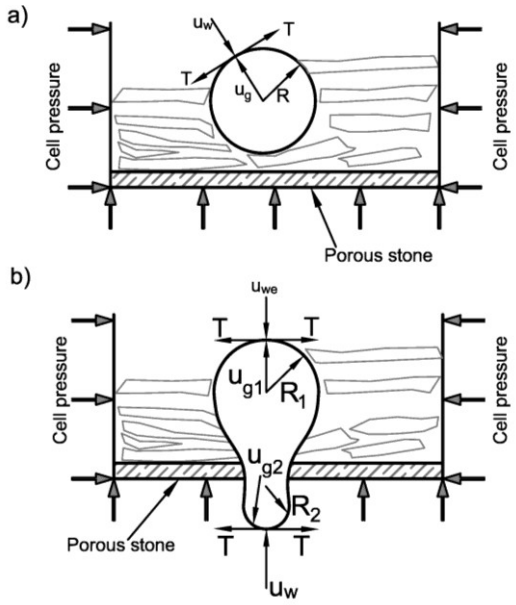

Figure 4.10. Schematic diagram showing conditions for (a) the equilibrium and dispersion of gas bubbles within the peat specimen, and (b) the escape of gas bubbles though the narrow pore at the drainage boundary during the isotropic consolidation of the peat specimens.

4.6 Conclusion

Extensive monitoring of pore pressures beneath a newly constructed railway embankment identified characteristic episodic increases and decreases in pore

pressures. Laboratory experiments on peat specimens subjected to isotropic consolidation were able to replicate this pore pressure response and show the mechanism associated with it. The accumulation of the pore pressure was shown to be a result of the build-up of gas within the peat structure. The rapid drops in pore pressure were shown to be the result of the expulsion of gas bubbles once pressures reached an *escape pressure* high enough to force the gas bubbles through the pore space towards the surface or drainage boundary.

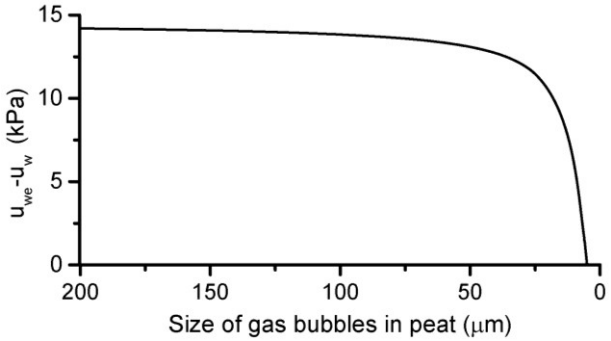

Figure 4.11. Plot of the theoretical increase in water pressure required to push the gas bubbles through narrow pores at the drainage boundary.

The field measurements showed that an increase in pore pressure occurred beneath the structures. In the upper portion of the peat layer, the increase in pore pressure was punctuated by rapid drops in pressure. These pressures peaked at magnitudes between 4 kPa and 15 kPa above the hydrostatic pressure. Similarly, the laboratory testing found the *escape pressure* to range from 3 kPa to 15 kPa and to be related to the applied confining stress.

This study has shown that changes in total stress or temperature result in these observed gas-related pore pressure behaviours. This has potential repercussions for the volumetric strain of peat and the settlement of structures constructed on top of peat. The volume reduction associated with primary consolidation and secondary compression under new construction can be accelerated due to the concurrent expulsion of gas within the soil. This was observed in the field measurements beneath the recently built railway embankment near Anzac in

northern Alberta after the addition of the fill, and in the laboratory during isotropic compression. The observed seasonal fluctuations in temperature result in pressures above the hydrostatic pressure in the peat subgrade that may drive a reoccurring consolidation process without the addition of externally applied loads. The cumulative volume change associated with these mechanisms may be significant enough to contribute to the long-term settlement of this railway embankment.

4.7 Acknowledgement

The authors would like to acknowledge Canadian National Railway (CN), and in particular, Tom Edwards, for providing both the project and funding. This research was made possible through the Railway Ground Hazard Research Program, which is funded by the Natural Sciences and Engineering Research Council of Canada, Canadian Pacific Railway, and CN.

4.8 References

Acharya, M.P., Hendry, M.T. and Martin, C.D. 2014. Thermal induced pore pressure in peat. *Proceedings, 67th Canadian Geotechnical Conference*, Regina, paper 106.

Adams, J.I. 1965. The engineering behaviour of Canadian muskeg. Proceedings, 6th International Conference on Soil Mechanics and Foundation Engineering, University of Toronto Press, I: 3-7.

ASTM D1997 Standard Test Method for Laboratory Determination of the Fiber Content of Peat Samples by Dry Mass.

ASTM D2974 Standard Test Methods for Moisture, Ash, and Organic Matter of Peat and Other Organic Soils.

Barden, L., 1974. Consolidation of clays compacted dry and wet of optimum water content. *Géotechnique*, 24(4): 605-625.

Berry, P.L., and Poskitt, T.J. 1972. The consolidation of peat. *Géotechnique*, 22(1): 27–52.

Den Haan, E. J. and Kruse, G. A. M. 2007. Characterisation and engineering properties of Dutch peats. In Proceedings of the 2nd international workshop on Characterisation and Engineering Properties of Natural Soils, Singapore: 2101-2133.

Edil, T.B., and Wang, X. 2000. Shear strength and K0 of peats and organic soils, Geotechnics of high water content materials. ASTM STP 1374, West Conshohocken, 209–225.

Gardescu, I. L., 1930, Behavior of gas bubbles in capillary spaces. Trans. AIME, 86: 351-370.

Hanrahan, E. T. 1954. An investigation of some physical properties of peat. *Géotechnique*, 4(3): 108-123.

Hayward, P. M. and Clymo, R. S. 1982. Profiles of water content and pore size in Sphagnum and peat, and their relation to peat bog ecology. Proceedings, The Royal society of London, B215, 299-325.

Hendry M. T., Martin C. D. and Barbour S.L. 2013. The measurement and analysis of the cyclic response of railway embankments and underlying soft peat foundations to heavy axle loads. *Canadian Geotechnical Journal*, 50(5): 467-415.

Hendry, M.T., Sharma, J.S., Martin, C.D., and Barbour, S.L. 2012. Effect of fibre content and structure on anisotropic elastic stiffness and shear strength of peat. *Canadian Geotechnical Journal*, 415: 403-415.

Hobbs, N. B. 1986. Mire morphology and the properties and behaviour of some British and foreign peats, Quarterly Journal of Engineering Geology and Hydrogeology, 19(1): 7-80.

Konrad, J. M., Grenier, S., and Garnier, P. 2007, Influence of Repeated Heavy Axle Loading on Peat Bearing Capacity. *In 60th Canadian Geotechnical Conference*, Ottawa: 1551-1558.

Landva, A.O. 2007. Characterization of Escuminac peat and construction on peatland. In Proceedings of the 2nd international workshop on Characterisation and Engineering Properties of Natural Soils, Singapore: 2135-2191.

Landva, A. O. and Pheeney, P.E. 1980. Peat fabric and structure. *Canadian Geotechnical Journal*, 17(3): 416-435.

Lea, N. D. and Brawner, C. O. 1963. Highway design and construction over peat deposits in lower British Columbia. *Highway Research Board*, Rec. 7, Washington, DC.: 1-33.

Lefebvre, G., Langlois, P., Lupien, C. and Lavallée, J.G. 1984. Laboratory testing and in situ behaviour of peat as embankment foundation. *Canadian Geotechnical Journal,* 21(2): 322-337.

MacFarlane, I.C. 1965. The consolidation of peat: A literature review. National Research Council of Canada Division of Building Research Ottawa, NRC, 8: 393.

Sills, G. C., Wheeler, S. J., Thomas, S. D. and Gardner T. N., 1991. Behaviour of offshore soils containing gas bubbles, *Géotechnique*, 41(2): 227-241.

Sobkowicz, J. C., and Morgenstern, N.R. 1984. The undrained equilibrium behavior of gassy sediments. *Canadian Geotechnical Journal*, 21: 439–448.

Sobkowicz, J. C., and Morgenstern, N.R. 1987. An experimental investigation of transient pore pressure behaviour in soils due to gas exsolution. Prediction and performance in geotechnical engineering, Calgary: 267-275

Thomas, S. D. 1987. The consolidation behaviour of gassy soil. D.Phill thesis, Oxford University.

Weber W.G. 1969. Performance of embankments constructed over peat. *Journal of the Soil mechanics and Foundations Division*, 95(1):53-76

Wheeler, S. J. (1988). A conceptual model for soils containing large gas bubbles. *Géotechnique*, 38(3): 389-397.

5 Chapter 5: Quantification of the settlement of an embankment constructed on peat due to expulsion of gases

5.1 Contribution of the Ph.D. candidate

All work reported in this chapter, including field installation, design of the experimental program, implementation of the experiments, review of the literature, analysis and discussion of the results, and writing of the text was carried out by the Ph.D. candidate. As supervisors, Dr. M. T. Hendry and Dr. C. D. Martin reviewed all parts of the work. This chapter will be submitted with the following citation:

Acharya M. P., Hendry, M. T. and Martin, C. D. 2015. Quantification of the settlement of an embankment constructed on peat due to expulsion of gases. *To be submitted to the International Journal of Geomechanics (ASCE).*

5.2 Abstract

The mechanisms that result in the settlement of structures constructed on peat foundations have been the subject of numerous investigations. A recent study of the behaviour of the peat subgrade below an embankment shows that gas bubbles within the peat strongly influence the pore pressure. The thermal expansion of these gas bubbles results in an increase in pore pressure during the warmer months and a displacement of water. The gas bubbles remain trapped until the pore pressure is sufficient enough to push them through the pore constrictions and towards the drainage boundary. The expulsion of the gas bubbles is followed by sharp drop in pore pressure and a rapid change in volume. This paper presents the analysis of field data conducted to quantify the impact of this mechanism on the settlement of an embankment constructed upon a peat subgrade. Measured pore pressures and deformations in the field are analysed to show the acceleration of vertical deformation during the pore pressure drops. An approach developed from laboratory isotropic consolidation testing results is presented to correlate the magnitude of the drop in pore pressure to the corresponding volumetric strain.

This correlation is then extrapolated to estimate the settlement of peat subgrade corresponding to the expulsion of gas. The results suggest that approximately 15% of the annual vertical settlement of the embankment occurs due to the cyclic dissipation of gas bubbles from the peat subgrade.

5.3 Introduction

Peat accumulates due to the addition of fragmented remains of dead vegetation in the presence of excessive moisture (MacFarlane, 1969; Hobbs, 1986). Due to the presence of excess moisture and the cellular structure of the fibres, peat is often characterized by high compressibility with a notably high rate of creep (Landva and La Rochelle, 1983). Embankments constructed on peat deposits are associated with instability and have been observed to continue to settle for decades after construction (Weber, 1969). Despite many years of effort to observe such settlement and pore pressure behaviour, difficulties remain with respect to the use of the measured properties of peat to predict its long-term deformation (Konrad et al., 2007; Long and Boylan, 2013).

Often ignored in the discussion of stress and strain response is the effect of the decomposition of peat and the generation and accumulation of gases, predominantly carbon dioxide (CO_2) and methane (CH_4), within the peat (MacFarlane, 1965; Hobbs, 1986). Recently, the instrumentation of a field site near Anzac, Alberta and a subsequent laboratory investigation of peat from this site have shown that the presence of the gas phase and the expansion of these gases during warmer seasons results in a significant (>10 kPa) increase in pore pressure (Acharya et al., 2015a). These pore pressures increase until the pressure is sufficiently great to push the bubbles through pore constrictions, after which the pore pressure rapidly declines; this is accompanied by a rapid change in volume (Acharya et al., 2015b). This led to the postulate that the seasonal, thermally driven pore pressures result in a recurring consolidation process, and that this mechanism may significantly contribute to the long-term settlement of embankments constructed on peat (Acharya et al., 2015b).

This paper completes the analysis of this thermally induced gas driven consolidation process to quantify the amount of settlement it has caused at the field site in Anzac, Alberta. This is accomplished by measurement of pore pressures as well as vertical and horizontal deformations in field, and the development of an empirical correlation between the magnitude of the pore pressure drops and the associated volume changes at differing confining pressures, based on isotropic consolidation testing of the peat and the application of this correlation. The measured vertical and horizontal displacements are presented and analyzed to quantify the deformation response to the pore pressure drops recorded by piezometers near the top of the peat and presented in Acharya et al. (2015b).

5.4 Description of field site

The site investigated for this study is located at MP 263.5 on Canadian National Railway's (CN) Lac-la-Biche subdivision (LLBS), just north of the town of Anzac, Alberta. At this site, the railway line crosses a large expanse of peat bog (Fig. 5.1). Fig. 5.2 features photographs of the instrumented site, showing the railway embankment and granular fill to the west side of the track. The alignment of this section of track was shifted westward in 2008 to accommodate a new bridge. The current embankment was constructed partly on peat that had never been loaded, and partly on the side slope of the pre-existing embankment. Additional fill was added to the west side of the embankment in October 2010 to serve as the base of a future stabilizing berm (Fig. 5.3).

A ground investigation conducted in May 2011 showed that the embankment consists of 2 to 3 m of granular fill at the surface overlying an undisturbed peat layer that is approximately 2.6 to 3.5 m thick (Fig. 5.3). Underlying the peat is an unoxidized medium plastic silt containing traces of sand and gravel. The silt layer extends more than 10 m below the track surface.

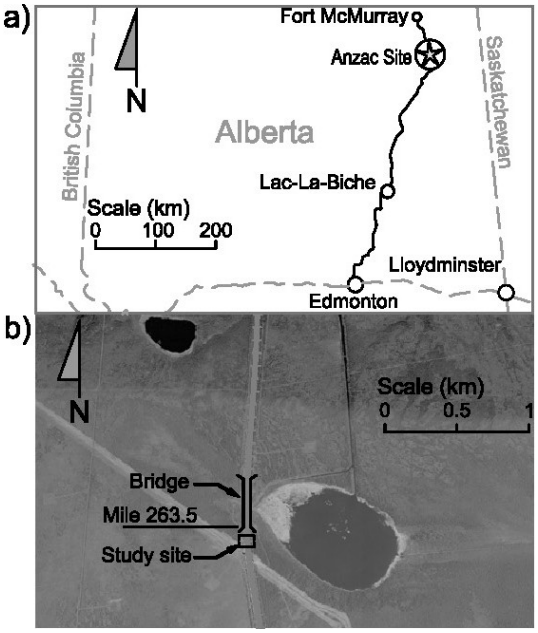

Figure 5.1. Location of (a) the Lac-la-Biche subdivision in northern Alberta and (b) the Anzac site near MP 236.5.

Figure 5.2. Photographs of (left) the instrumented site with the granular fill material to the west / left side of the track; and of (right) the old embankment and data logger to the east of track. Both photographs were taken facing northward near MP 263.5.

The samples retrieved from the field investigations were tested to quantify the water content and the fibre content as per the American Society for Testing Materials (ASTM) D2974 (ASTM, 2007) and D1997 (ASTM, 2008) standards. The water content was found to vary with depth, ranging from 800% at the top of

the peat layer to 400% at the bottom. The water content and fibre content within the peat were found to decrease with depth, with mean values of 580 and 67%, respectively. The peat was found to have a coarse fibrous texture and a yellow-brown colour. The degree of humification was determined to be insignificant, with the plant structures within the peat appearing to be intact. The peat was observed to have finer fibres and a more homogeneous consistency with increasing depth. The fibres at the silt-peat boundary had a more granular texture.

5.5 Site instrumentation

The instrumentation installed at the site consisted of five strain-gauge piezometers (SGP), four vibrating wire piezometers (VWP), five vibrating wire settlement gauges (VWSG), one extensometer, and three ShapeAccelArrays (SAA) (Figs. 5.3a, 5.3b). Two different types of piezometers were used because of their different capabilities and to provide additional assurance of the measured values. The SGPs are capable of recording high speed data. VWPs have a comparatively long life and are capable of recording temperature. The data logger recorded measurements from the instruments every two hours. The elevations for the top of all of the boreholes were measured relative to a common datum, on the bridge just north of the site, using a total station.

Four SGPs were installed under the centreline of the track at depths of 2.7, 3.80, 4.80, and 5.80 m. Three of the VWPs were installed at depths of 2.9, 3.5, and 4.4 m below the granular fill, respectively, and two VWPs were installed below the unloaded peat at depths of 1.50 and 3.2 m, respectively, on the west side of the granular fill. Both of the SGPs and the VWPs have a working range of up to 350 kPa and an accuracy of ±0.1% of the measured pressure.

Two of the VWSGs (VS4 and VS5) were installed 0.5 m below the top of fill. Two VWSGs (VS6 and VS7) were installed 0.3 m below the surface of the peat at 0.5 and 3.0 m, respectively, west of the western edge of the granular fill. The fifth VWSG (VS2) was installed at a depth of 7.0 m, within the silt layer, as a reference point to correct for settlement of the reservoir and changes in

barometric pressure. The VWSGs have a maximum depth of 7.0 m of hydrostatic head and an accuracy of ±0.1% of the measured depth below the reservoir.

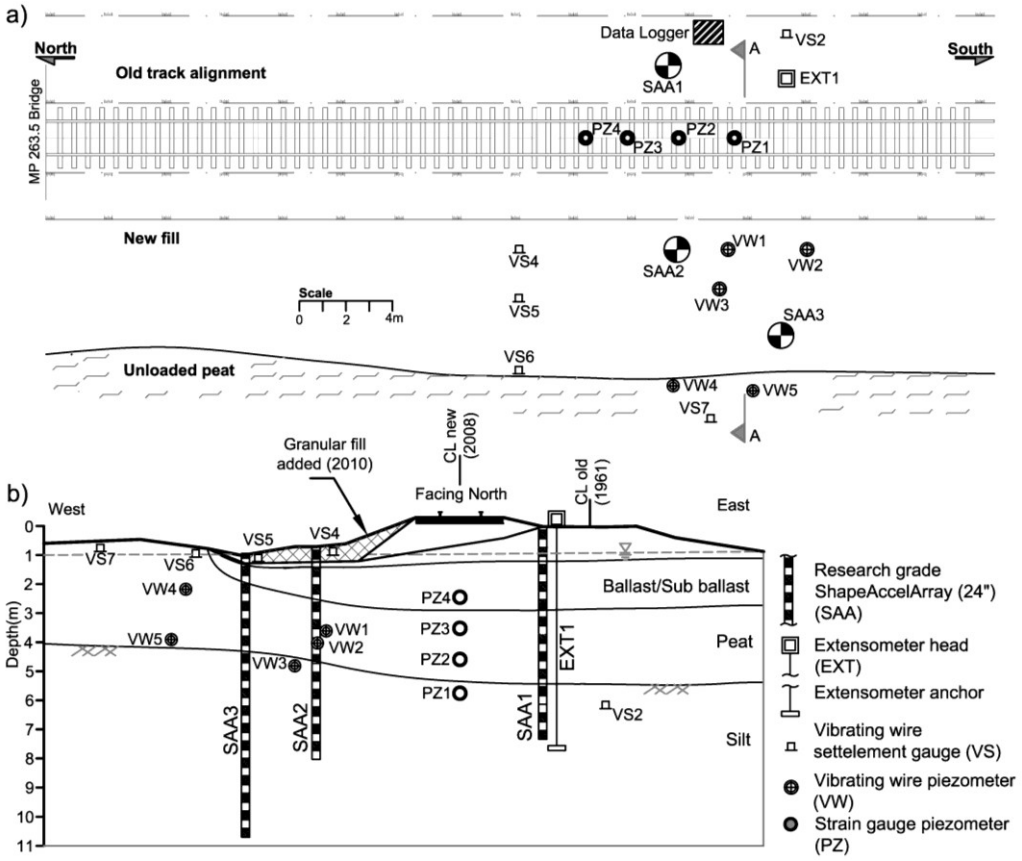

Figure 5.3. Summary of the instrumentation installed at the field site: (a) plan, and (b) cross-sectional elevation (section A-A) with summary of the stratigraphy, embankment geometry, and history of construction.

One extensometer was installed on the east side of the track and anchored at a depth of 8.5 m below the track in the underlying silt. The linear variable differential transducer (LVDT) used in the extensometer has an accuracy of ±0.1% of the measured displacement. Two SAAs (SAA1 and SAA2) each 7.3 m in length were installed vertically at 1.0 and 2.0 m, respectively, from the end of the ties (Fig. 5.3). SAA3 is a 9.8 m long array installed vertically at the toe of the recently added granular fill, 6.0 m west of the westernmost rail (Fig. 5.3). These SAAs consist of 305 mm long segments with sensors at two ends to record the

position, tilt, and angle of that segment relative to the base of the array. The short- and long-term accuracy of measurement relative to the starting shape are ±0.5 and ±1.5 mm, respectively.

5.6 Measured field data

5.6.1 Measured pore pressure response

Fig. 5.4 is reproduced from Acharya et al. (2015a) to present the pore pressures measured by the SGPs (Fig. 5.4a) and VWPs (Fig. 5.4b). The piezometers installed in the silt (PZ1 and VW3) recorded a relatively constant pore pressure whereas the piezometers installed within the peat beneath the track (PZ2), beneath the granular fill (VW2), and within the unloaded peat (VW4, VW5) showed an increase in pore pressure during summer and autumn for three consecutive years (2011, 2012, 2013). The piezometers near the top of the peat layer (PZ3 and VW1) recorded a series of gradual rises and sharp drops in pore pressure during the summer and autumn for all three years of monitoring. Beneath the fill, the peak pore pressure (Δu) and the magnitude of the pore pressure drops (Δu_d) reached a maximum in the summer of 2011 and were lower in the subsequent summers of 2012 and 2013 (Fig. 5.4b). Beneath the track, both Δu and Δu_d remained almost constant (Fig. 5.4a). The SGP installed at the peat-suballast boundary beneath the track (PZ4) recorded a relatively modest increase in pore pressure (3.5 kPa) during the summers (Fig. 5.4a), with series of increases and drops in pore pressures.

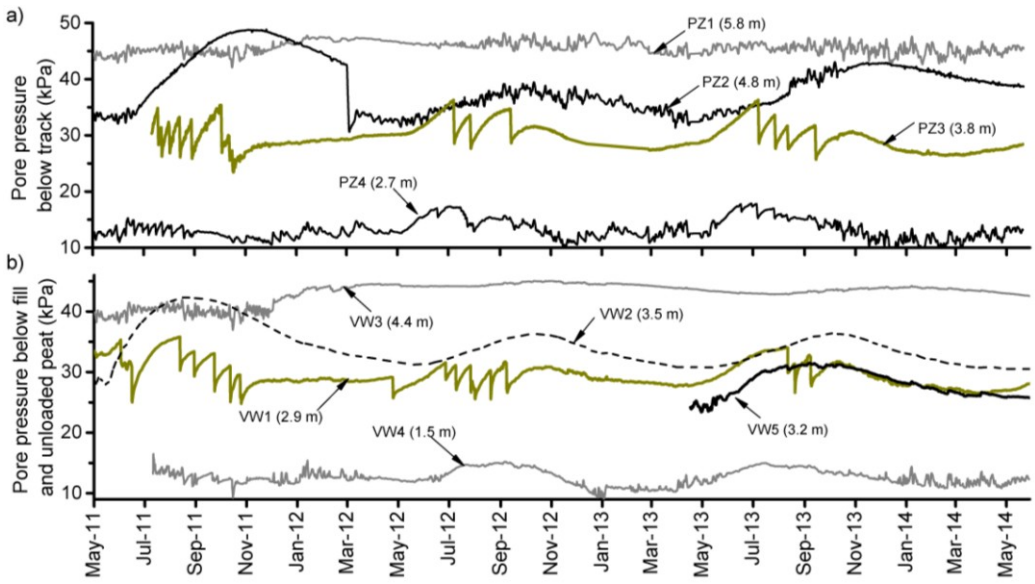

Figure 5.4. The pore pressure measured (a) below the centre of the track, and (b) below the fill and unloaded peat to the west of the track. (The noted depths are relative to ground surface at that location) (Acharya et al., 2015b).

5.6.2 Measured deformation of embankment and peat foundation

Fig. 5.5a presents the results of the vertical deformation recorded by the extensometer and the two VWSGs installed beneath the granular fill. The data from the extensometer are limited, as it did not function reliably after the first winter. The settlement recorded by the extensometer between May and September of 2011 was 28 mm. VWSGs (VS4 and VS5) recorded gradual downward and seasonal upward movement (when the ground surface was frozen or when the snow was melted). During the study period, the average cumulative settlement recorded by VS4 and VS5 was 173 and 189 mm, respectively. The average annual settlement recorded by these two VWSGs was 92, 64, and 25 mm, for the first, second and third years of the monitoring period, respectively (Fig. 5.5a). A 165 mm heave was measured at the western toe of the fill (VS6). Based on field inspection, this heave was determined to be local. The settlement recorded by the VWSG located 3 m west of the western edge of the granular fill (VS7) was 31 mm. The settlements recorded by VS6 and VS7 during winter months were correlated to the thickness of snow pile on top of the ground

surface. Field observation showed that thick snow piled up during the winters of 2012 and 2013. The deformation rebounded after snowmelt in the spring (May).

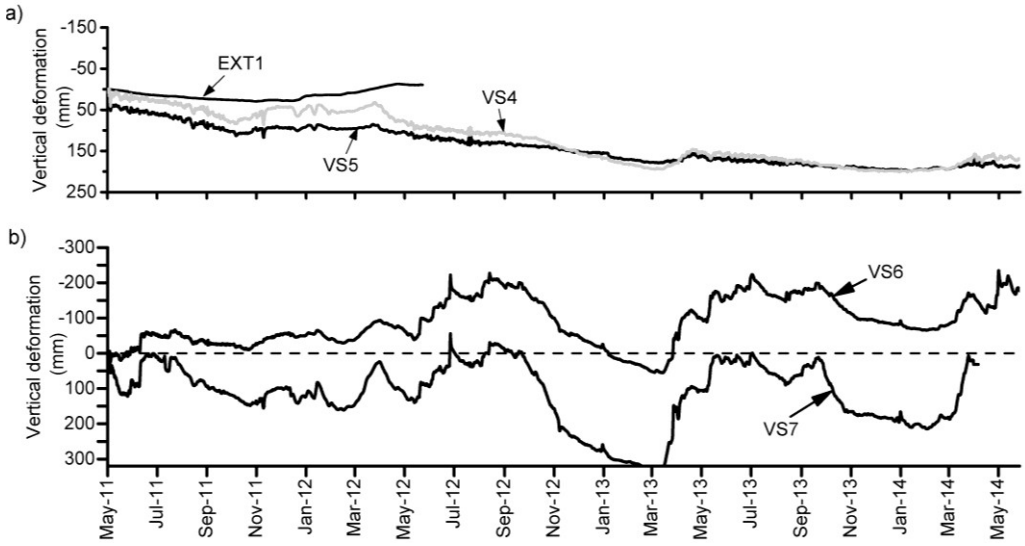

Figure 5.5. The vertical deformation measured (a) below the track and fill, and (b) at the surface of the unloaded peat.

Fig. 5.6 presents the horizontal deformation recorded by the vertically installed SAAs. The cumulative horizontal deformation recorded by the SAA at the boundary between the old and existing track (SAA1) was less than 6 and 8 mm towards the track at the mid-peat level and at the ground surface, respectively. The SAA between the fill and the existing track (SAA2) recorded a small deformation for the first and second years after the installation of instruments (Fig. 5.6). Similarly, the SAA at the western toe of the fill (SAA3) recorded seasonal deformation towards and away from the track during 2011 and 2012. Both SAA2 and SAA3 recorded significant horizontal deformation during the summer and autumn of 2013, the third year after installation (Fig. 5.6b). The cumulative horizontal deformation recorded by SAA2 was 48 and 33 mm towards the centre of the track at the ground surface and at the mid-peat level, respectively. The cumulative horizontal deformation recorded by SAA3 was 18 and 40 mm away from the centre of the track at the ground surface and at the mid-peat level, respectively (Fig. 5.6).

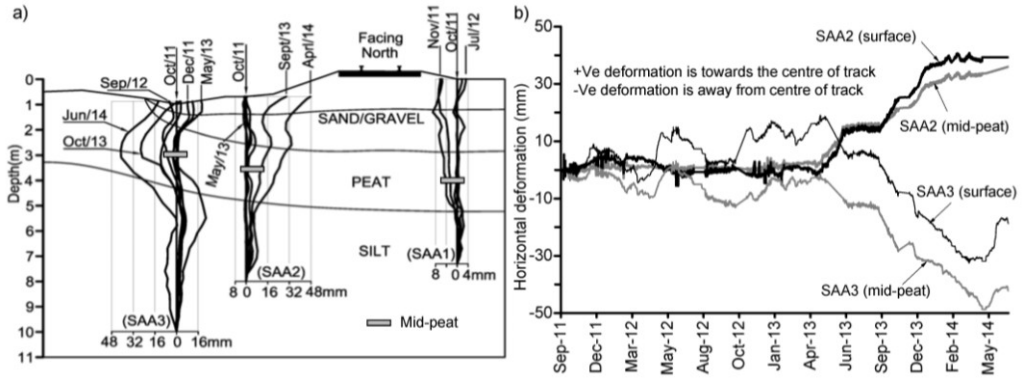

Figure 5.6. The horizontal deformation recorded by three vertically installed SAAs: (a) shape of the SAAs after different durations, and (b) deformation at surface and mid-peat level from May 2011 to June 2014.

5.6.3 Discussion of the field measurements

The pore pressure measured in the peat (Figs. 5.4a and 5.4b) showed an increase during the summer and autumn due to thermal expansion of gas bubbles (Acharya et al., 2015a). The periodic rise and sharp drops in pore pressure recorded by piezometers in the upper peat layer are a result of the movement of gas bubbles within the peat and expulsion of gas bubbles from the surface (Acharya et al. 2015b).

The effect of the pore pressure drops that occurred in the top peat layer (PZ3 and VW1) was not seen in the SGPs and VWPs that were installed deeper in the peat and silt layers (PZ1, PZ2, VW2, VW3) and in the VWPs installed in unloaded peat (VW4, VW5). The SGP at the peat-subballast boundary (PZ4) recorded the continuous rise and drops together with the drops at PZ3 and VW1. The drops were small, at 1 to 3 kPa, and subtle. The negative peaks in the plot of rate of change of pore pressure recorded by PZ4 (Fig. 5.7) show the drops in pore pressure and the corresponding expulsion of gas that occurs at the peat-subballast boundary.

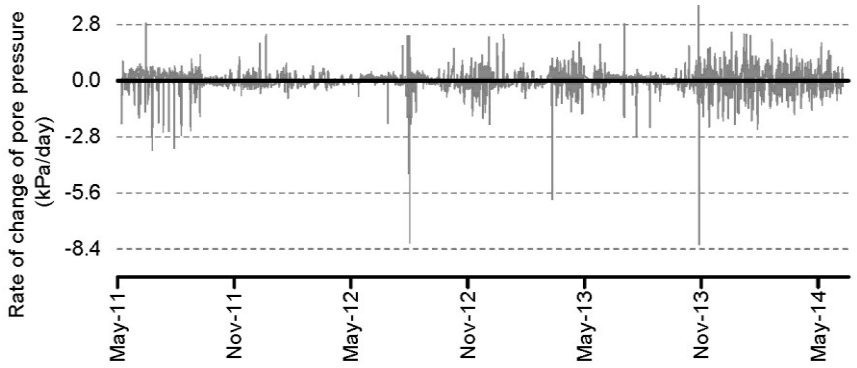

Figure 5.7. Rate of change in pore pressure recorded at the peat-subballast boundary.

The cumulative vertical settlement beneath the fill was more than three times the cumulative horizontal displacement measured at the ground surface. This suggests that the deformation is predominantly the result of volumetric change and not shear deformation. The vertical deformation (92 mm) and, consequently, the rate of vertical deformation were greatest in the summer and autumn of 2011 when both the peak pore pressure (Δu) and the magnitude of the pore pressure drops (Δu_d) were at their maximum. The maximum horizontal deformation (25 mm) occurred in 2013. The plots of vertical and horizontal deformation (Figs. 5.5 and 5.6, respectively) did not show any changes in vertical and horizontal deformation corresponding to the pore pressure drops that occurred in the top peat layer. This may in part be due to the distance between the VWPs and the settlement gauges and SAAs, and that the change of pore pressure due to the expulsion of gases is localized (Fig. 5.3).

To study the effect of the pore pressure drop, the rates of vertical settlement recorded by EXT1, VS4, and VS5 were plotted together with the pore pressure recorded by VW1 and PZ3 during the summer and autumn of 2011 (Fig. 5.8). Each pore pressure drop was followed by an increase in the rate of settlement (Figs. 5.8). There was a clear rise in the rate of settlement at EXT1, VS4, and VS5 corresponding to the pore pressure drop at PZ1. As VW1 and EXT1 are at the two opposite sides of the embankment (Fig. 5.3), the effect of pore pressure

drop at VW1 is not clear in the settlement measured by EXT1. This change in the settlement rate was not due to the temperature sensitivity of the sensors as the drop in pore pressure occurred during the summer and at an almost constant temperature.

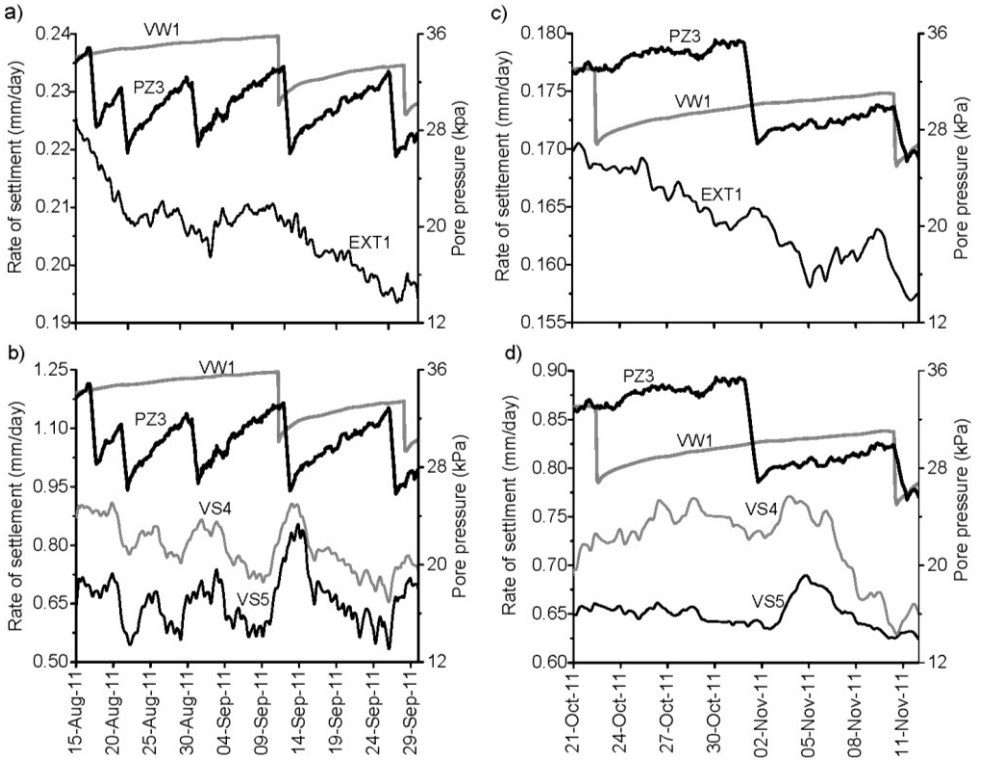

Figure 5.8. The rate of vertical deformation as calculated from the deformation measured between August 15 to September 29, 2011 by (a) EXT1, and (b) VS4 and VS5, and between October 21 to November 15, 2011 by (c) EXT1, and (d) VS4 and VS5.

A similar comparison was conducted for the rates of horizontal deformation recorded by SAA2 and SAA3 and the pore pressure response recorded by VW1 and PZ3 (Fig. 5.9). However, there was no apparent correlation between the measured rate of horizontal deformation and the pore pressure drops.

The field measurements show that vertical settlement is much greater than horizontal deformation. The pore pressure drops due to expulsion of gas are

coincident with a significant increase in the rate of vertical settlement and thus suggest that the volume loss due to the expulsion of gases from the peat are resulting in a vertical (*volumetric*) settlement of the peat foundation.

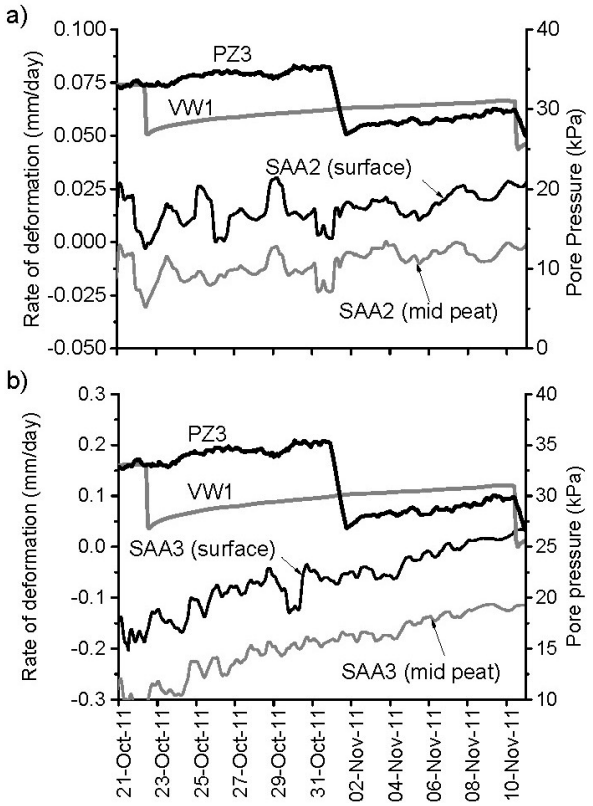

Figure 5.9. The rate of horizontal deformation as calculated from the deformation measured between October 21 to November 15, 2011 by (a) SAA2, and (b) SAA3 at the ground surface and at the middle of the peat layer as shown in Fig 5.6. Note: *positive deformations are towards the centre of the track and negative deformations are away from the centre of the track.*

5.7 Laboratory testing

Further confirmation of this mechanism can be seen in the laboratory testing results from Acharya et al. (2015b), presented in Fig. 5.10. The laboratory testing consisted of isotropic consolidation tests conducted at varying effective confining pressure (*p'*). These tests were conducted to reproduce the pore pressure generation and rapid drops measured at the field site. Six specimens were tested

with *p'* values ranged from 10 kPa and 40 kPa generated with a total confining pressures (*p*) ranging from 80 kPa to 230 kPa. The results of this testing showed that the rise in pore pressure was necessary to push the gas bubbles out through the pore constriction of both peat and porous stone (Acharya et al., 2015b). Notably, each drop in pore pressure was accompanied by a rapid change in volume (inset graph Fig. 5.10b).

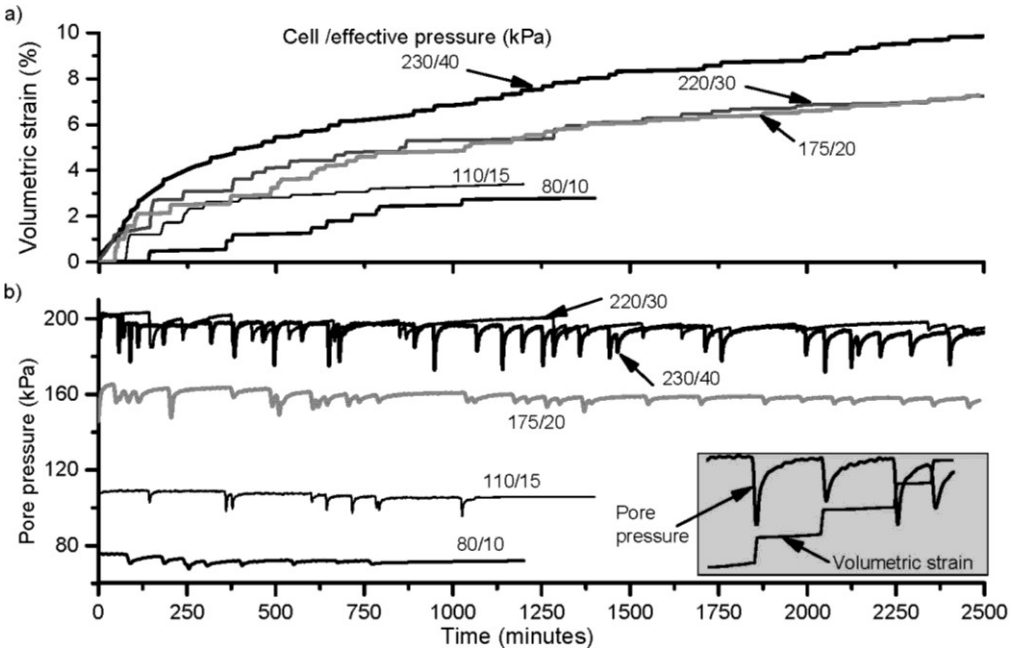

Figure 5.10. Results of isotropic consolidation tests on peat specimens: a) volumetric strain versus time, and b) pore pressure versus time. The inset graph shows the pore pressure drops and instant volume changes plotted with time (Acharya et al., 2015b).

The volume change of the specimens correlated with the number and magnitude of pore pressure drops (Fig. 5.10), with larger magnitude pore pressure drops (Δu_d) resulting in larger volume changes. The developed volumetric strain (ε_v) was correlated with effective stress (p)', such that higher volumetric strains corresponded to higher *p'* (Fig. 5.10a). This is consistent with the findings of Thomas (1987), who noted that the generation of volumetric strain in soil containing gas bubbles is correlated to the *p'*. The magnitude of pressure drops

measured in the laboratory are also better correlated with *p'*, with larger and more frequent drops observed at higher applied *p'* (Fig. 5.10) (Acharya et al., 2015b).

5.7.1 Correlation between Δu_d and associated volumetric change

This section describes the development of a correlation between the volumetric strain associated with pore pressure drop (ε_{vg}) and Δu_d; both result from the expulsion of gas bubbles in laboratory specimens, so this information can be extrapolated to estimate the settlement related to the expulsion of gas from the peat subgrade. Within the soil matrix, the size of the gas bubbles depends on temperature and the size of the pore space. During consolidation under isothermal conditions, the overall size of the pore space is a function of the stiffness of the soil matrix containing the gas bubble and the flow of pore water, and thus consequently a function of *p'* (Thomas, 1987; Sills at el., 1991).

In soil containing gases, any volume change that may occur due to the dissolution of gas into the pore water or expulsion of gas is difficult to separate from the volume change related to the dissipation of pore water (Thomas, 1987). The ε_v presented in Fig. 5.10a included volumetric strain developed due to the dissipation of both gas and water from the peat specimens. An attempt was made to quantify the volumetric strain that resulted from the dissipation of gas by separating the volumetric strain associated with the pore pressure drops (ε_{vg}) from ε_v.

Fig. 5.11a presents the variation of Δu_d, plotted with consolidation time. The Δu_d decreased with consolidation time. The semi-log plots show that the variation of Δu_d with time can be represented by a logarithmic function. Fig. 5.11b presents the ε_{vg} corresponding to each Δu_d, also plotted with consolidation time for all tests conducted. For all tests, the ε_{vg} decreases with time. This accounts for the larger pore pressure drops corresponding to the larger gas bubbles at the beginning of the tests and smaller pore pressure drops at the later stages of the

tests. As for Δu_d, the ε_{vg} decreases with time and suggests a correlation between these two variables.

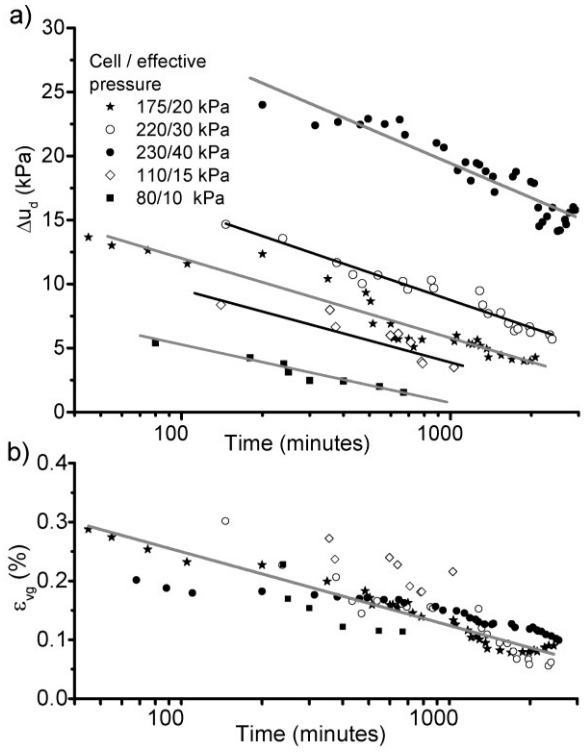

Figure 5.11. Results from isotropic consolidation tests of peat specimens plotted versus consolidation time: (a) magnitude of pore pressure drops (Δu_d), and (b) volumetric strain (ε_{vg}).

Fig. 5.12a presents the *log* ε_{vg} plotted with corresponding *log* Δu_d, which demonstrates a linear relationship between ε_{vg} and Δu_d; large Δu_d values resulted in larger ε_{vg} and smaller Δu_d produced smaller ε_{vg}. The parallel lines in Fig. 5.12a show that this relationship is constant for a given *p'*. The specimen with a lower *p'* experienced a larger volume change at constant Δu_d. This is due to the inverse relationship between the volume of gas bubbles and *p'*, i.e., under the higher *p'*, the gas bubbles will occupy a smaller volume in the pore space. The correlation between ε_{vg} and Δu_d in Fig. 5.12a can be represented by the power function in Eq. [5.1],

, -------[5.1]

where, b is the slope of the $log\ \varepsilon_{vg}$ - $log\ \Delta u_d$ plot and is constant at isothermal conditions, as the $log\ \varepsilon_{vg}$ - $log\ \Delta u_d$ plots for different p' are parallel to each other (Fig. 5.12a). For the four isotropic consolidation tests shown in Fig. 5.12a, the value of b ranged from 0.95 to 1.35 with an average of 1.21. Parameter A is the ordinate value of the $log\ \varepsilon_{vg}$ - $log\ \Delta u_d$ plot at $\Delta u_d = 1$ (Fig. 5.12a), or the maximum possible value of ε_{vg} corresponding to the applied p'. The A parameter decreased exponentially with increasing p' (Fig. 5.12b) and is represented by Eq. [5.2]:

. -------[5.2]

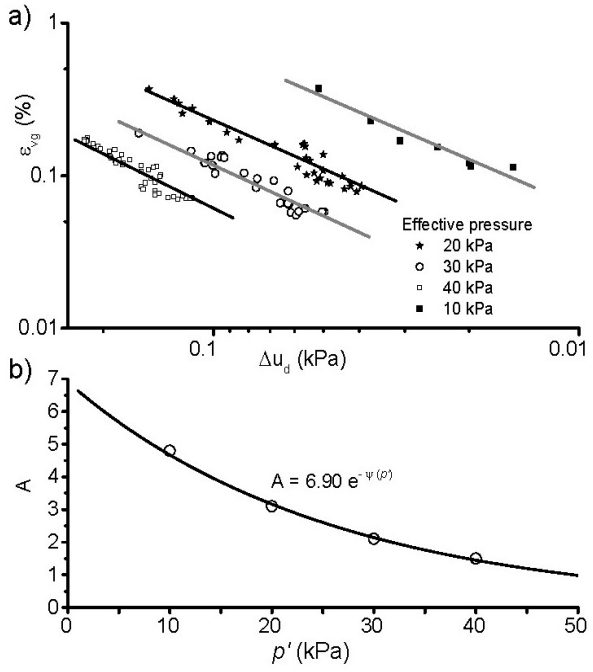

Figure 5.12. Plots of (a) the volumetric strain (ε_{vg}) versus the magnitude of pore pressure drop (Δu_d), and (b) factor A versus the effective confining pressure (p'). Note: *the pore pressure drops are normalised to atmospheric pressure.*

Eqs. [5.1] and [5.2] are combined to represent the correlation between ε_{vg} and Δu_d for the specimens tested at various p' as per Eq. [5.3]:

. ------[5.3]

The φ parameter depends on the compressibility of gas bubbles and indicates the decrease in volume of gas bubbles in the pore space; consequently, the volume change corresponds to Δu_d with increasing p'. For isothermal conditions, this parameter is assumed to be constant and equal to the slope of a *log A - p'* plot. Assuming φ and b are constant at values of -0.039 and 1.21, respectively, in Eq. [5.3], ε_{vg} values corresponding to various Δu_d were calculated for a series of mean confining pressures (p') and are presented in Fig. 5.13a. The *log* ε_{vg} – p' plots show the decrease in ε_{vg} with increasing confining pressure under constant Δu_d. This plot also presents the variation of ε_{vg} in peat specimens corresponding to different combinations of Δu_d and p'.

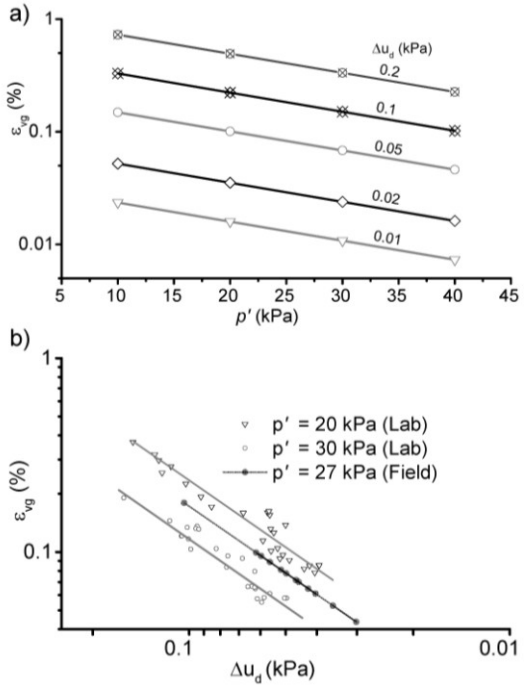

Figure 5.13. Plots of the calculated ε_{vg} (a) corresponding to different Δu_d with p', and (b) corresponding to different p' with Δu_d presented in Fig. 5.4. Note: *the* Δu_d *are normalised to atmospheric pressure*.

5.8 Settlement of peat subgrade

The field measurements showed a drop in pore pressure due to the expulsion of gas bubbles from the top peat layer beneath the field embankment (Fig. 5.4) and the associated vertical settlement of peat subgrade. The correlation developed between and ε_{vg} and Δu_d in Eq. [5.3] is used to calculate the part of the settlement that results from the expulsion of gas bubbles. Only the larger pore pressure drops recorded by PZ3 and VW1 from the top peat layer (Fig. 5.4) are considered in the calculation. The pore pressure drops recorded by PZ4 are too small and not considered in this calculation.

The average ground water level beneath the embankment at the instrumentation site near MP 263.5 is 1.30 m below the top of the track surface. Assuming an average density of the embankment material and peat of 22 and 12 kN/m^3, respectively, and thicknesses of the embankment material and peat of 2.75 and 2.60 m, respectively, the mean effective stress at the mid-peat level below the centre of the track is calculated to be 27 kPa. Using Eq. [5.3], the ε_{vg} corresponding to the Δu_d measured in field (Fig. 5.4) at a p' of 27 kPa are calculated and presented in Table 5.1 and plotted in Fig. 5.13b. The parameters b and φ are assumed constant as the pore pressure drops in the field occurred at constant confining pressure and temperature.

The cumulative ε_{vg} estimated for May to November of 2011 and 2012 from the measured Δu_d beneath the granular fill are 0.60 and 0.38% and below the track are 0.72 and 0.31%, respectively (Table 5.1). As the thickness of the peat is 2.6 m, these strains would result in vertical deformations of 15 and 10 mm below the granular fill and 18 and 8 mm below the track in 2011 and 2012, respectively (May to November). These values account for 17 and 16% of the vertical settlement below the granular fill and 65 and 30% of the vertical settlement below the track measured between May and November of 2011 and 2012, respectively. A lower percentage of settlement below the granular fill is only due to the large total settlement that occurred in 2011 and 2012.

Table 5.1. The calculated ε_{vg} associated with the major Δu_d measured at the field site in the summers of 2011 and 2012.

Location	Date	Pore pressure drop (Δu_d) (kPa)	Δu_d normalised to atmospheric pressure (kPa)	ε_{vg} (%)	Settlement (mm)
Fill	7/01/011	10.53	0.10	0.18	4.50
	9/09/011	5.69	0.06	0.09	2.22
	9/26/011	4.1	0.04	0.06	1.53
	10/20/011	6.28	0.06	0.10	2.49
	11/08/011	6.06	0.06	0.10	2.39
	11/19/011	5.06	0.05	0.08	1.94
			Total	**0.60**	**15.06**
	5/21/012	3.62	0.04	0.05	1.32
	7/24/012	3.06	0.03	0.04	1.09
	8/03/012	4.32	0.04	0.06	1.62
	8/23/012	4.63	0.05	0.07	1.75
	9/16/012	4.72	0.05	0.07	1.79
	10/03/012	5.25	0.05	0.08	2.03
			Total	**0.38**	**9.61**
Embankment	8/16/011	7.34	0.07	0.12	2.97
	8/20/011	6.9	0.07	0.11	2.77
	8/30/011	9.58	0.09	0.16	4.03
	9/11/011	7.04	0.07	0.11	2.83
	9/25/011	9.68	0.10	0.16	4.08
	10/31/011	8.52	0.08	0.14	3.53
	11/10/011	5.15	0.05	0.08	1.98
	11/13/011	3.66	0.04	0.05	1.34
			Total	**0.94**	**23.54**
	8/04/012	9.36	0.09	0.16	3.93
	8/24/012	7.14	0.07	0.12	2.88
	10/12/012	7.25	0.07	0.12	2.93
			Total	**0.39**	**9.74**

5.9 Conclusion

Field measurements of pore water pressure showed a series of rises and drops in pore pressure within the peat subgrade due to the movement and expulsion of gas bubbles. The vertical settlement accelerated following pore pressure drops in the top peat layer. The horizontal deformations were much smaller compared to the

vertical deformation and showed the seasonal movements towards and away from the track and are not affected by the pore pressure drops. Laboratory isotropic consolidation tests on the peat specimens replicated the field pore pressure behaviour and showed the volume change within peat specimens after each pore pressure drop. The volume changes associated with these pore pressure drops was found to be proportional to the magnitude of the pore pressure drops and inversely proportional to the effective confining pressure.

An empirical correlation was developed between the magnitude of pore pressure drop due to the expulsion of gas bubbles and the associated volumetric strain measured in the laboratory isotropic consolidation tests conducted on peat specimens at different confining pressures. This correlation was used to estimate the volumetric strain associated with the pore pressure drops measured in the peat subgrade beneath the railway embankment near MP 263.5. It was found that, during the first two consecutive years of monitoring (2011 and 2012), the settlements of peat subgrade related to the expulsion of gas bubbles were 15 and 10 mm below the granular fill and 18 and 8 mm below the embankment, respectively. These values represent 17 and 16% of the total settlement measured below the granular fill, and 65 and 30% of the total settlement measured below the track, respectively. These values are assumed to underestimate the settlement induced by the pressure fluctuations as the piezometers would not have detected all pore pressure drops below the embankment. However, it appears that more than 15% of the measured settlement every year is a result of the generation and expulsion of gas bubbles.

5.10 Acknowledgement

The authors would like to acknowledge the contribution of Canadian National Railways for providing both the project and funding. This research was made possible through the (Canadian) Railway Ground Hazard Research Program and the Canadian Rail Research Laboratory (www.carrl.ca), both of which are funded by the Natural Sciences and Engineering Research Council of Canada (NSERC), CPR, CN, and Transport Canada.

5.11 References

Acharya, M. P., Hendry, M. T. and Martin, C. D. 2015a. Thermally induced pore pressure response in peat beneath a railway embankment. *International Journal of Geotechnical Engineering*. *In press.*

Acharya, M. P., Hendry, M. T. and Martin, C. D. 2015b. Effect of the presence and movement of gas bubbles on pore pressure behaviours observed in peat. *Canadian Geotechnical Journal*, *In press.*

ASTM D1997-91 (2008), Standard Test Method for Laboratory Determination of the Fiber Content of Peat Samples by Dry Mass, ASTM International, West Conshohocken, PA, 2008, www.astm.org

ASTM D2974-07, Standard Test Methods for Moisture, Ash, and Organic Matter of Peat and Other Organic Soils, ASTM International, West Conshohocken, PA, 2007, www.astm.org

Hobbs, N. B. 1986. Mire morphology and the properties and behaviour of some British and foreign peats. *Quarterly Journal of Engineering Geology and Hydrogeology*, 19(1): 7-80.

Konrad, J., Grenier, S. and Garnier, P. 2007. Influence of repeated heavy axle loading on peat bearing capacity. Ottawa Geo2007: 1551-1558.

Landva, A. O. and La Rochelle, P. 1983. Compressibility and shear characteristics of Radforth peats. American Society for Testing and Materials, Testing of peat and organic soils, STP 820, West Conshohocken: 157-191.

Long, M. and Boylan N. 2013. Predictions of settlement in peat soils. *Quarterly Journal of Engineering Geology and Hydrogeology*, 46(3): 303-322.

MacFarlane, I. C. 1965. The consolidation of peat: A literature review. National Research Council of Canada Division of Building Research Ottawa, NRC: 8-393.

MacFarlane, I. C. 1969. Engineering characteristics of peat, *Muskeg Engineering Handbook,* I.C. McFarlane, ed., Univ. of Toronto Press, Canada: 78-126.

Sills, G. C., Wheeler, S.J., Thomas, S.D. and Gardner T.N. 1991. Behaviour of offshore soils containing gas bubbles. *Géotechnique*, 41(2): 227-241.

Thomas, S. D. 1987. The consolidation behaviour of gassy soil, D.Phil. thesis, Oxford University.

Weber W. G. 1969. Performance of embankments constructed over peat. *Journal of the Soil Mechanics and Foundations Division*, 95(1): 53-76

6 Chapter 6: Creep behaviour of remoulded and intact fibrous peat

6.1 Contribution of the Ph.D. candidate

All work reported in this chapter, including field installation, design of the experimental program, implementation of the experiments, review of the literature, development of the theoretical framework, analysis and discussion of the results, and writing of the text, was carried out by the Ph.D. candidate. As supervisors, Dr. M. T. Hendry and Dr. C. D. Martin reviewed all parts of the work. This chapter will be submitted with the following citation:

Acharya M. P., Hendry, M. T. and Martin, C. D. 2015. Creep behaviour of remoulded and intact fibrous peat. *To be submitted to the Canadian Geotechnical Journal*.

6.2 Abstract

This paper presents the creep behaviour of intact and remoulded specimens of fibrous peat obtained from a field site near Anzac, Alberta, Canada. The creep behaviour was investigated by means of long-term drained and undrained triaxial tests. The development of volumetric, axial, and undrained axial strain and strain rate during drained and undrained creep tests under variable stress states is presented. The *stress-strain-strain rate* (p'-ε_v-) relationship was found to be unique for different stress states and loading durations. The p'-ε_v- relationship is analysed and represented by creep isotaches. The applicability of different creep models developed for normally consolidated clay is discussed and applied to define the development of creep strain in fibrous peat under varying isotropic and deviatoric stress states. The validity of the use of the secondary consolidation coefficient for evaluating the volumetric strain rate of peat is considered and found to be applicable with some limits. The drained creep behaviour of remoulded peat specimens was found to differ from the behaviour shown by Shelby tube specimens, whereas the undrained creep behaviour in remoulded and Shelby tube specimens was similar.

Definition of symbols

C_c	=	Coefficient of compression
C_α	=	Coefficient of secondary compression
CU	=	Triaxial consolidated undrained compression tests
CD	=	Triaxial consolidated drained compression tests
1D	=	One-dimensional
p'_0	=	Preconsolidation pressure (kPa)
p'	=	Mean confining pressure (kPa)
’	=	Rate of effective stress change
q	=	σ_1-σ_3 = Deviatoric stress (kPa)
q_0	=	First deviatoric stress increment (kPa)
Δq	=	q_2-q_1 = Deviatoric stress increment (q increment)
σ'_3	=	$\sigma_3 – (\sigma_3 - p'_0) =$ Effective isotropic confining stress
$\Delta\sigma'_3$	=	$\sigma'_3 - p'_0$ = Isotropic stress increment (σ'_3 increment)
SIR	=	$\Delta q/q$ *or* $\Delta\sigma'_3 / \sigma'_3 =$ Stress increment ratio
w_0	=	Initial water content of specimen (%)
w_f	=	Water content at the end of the creep tests (%)
ρ_0	=	Density of specimen (g/cm^3)
ε_{vp}	=	Volumetric strain at the end of the pre-consolidation (%)
e_0	=	Initial void ratio
ε_v	=	Volumetric strain (%)
	=	Volumetric strain rate (% / minute)
ε_a	=	Axial strain (%)
	=	Axial strain rate (% / minute)
ε_{ad}	=	Undrained Axial strain (%)
	=	Undrained strain rate (% / minute)
u	=	Pore pressure developed during CD and CU tests (kPa)
α, β	=	Creep parameters
m	=	Slope of *log* – *log t* plot (the rate of decrease in strain rate)
ε_r	=	Lateral strain (%)
ν	=	Poisson’s ratio

6.3 Introduction

The long-term deformation behaviour of peat has been the subject of several studies (Macfarlane, 1965; Berry and Poskit, 1972; Dhowian and Edil, 1980; Fox and Edil 1996; Den Hann, 1996; Mesri et al., 1997; Madaschi and Gajo, 2015). These studies have investigated and modelled the consolidation behaviour of peat based on one-dimensional consolidation, and have done so using coefficients of primary consolidation and secondary compression (C_c and C_α) derived from oedometer tests (Macfarlane, 1965; Barden, 1968; Den Hann, 1996; Mesri et al., 1997)). Measured field settlements are often notably larger than those predicted from laboratory testing results as well as the models derived from oedometer tests and the resulting C_c and C_α coefficients. This discrepancy has been attributed to the variability of peat, the three-dimensional nature of creep, and the tendency of C_c and C_α to increase with time (Samson and La Rochelle, 1972; Landva and La Rochelle, 1983). Other studies have focused on the mechanisms behind this deformation and have described a more complex process of consolidation consisting of structural creep and a sequential or concurrent pressure-driven expulsion of water from between (inter-particle) and within (intra-particle) the organic structures that compose the particles (Barden, 1968; Berry and Poskit, 1972; Landva, 2007). Published field and laboratory findings have consistently shown that the secondary deformations in peat are significantly larger than those from primary consolidation (Macfarlane 1965; Weber, 1969; Mesri et al., 1997; Gunaratne et al., 1998).

The viscoplastic models based on one-dimensional deformation behaviour have defined the secondary compression or creep using creep functions developed for clays or have defined the creep functions in terms of parameters developed for similar one-dimensional behaviour in clay (Barden, 1969; Berry and Poskit, 1972; Den Haan, 1996). In contrast, clays have undergone more intense investigation, with creep behaviour studied under both one-dimensional and triaxial stress states (Sukje, 1957; Bjerrum, 1967; Singh and Mitchel, 1968; Tavenas et al., 1978; Graham et al., 1983; Lerouiel et al., 1985). These

investigations produced a general relationship between stress, stain, strain rate, and time and have provided a more robust framework for the development of one- and three-dimensional viscoplastic models (Yin and Graham, 1989; Morsy et al., 1995; Yin and Graham, 1999; Kim and Lerouiel, 2001; Kelln et al., 2008).

The purpose of this study was to expand the understanding of the long-term deformation behaviour of peat in triaxial stress states, to develop the *stress-strain-strain rate* (p'-ε_v-) relationships (Sukje, 1957; Bjerrum, 1967; Lerouiel et al., 1985), and to evaluate the applicability of the associated creep models developed for normally consolidated clay.

6.4 Study material

The study material was retrieved from a site located on the Canadian National Railway's (CN) Lac-la-Biche Subdivision near Anzac, Alberta (56°28'44.44"N 111°2'50.29"W), where a railway embankment crosses a large expanse of peat bog. The site was investigated in 2011 and samples were taken from the 2.6 to 3.5 m thick peat subgrade that underlies a 2 to 3 m thick embankment. Peat samples were collected both in Shelby tubes and as highly disturbed material from auger cuttings. The peat is classified as fibrous peat with light yellowish, highly coarse fibres, with fresh tree branches and roots in the top layer and finer fibres at greater depths. The water content ranges from 800% at the top to 400% for the coarse and fine fibrous layers. The degree of humification was determined to be insignificant, with the plant structures within the peat appearing to be intact. The classification of the peat as per Hobbs (1986) and the Von Post peat classification (Landva and Pheeney, 1980) system is H2B3F1R3W1N4.

6.5 Laboratory testing methodology

6.5.1 Specimen preparation

The specimens consisted of both remoulded specimens (reconstituted from the auger cuttings) and relatively intact specimens trimmed from Shelby tube samples. For preparation of the remoulded specimens, the cuttings were cleaned

of root and stone inclusions, and then placed inside a 38-mm-diameter steel tube up to a height of 130 ± 3 mm. The cuttings were then subjected to vertical compression under a vertical stress (σ'_v) of 55 kPa until the settlement-versus-time curve flattened, usually after 24 hours. The vertical strain at the end of compression varied from 5 to 26%. The compressed samples were extruded from the steel tube and trimmed to a length of 76 ± 4 mm for consolidated drained and undrained triaxial creep testing. The density of the remoulded specimens ranged from 0.97 to 1.09 g/cm^3, and the initial water content varied between 363 and 505%.

Shelby tube samples were trimmed to generate four peat specimens 72 ± 2 mm in diameter and 150 ± 15 mm in length, and one specimen 38 ± 2 mm in diameter and 76 ± 2 mm in length. The resulting specimens appeared relatively smooth and free from defects and large roots (Fig. 6.1). Some of the Shelby tube specimens (SD2, SU2) had shorter fibres (< 2 mm). The specimens had a measured density between 0.94 to 1.08 g/cm^3. The water content of these specimens varied between 440 and 730%, which was a wider range than for the remoulded specimens. Physical properties of the specimens are summarized in Table 6.1.

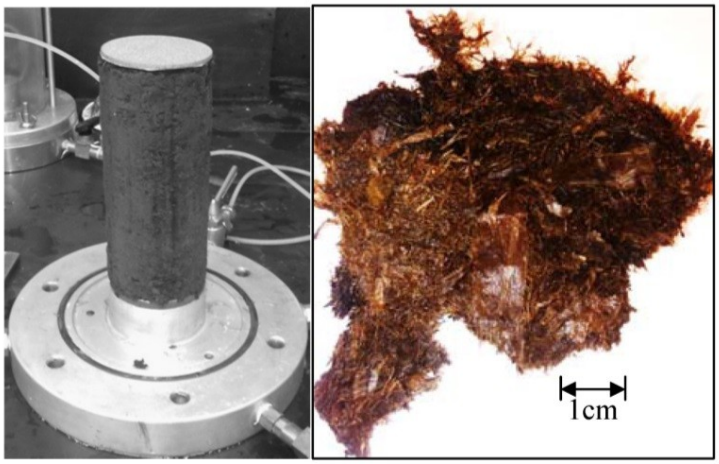

Figure 6.1. Peat specimens: (left) trimmed to size and placed at the base of the triaxial cell and (right) cuff off showing intact fibres.

Table 6.1. Summary of physical properties of peat specimens

Specimen type	Specimen ID	Diameter (mm)	w_0 (%)	ρ_0 (g/cm3)	e_0	p'_0 (kPa)	ε_{vp} (%)	w_f (%)
Intact	SD1	70.7	668.5	1.022	12.5	30	16.12	420
	SD2	69.5	616	1.002	11.9	20	1.08	481
	SD3	37.63	469.5	0.94	9.9	30	3.34	345
	SU1	71.11	536.5	1.08	9.6	30	6.87	430
	SU2	70.9	601	0.99	11.7	20	7.26	533
Remoulded	RD1	38.08	475	0.97	9.7	30	4.12	435
	RD2	37.63	398	1.09	7.2	30	2.2	341
	OD1	70.95	521	0.97	9.2		29	390
	OD2	63	475	1.02	9.1		23	190
	RU1	37.94	421	1.044	8.0	30	5.78	336
	RU2	38.21	505	1.02	9.7	40	3.9	305

6.5.2 Laboratory creep tests

Two remoulded and three Shelby tube peat specimens were subjected to a consolidated drained (CD) creep test and two remoulded and two Shelby tube peat specimens were subjected to a consolidation undrained (CU) creep test. The CU testing was conducted to isolate the shear component of the deformation behaviour; it was not intended to represent conditions of peat that can be realized in the field.

A schematic diagram of the triaxial testing apparatus used in these tests is presented in Fig. 6.2. The pore pressure was measured with pressure transducers (accuracy: ± 0.08% of the measured value) and the axial displacements were measured with a linear variable differential transformer (LVDT) (accuracy: ± 0.2% of the measured value). Teledyne ISCO pumps measured the amount of water expelled during the CD test, thus the volumetric strain (ε_v), with an accuracy of ± 0.05%.

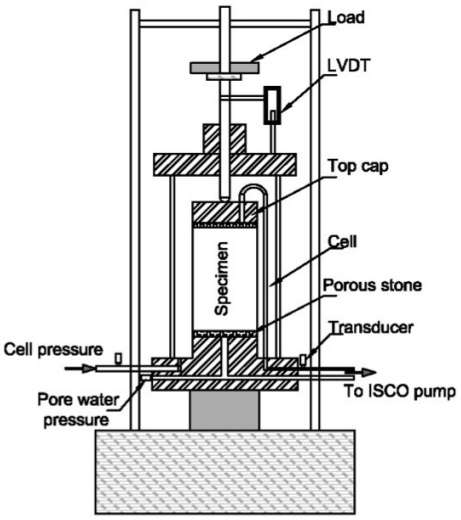

Figure 6.2. Schematic diagram of triaxial setup for creep tests.

All specimens were subjected to backpressure saturation using a backpressure of 190 kPa and a cell pressure of 200 kPa. The Skempton's B value was calculated and found to be greater than 0.97 before the start of each test. The specimens were then consolidated to the desired effective confining pressure (p'_0), which was varied between 10 and 40 kPa. The consolidation was continued until the volume change verses time curve flattened or the pore pressure remained stable. The duration of the consolidation ranged from a few days to a few weeks. After consolidation, deviatoric stresses (q) were applied in increments (Δq) ranging from 5 to 20 kPa. A stepped stress application procedure, as described in Tavenas et al. (1978), was applied. In isotropic creep tests, the effective confining stresses (σ'_3) were applied in increments ($\Delta\sigma'_3$) ranging from 3.5 to 80 kPa. The stress increment ratio (SIR) for both Δq and $\Delta\sigma'_3$ increments ranged from 0.2 to 1. A small SIR was used to minimize the effect of primary consolidation, and a higher increment ratio was used to study the strain behaviour not affected by the loading history (e.g., Barden, 1969). Each Δq *or* $\Delta\sigma'_3$ was maintained for whichever time period was longer: seven days or when the strain rate slowed to 1×10^{-4} %/minute. The tests were stopped when either the specimens failed or the axial strain exceeded 25%. The duration of these tests ranged from 4 to 17 weeks. Table 6.1 presents the summary of the test program, including the details of the deviatoric

and isotropic stresses applied during the tests and the SIRs used. Fig. 6.3 presents the stress path followed by specimens subjected to creep stress during drained and undrained conditions. Each point in Fig. 6.3 represents the stress state of the specimen in the q - p' space at the beginning of each Δq or $\Delta\sigma'_3$ increment.

Table 6.2. Summary of CD, CU, and 1D tests (D = deviatoric, I = isotropic, and 1D = one dimensional)

Specimen type	Tests	Specimen ID	Type of Stress	q, σ_3, and $\sigma'v$ (kPa)	Δq or $\Delta\sigma_3$ (kPa)	SIR
Intact	CD	SD1	D	q = 20, 30, 40, 50, 60	Δq = 10	0.2 to 0.5
		SD2	D	q = 5, 10, 20, 30, 40	Δq = 5, 10, 20	1
		SD3	I	σ'_3 = 33.5, 37.0, 40.5, 44.0, 47.5, 51.0, 54.5, 64.5, 84.5, 124.5, 204.5	Δp = 3.5, 10, 20, 40, 80	0.2 to 1
	UD	SU1	D	q = 5, 10, 20, 40	Δq = 5, 10	1
		SU2	D	q = 5, 10, 20, 40	Δq = 5, 10	0.5 to 1
Remoulded	CD	RD1	D	q = 10, 20	Δq = 10	1
		RD2	D	q = 10, 20, 30, 40, 50, 60	Δq = 10	0.2 to 1
		OD1	1D	$\sigma'v$ = 6.25, 12.5, 25, 50, 100	$\Delta\sigma'v$ = 6.25, 12.5, 25, 50	1
		OD2	1D	$\sigma'v$ = 25, 50, 100, 200	$\Delta\sigma'v$ = 25, 50, 100	1
	UD	RU1	D	q = 20, 30, 40, 50, 60,	Δq = 10	0.2 to 0.5
		RU2	D	q = 10, 20, 30,40, 50, 60, 70, 80	Δq = 10	0.2 to 1

Additionally, to compare the creep behaviour of peat in triaxial and one-dimensional consolidation (1D) loading, two remoulded specimens were subjected to 1D loading. The first specimen was prepared by placing the peat in a tube 75 mm in diameter and 150 mm in height and subjecting it to vertical pressure increments ranging from 6.5 to 105 kPa. The second specimen was placed on a standard oedometer apparatus and subjected to pressure increments ranging from 25 to 200 kPa. The SIR was kept equal to 1. Each increment was

held for two days. Drainage was allowed from both ends. The vertical displacement was measured using a LVDT.

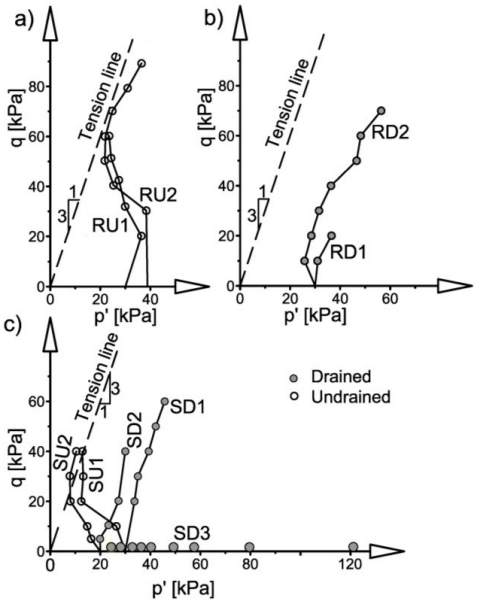

Figure 6.3. Stress state of peat specimens during (a) CU creep tests (remoulded), (b) CD creep tests (remoulded), and (c) CU and CD creep tests (Shelby tube).

6.6 Test results and analysis

The following sections present the results of the laboratory CD and CU tests conducted on remoulded and intact peat specimens under different stress conditions (Fig. 6.3). They describe the development of volumetric creep strain and strain rate (ε_v and), development of pore pressure (u), analysis of rheological behavior, the development of an expression for volumetric creep rate, the development of axial strain and strain rate (ε_a and), the analysis of Poisson's ratio, and the development of shear strain and strain rate (ε_{ad} and).

6.6.1 Development of volumetric strain during CD tests

Fig. 6.4 presents the volumetric strain (ε_v) and the volumetric strain rate ( ) developed over the course of the three CD tests conducted on Shelby tube specimens. The loading of specimen SD1 was started with a larger deviatoric stress increment (Δq) of 20 kPa. Four more Δq of 10 kPa each were added,

resulting in creep tests conducted with q's of 20, 30, 40, 50, and 60 kPa. The resulting SIRs varied from 0.5 to 0.2. The resulting ε_v – *log t* curves presented in Fig. 6.4a are all similar in shape. The developed ε_v was highest under the first Δq (i.e., q = 20 kPa) (9.28%). The ε_v did not increase proportionally with increasing q. The net ε_v generated under the next four Δq, each 10 kPa, were 1.80, 1.94, 3.07, and 2.56 %, respectively. No sign of failure was detected even after a ε_v of 18.5% and a loading duration of 10^5 minutes.

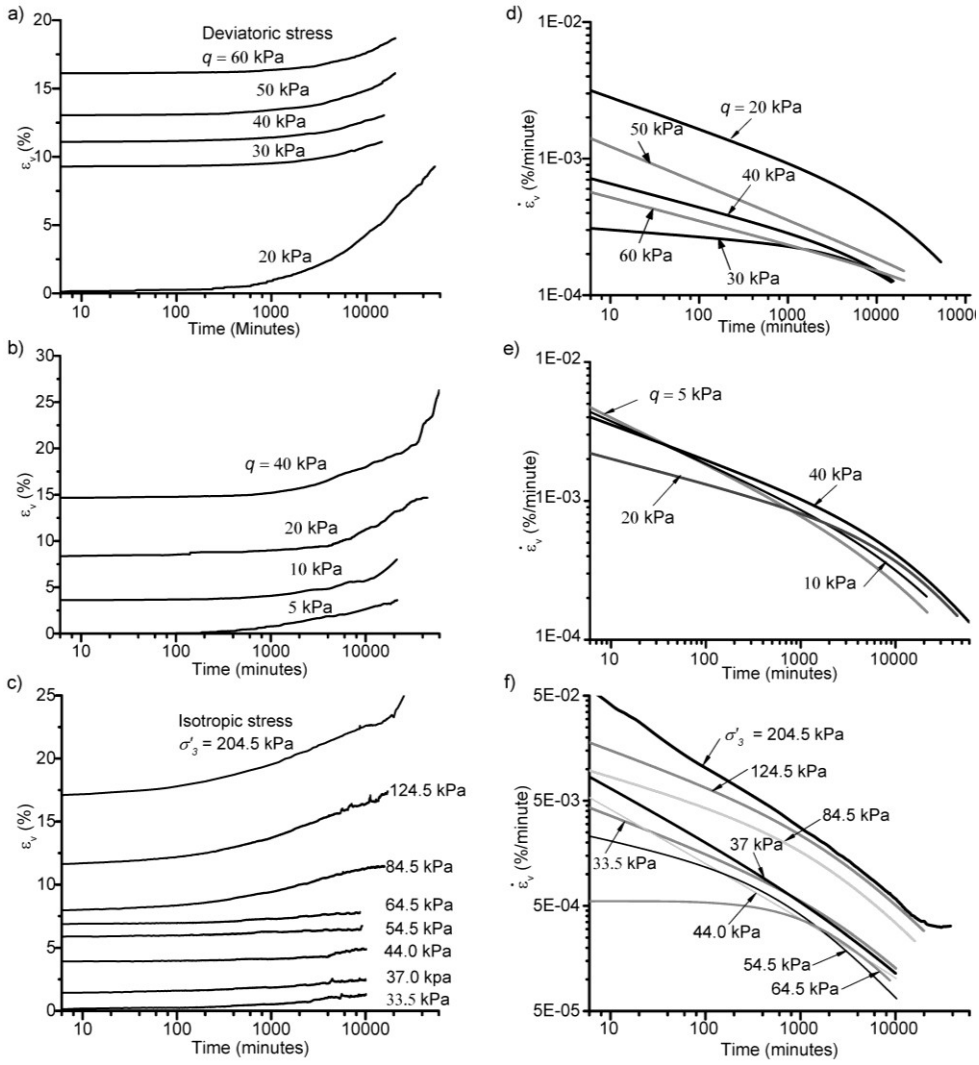

Figure 6.4. Development of ε_v, (a) SD1 (p'_0 = 30 kPa), (b) SD2 (p'_0 = 20 kPa), and (c) SD3 (p'_0 = 30 kPa), and , (d) SD1, (e) SD2, and (f) SD3, for the three Shelby tube peat specimens subjected to drained triaxial creep testing.

The was calculated for each strain value relative to the strain value at the beginning of each stress increment. Irrespective of the magnitude of the SIR used, the initial was the highest under the first q increment. The measured was the smallest under the second Δq and slightly higher under the subsequent Δq, at higher q. Thus, the trend indicates that, over the long term, the strain rate under the higher q could be higher than the under the smaller q.

The creep test in specimen SD2 began with a small Δq of 5 kPa (Table 6.2) and the SIR was kept equal to 1. The resulting ε_v – $log\ t$ curves (Fig. 6.4b) are similar in shape to that of specimen SD1 (Fig. 6.4a). Although the measured ε_v was the smallest, the was at its maximum under the first Δq irrespective of the SIR used. The decreased sharply with time under the smaller q and gradually under the larger q (Fig. 6.4e). was higher under the larger q during the later stage of tests. At the end of the test, the highest was under a q of 40 kPa (Fig. 6.4e).

Specimen SD3 was isotropically compressed under constant σ'_3 ranging from 33.5 to 204.5 kPa. The isotropic stress increments ($\Delta\sigma'_3$) varied between 3.5 and 80 kPa and the SIR from 0.2 to 1. The shape of the ε_v – $log\ t$ plots (Fig. 6.4c) at constant $\Delta\sigma'_3$ (3.5 kPa) were almost the same and the magnitude of ε_v was about 1% or less. A higher ε_v, ranging from 0.6 to 12.3%, was generated under larger $\Delta\sigma'_3$ (10 to 80 kPa). There was no unique trend in the plotted with time (Fig. 6.4f). The shapes of – $log\ t$ plots under constant $\Delta\sigma'_3$ (σ'_3 < 54.5 kPa) were similar, with a slightly higher strain rate under the first $\Delta\sigma'_3$. Similar to specimens SD1 and SD2, there was a faster decrease in under the smaller σ'_3 and a slower decrease in under higher σ'_3. For larger $\Delta\sigma'_3$ (SIR = 1), the – $log\ t$ plots are parallel to each other and there was higher under the higher σ'_3 (Fig. 6.4f).

Fig. 6.5 presents the development of ε_v and on two remoulded peat specimens under different q increments. Specimen RD1 was subjected to two stress increments and RD2 was subjected to seven stress increments of 10 kPa (SIR =

0.2 to 1) (Table 6.2). RD1 failed due to mechanical failure in the test setup at the beginning of the third stress increment.

Unlike the Shelby tube peat specimens, the development of ε_v in the remoulded peat specimen was not gradual (Fig. 6.5). In specimen RD1, higher ε_v and were measured under the second stress increment. ε_v – *log t* and – *log t* plots were similar and have almost parallel slopes (Figs. 6.5a, 6.5c). A number of sharp increases in volume change were observed. Specimen RD2 went through a series of compressions and dilations. Consequently, the ε_v – *log t* plots were not smooth (Fig. 6.5b). There was a decrease in ε_v during the dilation of the specimen. The total ε_v developed under all stress increments was 4.14%, which was much smaller than the ε_v developed in the Shelby tube specimen under similar stress increments. The was slightly higher under the first stress increment and almost the same under subsequent stress increments. The became negative under magnitudes of *q* above 50 kPa (Fig. 6.5d). There was reverse flow of drained water back to the peat specimen.

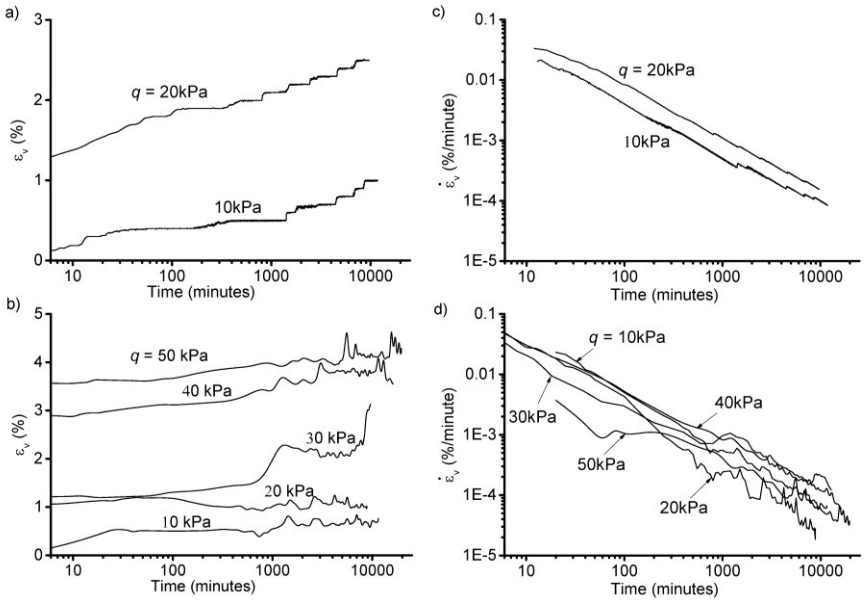

Figure 6.5. Development of ε_v, (a) RD1 (p'_0 = 40 kPa), (b) RD2 (p'_0 = 20 kPa), and (c) RD1, and (d) RD2, for two remoulded peat specimens under different *q* increments.

6.6.2 Development of pore pressure with time

Fig. 6.6 presents the measured pore pressure during the CD creep tests in three Shelby tube specimens. Under every stress increment, pore pressure increased instantly to the maximum value and gradually dissipated. The magnitude of the pore pressure generated depended on the SIR and the magnitude of Δq or $\Delta\sigma'_3$. In specimen SD1 (SIR < 0.5), the highest pore pressure (18 kPa) was generated under the first q (20 kPa) (Fig. 6.6a); in SD2 (SIR =1), the highest pore pressure (16 kPa) was recorded under larger q (2 and 40 kPa) (Fig. 6.6b). This pore pressure decreased significantly after 24 hours and remained below 5 kPa after one week (10^4 minutes). Under every other q increment, the pore pressure decreased to less than 5 kPa within 24 hours after the loading started.

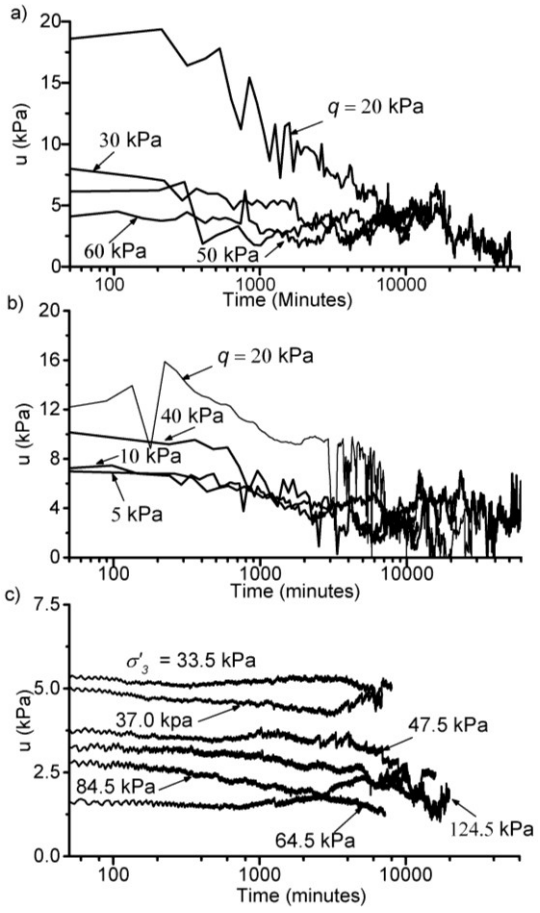

Figure 6.6. Measured pore pressure during CD creep tests on Shelby tube peat specimens (a) SD1, (b) SD2, and (c) SD3 under applied q and σ'_3 increments.

In specimen SD3, the pore pressure increased up to 5.5 kPa and remained near 5 kPa under every $\Delta\sigma'_3$. This small pore pressure generation is attributed to the application of small magnitude of $\Delta\sigma'_3$ (< 3.5 kPa) and SIR (< 0.5). There was a decreasing trend in pore pressure 24 hours after the loading started. This trend was significant under larger $\Delta\sigma'_3$ and under higher SIR.

In general, higher pore pressures were generated under the higher stress increments or under the first stress increment if the SIR was small. Under the same magnitude of q, higher pore pressures were observed in Shelby tube specimens than in remoulded peat specimens.

6.6.3 Development of creep strain and strain rate

The *log* – *log t* plots from CD creep tests in Shelby tube specimens (Fig. 6.4d, e, f) are not linear except for some stress increments with smaller SIR. These plots showed that, after some time elapsed following loading, a significant change occurred in the . Such deviations in *log* – *log t* plots have been reported in one-dimensional consolidation test results in peat (Wilson et al., 1965). The CD creep tests of the remoulded peat specimens did not show this behaviour (Figs. 6.5a, 6.5b). For most of the stress increments, this deviation of occurred at the same time after the pore pressure within the specimen gradually decreased to around 5 kPa. In specimens SD1 and SD2, this change occurred between 24 hours and one week (Figs. 6.4c, 6.4d). In specimen SD3, this deviation occurred at around 24 hours under smaller $\Delta\sigma'_3$ and between 24 hours and one week under large $\Delta\sigma'_3$ (Fig. 6.4f). In specimens SD1 and SD3, no significant change occurred in under stress increments in which the pore pressure remained almost constant throughout the loading period.

The initial slope of the *log* – *log t* curve was comparable to primary consolidation. The later stage of straining, which mostly occurred under constant or minimum pore pressures, was creep strain under constant stress conditions. At this later stage, the in all peat specimens under most of the stress increments was less than 10^{-3} %/minute. Thus, the below 10^{-3} %/minute could be

considered creep strain. The generated at the later stage in creep tests of Shelby tube specimens can be expressed in terms of Eq. [6.1], which represents the linear decrease of *log* with *log t*, such that

– , ----- [6.1]

where *m* is the slope of *log* – *log t* plots or the measure of the decrease in strain rate with time. According to the classical approach of volumetric creep (is only the function of time), this parameter should be equal to 1.0 in 1D loading (Tavenas et al., 1978). However, the test results indicate much lower values of *m,* which vary between 0.6 to 0.2, for Shelby tube specimens under deviatoric stress incrments. An almost constant value of *m* (≈ 0.70) is found for all stress increments applied to isotropically compressed Shelby tube specimens. Higher values of *m* (0.75 to 0.9) were found for remoulded peat specimens. The parameter β includes a stress function that defines the development of at different stress states. t_i and *t* are the current and reference time, respectively.

The small values of *m* for the Shelby tube specimens might account for the presence of highly compressible layers of peat fibres with gas bubbles (Acharya et al., 2015). These layers are continuously compressed without decreasing the strain rate. Thus, the development of strain was gradual in Shelby tube specimens whereas the ε_v developed instantly after the placement of the stress increment and considerably decreased later in remoulded peat specimens.

A higher *m* value indicated a faster decrease in with time and a smaller *m* value indicated a slower decrease in . In the Shelby tube specimens, the value of *m* was dependent on the magnitude of the stress increment (Δq or $\Delta\sigma'_3$), SIR, and the difference between the current mean pressure (p') and initial consolidation pressure (p'_0). Higher initial stress increments generated higher ε_v but the decreased rapidly and, consequently, the *m* value was higher. A comparatively longer time was needed to decrease the same amount of under the small stress increments and ε_v. similar behaviour has been reported in

relatively over-consolidated clay (Tavenas et al., 1978). Decreasing the equal magnitude of in *log* – *log t* plots under different stress increments may take the same amount of time but will generate a lower or higher ε_v unless the *log* – *log t* plots are parallel to each other.

6.6.4 The rheological behaviour of peat

Fig. 6.7 presents the ε_v - *log* plot for different stress increments from specimens SD1, SD2, and SD3. There is first a rapid decrease in at small values of ε_v followed by a sharp increase in the ε_v. At a higher ε_v, the decreased progressively. In specimens SD1 and SD2 , 1 to 10% of the ε_v was developed with the decrease in from 1×10^{-3} to 1×10^{-4} %/minute (Fig. 6.7a). In specimen SD3, the ε_v was 0.5 to 6% corresponding to a decrease in the strain rate from 1.5×10^{-2} to 1×10^{-4} %/minute (Fig. 6.7b). From these portions of the ε_v - *log* plots, the stress-strain relationship for the development of creep rate ( ) can be defined.

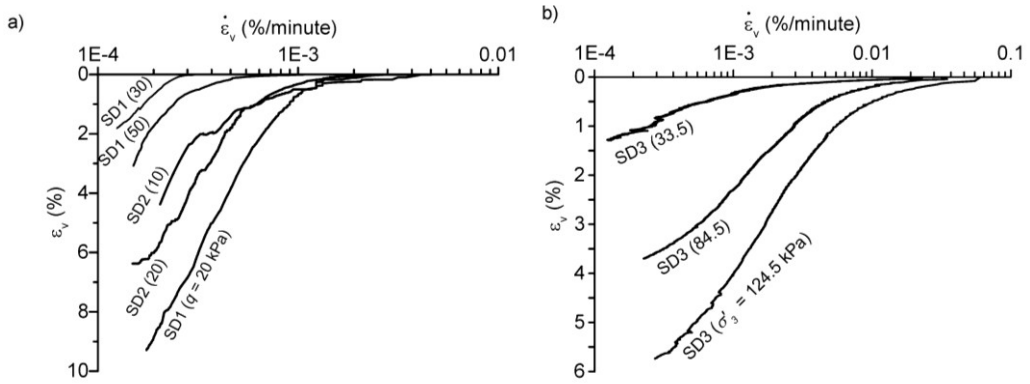

Figure 6.7. Strain-strain rate variation for creep tests on Shelby tube specimens under (a) q and (b) σ'_3 increments.

The rheological behaviour of clay has been expressed for three different conditions, including the analysis of (a) strain at a constant strain rate, (b) strain rate at a constant loading duration, and (c) strain rate at a constant strain. Fig. 6.8 presents the ε_v developed at a constant under multiple stress increments. These

ε_v - *log p'* plots for both q (Fig. 6.8a) and σ'_3 loading (Fig. 6.8b) produced a series of parallel lines. These constant strain rate lines are the creep isotaches in the strain-stress plane. Creep isotaches for specimens SD1 and SD2 are plotted parallel to each other regardless of the different SIRs and loading durations used during the creep tests. The creep isotaches under σ'_3 (specimen SD3) (Fig. 6.8b) had a lower slope than the creep isotaches produced under q loading (specimens SD1 and SD2).

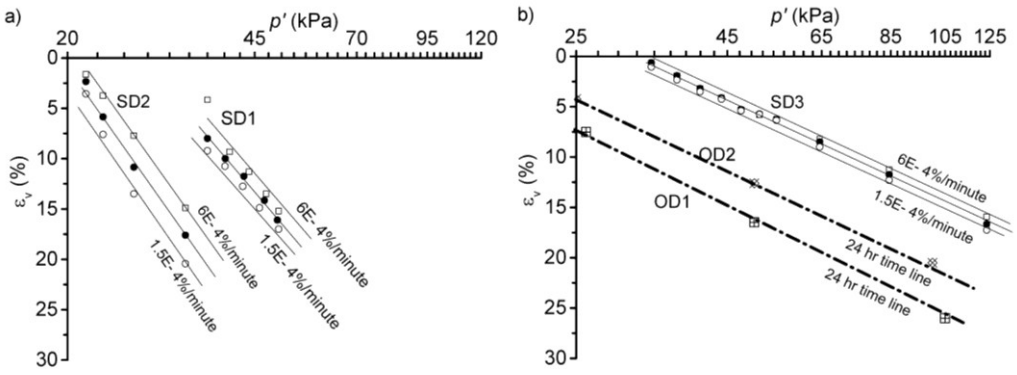

Figure 6.8. Plot of creep isotaches versus mean pressure (p') to define the stress-strain relationship during CD creep tests on Shelby tube specimens under (a) q and (b) σ'_3 increments.

Together with the isotaches, Fig. 6.8b presents the plot of strain measured during one-dimensional consolidation tests (OD1 and OD2) under 1D stress increments ($\Delta\sigma'_v$) varying between 25 and 100 kPa. The lines joining the strains developed 24 hours after the beginning of loading, i.e., normal consolidation lines (NCL) are plotted parallel to the isotaches from SD3. As the slopes of the Isotropic consolidation lines (Iso-NCL) and NCL plots are parallel to each other (Atkinson, 1978), this implies that, in the strain-stress (ε_v - p') plane, the isotaches derived for σ'_3 loading are parallel to both 1D NCLs and Iso-NCL respectively, whereas the creep isotaches derived for q loading plot away from the Iso-NCL line. Similar behaviour is reported for normally consolidated clay (Graham et al., 1983). This result is analogous to the variation of specific volume

in the ε_v - p' plane during conventional CD tests on normally consolidated soil. Within the same specimen, the linearity of creep isotaches showed that the slope of ε_v - *log* t plots under different $\Delta\sigma'_3$ and Δq at values smaller than 1×10^{-3} %/minute can be considered parallel to each other. At this or smaller , the constant lines presented in Fig. 6.8 will be identical to the equal duration of loading lines defined by Bjerrum (1967). This implies that the magnitude and number of stress increments ($\Delta\sigma'_3$ or Δq), i.e., the history of loading, do not influence the development of creep strain. Thus, the rheological behaviour of peat can be uniquely expressed in terms of current stress, strain, and strain rate using

$$R\ (p',\ \varepsilon_v,\ \ ) = 0. \qquad \text{-----[6.2]}$$

From the series of constant strain and constant stress tests, Leroueil et al. (1985) proved this expression for the rheological behaviour of clay. They found that the rate of effective stress (') did not influence the rheological behaviour of clay. This uniqueness of p'-ε_v- has been used to define the 1D creep behaviour of clay and peat (Den Haan, 1996; Kim and Leroueil, 2001). The isotaches presented in Fig. 6.8b are equivalent to the creep isotaches reported by Den Hann (1996) for 1D loading conditions. Thus, even in a non-isometric stress state, the development of at a particular void ratio (e) or strain (ε_v) and under stress conditions (p') can be defined relative to the NCL or Iso-NCL. According to the Taylor-Bjerrum model, the NCL and Iso-NCL are also the line of constant where C_α is constant (Tavenas et al., 1978).

Some scatter in the plot of ε_v (Fig. 6.8a) for specimens SD1 and SD2 was due to the faster decrease of strain rate under the first Δq (Fig. 6.7a). The linearity was mostly valid between the ε_v and p' for values less than 1×10^{-3} %/minute. The vertical distance between two isotaches represented the development of strain at constant p' while the decreased with time. The constant gap between creep isotaches, except some scatter at smaller initial stress increments, indicated the development of almost constant creep strain under different p' at the same rate of

decrease in . Some variation in the development of ε_v under *p'* higher than 100 kPa was noted for specimen SD3. For the same decrease in , a higher creep strain was developed under higher *p'*. This indicated that there was an increase in C_α under higher mean pressure in specimen SD3, but C_α was almost constant for the loading range applied in specimens SD1 and SD2.

There was a notable difference in the ε_v developed at a constant in specimens SD1, SD2, and SD3 (Fig. 6.8). This variation accounted for the effect of the stress state in the development of creep strain. Under the same *p'* and same magnitude of the decrease in , a smaller amount of ε_v developed under σ'_3 increments (specimen SD3), which can be seen from the smallest gap between isotaches (Fig. 6.8b). Comparing specimens SD1 and SD2 under *q* increments, more ε_v developed in specimen SD2. The loading of specimens SD2 and SD1 began at p'_0 = 20 and 30 kPa, respectively. Thus, in *q* - *p'* space, the stress state in SD2 was near the tension line, resulting in the development of higher strain (Fig. 6.3c).

Fig. 6.9 presents the plot of variation of with *p'* at various loading durations (*t*) for specimens SD1, SD2, and SD3. For specimen SD3, the strain rate only from σ'_3 increments with SIR values greater than 0.5 are considered. These *log* - *p'* plots are different from the equal duration of loading lines (e.g., Bjerrum, 1967) mentioned previously. At any given time and stress state, a linear relationship exists between *log* and *p'*. Similar to the ε_v, the was smaller under σ'_3 increments at any loading duration (specimen SD3) (Fig. 6.9b). This is valid for the range of *p'* between 20 and 130 kPa. The highest values were recorded in specimen SD2. In spite of the smaller SIR used in specimen SD1, the between t = 5,000 to 15,000 minutes are plotted between specimens SD2 and SD3. For the time range considered in specimens SD2 and SD3, there is a faster decrease in the in specimen SD3 (σ'_3 increments).

The relationship proposed by Singh and Mitchel (1968) to describe the axial and deviatoric strain was used to describe the development of at different stress

states. This correlation is also used to express volumetric strain rate (Tavenas et al., 1978). The correlation between , *p'*, and time (*t*) is presented in combination with Eq. [6.1] in Eq. [6.3]:

– . ----- [6.3]

The first part (additional to Eq. [6.1]) in Eq. [6.3] is the stress function required to define the . The creep parameter α, which is the slope of the *log* - *p'* lines, varied with time and stress state. For the loading duration considered in Fig. 6.9, α slightly increased with time. α is also slightly higher in the isotropic stress state than in the deviatoric stress state. β is the ordinate value of at the beginning of creep and a function of *p'*. For the strain rate presented in Fig. 6.9, the at the beginning of creep is assumed to be 1×10^{-3} %/minute. This reference depends on many factors, including the stress state, SIR, and magnitude of *p'*.

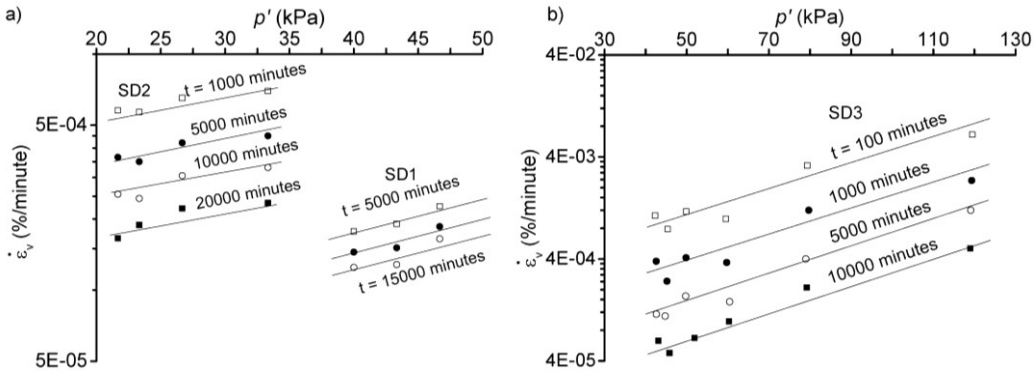

Figure 6.9. Plot of development of at constant loading duration with *p'* from CD tests on Shelby tube specimens under a) *q* and b) σ'_3 increments.

Fig. 6.10 presents a plot of the variation of with mean pressure (*p'*) at various strains (ε_v) in specimens SD2 and SD3. The strain rates considered are those from stress increments with SIR values greater than 0.5, as the strain rate developed from stress increments with SIRs less than 0.5 are influenced by stress history. At any time, a linear relationship exists between log and *p'*. The relationship between the axial strain and shear stress based on rate process

theory, proposed by Murayama and Shibata (1964), is found to be applicable for describing the presented in Fig. 6.10. The values are expressed in terms of *p'* such that

— . ----- [6.4]

This relationship has been used to describe the rate of secondary consolidation in the one-dimensional consolidation of fibrous peat (Berry and Poskitt, 1972). The creep parameters α and β are found to decrease with the increase in strain but be almost constant at different stress states. β is the ordinate value of the at the beginning of creep and α is the slope of the *log* - *p'* line (Fig. 6.10). The limitation of using this approach to express the relationship between and *p'* is that the relationship can only be verified for strain developed under smaller stress increments.

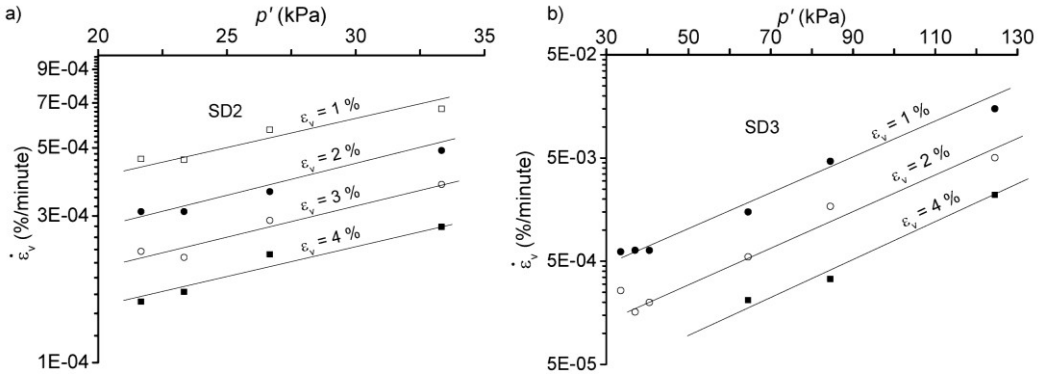

Figure 6.10. Plot of development of at constant strain with (*p'*) in CD tests on Shelby tube specimens under a) *q* and b) σ'_3 increments.

6.6.5 Development of axial strain during CD test

The time dependency of strain developing in clay subjected to any type of stress condition has been described by separate consideration of ε_v and ε_q (Kavezajian and Mitchell, 1977; Tavenas et al., 1978; Yin and Graham, 1999). Shear strain can be directly investigated by means of undrained triaxial tests or calculated indirectly from measured ε_a and ε_v. This calculation needs to assume some value

of Poisson's ratio. In fibrous peat, the calculation of Poisson's ratio (ν) is rather vague. The development of axial strain is presented, as this also includes shear strain.

Fig. 6.11 presents the development of ε_a and on two Shelby tube specimens, SD1 and SD2, under different Δq. The shapes of the ε_a - *log t* curves (Figs. 6.11a, 6.11b) are similar to those of the ε_v - *log t* curves presented in Fig. 6.4. At small Δq, the axial strain remained small; at large Δq, large deformations developed rapidly. Similar to ε_v, the development of ε_a depended on SIR. Higher initial Δq and small SIR (< 0.5) in specimen SD1 produced a higher ε_a under the first stress increment. A smaller initial Δq and higher SIR in specimen SD2 produced a smaller ε_a under the first stress increment. The ε_a measured for specimens SD1 and SD2 was about 18 and 15% higher, respectively, than the magnitude of the ε_v.

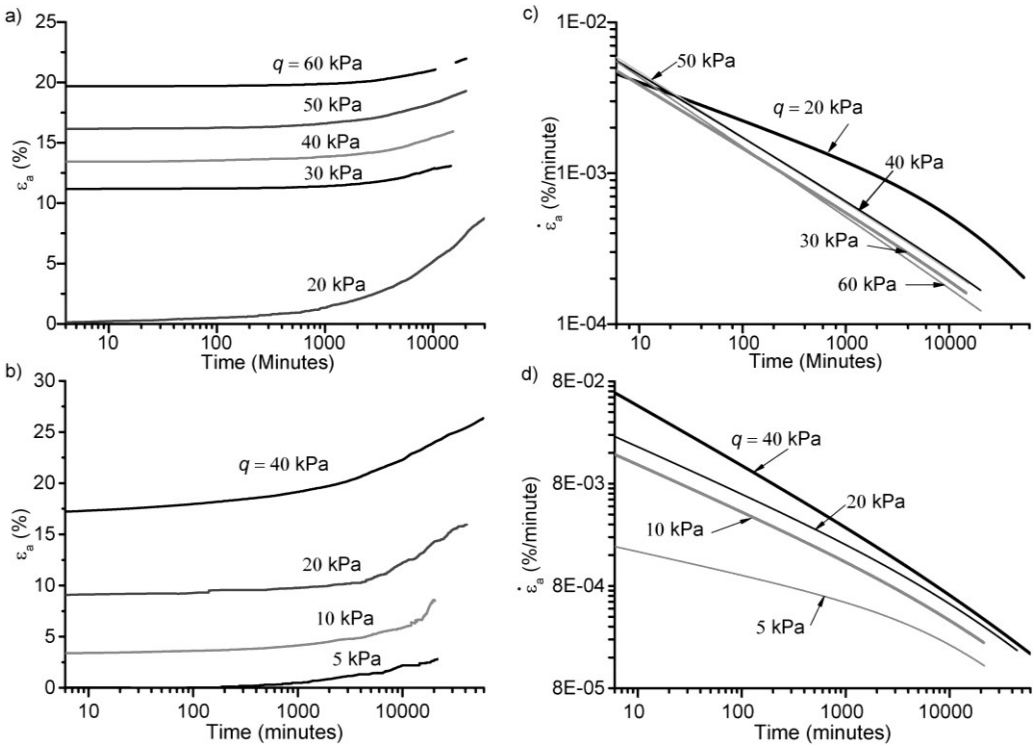

Figure 6.11. Development of ε_a in specimens a) SD1, and b) SD2 and in specimens c) SD1, and d) SD2 with time under different q increments.

The - *log t* plots (Figs. 6.11c, 6.11d) varied slightly from the - *log t* plots presented in Fig. 6.4. The again depended on the SIR. In specimen SD1 (SIR < 0.5), the was highest under the first Δq (Fig. 6.11c) and decreased significantly nearly 1,000 minutes after the loading started. Unlike the - *log t* plots, the - *log t* plots for subsequent q increments were linear with almost parallel slopes. At the end of the tests, there was a higher rate of decrease of under the first Δq than under subsequent Δq (higher q). In specimen SD2 (SIR =1), the increased under larger Δq (higher q) (Fig. 6.11d). The was largest under the largest Δq (q = 40 kPa). The – *log t* plot showed that there was a slight decrease in after 24 hours. At the final stage of the test, the slopes of the – *log t* plots under each Δq were almost parallel to each other, suggesting a constant decrease in axial strain rates.

Fig. 6.12 presents the development of ε_a and on two remoulded peat specimens under different Δq. Except for some sharp increases in ε_a, the ε_a – *log t* plots are smooth and have slopes that parallel one other (Figs. 6.12a, 6.12b). In specimen RD1 (SIR = 1), higher ε_a and were developed under the second Δq. The slopes of the log – *log t* plots were almost parallel to each other (Fig. 6.12c).

The ε_a – *log t* plots for specimen RD2 (Fig. 6.12b) are different from the ε_v – *log t* plots (Fig. 6.5b). Irrespective of lower SIR (<1), larger ε_a were developed under subsequent Δq (higher q). This development of larger ε_a under higher q was due to the dilation of the specimen. The total ε_a developed under all Δq was 12%, nearly three times the total ε_v generated (Figs. 6.5b, 6.12b). The – *log t* plots for the first and second Δq (SIR =1) were parallel to each other but the plots became flatter under subsequent Δq (higher q) (Fig. 6.12d). At the initial stage of loading, the maximum was developed under the first Δq (q = 10 kPa) but at the later stage was at a maximum for q = 50 kPa.

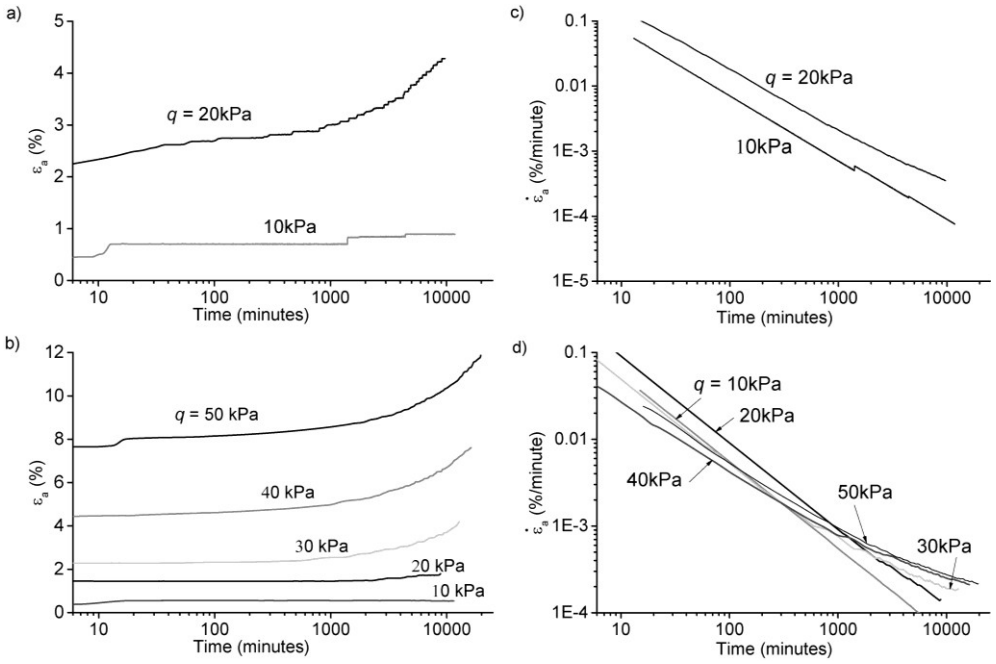

Figure 6.12. Plot of development of ε_a in specimen a) RD1, and b) RD2 and in c) RD1, and d) RD2 with time.

6.6.6 Development of axial creep strain and strain rate

The *log* – *log t* plots (Figs. 6.11c, 6.11d, 6.12c, 6.12d) are not linear except under Δq with smaller SIR in the Shelby tube specimens and under smaller Δq in remoulded peat specimens. For specimen SD2, this linearity increased at higher q. Similar to that in the *log* – *log t* plots (Fig. 6.4), there was some decrease in the in Shelby tube specimens (Fig. 6.11) together with the decrease in u after some time (between 1,000 to 10,000 minutes) elapsed following loading (Figs. 6.11c 6.11d). The *log* – *log t* plots for remoulded peat specimens did not show this deviation (Figs. 6.12c, 6.12d). In specimen RD2, the decrease in slowed down 24 hours after the loading began, following dilation of the specimens.

Similar to the ε_v, the ε_a that developed at the later stage of tests under constant pore pressure is axial creep strain developed at constant stress. At this stage, the values in both the Shelby tube and remoulded peat specimens under all Δq are

less than 1×10^{-3} %/minute. These at the later stages of the creep tests can be expressed by the same relationship presented in Eq. [6.1], i.e.,

– , ----- [6.5]

where m is the slope of the *log* – *log t* plots (Figs. 6.11c, 6.11d, 6.12c, 6.12d). The values of m varied between 0.45 and 0.7 for the Shelby tube specimens. Higher values of m (0.55 to 0.95) were observed in remoulded peat specimens. The parameter β includes a stress function that defines the development of under different stress conditions. A higher m value indicates a faster decrease in with time. The value of m was dependent on the magnitude of Δq and the SIR. The higher ε_a that developed under higher initial Δq or under higher SIR has a faster decrease in , resulting in a higher m value. The smaller ε_a that developed under the smaller initial Δq and smaller SIR resulted in a smaller m value. The higher value of m in the *log* – *log t* plots compared to the *log* – *log t* plots was due to the development of higher axial strain at the later stages of the tests.

Fig. 6.13a presents the ε_a plotted with *log* for different Δq from specimens SD1 and SD2. Depending on the magnitude of Δq and SIR, there was first a rapid decrease in at low ε_a followed by a sharp increase in ε_a. At higher ε_a, the decreased progressively. The ε_a developed between 2 to 10% with the decrease in from 1×10^{-2} to 1×10^{-4} %/minute. Fig. 6.13b presents the cumulative ε_a developed at constant under multiple Δq in specimens SD1 and SD2. Similar to constant lines presented in Fig. 6.8b, constant lines plotted against q produced a series of parallel lines or creep isotaches for ε_a. The creep isotaches from specimens SD1 and SD2 plotted parallel to each other irrespective of the magnitude of the Δq and SIR applied. However, at higher q the constant lines for SD1 and D2 diverged from one another. Similar to that for ε_v, a larger magnitude of ε_a developed in specimen SD2 for the same decrease in . The linearity of constant lines showed that the history of loading did not influence

the development of axial strain. Thus, Eq. 6.2 is equally valid for the development of axial creep strain and consequently for shear strain. Except for some scatter in the initial phase of the tests, the linearity of ε_a - *log q* was largely valid for values less than 1×10^{-3} %/minute. The vertical distance between two isotaches represented the development of ε_a at constant q while the decreased with time (Fig. 6.13b). This gap was almost constant in specimen SD1 but this gap increased in SD2 at the later stage of loading. This showed the gradual development of larger axial strain (shear strain) at higher q, i.e., near the tension line (Fig. 6.3).

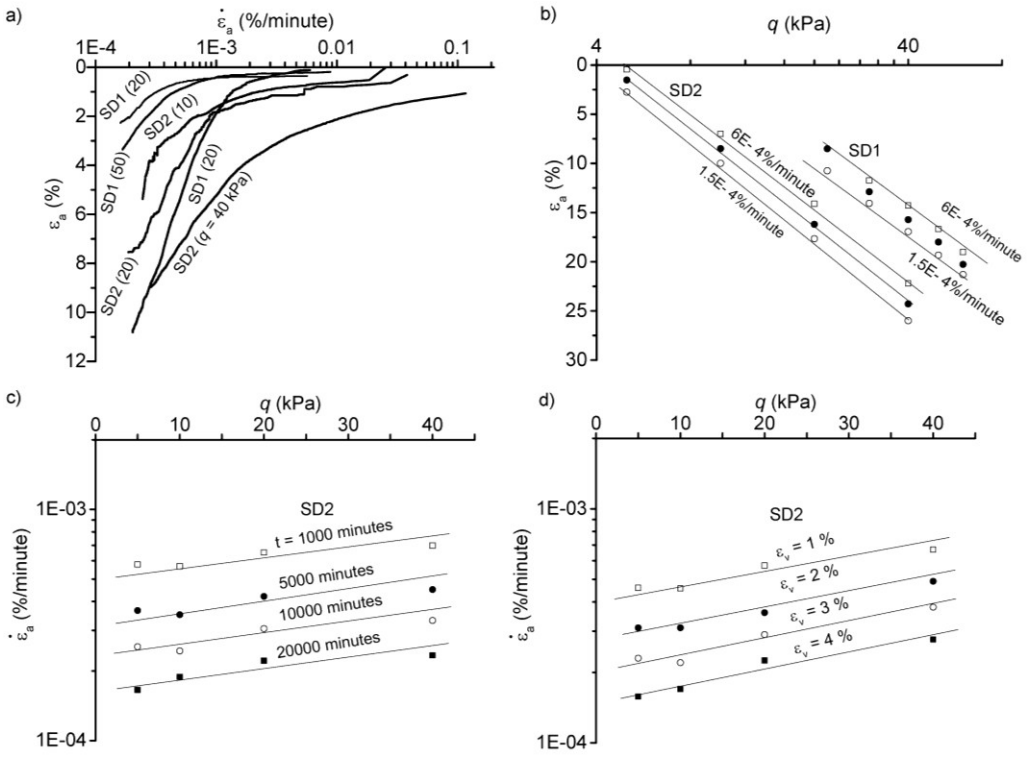

Figure 6.13. Plot of development of a) ε_a with , b) ε_a at constant , c) at constant duration (t), and d) at constant ε_a in Shelby tube specimens under different q increments.

Figs. 6.13c and 6.13d respectively present plots of the variation of with q at various loading durations and various ε_a in specimen SD2. At any time, a linear relationship exists between *log* and q, and the lines are identical to the *log* –

p' lines (Fig. 6.9). At any loading duration, is larger than (Figs. 6.9a, 6.13c). The *log* - *q* lines are not exactly parallel; there is a tendency to have a larger decrease in strain rate under a large *q*. The relationship proposed by Singh and Mitchel (1968) presented in Eq. [6.3] can again be used to describe the in terms of *q* and *t* in combination with Eq. [6.5], as follows:

– . ----- [6.6]

For the time considered in this correlation, α (the slope of the *log* - *q* lines) increased with time. β is the ordinate value of at the beginning of creep. For these tests, at the beginning of creep is assumed to be 1×10^{-3} %/minute. t_i and *t* are the current and reference times, respectively. The reference varied with the size of the *q* increment.

Similarly, the linearity between *log* and *q* at various strain states (Fig. 6.13d) can be described by the relationship presented in Eq. [6.4]. The mean pressure is replaced by *q*, such that:

— . ----- [6.7]

The creep parameters α and β are found to decrease with the increase in ε_a. β is again the ordinate value of the strain rate at the beginning of creep and α is the slope of *log* - *q* line.

6.6.7 Poisson's ratio

Fig. 6.14 presents the plot of ε_v versus ε_a for two Shelby tube specimens (Fig. 6.14a) and two remoulded peat specimens (Fig. 6.14b). Irrespective of the number of stress increments, different SIR values, and the unequal duration of loading, the ε_v - ε_a plots were linear for the Shelby tube specimens and linear to an extent for the remoulded peat specimens. In specimen RD2, there was some scatter in the plot as the specimen went through a series of compressions and dilations. After 4.5% of ε_v, the generation of ε_a was almost at a constant volume.

The slopes ($\varepsilon_v/\varepsilon_a$) of the ε_v - ε_a plots were 0.85 and 0.82 for specimens SD1 and SD2, and 0.58 and 0.62 for specimens RD1 and RD2, respectively. A slope ($\varepsilon_v/\varepsilon_a$) near to unity represents the straining for the 1D condition with a negligible deviatoric strain. The $\varepsilon_v/\varepsilon_a$ also represents the ratio of change in a cross-sectional area of specimens relative to the cross-sectional area at the beginning of the tests. The calculated ratios were consistent with the measured dimensions of the specimens after the tests.

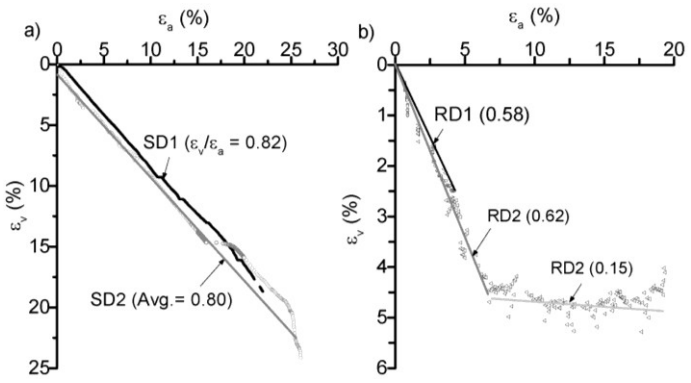

Figure 6.14. Plot of ε_v verses ε_a developed during CD creep tests on a) Shelby tube, and b) remoulded peat specimens.

Fig. 6.15 presents the calculated lateral strain (ε_r) and drained Poisson's ratio (ν) for Shelby tube (Figs. 6.15a, 6.15c) and remoulded (Figs. 6.15b, 6.15d) peat specimens. The CD test specimens underwent lateral compression during pre-consolidation and bulged very slightly under q increments, essentially undergoing one-dimensional compression. The calculated value of ν ranged from 0.08 to 0.13 for the Shelby tube specimens and 0.19 to 0.27 for the remoulded peat specimens. The ν for constant volume straining at the later stage of the tests of specimen RD2 varied between 0.4 and 0.45. These values of ν for Shelby tube and remoulded peat from northern Alberta, Canada are within the range reported in the literature (Rowe et al., 1984; Zwanenberg, 2005; Tan, 2008; O'Kelly and Zhang, 2013).

6.6.8 Development of undrained creep strains

Figs. 6.16 and 6.17 respectively present the measured undrained axial strains (ε_{ad}) and undrained axial strain rate ( ) in two Shelby tube specimens, SU1 and SU2, and two remoulded peat specimens, RD1 and RD2. Each specimen was subjected to four to seven q increments (Δq) at SIR values ranging from 0.15 to 1 (Table 6.2).

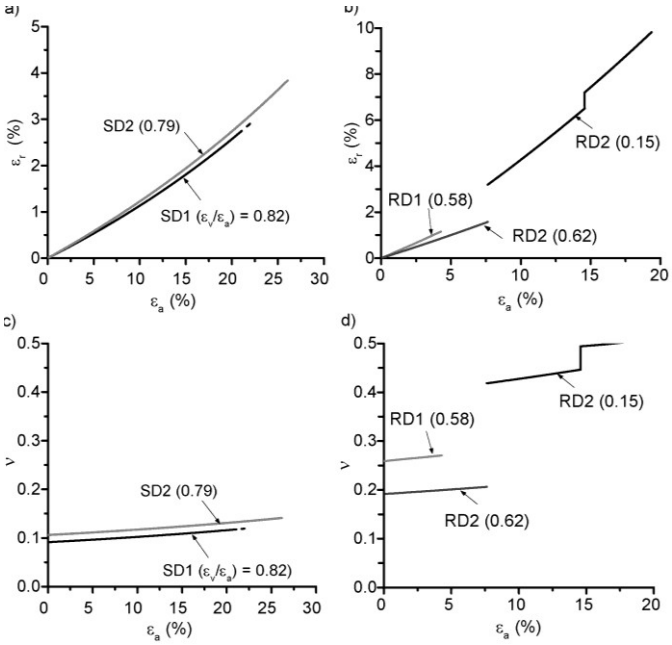

Figure 6.15. Plot of calculated ε_r versus measured axial strain on a) Shelby tube, and b) remoulded peat specimens and ν versus axial strain on c) Shelby tube, and d) remoulded peat specimens.

In both Shelby tube and remoulded peat specimens, the shapes of the ε_{ad} - *log t* curves (Figs. 6.16a, 6.16b, 6.17a, 6.17c) are similar to those of the ε_a - *log t* curves (Figs. 6.11 6.12) except at the time of failure. The Shelby tube specimens underwent a slow and small deformation under a small q (< 20 kPa) and rapid and large deformations at q values above 20 kPa (Figs. 6.16a, 6.16b). The remoulded peat specimens gradually deformed under q increments varying between 20 to 50 kPa and rapidly deformed to failure at q values above 50 kPa. Both the Shelby tube and remoulded specimens failed when ε_{ad} exceeded 15%.

Both Shelby tube specimens, SU1 and SU2, failed at a q of 40 kPa. Two remoulded peat specimens, RD1 and RD2, failed at a q of 60 and 80 kPa, respectively. Unlike the ε_a developed in CD tests, the ε_{ad} in CU tests were larger under the larger q, regardless of the magnitude of Δq and SIR applied. Some periodic sharp rises in ε_{ad} were observed in both remoulded and Shelby tube specimens. These rises were more significant under small q.

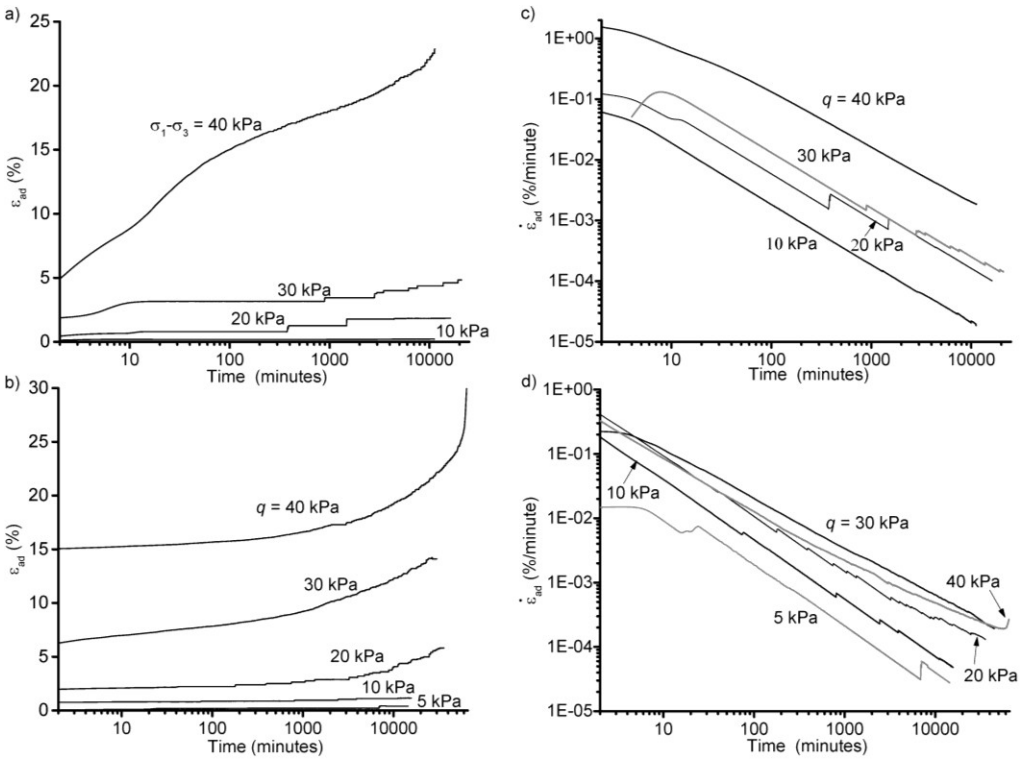

Figure 6.16. Plot of development of ε_{ad} in Shelby tube peat specimens a) SU1 (p'_0 = 30 kPa) and b) SU2 (p'_0 = 20 kPa) and in specimens c) SU1 and d) SU2 with time during CU creep tests.

The linear decrease in the slope of the *log* – *log t* plots (Figs. 6.16c, 16d, 6.17c, 6.17d) was identical in both Shelby tube and remoulded peat specimens. The plots were similar to what has been reported for undrained tests on clay (Tavenas et al., 1978; Zhu et al., 2011) but different from the *log* – *log t* plots of the CD test results (Figs. 6.11, 6.12). Similar to ε_{ad}, a larger developed under a higher q, irrespective of SIR. The highest was measured under the Δq

causing the failure of the specimen. The failure was initiated by rapidly increasing either just after loading began (specimen SU1) (Fig. 6.16c) or by slowly accelerating the strain rate for a long time after the placement of that stress increment (specimens SD2, RD1, and RD2) (Figs. 6.16d, 6.17c, 6.17d). A strain hardening effect resulting in the deceleration of the strain rate under some stress increments was observed (Figs. 6.16c, 6.17d). Except for specimen SU2, the failure occurred under the q value that was twice the p'_0. Under some stress increments, there were a series of sharp rises in associated with the sharp increase in ε_{ad}. Due to these sharp increases in , the slope of the log $-$ log t plot decreased in the later stages of the tests.

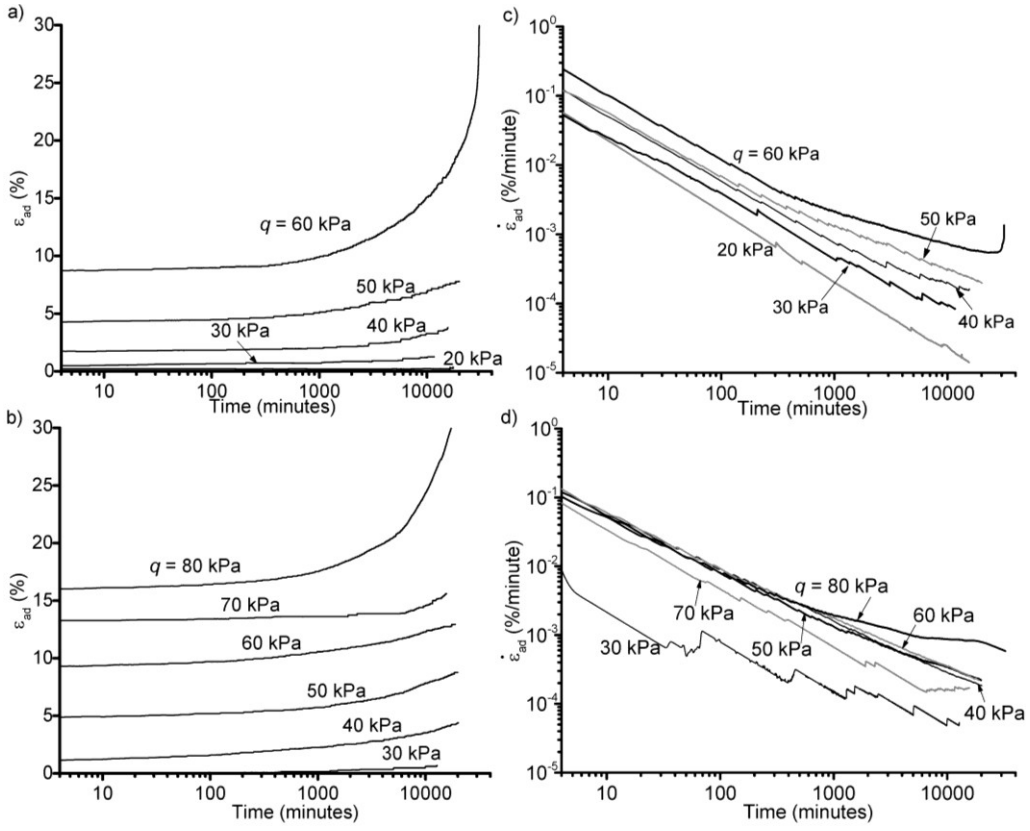

Figure 6.17. Plot of development of ε_{ad} in remoulded peat specimens a) RU1 (p'_0 = 30 kPa) and b) RU2 (p'_0 = 40 kPa) and in specimens c) RU1 and d) RU2 with time during CU creep tests.

6.6.9 Development of undrained pore pressure with time

Fig. 6.18 presents the measured increased in pore pressure (u) during the CU creep tests on the Shelby tube and remoulded peat specimens. The generation and dissipation of the pore pressure was independent of SIR and the magnitude of the stress increments. In both the Shelby tube and remoulded peat specimens, the pore pressure instantly increased after the placement of stress increments. The magnitude of the instant increase in pore pressure was largest under the first stress increment and decreased under the subsequent increments. In Shelby tube specimens SU1 and SU2, the pore pressure that developed under the first q increment was more than the applied magnitude (Figs. 6.18a, 6.18b). In the remoulded peat specimens, the increase in pore pressure was nearly two-thirds of the magnitude of the first stress increment (Figs. 6.18c, 6.18d). Under the subsequent stress increments in both the remoulded and Shelby tube specimens, the pore pressure increased gradually to a maximum value equal to (Figs. 6.18a, 6.18c, 6.18d) or even larger (Fig. 6.18b) than the effective confining pressure. In specimen SU2, the increase in pore pressure was higher than the effective confining pressure by 7 kPa.

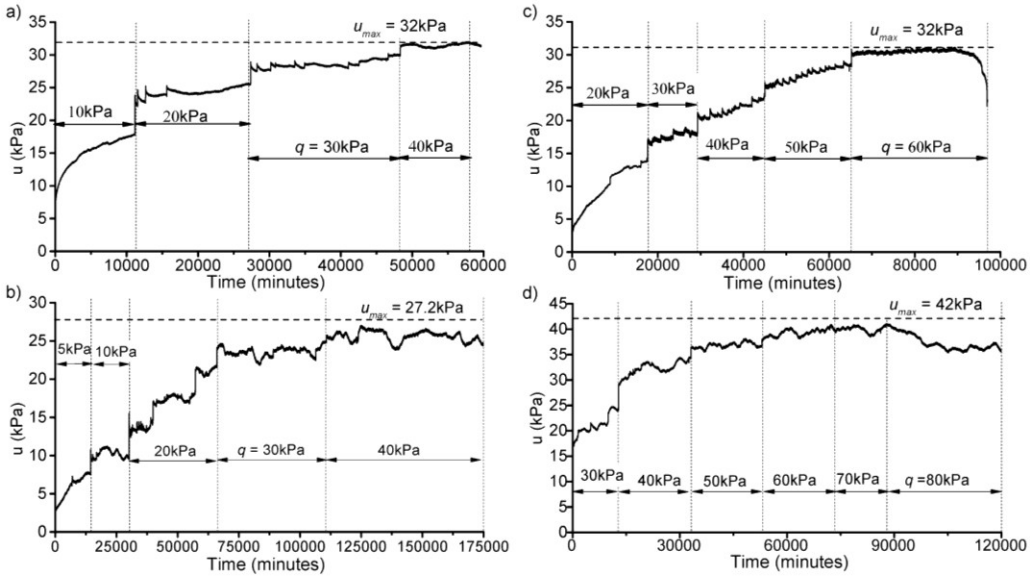

Figure 6.18. Measured pore pressure during CU creep tests on Shelby tube and remoulded peat specimens a) SU1, b) SU2, c) RU1, and d) RU2.

Previous studies have reported the development of higher pore pressures, higher or equal to the cell pressure, during undrained tests in peat (Yamaguchi et al., 1985; Farrell and Habib, 1998; Farrell, 2012). Some of the given reasons for the development of pore pressure higher than the applied q include: i) the anisotropic nature of peat specimens with higher stiffness in the horizontal direction (Hendry et al., 2012) and ii) the compression of gas bubbles existing within the peat fibres (Acharya et al., 2015). The higher pore pressure measured in Shelby tube specimens supports both of these concepts. The Shelby tube specimens have intact horizontally-oriented fibres and might have higher gas content within the fibres.

Some periodic sharp increases in pore pressure were observed in both remoulded and Shelby tube peat specimens. These increases were associated with the sharp increase in axial strain discussed in section 6.5.8 (Fig. 6.18). These sharp increases in pore pressure under the constant q dissipated gradually to the lower value, and then the next cycle started. The duration of the dissipation was proportional to the rise in pore pressure. These sharp rises in pore pressure were considered to be due to the release of gas bubbles from the peat fibre to the pore voids of the peat matrix.

The failure of the specimens started when the pore pressure approached the effective confining pressure (ε_{ad} = 10 to 15%). The developed rapidly and reached its maximum value within 30 minutes to two hours. At the time of failure, the pore pressure inside the specimen was higher than the cell pressure. Thus, it was rather difficult to judge the reason for failure. The failure of some specimens was due to bulking, and at least one (specimen SU2) failed under shear deformation. The pattern of failure might have some correlation with the length of the fibres. Specimen SU2, still a Shelby tube specimen, had a much shorter fibre length than specimen SU1, which might be what made it possible to develop a shear plane.

6.6.10 Development of undrained creep strain rate

The *log* – *log t* plots from CU creep tests of the Shelby tube and remoulded specimens (Figs. 6.16c, 6.16d, 6.17c, 6.17d) are mostly linear except at the time of failure. Irrespective of the SIR, was higher under higher *q* except in specimen RD2. In specimen RD2, strain hardening behaviour was observed for *q* values greater than 50 kPa, resulting in the development of a strain rate less than under the smaller *q*. The increase in occurred together with the increase in axial strain under the higher *q*. Consequently, pore pressure within the specimen increased to the maximum value. As it was difficult to conclude whether failure occurred due to the shearing or buckling of specimens, the during the failure of specimens is not only the the shear creep strain rate.

Similar to the developed at the later stage of CD creep tests, the developed both in the remoulded and Shelby tube specimens during the CU tests except at failure can be expressed by the relationship presented in Eq. [6.1], as follows:

– . ----- [6.8]

The parameter β includes a stress function that defines the development of at different *q*. *m* is the slope of the *log* – *log t* plots (Figs. 6.16c, 6.16d, 6.17c, 6.17d). The value of *m* varied between 0.75 and 0.95 for Shelby tube specimens and between 0.6 and 0.95 for remoulded peat specimens. Smaller values of *m* indicated a slower decrease in and higher values of *m* indicated a faster decrease in with time. *m* values below 0.6 were associated with a sharp increase in the strain rate, corresponding to the sharp increase in axial strain at the later stages of the tests. The value of *m* was largely independent of the magnitude of stress and the SIR. Under small *q,* the strain developed instantly and stayed almost constant, resulting in a faster decrease of and a higher *m* value. Under higher *q*, ε_{ad} developed gradually over a long time, resulting in a slower decrease of with time and a smaller *m* value. For strain rates below 5×10^{-2} %/minute, the *log* – *log t* plots for all stress increments except during

failure can be considered parallel to each other and be used to analyse the stress function mentioned in Eq. 6.7.

Figs. 6.19a and 6.19b present the plots of the variation of with q at various loading durations t in two Shelby tube specimens, SU1 and SU2. At any time, a linear relationship exists between log and q. The relationship proposed by Singh and Mitchel (1968) and presented in Eq. [6.3] can again be used to describe the in terms of q and time t in combination with Eq. [6.8], as follows:

– . ----- [6.9]

For the time considered in this correlation α, the slope of the log – log t plot, increased with time. β is the ordinate value of under the current q at the beginning of creep. For these tests, β (also called the reference strain rate) is assumed to be 5×10^{-2} %/minute. t_i and t are the current and reference times, respectively. The reference strain rate may change with the amount of the q increment.

6.7 Discussion

The present investigation considered the time-dependent development of volumetric, axial, and shear strain in Shelby tube and remoulded peat specimens collected from beneath a railway embankment in northern Alberta, Canada. Peat itself is characterized by physical variability. The specimens studied varied in terms of density as well as water and fibre content (Table 6.1). Some of the specimens were not homogeneous and the surfaces were not smooth. By saturating and consolidating all of the specimens at a similar total or effective stress, it is assumed that all specimens achieved homogeneity. However, significant variability in the test results was expected and consequently the comparative analysis of such test results was a big challenge.

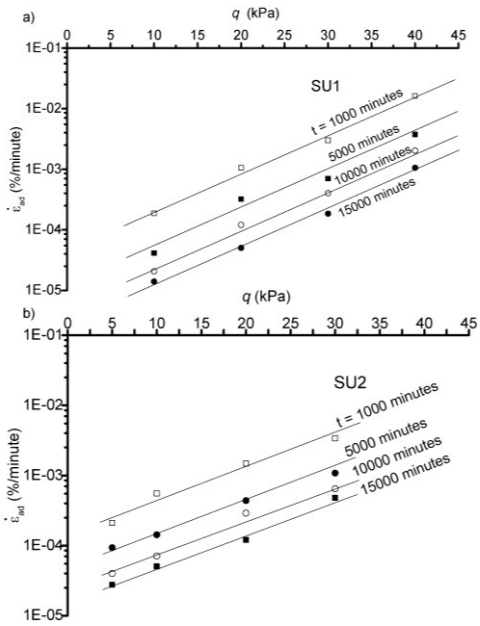

Figure 6.19. Plot of with q at a constant loading duration during CU creep tests on Shelby tube specimens a) SD1 and b) SU2.

At the end of pre-consolidation, conducted over duration of three to five days, the Shelby tube specimens underwent a larger volume change than the remoulded specimens. This accounts for the higher water and air content of the peat matrix, as well as some irregularities in the shape of the specimens. Specimens with relatively fine fibres were smooth and underwent faster consolidation but produced a smaller strain (specimens SD2 and SU2). The smaller size of the remoulded specimens might have made some contribution to their smaller volume change during consolidation. But, most important was that the remoulded specimens were compacted under 55 kPa of vertical stress during the time of preparation. Specimen SD1 was consolidated for a significantly longer time that resulted in 15.1% volumetric strain (ε_{vp}) at the end of pre-consolidation. As an effect of this consolidation, there was less variability in the test results, including measured deformation, volume change, and pore pressure.

The conventional consensus with respect to fibrous peat is that, because of fibre effects, peat specimens should mobilize greater shear resistance in the triaxial

mode of shear. During CD tests, this shear resistance provides better stability through higher lateral resistance (Landva and La Rochelle, 1983). The present study showed that the axial strain developed gradually with no signs of failure in both remoulded and Shelby tube specimens, even at $\varepsilon_a > 30\%$. This result is in accordance with the conclusion of Farrell (2012) that, because of the continual compression of peat fibre, fibrous peat specimens generally do not fail in CD compression tests. Long (2005) reported that, for peats with low fibre content, fibre reinforcement effects are insignificant and shear failure may be expected. However, specimens with significantly finer fibres (specimen SD2) showed no sign of developing shear failure, even at $\varepsilon_a > 30$ %. Under some stress increments, the development of shear strain due to drainage obstruction was observed in specimen SD2, followed by an increase in pore pressure (Fig. 6.6b). This pore pressure development is due to the transitional obstruction of drainage by gas bubbles (Acharya et al., 2015). This development was transient, and the volume change occurred rapidly after the pore pressure dissipated (Fig. 6.4b). This behaviour was also seen in specimens with coarse fibres (specimen SD1), suggesting that, when it comes to limiting the development of shear strain during CD creep tests, the continual compression of fibres in the vertical direction (Farrell, 2012) is more dominant than the reinforcing effect of peat fibres. Similar findings have been previously reported (Edil and Wang, 2000; O'Kelly et al., 2013).

During the CD creep tests on the Shelby tube specimens, both the axial and volumetric strain developed continuously even for $\varepsilon_a \approx 30\%$. This accounts for the continuous expulsion of pore water after the application of stress. No distinct boundary between the primary and secondary compression was observed. Consequently, no distinction could be found between deformation due to the expulsion of inter-particle and intra-particle water as previously considered (Barden, 1969; Berry and Poskitt, 1972). This finding supports the conclusion of Landva (2007) that, due to highly porous nature of peat fibres, the intra-particle and inter-particle water drain at the same time. Only under very high σ'_3 (> 200

kPa) and $\varepsilon_v > 30\%$ (Fig. 6.4c) was there a rapid increase in the strain rate and pore pressure. This behaviour is attributed to the breaking of fibres and increases in the compressibility of peat specimens (Landva and La Rochelle, 1983). Observations of peat specimens at the end of creep tests showed that the peat fibres were broken into very fine peat grains (Fig. 6.20a). The breaking occurred in layer after layer, starting from the drainage boundary. At this stage, higher shear strain can develop. The development of a higher axial strain rate under the higher q in specimens SD1 and SD2 might be attributed to this change in state of material.

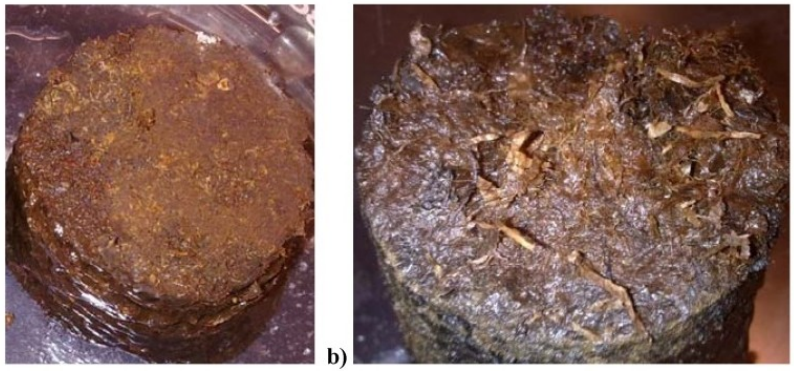

Figure 6.20. Pictures showing the state of fibres at the end of a) CD creep tests on specimen SD3 and b) CU creep tests on specimen SU1.

In one remoulded peat specimen (RD2), deformation at a constant volume was observed when the axial strain exceeded 5% and q surpassed 50 kPa (Fig. 6.6b). This might account for the disturbance in the layout of the peat fibres, loss of moisture, and the change in compressibility of the specimens. The possibility of drainage obstruction was avoided as the specimens had gone through a series of dilations and contractions. Both remoulded specimens demonstrated significantly smaller ε_v and ε_a under the same magnitude of q. Due to these complexities and differences in compression behaviour, the CD creep tests on smaller remoulded peat specimens were not useful when analysing the drained creep behaviour of peat.

Unlike the CD creep tests, the development of strain, strain rate, and pore pressure during CU creep tests in both remoulded and Shelby tube specimens was similar (Figs. 6.16, 6.17, 6.18). Except for some degradation of peat material that had been kept inside the triaxial cell for a long time, the fibres inside the specimens were intact (Fig. 6.20b). Each specimen gradually compressed to $\varepsilon_{ad} >$ 10% and failed due to a lack of confinement when the pore pressure inside the specimens exceeded the confining pressure. This implies that the failure in CU tests in fibrous peat is not associated with the breaking of fibres or shearing of specimens. Thus, the measured shear strains at the failure of specimens is not only the deviatoric creep strain.

The lower values of v ranging from 0.08 to 0.13 and the higher values of v ranging from 0.19 to 0.27 were deduced over a range in ε_a of 0 to 25 % for CD creep tests of the Shelby tube and remolded peat specimens, respectively. These variations in v are usually accounted for and reflect the greater effect of the peat's cross-anisotropic "mat" fabric in the Shelby tube specimens relative to the transitional isotropic-to-cross-anisotropic structure of the remolded peat specimens (O'Kelly, 2013). However, the similarity of the v value from the two Shelby tube specimens with long and fine fibers (SD1 and SD2) implies that, during CD tests, the reinforcing effect of peat fibers does not appear to have a significant effect on the almost one-dimensional compression. The slight increase in the v value in SD2 and a very high v value in the later stage of RD2 compared to specimen SD1 is analogous to the increase in v with the decreasing effective confining pressure, as reported by Hollingshead and Raymond (1972).

6.8 Conclusions

This paper presented the results from a number of triaxial consolidated drained and consolidated undrained creep tests conducted under various confining pressures and deviatoric and isotropic stress increments on remoulded and Shelby tube specimens of fibrous peat from northern Alberta. From this study, many novel understandings have been made with respect to the creep behaviour of peat.

The creep behaviour of peat can be explained based on the framework developed for soft, normally consolidated clay. The uniqueness of the p'-ε_v - relationship devised for clay was also applicable to peat. For the applied stress range, this uniqueness held true for all Shelby tube specimens, regardless of the number and magnitude of stress increments applied and the SIR used.

The volumetric creep deformation in peat followed the creep behaviour of normally consolidated clay. At the same volumetric strain rate ( ), a higher volumetric strain (ε_v) developed in specimens pre-consolidated under lower stress (p'_0). At any and at the same mean pressure (p'), higher values of ε_v developed under deviatoric stress (q) increments than under isotropic stress (σ'_3) increments. Similarly, at any constant p' and loading duration, the values were higher under the q increments. This softening behaviour of specimens under q increments or hardening of specimens under σ'_3 increments was not related to the shearing of specimens, but due to the anisotropic nature of peat related to the layering of peat fibres in a horizontal direction and the continual compression of peat fibres in a vertical direction. This implies that the widely used assumption in creep deformation of clay, i.e., that the development of volumetric creep rate is independent of the stress state, might not be valid for fibrous peat.

The creep equation proposed by Singh and Mitchell was found to be able to represent the development of volumetric and axial creep in fibrous peat under isotropic as well as deviatoric stress states. Compared to that in normally consolidated clay, the measured strain rates are higher and the decrease of strain rates are much slower in peat, and this results in the considerable difference in the value of creep parameters. The volumetric and, consequently, the axial creep rate in CD tests can be defined with respect to the Iso-NCL or NCL. The stress functions can be defined in terms of the ratio of the current and first mean pressure or deviatoric stress increments. The use of a creep expression based on rate process theory is limited as it can only be verified for the strain developed under smaller stress increments.

The CD creep tests on fibrous peat also verified the validity of using C_α to define the volumetric creep rate. As there is no clear division between primary and secondary consolidation, the use of this parameter must be limited to the strain time plots with slopes that parallel one other. The use of rather than pore pressure has been found adequate to describe the range. For the peat specimens tested, strain rates less than 1×10^{-3} %/minute developed almost independent of the stress state. The use of C_α will be valid below this range of strain rate. However, under higher stress, the strain rate might increase due to the breaking of fibres, consequently increasing the C_α.

Poisson's ratio (ν) was calculated from drained creep tests. For the Shelby tube specimens, the average ν ranged from 0.8 to 0.14, resulting in almost one-dimensional compression; slightly higher values between 0.19 and 0.27 were noted for the remoulded peat specimens. This value went up to 0.4 for constant volume deformation. Some dependency on the confining pressure was found. The ν was smaller under higher confining pressures. Because of the small value of ν in the Shelby tube specimens, the development of shear strain could be less significant in CD creep tests; a separate analysis is thus not presented.

CU tests are routine tests conducted to define the strength parameters of fibrous peat. The problem with CU tests is the rapid growth of pore pressure, which surpasses the cell pressure and results in failure of the specimens due to a lack of lateral confinement. Of the four specimens tested, three failed without developing a shear plane when the axial strain reached 10 to 15%. Thus, creep strain generated under undrained loading is not exactly deviatoric creep strain. Moreover, undrained creep tests are not very useful for measuring deviatoric creep strain in peat.

6.9 Acknowledgement

The authors would like to acknowledge the contribution of Canadian National Railways for providing both the project and funding. This research was made possible through the (Canadian) Railway Ground Hazard Research Program and

the Canadian Rail Research Laboratory (www.carrl.ca), both of which are funded by the Natural Sciences and Engineering Research Council of Canada (NSERC), CPR, CN, and Transport Canada.

6.10 References

Acharya, M. P., Hendry, M. T. and Martin, C. D. 2015. Effect of the presence and movement of gas bubbles on pore pressure behaviours observed in peat, *Canadian Geotechnical Journal*, *In press.*

Atkinson , J. H. 1978. The Mechanics of Soils: An Introduction to Critical State Soil Mechanics (McGraw-Hill University Series in Civil Engineering).

Barden, L. 1968. Primary and secondary compression of clay and peat. *Geotechnique*, 18: 1-24.

Barden, L. 1969. Time dependent deformation of normally consolidated clays and peats. *Journal of Soil Mechanics and Foundations Division*, 95(1):1-31

Berry, P.L., and Poskitt, T.J. 1972. The consolidation of peat. *Géotechnique*, 22(1): 27–52.

Bjerrum, L. 1967. Engineering geology of Norwegian normally consolidated marine clays as related to settlements of buildings. *Géotechnique,* 17(2): 83–118, http://dx.doi.org/10.1680/ geot.1967.17.2.83.

Den Haan, E. J. 1996. A compression model for non-brittle soft clays and peat. *Géotechnique*, 46(1): 1-16.

Dhowian, A. W. and Edil, T. B. 1980. Consolidation behavior of peats. *Geotechnical Testing Journal*, 3(3): 105–114.

Edil, T. B. and Wang, X., 2000. Shear Strength and Ko of Peats and Organic Soils. Geotechnics of High Water Content Materials, ASTM STP 1374, T. B. Edil and P. J. Fox, Eds., ASTM International, West Conshohocken, PA: 209–225.

Farrell, E. R., 2012. Organics/Peat Soils. ICE Manual of Geotechnical Engineering, Vol. 1, J. Burland, T. Chapman, H. Skinner, and M. Brown, Eds. ICE Publishing, London: 463–479.

Farrell, E. R. and Hebib, S., 1998. The Determination of Geotechnical Parameters of Organic Soils, Proceedings of the International Symposium on Problematic Soils (IS-TOHOKU 98), Vol. 1, Sendai, Japan, October 28–30, 1998: 33–36.

Fox, P. J. and Edil, T. B. (1996). Effects of stress and temperature on secondary compression of peat. *Canadian Geotechnical Journal*, 33(3), 405–415.

Graham, J., Crooks, J.H.A., and Bell, A.L. 1983. Time effects on stress–strain behaviour of natural soft clays. *Géotechnique*, 3(3): 327–340.

Gunaratne, M., Stinnette, P. and Mullins, A. G. 1998. Compressibility relations for peat and organic soil. *J. Testing Evaluation*, 26 (1): 1–9.

Hendry, M. T., Sharma, J.S., Martin, C.D. and Barbour, S.L. 2012. Effect of fibre content and structure on anisotropic elastic stiffness and shear strength of peat. *Canadian Geotechnical Journal*, 49(4): 403-415.

Hobbs, N. B. 1986. Mire morphology and the properties and behaviour of some British and foreign peats. *Quarterly Journal of Engineering Geology and Hydrogeology*, 19(1): 7-80.

Hollingshead, G. W. and Raymond, G. P. 1972. Field loading tests on muskeg. *Canadian Geotechnical Journal*, 9(3): 278–289.

Kavezajian, E. and Mitchel, J. K., 1977. A general stress-strain time formulation for soils. Proceedings, Specialty Session 9, 9th International Conference on Soil Mechanics and Foundation Engineering, Tokyo, Japan: 113-120,

Kelln, C., Sharma, J., Hughes, D. amd Graham, J. 2008. An improved elastic-viscoplastic soil model. *Canadian Geotechnical Journal,* 45(10): 1356-1376.

Kim, Y. T. and Leroueil, S. 2001. Modelling the Visco plastic behaviour of clays during consolidation: application to Berthierville clay in both laboratory and field conditions. *Canadian Geotechnical Journal*, 38: 484–497.

Landva, A.O. 2007. Characterization of Escuminac peat and construction on peatland. In Proceedings of the 2nd international workshop on Characterisation and Engineering Properties of Natural Soils, Singapore: 2135-2191.

Landva, A. O. and La Rochelle, P. 1983. Compressibility and shear characteristics of Radforth peats. American Society for Testing and Materials, Testing of peat and organic soils, STP 820, West Conshohocken: 157-191.

Landva, A. O. and Pheeney, P.E. 1980. Peat fabric and structure. *Canadian Geotechnical Journal*, 17(3): 416-435.

Leroueil, S., Kabbaj, M., Tavenas, F., and Bouchard, R. 1985. Stress – strain – strain rate relation for the compressibility of sensitive natural clays. *Géotechnique*, 35(2): 159–180.

Long, M., 2005. Review of Peat Strength, Peat Characterization and Constitutive Modelling of Peat With Reference to Landslides, *Studia Geotechnica et Mechanica*, 27(3–4): 67–90.

MacFarlane, I.C. 1965. The consolidation of peat: A literature review. *National Research Council of Canada Division of Building Research Ottawa*, NRC: 8-393.

Madaschi, A., & Gajo, A. 2015. One-dimensional response of peaty soils subjected to a wide range of oedometric conditions, *Géotechnique*, 65(4): 274-286.

Mesri, G., Stark, T. D., Ajlouni, M. and Chen, C. S. 1997. Secondary compression of peat with or without surcharging. *Journal of Geotechnical and Geoenvironmental Engineering*, 123(5): 411–421.

Morsy, M. M., Chan, D. H. and Morgenstern, N. R. 1995. An effective stress model for creep of clay. *Canadian geotechnical journal*, 32(5): 819-834.

Murayama, S. and Shibata, T. 1964. Flow and stress relaxation of clays. International Union of Theoretical and Applied Mechanics Symposium Rheological Soil Mechanics, Grenoble, France: 0- 99.

O'Kelly, B.C. and Zhang, L. 2013. Consolidated-drained triaxial testing of peat. *ASTM Geotechnical Testing Journal*, 36(3): 310-321.

Rowe, R. K., MacLean, M. D., and Soderman, K. L., 1984. Analysis of a Geotextile Reinforced Embankment Constructed on Peat. *Canadian Geotechnical. Journal*, 21(3): 563–576.

Samson, L. and La Rochelle, P. 1972. Design and performance of an expressway constructed over peat by preloading. *Canadian Geotechnical Journal*, 9: 447–466.

Singh, A., and Mitchel, J. K. 1968. General stress strain-time function for soils. *ASCE Journal of the Soil Mechanics and Foundations Division*, 94(SM1): 21-46.

Sukje, L. 1957. The analysis of the consolidation process by the isotaches method. Proceedings, 4th International Conference on Soil Mechanics and Foundation Engineering, London, England, (I): 200-206.

Tan, Y. 2008. Finite Element Analysis of Highway Construction in Peat Bog. *Canadian Geotechnical Journal*, 45(2): 147–160.

Tavenas, F., Leroueil, S., La Rochelle, P., and Roy, M. 1978. Creep behaviour of an undisturbed lightly over consolidated clay. *Canadian Geotechnical Journal*, 15: 402–423. doi:10.1139/ t78-037.

Weber W. G. 1969. Performance of embankments constructed over peat. *Journal of the Soil Mechanics and Foundations Division*, 95(1): 53-76

Wilson, N. E., Radforth, N. W., MacFarlane, I. C. and Lo, M. B. 1965. The rates of consolidation for peat. Proceedings, 6th international conference, Soil Mechanics, Montreal, 1: 407-411

Yamaguchi, H., Ohira, Y., Kogure, K., and Mori, S., 1985, Undrained Shear Characteristics of Normally Consolidated Peat under Triaxial Compression and Extension Conditions. *Soil Mechanics and Foundation Engineering*, 25(3): 1–18.

Yin, J.-H., and Graham, J. 1989. Viscous–elastic–plastic modelling of one-dimensional time-dependent behaviour of clays. *Canadian Geotechnical Journal*, 26: 199–209.

Yin, J.-H., and Graham, J. 1999. Elastic viscoplastic modelling of time-dependent stress–strain behavior of soils. *Canadian Geotechnical Journal*, 36: 736–745.

Zhu, J. G., Zhao, Y. H., & Yin, J. H. 2011. Undrained Creep Behavior of a Silty Clay in Triaxial Tests. In Instrumentation, Testing, and Modeling of Soil and Rock Behavior, ASCE: 139-146.

Zwanenberg, C., 2005. The Influence of Anisotropy on the Consolidation Behavior of Peat. Ph.D. thesis, TU Delft, Delft, The Netherlands.

7 Chapter 7: Conclusions and Recommendations

7.1 General conclusions

The focus of this research program was to understand the mechanism of long-term settlement and pore pressure generation in peat subgrade. It is a component of a large research program studying the response of peat subgrade underlying Canadian railway embankments that was initiated after a recommendation by the TSB (2008). This research is a continuation of a study conducted on the response of peat foundations underlying railway embankments (Hendry, 2011) that highlighted the necessity of understanding the development of long-term deformation and pore pressure in peat subgrade.

This research included the installation of instrumentation at a field site to measure the in situ pore pressure, horizontal and vertical deformation, and temperature within peat subgrade beneath an embankment. Measurements were taken at two hours intervals for more than three years. Laboratory tests, including isotropic consolidation tests on peat and cellulose specimens and temperature controlled undrained compression tests on peat specimens, were conducted to study the mechanism of generation of pore pressure in peat. Triaxial drained and undrained creep tests were conducted to study the mechanism of long-term deformation of peat. Incubation of peat under anaerobic conditions was done to observe the decomposition of peat and to detect the amount and type of gas produced.

This study revealed that gas bubbles present in the peat subgrade are due to the decomposition of organic materials that comprise the peat. These gas bubbles are associated with the anomalous pore pressure behaviours that have been reported in the literature and measured during the course of this study. The long-term deformation of peat involved multiple mechanisms, including deformation due to periodic expulsion of gases and time-dependent consolidation and creep. The field and laboratory measurements suggested almost one-dimensional

deformation. The creep behaviour could be effectively described based on the understanding developed for normally consolidated soil.

7.2 Observed pore pressure and existence of gas in peat subgrade

Chapter 3 presents the results of a study investigating the behaviour of peat subgrade beneath a railway embankment that included analysis of the measured pore pressure, temperature, and settlement measured beneath the railway embankment, granular fill, and unloaded peat. The pore pressure in the peat subgrade and within the peat away from the influence of the embankment showed a seasonal increase in pore pressure in excess of hydrostatic pressure and strongly correlated to the temperature measured at the same location. The pore pressures were not the result of a total stress change and not correlated to the vertical settlement. These seasonal variations in pore pressure were found to be the result of thermal expansion of gas bubbles existing in peat beneath the water table (Chapter 3).

The laboratory incubation of peat specimens at room temperature and under anaerobic conditions showed the decomposition of peat and generation of CO_2 and CH_4. Further, the peat specimens compressed at constant pressure with incrementally increasing and decreasing temperature replicated field pore pressure behaviour. The volume of gas was estimated to be 9.5 ± 2% of the total volume of the peat specimens.

The cyclic increase and decrease in pore pressure in peat subgrade was measured for three consecutive years. The increase in pore pressure above hydrostatic pressure during the summer months remained fairly constant. Both the measured temperature and pore pressure beneath the embankment were higher than measured at the same elevation beneath the fill and unloaded peat. This was attributed to the higher thermal conductivity of the embankment material. Previously published work suggests that the higher temperatures beneath the embankment could accelerate the decomposition of peat at this location.

The results presented in Chapter 3 showed that the peat beneath the ground water table continuously decomposes to form gas bubbles and the volume of gas is sufficient to alter the compression behaviour of the peat (Chapters 4 and 5) as compared to the inorganic saturated soils.

7.3 Effect of movement of gas bubbles on pore pressure

Chapter 4 focused on the analysis of the mechanism associated with the characteristic episodic increases and decreases in pore pressure at the top of the peat layer described in Chapter 3. Further analysis of the field data and additional laboratory testing were conducted to examine how the mobility of the gas through the cellular voids of the peat contributes to this behaviour.

The pore pressure varied at constant total pressure, and at constant temperature this variation is thus a function of the movement of pore fluid including gas and water within and out of the peat matrix. With the help of theoretical analysis, it was found that the accumulation of pore pressure was the result of the restriction of the flow of gas bubbles through the constriction towards the drainage boundary. The rapid drop in pore pressure was the result of the expulsion of gas bubbles once the pore pressure reached a peak value, or *escape pressure*, high enough to force the gas bubbles through the pore space and out of the drainage boundary.

Beneath the embankment, the pore pressures (*escape pressures*) peaked at magnitudes between 4 and 15 kPa above the hydrostatic pressure. In laboratory peat specimens, the *escape pressures* ranged from 3 to 15 kPa and were related to the applied confining pressure. The increase in pore pressure was proportional to the size of the gas bubbles or the pore space. Thus, higher increases in pore pressure could occur in fibrous peat with larger pore spaces. Moreover, this study showed that the episodic increases and decreases in pore pressure are a continuous phenomenon that could be initiated even for small changes in effective stress or increases in pore pressure.

7.4 Effect of movement of gas bubbles on volume change

The isotropic consolidation tests described in Chapters 4 and 5 along with field measurements of deformation and rate of vertical deformation presented in Chapter 5 showed that the pore pressure drops related to the expulsion of gas bubbles preceded a temporary acceleration in volume change and vertical settlement. This observation gave new insight, i.e., that the long-term deformation of peat subgrade is also a function of the expulsion of gases.

During the isotropic consolidation tests, the amount of volume change was proportional to the magnitude of the pore pressure drops and inversely proportional to the confining pressure. Based on this finding, a correlation was developed between the volume change corresponding to the dissipation of gas bubbles and the magnitude of pore pressure drops under different confining pressures. This correlation was extrapolated to estimate the settlement of the peat layer beneath the railway embankment. It was estimated that at least 15% of the total settlement measured is associated with the expulsion of gas bubbles. This might be an underestimate of the settlement due to the expulsion of gases, as it is not possible to detect all pore pressure drops below the embankment. Continuous flow of gas bubbles out of the saturated peat layer beside the embankment was observed throughout the summer (Chapter 3).

7.5 Time-dependent deformation of peat

The results of consolidated drained (CD) and consolidated undrained (CU) triaxial creep tests on remoulded and Shelby tube specimens revealed the creep behaviour of peat at various stress states. During the drained creep tests, peat specimens underwent continuous compression that resulted in more than 30% axial strain without any sign of failure. This strain occurred in less than three months under constant deviatoric stress increments of less than 50 kPa. The deformation occurred continuously without any deviation in the strain time plot, as usually occurs in inorganic clays. The breaking of fibres occurred only under relatively high values of stress and axial strain. More than two-thirds of the volume change occurred at an almost constant pore pressure of around 5 kPa but

with continuous dissipation of pore water. The strains developed at constant pore pressure are considered to be creep strains under constant stress. Thus, secondary compression or creep is dominant in peat compression.

The creep behaviour of peat was found to be similar to that of soft, normally consolidated clay. The uniqueness of p'-ε_v- , a relationship which had been devised for clay, was also found to be applicable for peat. This uniqueness held true in all Shelby tube specimens irrespective of the different magnitudes of stress increments and stress increment ratios (SIR) applied.

The volumetric creep deformation under constant stress conditions was similar to the behaviour of normally consolidated clay. At the same volumetric strain rate ( ), a higher volumetric strain (ε_v) developed in specimens consolidated under lower confining stress (p'_0). At any and at same mean pressure (p'), higher ε_v developed under deviatoric stress (q) increments than under isotropic stress (σ'_3) increments. Similarly at any constant p' and loading duration, was also higher under the q increments. This behaviour was attributed to the layering of peat fibres in the horizontal direction, which results in the higher compressibility of the specimen in the vertical direction. This implies that the widely used assumption of volumetric creep rate independent of stress state may not be a good representation of the behaviour of fibrous peat.

The relation proposed by Singh and Mitchell (1968) for the development of axial creep strain was found to be able to represent the development of volumetric and axial creep in fibrous peat under isotropic as well as deviatoric stress states. Similar to that in normally consolidated soil, the constant strain rate lines (creep isotaches) derived from isotropic stress increments plotted parallel to both the one-dimensional consolidation lines (NCL) and isotropic consolidation lines (Iso-NCL) (Chapter 6). Thus, the volumetric creep and consequently the axial creep deformation may best be defined with respect to the Iso-NCL or NCL. The stress functions can be defined in terms of the ratio of the current and first mean pressure or deviatoric stress increments. Compared to that in normally

consolidated clay, the measured strain rate is higher and the decrease of strain rate much slower in peat, which results in the considerable difference in the value of creep parameters.

The CD creep tests on fibrous peat also verified the validity of the use of C_α to define the volumetric creep rate. As there is no clear division between primary and secondary consolidation, use of this parameter must be limited to strain time plots with slopes that parallel one other. Use of strain rate rather than pore pressure was found to be adequate to describe the range. For the laboratory peat specimens tested, strain rates less than 1×10^{-3} %/minute developed almost independently from stress state. Thus, the use of C_α may be valid for a range of strain rates less than 1×10^{-3} %/minute.

The drained Poisson's ratio (ν) ranged from 0.08 to 0.14 for Shelby tube specimens and 0.19 to 0.27 for remoulded peat specimens. The value of Poisson's ratio was found to be slightly smaller under higher confining stresses. The small value of Poisson's ratio in the Shelby tube specimens indicated almost one-dimensional compression. This was also found in the field measurements, in that lateral deformation of the peat subgrade measured for three years was less than the 20% of vertical settlement (Chapter 5). The development of creep shear strain was less significant in the CD creep tests.

CU creep tests were not useful in the investigation of the long-term deformation and the deviatoric stress state. In every peat specimen tested, a rapid growth of pore pressure was observed that surpassed the cell pressure. Thus, the peat specimens failed due to lack of lateral confinement. Of the four specimens tested, three failed without developing a shear plane when the axial strain reached 10 to 15%. Due to the open structure of the peat fibres and the very high initial permeability of the peat matrix, pure undrained loading conditions are less likely to exist in the field.

7.6 Implications of Study

The major objective of this research was to determine the mechanisms that govern the variation in pore pressure and the development of long-term settlement within the peat foundation of railway embankments. The variation of pore pressure in peat subgrade was found to be related to the thermal expansion, contraction, and expulsion of gas bubbles existing in the peat. The long-term settlement was a combination of the settlement associated with the expulsion of gas and pore water and time-dependent deformation under constant loading.

The peat from Anzac, Alberta had $9 \pm 2\%$ gas by volume. Due to the high degree of saturation of peat, gas exists as isolated bubbles. Therefore, the structure of peat is different from both saturated and unsaturated soils. Such soils are sometimes classified as gassy soils. Due to the low stiffness of natural peat, these gas bubbles control the deformation and pore pressure behaviours.

The decomposition of peat is a continuous process. Higher temperatures accelerate the rate of decomposition. Thus, the state of peat could be related to the average temperature of a site. In Canada, peat near the southern border could be more humified than northern fibrous peat. Tropical peats are often reported to be highly humified amorphous peat. This geographic variation of the type of peat consequently varies the compression behaviour of the peat, so characterization should consider the average annual temperature of the study site. Due to the high compressibility of peat fibres, however, the long-term compression behaviour of peat (except for highly humified amorphous peat) could be the same irrespective of higher variation in the initial stages.

The second objective of the research was to determine the implications of understanding gained so far with respect to the stability of railway embankments overlying peat subgrades. A long-standing concern is the stability of railway embankments with underlying thick peat layers containing more than 85% water by volume and their ability to carry excessively long and heavy trains. This study showed the formation of gas and the existence of gas bubbles within peat fibres

that do not drain readily. This suggests that the equilibrium in the peat subgrade may be a hydrodynamic equilibrium at the interface of the water film, gas bubbles, and organic materials in multiple layers of peat fibres. Consequently, the stress transfer is not grain-to-grain as in transported soil. This mechanism might be the reason behind the elastic response of peat foundations; further study is required to confirm this mechanism.

The presence of gas together with the high water content (low solid content) in the peat matrix makes it difficult to reinforce the peat, as many materials cannot develop bonds with peat. One effective way to reduce the rate of settlement might be to maintain a constant vertical stress. Additional stresses as low as few kPa may initiate further settlement. Piles that are capable of transferring the full load of the embankment might help to maintain a constant load on the peat subgrade and may significantly reduce the settlement.

7.7 Recommendations

The research included within this thesis is part of a larger ongoing program. This study produced new understanding of the long-term settlement behaviour of peat under constant embankment loading. The following recommendations for additional work will aid in the progression of this research area.

- Continuation of field monitoring at the current study site: The current study included the measurement of vertical and horizontal deformation beneath the granular fill on the west side of the track near MP 263.5. CN built a berm on top of the fill in September 2014. The existing instruments are recording the deformation and pore pressure beneath the berm. Measurement of the response of the peat under the new berm will help to further define the mechanism of settlement and pore pressure generation presented in this thesis. As the instruments measuring deformation are well below the ground surface, the measured settlement will be free from the effect of variation of temperature at the ground surface. The measured settlement can be used to calculate the rate of vertical settlement, which

might be useful to study and understand the stability of embankments and tracks overlying peat foundations. In addition, the measured settlement together with the settlement measured under the soil fill presented in this thesis can be used to develop a chart to predict settlement under future load increments. The possibility of this superposition in laboratory test results was discussed in Chapter 6 of this thesis. This should provide usable data to CN, allowing them to quantify the amount of new gravel that can be added on top of the track without accelerating the rate of settlement.

- Understanding of the impact of train load on long-term deformation: Current and previous field measurements included the measurement of dynamic data including vertical and horizontal deformation and pore pressure. These data were not analysed. Previous studies have shown both elastic and non-elastic responses of peat foundations under heavy axle loading. Further analysis of these recorded data considering the peat subgrade as a continuum consisting of gas bubbles might help to better understand the impact of length, speed, and axle load of passing trains on the long-term deformation of the peat subgrade.
- Understanding the hydro-mechanical equilibrium at the interface between water film, gas bubbles, and peat skeletons: This research provided new insight into the mechanism of generation of pore pressure and settlement due to the movement and expulsion of gas bubbles. The laboratory isotropic consolidation tests on peat showed very little volume change between two consecutive pore pressure drops during the expulsion of gas bubbles. Further study of the mechanism of the equilibrium between gas bubbles, water film, and solid skeletons will provide a better understanding of the stability of embankments over peat subgrade, which is generally considered to be a floating foundation, and the mechanism of the long-term settlement of peat.
- Development of a complete viscoplastic model: This research provided fundamental insight on the creep behaviour of peat at various stress states. The uniqueness of the stress, strain, and strain rate concept developed for

clay was validated and the creep function was derived for both volumetric and axial strain rates. This finding could be extended to full three-dimensional models to predict the creep deformation in peat subgrade.

Study of the ecological evolution of peatlands surrounding the railway line and use of this understanding to reinforce the embankment passing through peatlands: During the three years of monitoring the railway embankment at CN's Lac-la-Biche subdivision near MP 263.5, it was found that the peatland surrounding the railway embankment continuously evolved with noticeable changes in drainage pattern, topography, and ecology. Due to the slight reduction in the water table, new species of plants came up and helped to strengthen the peatland surrounding the railway embankment. This natural process of ecological development could be used to laterally reinforce the railway embankment. A poster made to further clarify this process is included in the appendix. Further study in this regard could focus on the selection of appropriate plant species, modification of the embankment geometry, and quantitative evaluation of the effectiveness of this approach to strengthen the existing railway embankment.

References

Acharya, M. P., Hendry, M. T. and Martin, C. D. 2015a. Thermally induced pore pressure in peat. *International Journal of Geotechnical Engineering*. *In press.*

Acharya, M. P., Hendry, M. T. and Martin, C. D. 2015b. Effect of the presence and movement of gas bubbles on pore pressure behaviours observed in peat. *Canadian geotechnical Journal*, *In press.*

Acharya, M. P., Hendry, M. T. and Martin, C. D. 2014. Thermal induced pore pressure in peat. In 67th Canadian Geotechnical Conference, GeoRegina 2014, Paper no. 106.

Adams, J. I. 1965. The engineering behaviour of a Canadian muskeg. Proceedings, 6th International Conference on Soil Mechanics and Foundation Engineering, (I): 3-7.

Ajlouni, M. H. 2000. Geotechnical Properties of peat and Related Engineering problems. PhD thesis, University of Illinois at Urbana-Champaign.

ASTM D854 Standard Test Methods for Specific Gravity of Soil Solids by Water Pycnometer.

ASTM D1997 Standard Test Method for Laboratory Determination of the Fiber Content of Peat Samples by Dry Mass.

ASTM D2974 Standard Test Methods for Moisture, Ash, and Organic Matter of Peat and Other Organic Soils.

ASTM D2976 Standard Test Method for pH of Peat Materials.

ASTM D2980 Standard Test Method for Volume Weights, Water-Holding Capacity, and Air Capacity of Water-Saturated Peat Materials.

ASTM D4318 Standard Test Methods for Liquid Limit, Plastic Limit, and Plasticity Index of Soils.

ASTM D4427 Standard Classification of Peat Samples by Laboratory Testing.

ASTM D4531 Standard Test Methods for Bulk Density of Peat and Peat Products.

ASTM D5715 Standard Test Method for Estimating the Degree of Humification of Peat and Other Organic Soils (Visual/Manual Method).

Atkinson J. H. 1978. The Mechanics of Soils: An Introduction to Critical State Soil Mechanics (McGraw-Hill university series in civil engineering).

Barden, L. 1965. Consolidation of clay with nonlinear viscosity. *Géotechnique* 15, (4): 345-362.

Barden, L. 1974. Consolidation of clays compacted dry and wet of optimum water content. *Géotechnique*, 24(4) 605-625.

Barden, L. 1968. Primary and secondary compression of clay and peat. *Géotechnique*, 18: 1-24.

Barden, L. 1969. Time dependent deformation of normally consolidated clays and peats. *Journal of Soil Mechanics and Foundations Division*, 95(1): 1-31.

Beckwith, C.W., and Baird, A.J., 2001. Effect of biogenic gas bubbles on water flow through poorly decomposed blanket peat. *Water Resources Research*, 37 (3): 551-558.

Beer J. and Blodau C. 2007. Transport and thermodynamics constrain belowground carbon turnover in a northern peatland. *Geochimica et Cosmochimica Acta*, 71: 2989-3002.

Berry, P.L., and Poskitt, T.J. 1972. The consolidation of peat. *Géotechnique*, 22(1): 27–52.

Bjerrum, L. 1967. Engineering geology of Norwegian normally consolidated marine clays as related to settlements of buildings. *Géotechnique*, 17(2): 83–118.

Briaud, J. L. 1974. Development of peat mechanics at UNB (1972-1974). M. Sc. Engineering thesis, Department of Civil Engineering, University of New Brunswick.

Buisman, A. S. K. 1936. Results of long-duration settlement tests. Proceedings, 1st International Conference SMFE, vol. 1, Cambridge, MA.

Christensen, R. W., and Wu, T. H. 1964. Analysis of Clay Deformation as a Rate Process. *Journal of the Soil Mechanics and Foundations Division*, ASCE, 90 (SM6): 125– 57.

Clymo, R. S. and Bryant, C. L. 2008. Diffusion and mass flow of dissolved carbon dioxide, methane, and dissolved organic carbon in a 7-m deep raised peat bog. *Geochimica et Cosmochimica Acta*, 72: 2048-2066.

Clymo, R.O., and Hayward, P.M. 1982. The ecology of peat sphagnum. Bryophyte ecology, A. J. E. Smith, ed., Chapman and Hall, London, 221–289.

Colley, B. E. 1950. Construction of highways over peat and muck areas. *American highways, Washington*, D.C., 29(1): 3–6.

Dalton, J. 1954. Air drying of peat. *International peat Symposium*, Dublin.

Davis, J. H. 1997. The peat deposits of Florida, their occurrence, development and uses. Geological bulletin no. 3, Florida Geological Survey, Tallahassee, Fla.

De Jong, G. D. J. 1968. Consolidation models consisting of an assembly of viscous elements on a cavity channel network. *Geotechnique*, 18(2): 195-228.

De Jong, J., and Verujit, A. 1965. Primary and Secondary Consolidation of a Spherical Clay Sample. *Proceedings, 6th international conference on Soil Mechanics and Foundation Engineering*, 1.

Den Haan, E. J. 1996. A compression model for non-brittle soft clays and peat. *Géotechnique*, 46(1): 1-16.

Den Haan, E.J. and Kruse, G.A.M. 2007. Characterisation and engineering properties of Dutch peats, Proceedings, 2nd international workshop on Characterisation and Engineering Properties of Natural Soils, Singapore: 2101-2133.

Dhowian, A. W. and Edil, T. B. 1980. Consolidation behavior of peats. *Geotechnical Testing Journal*, 3(3): 105–114.

Edil, T. B., Simon-Gilles D. A. 1986. Settlement of Embankments on peat: two Case Histories. In Proceedings on, Advances in Peatlands Engineering, Carleton University, Ottawa: 147-154.

Edil, T. B. and Wang, X., 2000. Shear Strength and K_0 of Peats and Organic Soils. Geotechnics of High Water Content Materials, ASTM STP 1374, (Ed., T. B. Edil and P. J. Fox), ASTM International, West Conshohocken, PA: 209–225.

Elsayed, A. A. 2003. The Characteristics and Engineering Properties of Peat. In Bogs, PhD Thesis, University of Massachusets Lowell.

Farrell, E. R., 2012. Organics/Peat Soils, ICE Manual of Geotechnical Engineering. Eds.: J. Burland, T. Chapman, H. Skinner, and M. Brown, ICE Publishing, London, (1): 1463-479.

Farrell, E. R. and Hebib, S., 1998. The Determination of Geotechnical Parameters of Organic Soils, Proceedings of the International Symposium on Problematic Soils (IS-TOHOKU 98), Sendai, Japan, October 28–30(1): 33–36.

Fechner-Levy, E. J., and Hemond, H. F. 1996. Trapped methane volume and potential effects on methane ebullition in a northern peatland. *Limnology and Oceanography*, 41(7): 1375-1383.

Fox, P. J. and Edil, T. B. 1996. Effects of stress and temperature on secondary compression of peat. *Canadian Geotechnical Journal*, 33(3), 405–415.

Forest, J. B. 1967. Field studies of the consolidation response of peat. Report 344, National Research Council of Canada, Division of Building Research Ottawa.

Gardescu, I. I. and Pittsburgh, PA. 1930. Behavior of gas bubbles in capillary spaces. Transactions of the AIME, 86(01): 351-370.

Graham, J., Crooks, J. H. A., and Bell, A. L. 1983. Time effects on stress–strain behaviour of natural soft clays. *Géotechnique*, 3(3): 327-340.

Gunaratne, M., Stinnette, P. and Mullins, A. G. 1998. Compressibility relations for peat and organic soil. *J. Testing Evaluation*, 26 (1): 1–9.

Hanrahan, E.T. 1954. An investigation of some physical properties of peat. *Geotechnique*, 4(3): 108-123.

Hayward, P. M. and Clymo, R. S. 1982. Profiles of water content and pore size in Sphagnum and peat, and their relation to peat bog ecology. Proceedings, The Royal society of London: B215, 299-325.

Henry M. T., 2011. The geomechanical behaviour of peat foundations below rail-track structures, PhD Thesis, University of Saskatchewan, and Saskatoon, Canada.

Hendry, M.T., Barbour, S.L., and Martin, C.D. 2011. An evaluation of realtime deformation monitoring using motion capture instrumentation and its application in monitoring railway foundations. *ASTM geotechnical testing journal*, 34(6): 602-612.

Hendry, M. T., Martin, C. D. and Barbour, S. L. 2013. The measurement and analysis of the cyclic response of railway embankments and underlying soft peat foundations to heavy axle loads. *Canadian Geotechnical Journal* 50(5): 467-415.

Hendry, M.T., Martin, C.D., Barbour, S.L., and Edwards, T. 2008. Monitoring cyclic strain below a railway embankment overlying a peaty foundation using

novel instrumentation. 61st Canadian geotechnican conference, Edmonton, Alberta, Paper no. 443.

Hendry, M. T., Sharma, J. S., Martin, C. D. and Barbour, S. L. 2012. Effect of fibre content and structure on anisotropic elastic stiffness and shear strength of peat. *Canadian Geotechnical Journal*, 49(4): 403-415.

Hobbs, N. B. 1986. Mire morphology and the properties and behaviour of some British and foreign peats. *Quarterly Journal of Engineering Geology and Hydrogeology*, 19(1): 7-80.

Hogan, J. M., Kamp, G. V. D., Barbour, S.L., and Schmidt, R. 2006. Field methods for measuring hydraulic properties of peat deposits. *Hydrological Processes*, 20: 3635–3649.

Hollingshead, G. W. and Raymond, G. P., 1972. Field Loading Tests on Muskeg. *Canadian Geotechnical Journal*, 9(3): 278-289.

Kavezajian, E. and Mitchel, J. K., 1977. A general stress-strain time formulation for soils. Proceedings, Specialty Session 9, 9th International Conference on Soil Mechanics and Foundation Engineering, Tokyo, Japan: 113-120,

Kelln, C., Sharma, J., Hughes, D. amd Graham, J. 2008. An improved elastic-viscoplastic soil model. *Canadian Geotechnical Journal,* 45(10): 1356-1376.

Kim, Y. T. and Leroueil S. 2001. Modelling the Visco plastic behaviour of clays during consolidation: application to Berthierville clay in both laboratory and field conditions. *Canadian Geotechnical Journal*, 38: 484-497.

Kogure, K. Yamaghuchi, Y. Ohira, and Ishiorosi, Y. 1986. Physical and engineering properties of peat ground. Proceedings, Advances in Peatlands Engineering, Carleton University, Ottawa: 95-101.

Konrad, J.M., Grenier, S. and Garnier, P. 2007, Influence of Repeated Heavy Axle Loading on Peat Bearing Capacity. In 60th Canadian Geotechnical Conference, Ottawa: 1551-1558.

Lan, L. T. 1992. A model for one dimensional compression of peat. Ph. D. Thesis, University of Wisconsion, Madison, Wisconsin.

Landva, A.O. 1980. Geotechnical behaviour and testing of peat. PhD thesis, Université Laval Quebec.

Landva, A.O. 2007. Characterization of Escuminac peat and construction on peatland. Proceedings, 2nd international workshop on Characterisation and Engineering Properties of Natural Soils, Singapore: 2135-2191.

Landva, A. O., Clark, J. I., Crooks, J. H. A. and Burwash, W. J. 1986. Degradation of peats and organic soils under engineered structures - A preliminary study. Proceedings of Advances in Peatlands Engineering, Ottawa: 110 -115.

Landva, A.O. and La Rochelle, P. 1983. Compressibility and shear characteristics of Radforth peats. American Society for Testing and Materials, Testing of peat and organic soils, STP 820, West Conshohocken: 157-191.

Landva, A.O. and Pheeney, P.E. 1980. Peat fabric and structure. *Canadian Geotechnical Journal*, 17(3): 416-435.

Landva, A.O., Pheeney, P.E., La Rochelle, P. and Briuad, J. –L. 1986. Structures on peatland – Geotechnical Investigations. Proceedings, Advances in Peatlands Engineering, Carleton University, Ottawa: 16-29.

Lea, N. D. and Brawner, C. O. 1963. Highway design and construction over peat deposits in lower British Columbia. Highway Research Board, Record 7, Washington, DC.: 1-33.

Lechowicz, Z., Szymanski, A. and Baranski, T. 1996. Laboratory investigation. Proceedings on Embankments on Organic Soils, Delft, Netherlands, 167-179

Lefebvre, G., Langlois, P., Lupien, C. and Lavallée, J.G. 1984. Laboratory testing and in situ behaviour of peat as embankment foundation. *Canadian Geotechnical Journal*, 21(2): 322-337.

Leger, S. Chornet, E. and Overrend, R. P. 1987. Characterization of peat residues derived from the Udes/NRC process: an application of differential thermal analysis. Proceedings, Symposium' 87 Wetlands/peatlands, Edmonton, Alberta, Canada: 71-75.

Leonards, G. A. and Girault, P. 1961. A study of the one-dimensional consolidation test. Proceedings, 5th Conference on Soil Mechanics and Foundation Engineering, 1: 213-218.

Leroueil, S., Kabbaj, M., Tavenas, F., and Bouchard, R. 1985. Stress – strain – strain rate relation for the compressibility of sensitive natural clays. *Géotechnique*, 35(2): 159–180.

Lewis, S. 2014. Sample of Congo peat, *BBC.com.* Web. 14 May 2014. (http://www.bbc.com/news/science-environment-27492949)

Liingaard, M., Augustesen, A. and Lade, P. V. 2004. Characterization of Models for Time-Dependent Behavior of Soils. *International Journal of Geomechanics*, ASCE, 30(3): 157 – 177.

Lishtvan, I. I. 1982. Physico-chemistry and probable of peat integrated processing. Proceedings, International Peat Symposium of IPS Commissions IV and II, Peat its Properties and Perspectives of Utilization, Minsk, 11-18.

Lishtvan, I. I. 1981. Physicochemical fundamentals of chemical technology of peat. Proceedings, International Peat Symposium, Bemidji, Minnesota, USA: 321-334.

Long, M., 2005. Review of Peat Strength, Peat Characterization and Constitutive Modelling of Peat With Reference to Landslides. *Studia Geotechnica et Mechanica*, 27(3–4): 67–90.

Long, M. and Boylan, N. 2013. Predictions of settlement in peat soils. *Quarterly Journal of Engineering Geology and Hydrogeology*, 46(3): 303-322.

MacFarlane, I.C. 1969. Engineering characteristics of peat, Muskeg Engineering Handbook. University of Toronto Press, Toronto, Canada: 78-126.

MacFarlane, I.C. 1965. The consolidation of peat: A literature review. *National Research Council of Canada Division of Building Research Ottawa*, NRC: 8-393.

MacFarlane, I. C., Radforth, M. W. 1964. A study of the physical behaviour of peat derivatives under compression. Proceedings, 10th Muskeg Conference, Technical Memorandum 85, Ottawa.

MacKenzie, W. B. 1902. Notes on railway work. Lecture given to the Engineering Society of the University of New Brunswick, October 1902, Constitution and Lectures: 1902-1904.

Madaschi, A., & Gajo, A. 2015. One-dimensional response of peaty soils subjected to a wide range of oedometric conditions. *Géotechnique*, 65(4): 274-286.

Mesri, G. and Ajlouni, M. A. 2007. Engineering properties of fibrous peat. *Canadian Geotechnical Journal*, 133(7).

Mesri, G., Stark, T. D., Ajlouni, M. A., and Chen, C. S. 1997. Secondary compression of peat with or without surcharging. *Journal of Geotechnical and Geoenvironmental Engineering*, 123(5): 411–421.

Morsy, M. M., Chan, D. H. and Morgenstern, N. R. 1995. An effective stress model for creep of clay. *Canadian geotechnical journal*, 32(5): 819-834.

Murayama, S. and Shibata, T. 1961. Rheological Properties of Clays. Proceedings, 5th International Conference on Soil Mechanics and Foundation Engineering, Paris, France, 1: 269 – 273.

Murayama, S. and Shibata, T. 1964. Flow and stress relaxation of clays. International Union of Theoretical and Applied Mechanics Symposium Rheological Soil Mechanics, Grenoble, France: 0- 99.

Nageswaran, S. 1983. Effect of Gas Bubbles on the Seabed Behaviour. D. Phil. Thesis, Oxford University.

Ohira, Y. 1977. Methods of tests and investigation. Engineering Problems of Organic Soils in Japan. Special report by Research Committee on Organic Soils: 19-33.

O'Kelly B. C. and Zhang, L. 2013. Consolidated-drained triaxial testing of peat. *Geotechnical testing journal* 36(3).

Ripley, C. F. and Leonoff, C. E. 1961. Embankment settlement behaviour on deep peat. Proceedings, 7th Muskeg Research Conference, NRC, Associated Committee on Soil and Snow Mechanics, Technical Memorandum 71, Ottawa, 185-204.

Rowe, R. K., MacLean, M. D. and Barsvary, A. K. 1984. The observed behaviour of a geotextile-reinforced embankment constructed on peat. *Canadian Geotechnical Journal*, 21(2): 289-304.

Samson, L. and La Rochelle, P. 1972. Design and performance of an expressway constructed over peat by preloading. *Canadian Geotechnical Journal*, 9: 447–466.

Schuurman, I. E., 1966. The compressibility of an air/water mixture and a theoretical relation between the air and water pressures, *Géotechnique*, 16: 269-281.

Sedano J. A. I., Vanapalli, S. K. and Garga, V. K., 2013. Modified Ring Shear Apparatus for Unsaturated Soils Testing. *Geotechnical Testing Journal*, 30(1): 39-47.

Sills, G. C., Wheeler, S.J., Thomas, S.D. and Gardner T.N. 1991. Behaviour of offshore soils containing gas bubbles, *Geotechnique*, 41(2): 227-241.

Singh, A. and Mitchel, J. K. 1968. General stress, strain - time function for soils. *ASCE Journal of the Soil Mechanics and Foundations Division*, 94(SM1): 21-46.

Sobkowicz, J. C. and Morgenstern, N. R. 1984. The undrained equilibrium behavior of gassy sediments. *Canadian Geotechnical Journal*, 21: 439–448.

Sobkowicz, J. C., and Morgenstern, N. R. 1987. An experimental investigation of transient pore pressure behaviour in soils due to gas exsolution, Prediction and performance in geotechnical engineering*, Calgary*: 267-275.

Stanek, W. and Worley, I. A. 1983. A terminology of virgin peat and peatlands. Proceedings, international Symposium on Peat Utilization, Bemidji, USA: 75-104.

Sukje, L. 1957. The analysis of the consolidation process by the isotaches method. Proceedings, 4th International Conference on Soil Mechanics and Foundation Engineering, London, England, I: 200-206.

Tan, Y., 2008, Finite Element Analysis of Highway Construction in Peat Bog. *Canadian Geotechnical Journal*, 45(2): 147–160.

Tarnokai, C., Kettles, I. M. and Lacelle, B. 2002. Peatlands of Canada Database. Geological Survey of Canada, Open File 4002.

Tavenas, F., Leroueil, S., La Rochelle, P. and Roy, M. 1978. Creep behaviour of an undisturbed lightly over consolidated clay. *Canadian Geotechnical Journal*, 15: 402–423.

Taylor, D. W. 1948. Fundamentals of soil Mechanics. John Wiley, New York.

Terzaghi, C. 1931. The Static Rigidity of Plastic Clays. *Journal of Rheology*, 2(3): 253 – 262.

Teunissen, J. A. M. 1982. Mechanics of a fluid-gas mixture in a porous medium. *Mechanics of materials*, 1(3): 229-237.

Thomas, S. D. 1987. The consolidation behaviour of gassy soil, D. Phill thesis. Oxford University.

Transportation Safety Board of Canada (TSB), 2008. Railway Investigation Report R04Q0040. Cat. No. TU3-6/04-2E, ISBN 978-0-662-47573-6

Turchenek L.W. and Pigot, M. E. 1988. Peatland distribution in Alberta. Alberta Research Council, Natural Resources Division Terrain Sciences Department, map 212.

Van Hulzen, J. B., Segers, R., Van Bodegom, P. M. and Le, P. A. 1999. Temperature effects on soil methane production: an explanation for observed variability. *Soil Biology and Biochemistry*, 31: 1919-1929.

Van Winden J. F., Reichart G. J., McNamara N. P., Benthien A. and Damste´ J. S. S. 2012. Temperature - induced increase in methane release from peat bogs: A mesocosm experiment. *PLoS ONE 7(6)*

Wardwell, R. E., Charlie, W. A. and Doxtador, K. A., 1983. Test methods for determining the potential for decomposition in organic soils. In STP 820, P.M. Jarrett (Ed.), ASTM Committee D-18 Symposium, Toronto, Canada: 218-229.

Weber W. G. 1969. Performance of embankments constructed over peat. *Journal of the Soil mechanics and Foundations Division*, 95(1): 53-76

Wehling, T. H., Boulanger, R. W., Arulnathan, R., Harder, L. F. J., and Driller, M. W. 2003. Nonlinear Dynamic Properties of a Fibrous Organic Soil. *Journal of Geotechnical and Geoenvironmental Engineering*, 129(10): 929-939.

Wheeler, S. J. 1988. The undrained shear strength of soils containing large gas bubbles. *Geotechnique*, 38(3): 399-413.

Wilson, N. E., Radforth, N. W., MacFarlane, I. C. and Lo, M. B. 1965. The rates of consolidation for peat. Proceedings, 6th international conference, Soil Mechanics, Montreal, 1: 407-.411

Wong, R. C. K. and Maini, B. B. 2008. Gas bubble growth in heavy oil-filled sand packs under undrained unloading. Journal of Petroleum Science and Engineering, 55: 259–270

Wong, R. C. K., Thomson, P. R. and Choi E. S. C. 2006. Insitu pore pressure responses of native peat and soil under train load. *Journal of Geotechnical and Geoenvironmental Engineering*, ASCE, 132(10): 1360-1369.

Wood, D. M. 1990. Soil Behaviour and Critical State Soil Mechanics. Cambridge University press.

Wu, T. H., Resendiz, D. and Neukirchner, R. J. 1966. Analysis of clay deformation as a rate process. *Journal of Soil Mechanics and foundation division*, 92, (SM6): 229-248.

Yamaguchi, H., Ohira, Y., Kogure, K., and Mori, S., 1985. Undrained Shear Characteristics of Normally Consolidated Peat under Triaxial Compression and Extension Conditions. *Soil Mech. Found. Eng.*, 25(3): 1–18.

Yin, J. H., Zhu, J. G. and Graham, J. 2002. A new elastic viscoplastic model for time dependent behaviour of normally and overconsolidated clays: theory and verification. *Canadian Geotechnical Journal*, 39: 157–173.

Yin, J. H. and Graham, J. 1999. Elastic viscoplastic modelling of time-dependent stress–strain behavior of soils. *Canadian Geotechnical Journal*, 36: 736–745.

Yin, J. H., and Graham, J. 1989. Viscous–elastic–plastic modelling of one-dimensional time-dependent behaviour of clays. *Canadian Geotechnical Journal*, 26: 199-209.

Zhu, J. G., Zhao, Y. H., & Yin, J. H. 2011. Undrained Creep Behavior of a Silty Clay in Triaxial Tests. In Instrumentation, Testing, and Modeling of Soil and Rock Behavior, ASCE: 139-146.

Zwanenberg, C., 2005. The Influence of Anisotropy on the Consolidation Behavior of Peat. Ph.D. thesis, TU Delft, Delft, The Netherlands.

Appendix A: Site Characterization and instrumentation

This appendix provides a record of the site investigations, sampling and instrumentation installation at Anzac site. This site is referred as Anzac site.

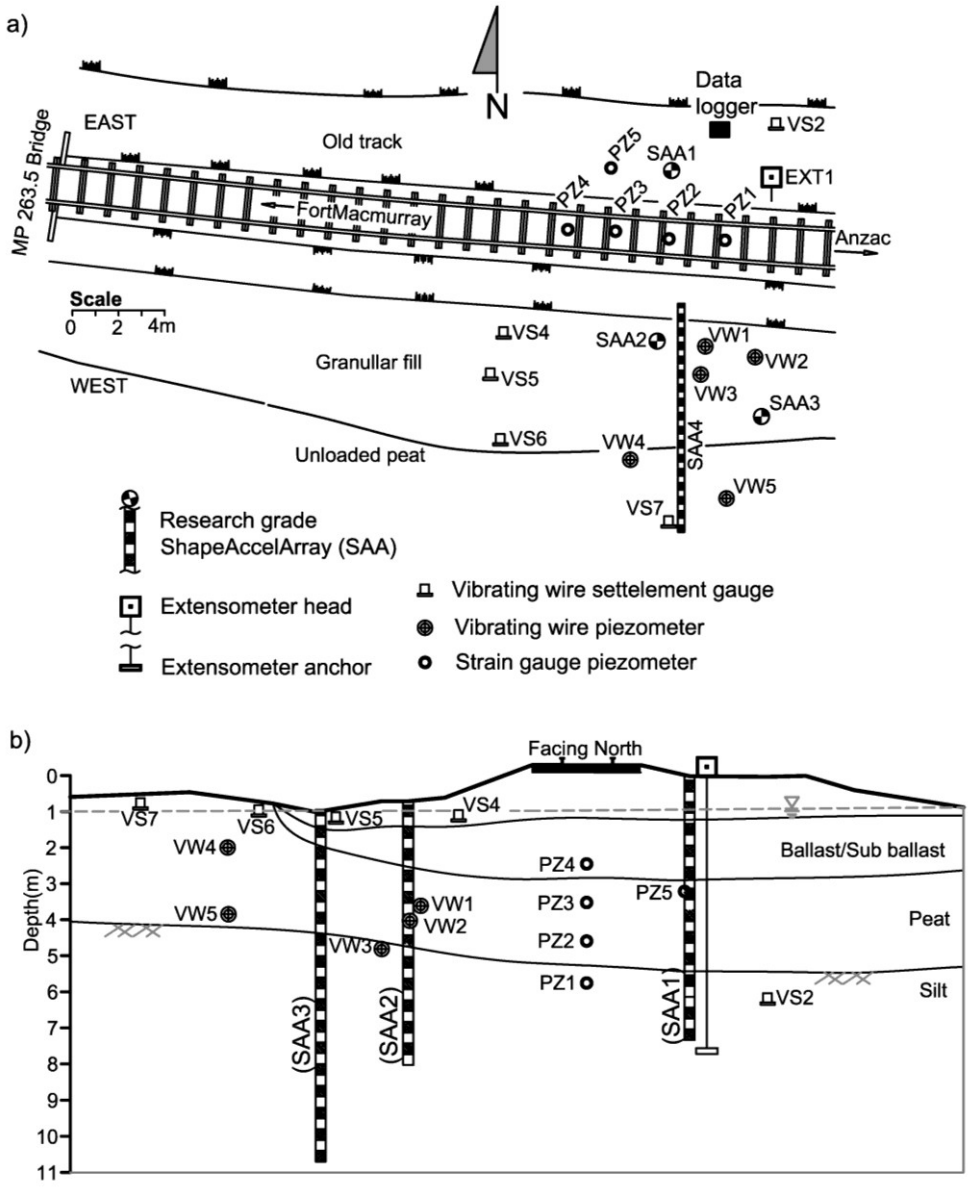

Figure A1. Plan and sectional elevation of study site and instruments installed at MP 263.5.

Borehole Logs (MP 263.5)

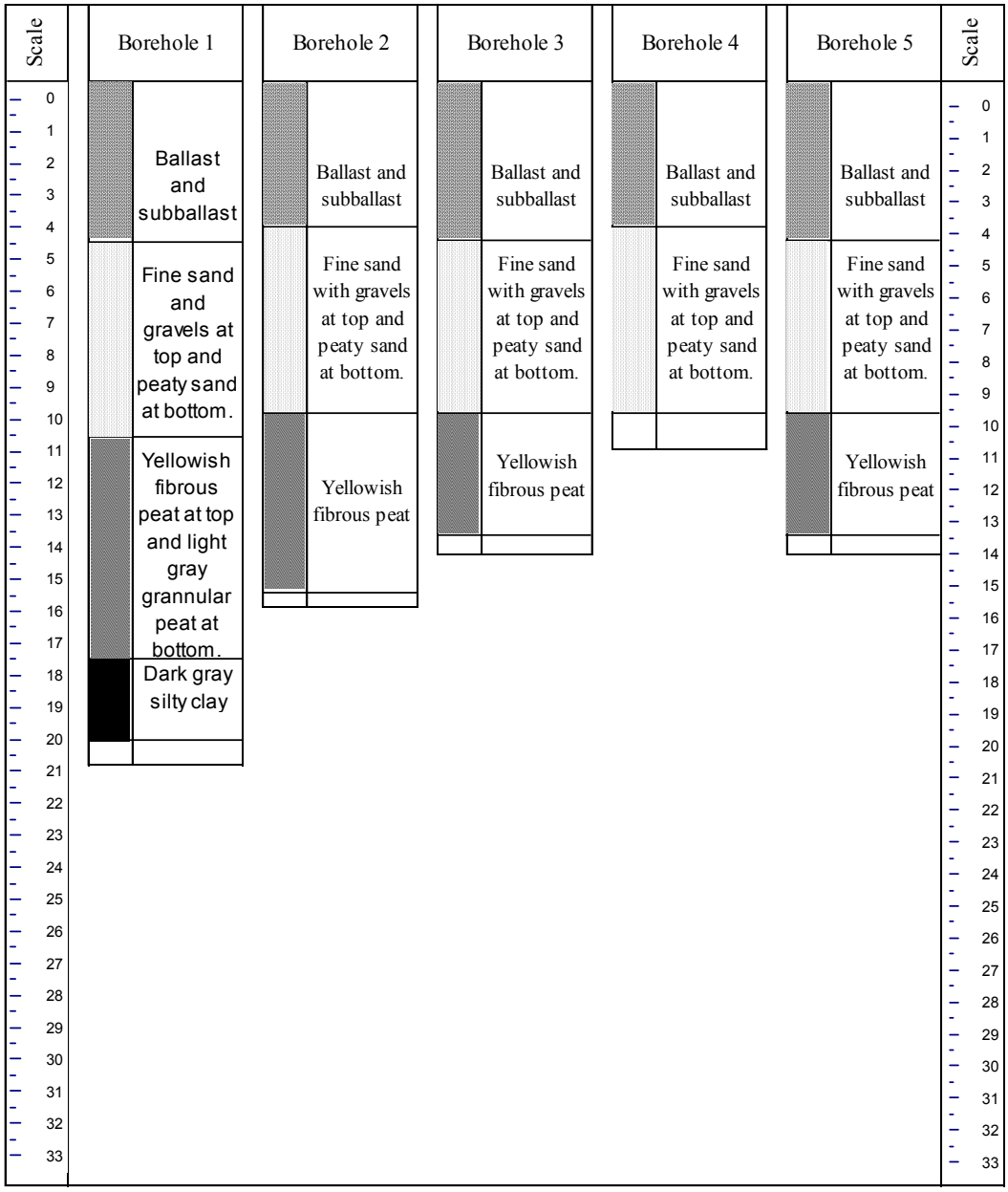

Borehole Logs (MP 263.5)

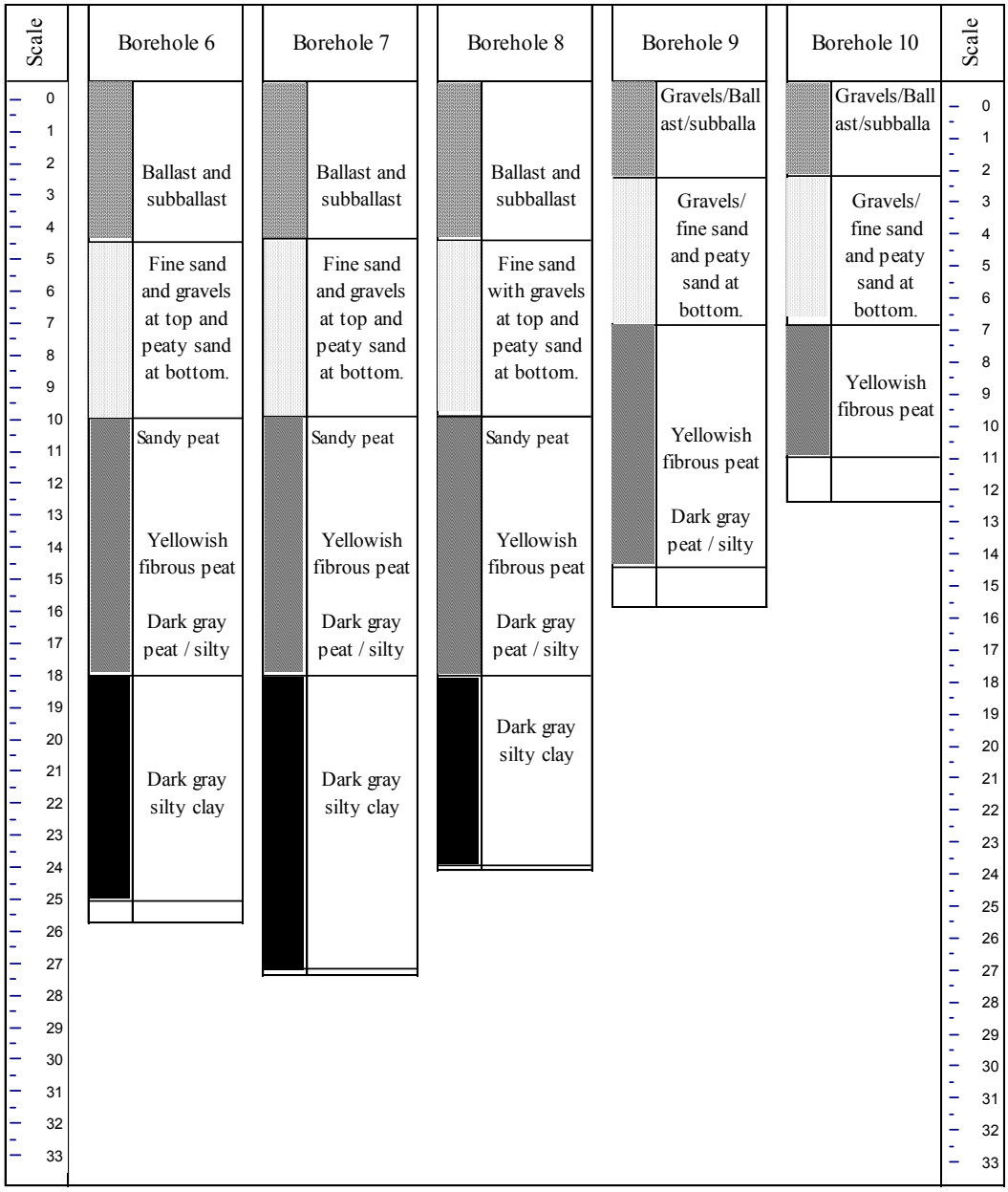

Borehole Logs (MP 263.5)

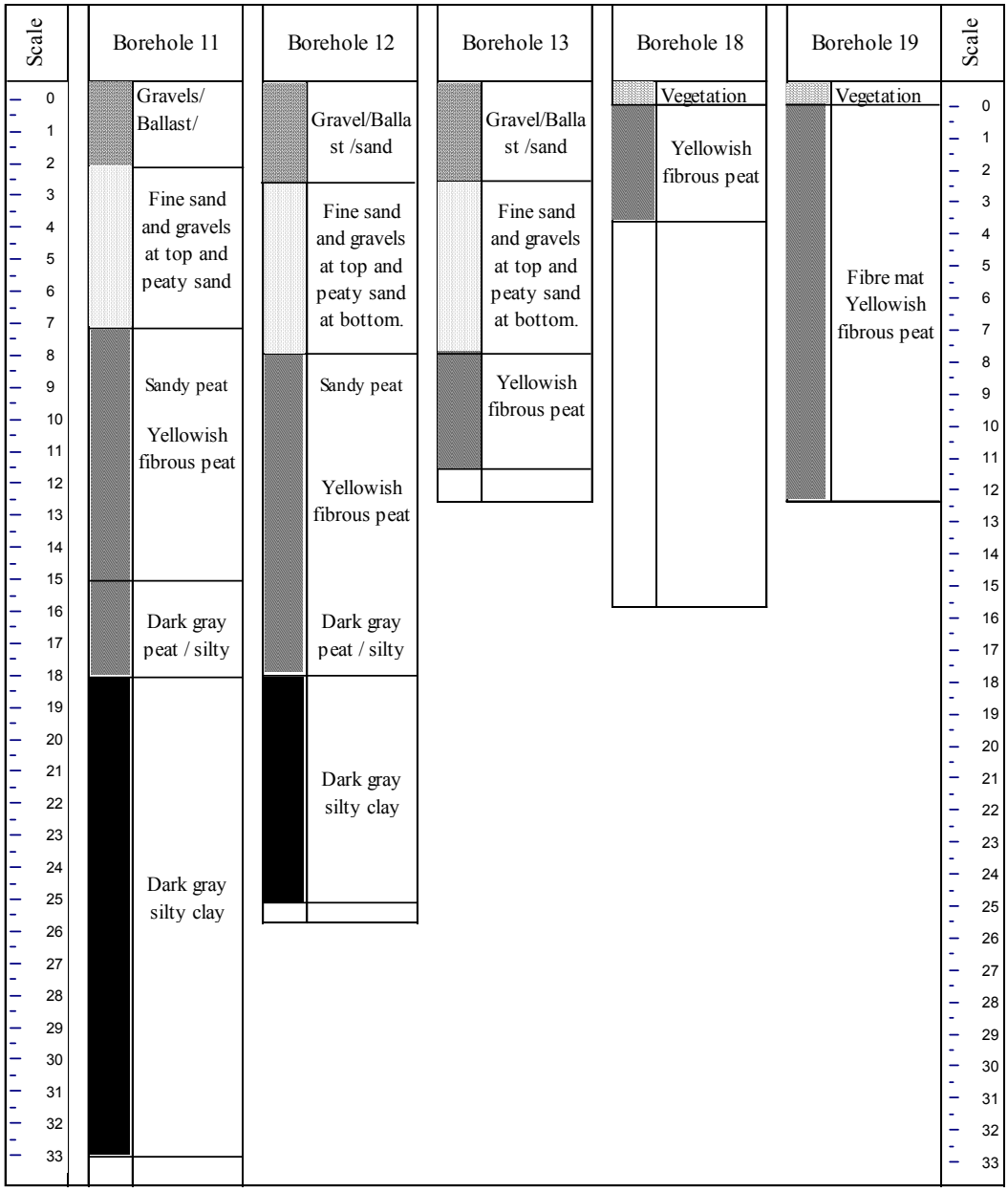

Boreholes 14 to 17 are less than 0.5 m deep.

Table A1. Instruments installation and Shelby tube sample collection

Bh. No	Depth of Bh (ft)	Instruments	Instruments ID	Instruments serial no.	Installed depths (m)	Ground surface elevation (m)	Shelby tube sample collected at depths (m)
Bh1	20	SGP	PZ1	15991	5.8	1000.15	2.0, 3.2, 3.6, 5.2
Bh2	16	SGP	PZ2	62894	4.8	1000.16	3.0, 3.8
Bh3	13	SGP	PZ3	62915	3.8	1000.19	
Bh4	9	SGP	PZ4	15982	2.7	1000.19	
Bh5	12	SGP	PZ5	62913	3.4	999.95	
Bh6	25	SAAR	SAA1	45521-24	7.5	999.88	3.3, 4.9
Bh7	28	EXT	EXT1	34129	8.5	999.87	4.0, 5.2
Bh8	24	VWSG	VS2	VS502	7	999.85	
Bh9	13	VWP	VW3	VW15434	4.4	999.18	
Bh10	9	VWP	VW1	VW15431	2.9	999.28	2.3
Bh11	33	SAA	SAA3	45882-32	10	998.87	
Bh12	25	SAAR	SAA2	45731-24	7.5	999.21	2.75, 4.3
Bh13	11	VWP	VW2	VW15432	3.5	999.17	3.0
Bh14	1.5	VWSG	VS4	VS505	0.5	999.06	
Bh15	1.5	VWSG	VS5	VS504	0.5	998.99	
Bh16	1	VWSG	VS6	VS506	0.3	999.14	
Bh17	1	VWSG	VS7	VS507	0.3	999.21	
Bh18	4.5	VWP	VW4	VW15429	1.5	999.13	
Bh19	11	VWP	VW5	VW15433	3.2	999.42	

SAA = ShapeAccelArrays

VW = Vibrating wire piezometers

SGP = Strain gauge piezometers

EXT = Borehole extensometers

VWSG = Vibrating wire settlment gauge

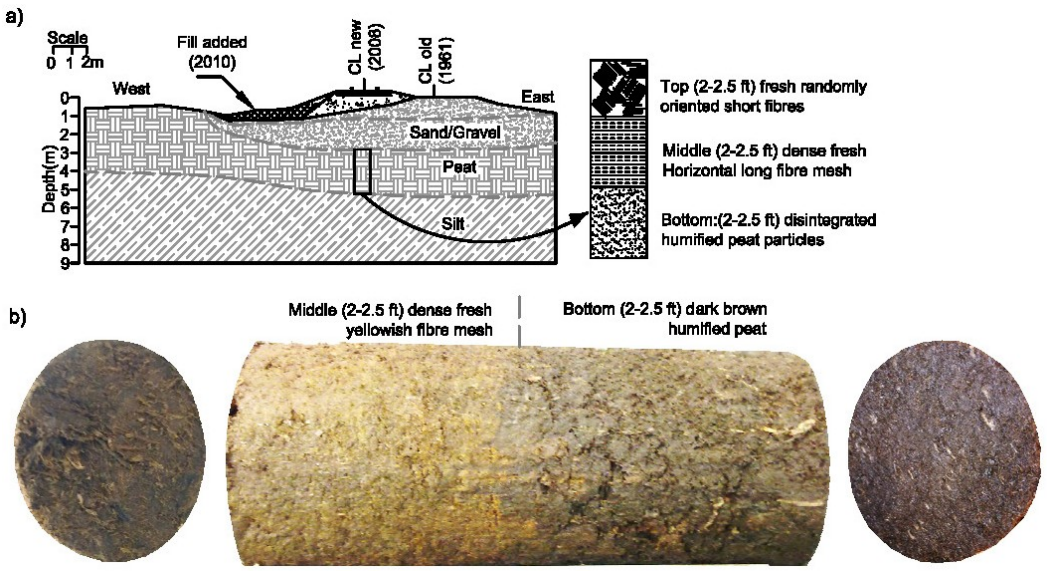

Figure A2. Summary of stratigraphy, embankment geometry and history of construction and peat specimen showing the transition from coarse fibrous to fine fibrous peat at MP 263.5, Anzac Alberta Canada.

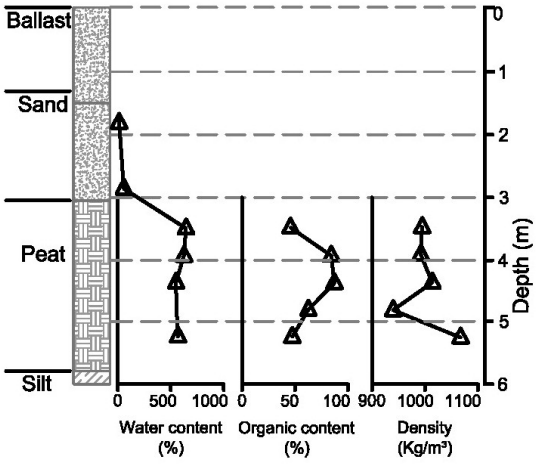

Figure A3. Soil profile, water content profile and density of peat layer at MP 263.5, Anzac Alberta Canada.

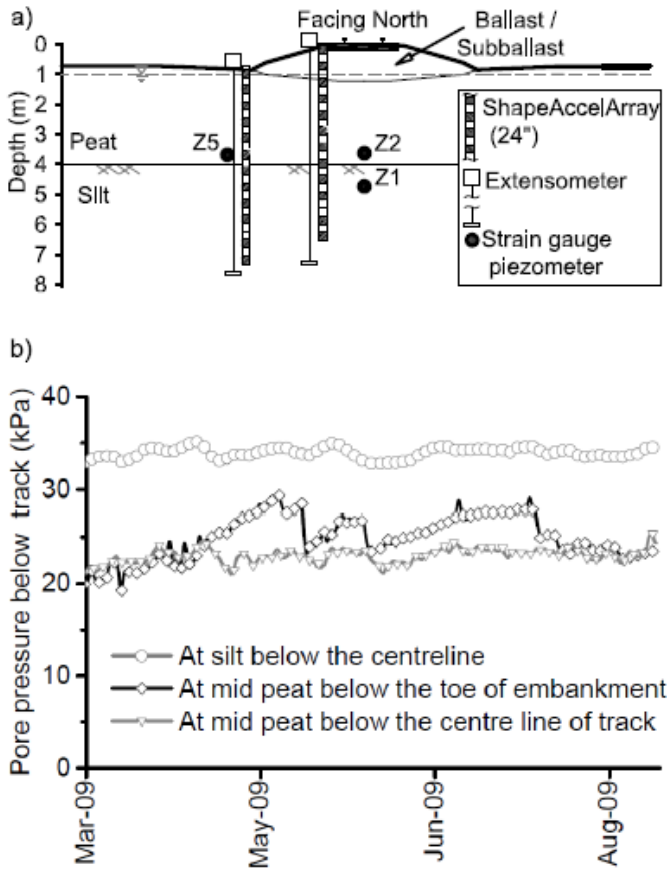

Figure A4. a) Summary of instruments installed at MP 263.9 at Anzac, Alberta, and b) plot of pore pore pressure (piezometer) data. (Reproduced with permission from Michael Hendry, University of Alberta.)

Appendix B: Data sets and time lapse pictures from field Site.

This appendix provides a record of the field data collected at the field site in Anzac. The data sets provided here are data measured in field additional to that presented in Chapter # 3, # 4 and # 5. The data included i) the horizontal deformation record of each node of three SAAs, and ii) the comparative plots of train time temperature, vertical deformation and pore pressure measured beneath the track.

The time lapse pictures included pictures taken at field site at different time during the period of monitoring to show the settlement of peat foundation.

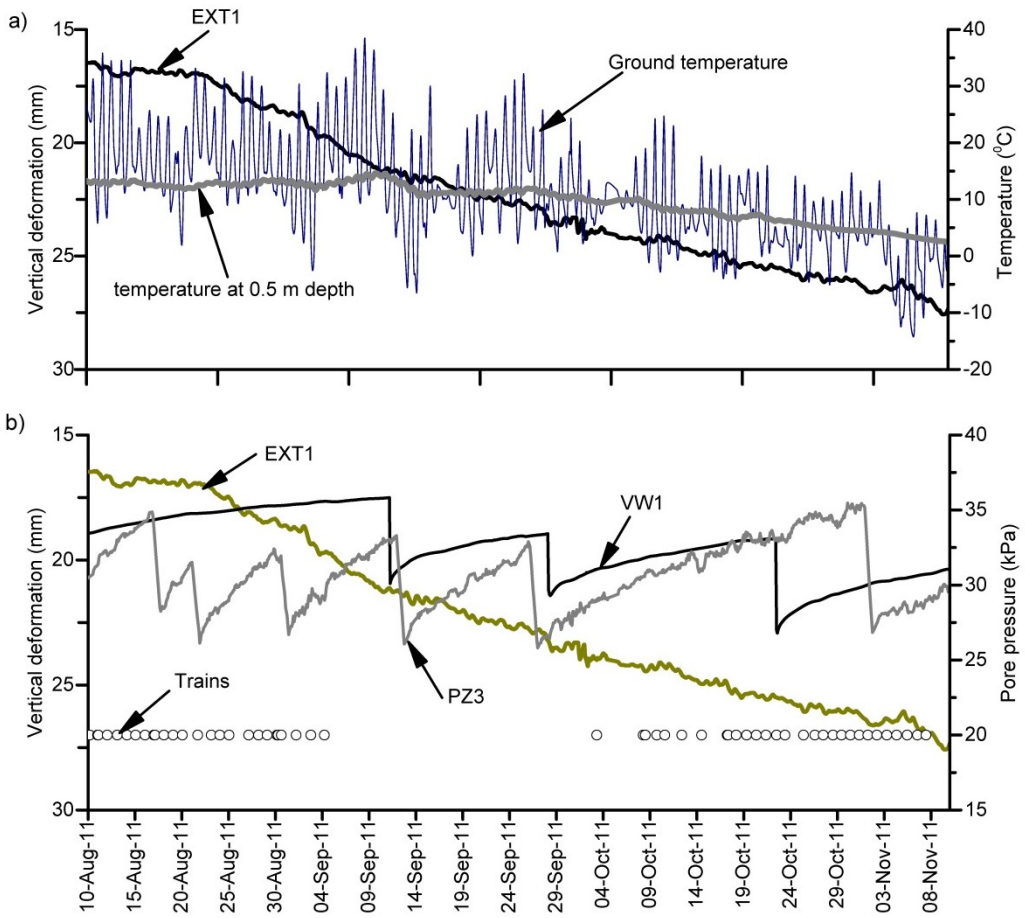

Figure B1. Plot of a) vertical deformation of track and temperature variation, and b) the vertical deformation, and pore pressure measured by two piezometers at the top peat layer together with the passing of loaded train in summer of 2011.

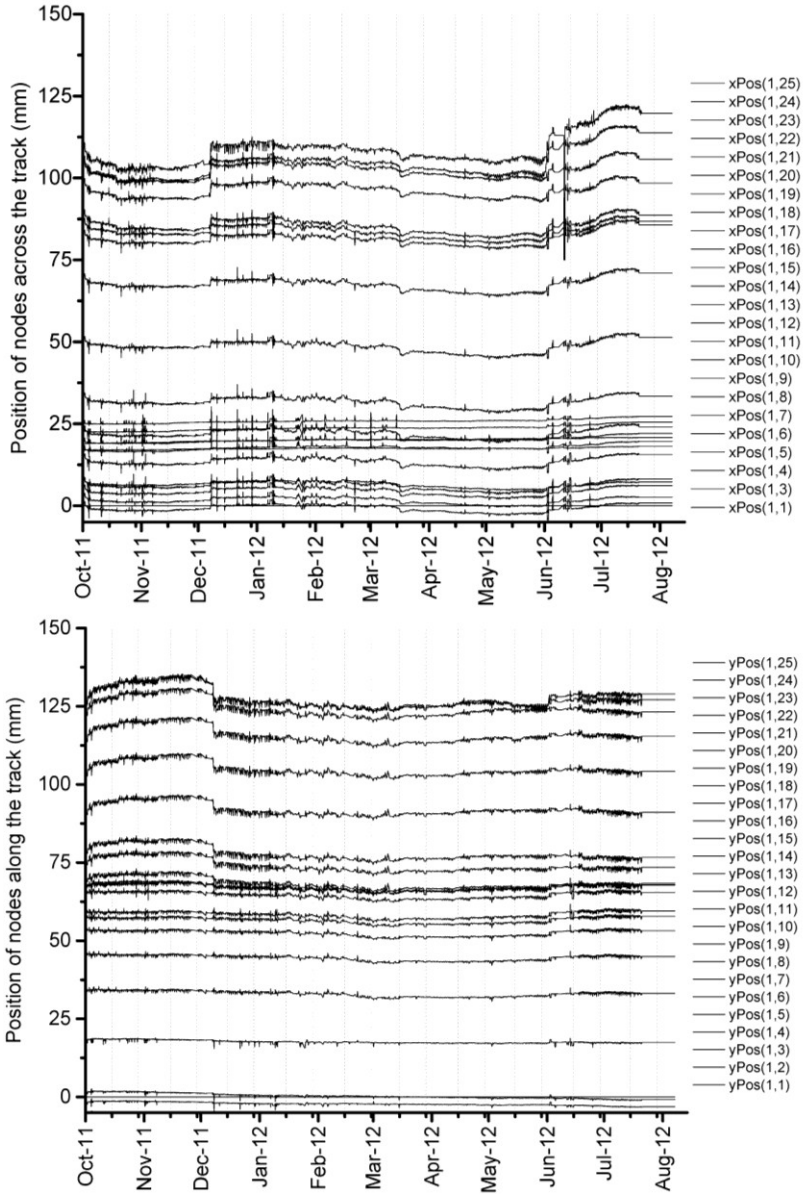

Figure B2. Plot of horizontal deformation record of SAA1, a) across the track, and b) along the track.

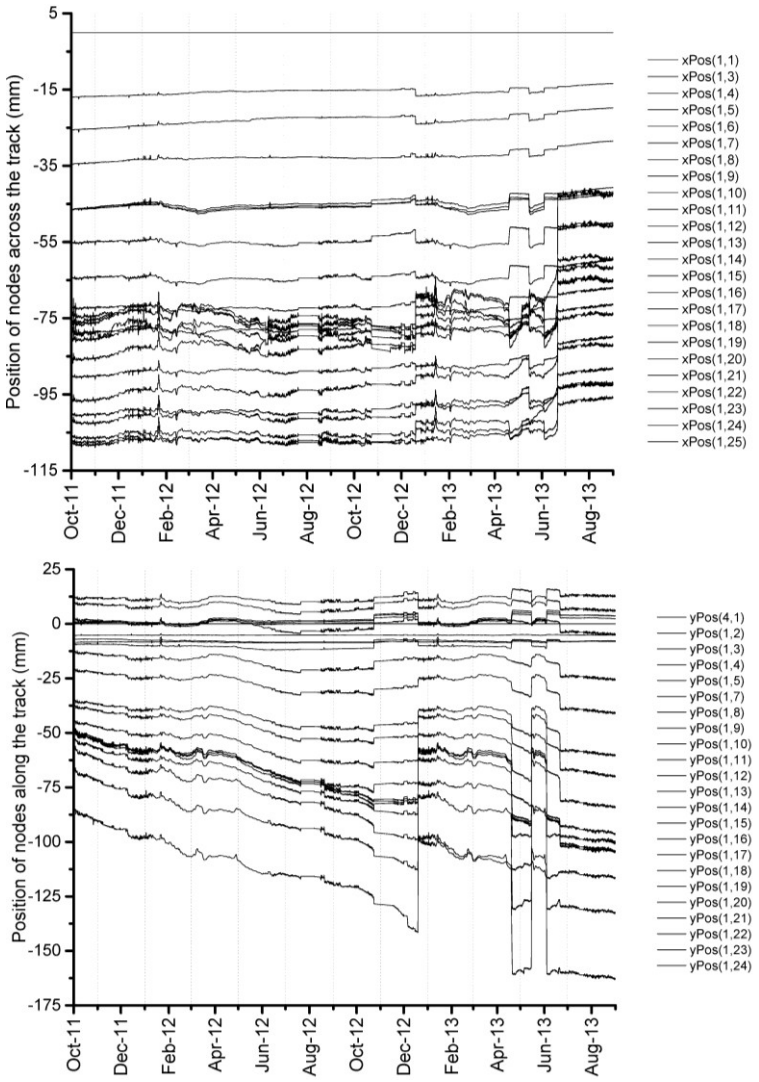

Figure B3. Plot of horizontal deformation record of SAA2, a) across the track, and b) along the track.

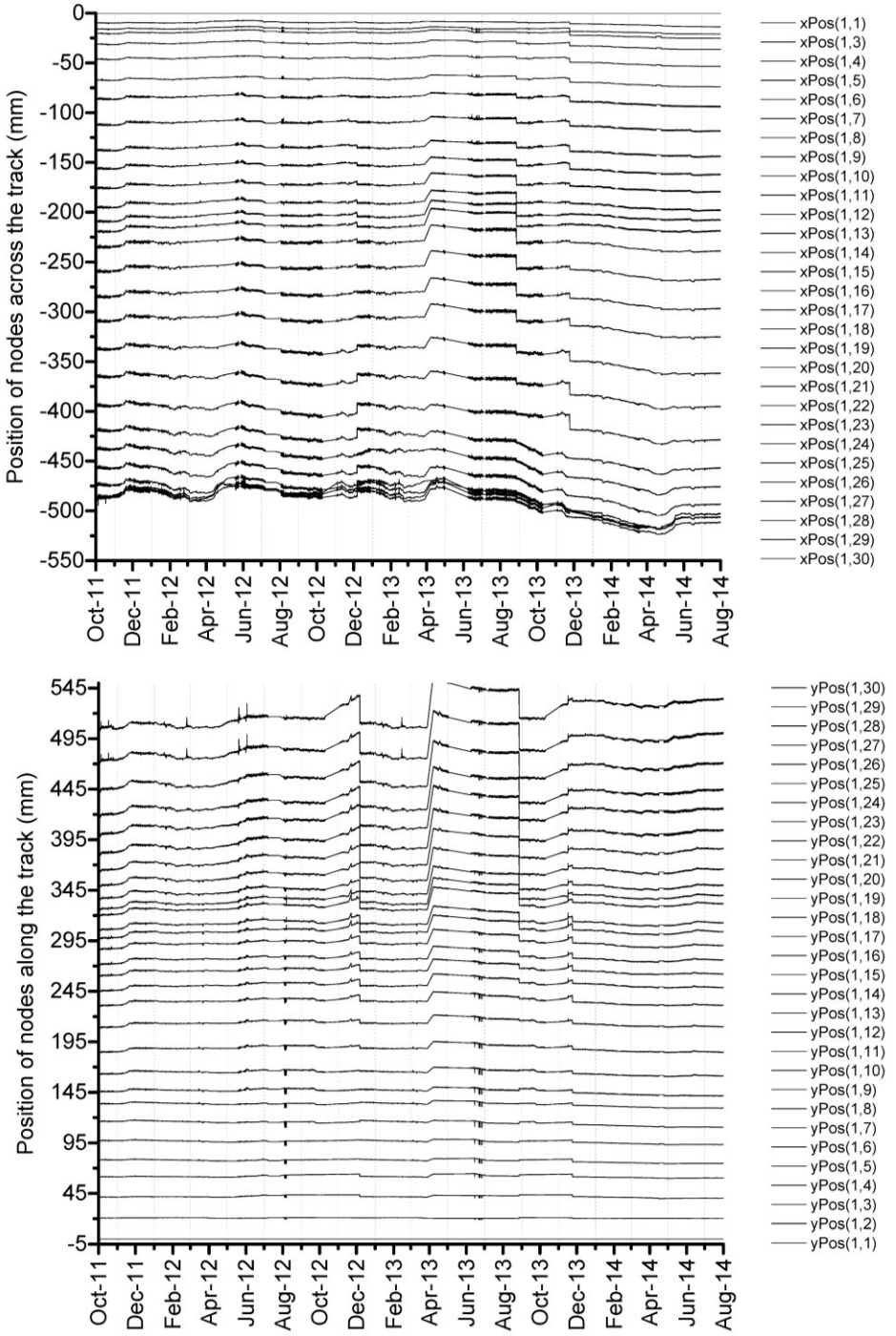

Figure B4. Plot of horizontal deformation record of SAA3, a) across the track, and b) along the track.

Figure B5. Time lapse pictures showing gradual settlement of granular fill the platform for future berm and instruments installation built in November 2010 at MP 263.5 Anzac, Alberta, a) before installation of instruments in May 2011, b) after instrumentation, May 2011, c) frozen ground surface, December 2011, d) platform settlement; went down beneath ground water table, Aug 2012, e) covered with 1 m thick snow, December 2012, f) and g) completely submerged and plat growth, June and September 2013, h) nearly beneath the plants and formation of peat cover, September 2014.

Appendix C: Results from laboratory testing of peat specimens

This appendix provides a record of the data collected during the course of the laboratory testing of samples retrieved from the Anzac site. These data sets are used or additional to the data sets already included in Chapter # 3, # 4 , #5 and # 6. These data includes i) the tests results of index properties of peat, including water content, fibre content, and atterbergs limits, ii) the results of two one-dimensional consolidation tests done on remoulded peat specimens, and iii) a comparative plot of time settlement curve obtained from one-dimenaional and triaxial consolidation tests in clay and peat.

The analysis of time tests results presented in C4 is additional analysis of laboratory tests results based on the description presented in Chapter 6.

C1: Index properties of Shelby tube specimens retrieved from MP 263.5

BH:	1			
Depth:	6, 10"	ft	2.19	m
Sample recovered:	15	cm		
Tube length:	60	cm		
Peat description:	Mix of gravel and fine sand, light gray colour.			
Water content:	11.02	%		

BH:	1			
Depth:	10	ft	3.13	m
Sample recovered:	10	cm		
Tube length:	60	cm		
Peat description:	Medium to fine grained sand core sample with visible fresh peat fibres, no odour.			

BH:	1			
Depth:	12	ft	3.75	m
Sample recovered:	45	cm		
Tube length:	60	cm		
Peat description:	Highly fibrous peat/ with fresh roots and leafs, visible tree trunk, light brown in color.			
Water content:				
Top part	454.47	%		
Mid part (12 ft)	388.76	%		
Bottom part	449.39	%		
Fibre content:				
Mid part (12 ft)	82.44	%		

BH:	2			
Depth:	10	ft	3.13	m
Sample recovered:	30	cm		
Tube length:	60	cm		
Peat description:				
Top	15 cm long core of mixes of medium fine sand, fresh, clear and washed, with 10% peat fibres.			
Bottom	15cm long core of light to dark brown, fibrous peat, high water content, coarse but short fibres.			
Water content:				
Top part /sand mix	53.46	%		
Bottom part	543.51	%		

BH:	2			
Depth:	12.5	ft	3.91	m
Sample recovered:	45	cm		
Tube length:	60	cm		
Peat description:				
Top	Mixed dark and light brown. Mix of humified and fresh fibres, randomly, oriented shorter -disintegrated, with wooden twigs.			
Middle	Light brown fresh -highly fibrous contains visible coarse fibre net, non-plastic, not penetrable by van shear apparatus.			
Bottom	10 cm plastic dark brown highly plastic at plastic limit			
Water content:				
Top peat (12.5 ft)	537.22	%		
Mid peat (13 ft)	603.88	%		
Bottom Peat (14')ft	734.88	%		
Liquid limit :				
Bottom peat (14 ft)	1050.15	%		
Fibre content:	96.12	%		

BH:	6		1.88	m
Depth:	11	ft		
Sample recovered:	30	cm		
Tube length:	60	cm		
Peat description:	Fresh light brown peat fibres, completely dry at lab temperature and air. Short and medium long fibres, none plastic, visible fibres, Light brown at top and dark brown at bottom.			
Water content:				
Bottom peat	424.069	%		
Top peat	431.954	%		

BH:	6			
Depth:	16	ft	5	m
Sample recovered:	40	cm		
Tube length:	60	cm		
Peat description:				
Top	Dark brown peat fine fibres, Very short and fibres, plastic, very fine fibres, nearly decomposed to inorganic soil.			
Bottom	Dark brown peat fine fibres, with visible but fine and short fibres, slightly decomposed or better to say compressed at high pressure.			
Water content:				
Bottom peat	193.71	%		
Top peat	405.11	%		

BH:	7	(beneath the old track)		
Depth:	13	ft	4.06	m
Sample recovered:	30	cm		
Tube length:	60	cm		
Peat description:				
Top	Coarse fibres			
Bottom	Dark gray, humified , less fibrous with some odour of decayed wood.			
Water content:	507.17	%		
Plastic Limit:	706.47	%		
Liquid limit:	817.00	%		
Fibre content:	40.00	%		

BH:	9			
Depth:	10	ft	3.13	m
Sample recovered:	35	cm		
Tube length:	60	cm		
Peat description:	Highly humified and plastic dark brown peat.			
Water content:				
Top part	578.49	%		
Bottom part	624.12	%		
Middle part	587.78	%		
Plastic Limit:				
Mid peat (14 ft)	589.08	%		
Liquid limit:				
Mid peat (11 ft)	709.85	%		
Fibre content:				
Top Peat (10.5 ft)	83.87	%		

BH:	10			
Depth:	7.5	ft	2.34	m
Sample recovered:	39	cm		
Tube length:	60	cm		
Peat description:				
Top	13 cm long core: Mixes of coarse sand, pebbles, and twigs, fibres, humified and fresh.			
Bottom	26 cm long core of dark brown, fibrous peat, with trunks, twigs, fair odour, with humified fibres.			
Water content:				
Top peat /sand mix	68.98	%		
Bottom peat	454.57	%		
Bottom peat	669.23	%		

BH:	12			
Depth:	9.5	ft	2.97	m
Sample recovered:	16	cm		
Tube length:	60	cm		
Peat description:				
Top	Very fibrous, light and dark brown mixed fibres.			
Bottom	Highly humified dark brown, with strong smell.			
Water content:				
Top peat	530.43	%		
Bottom peat	530.80	%		

BH:	13			
Depth:	10	ft	3.13	m
Sample recovered:	25	cm		
Tube length:	60	cm		
Peat description:	Mixed dark gray humified and light brown fresh fibres odour of decayed wood.			
Water content:	644.68	%		
Fibre content:	44.27	%		

C2: One dimensional consolidation tests results

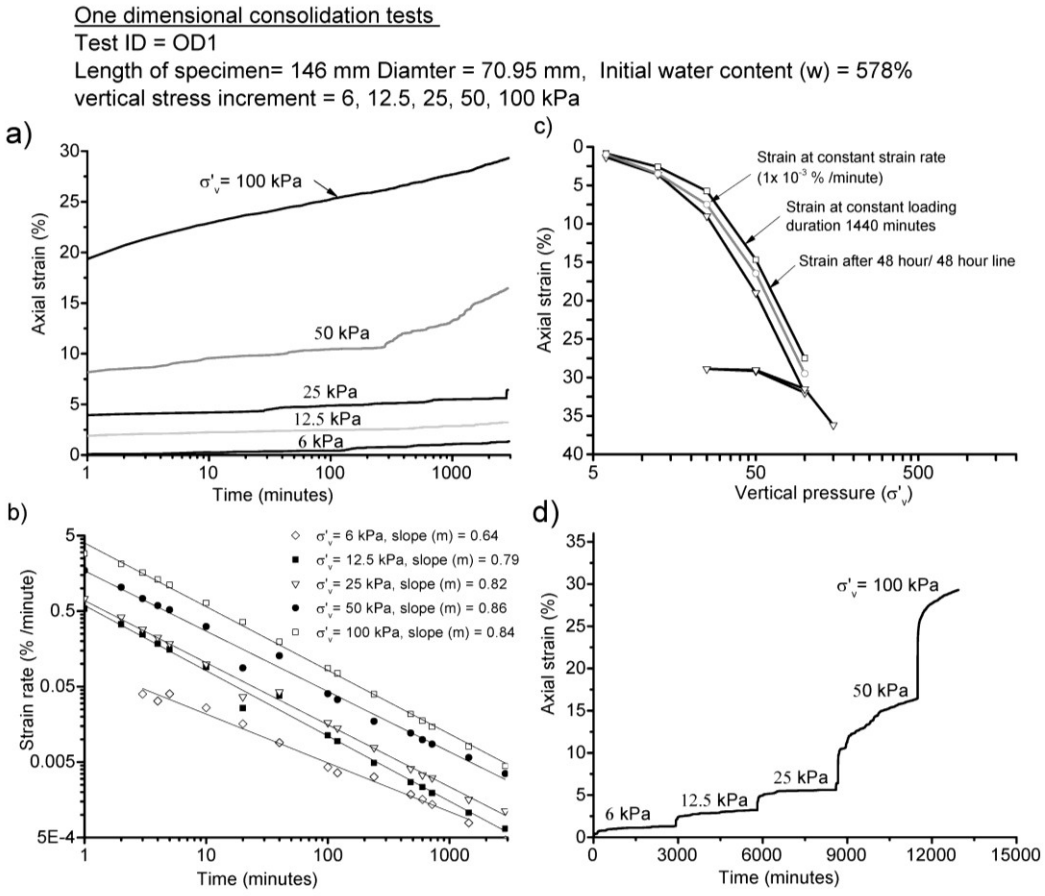

Figure C1. Data set from one-dimensional consolidation tests conducted on remoulded peat specimen, a) axial strain developed under multiple vertical stress (σ'_v) increments each kept for 48 hours, b) axial strain rate versus time, c) the strain developed at constant loading duration, constant strain rate, and at the end of consolidation plotted with σ'_v, and d) cumulative strain developed under multiple σ'_v increments. The results are included in Chapter 6 for comparison.

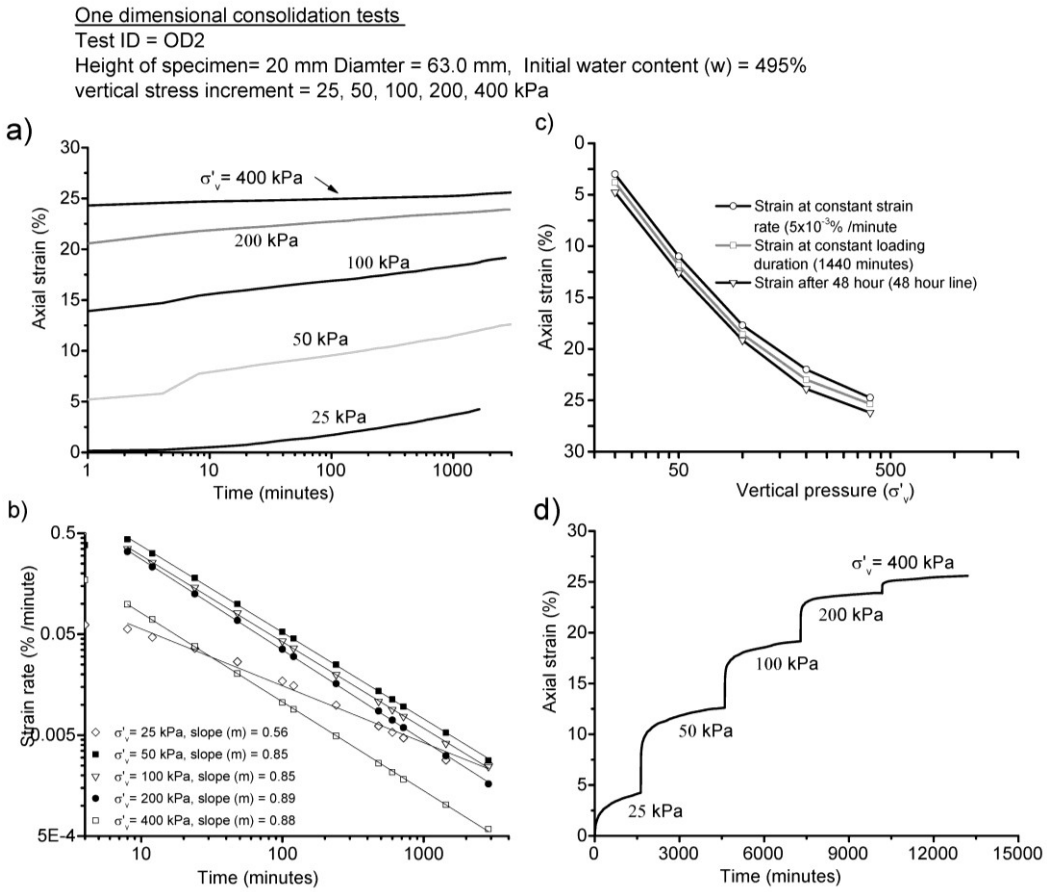

Figure C2. Data set from one-dimensional consolidation tests conducted on thin remoulded peat specimen, a) axial strain developed under multiple vertical stress (σ'_v) increments each kept for 48 hours, b) axial strain rate versus time, c) the strain developed at constant loading duration, constant strain rate, and at the end of consolidation plotted with σ'_v, and d) cumulative strain developed under multiple σ'_v increments. The results are included in Chapter 6 for comparison.

C3: Time settlement curves in peat and silt results

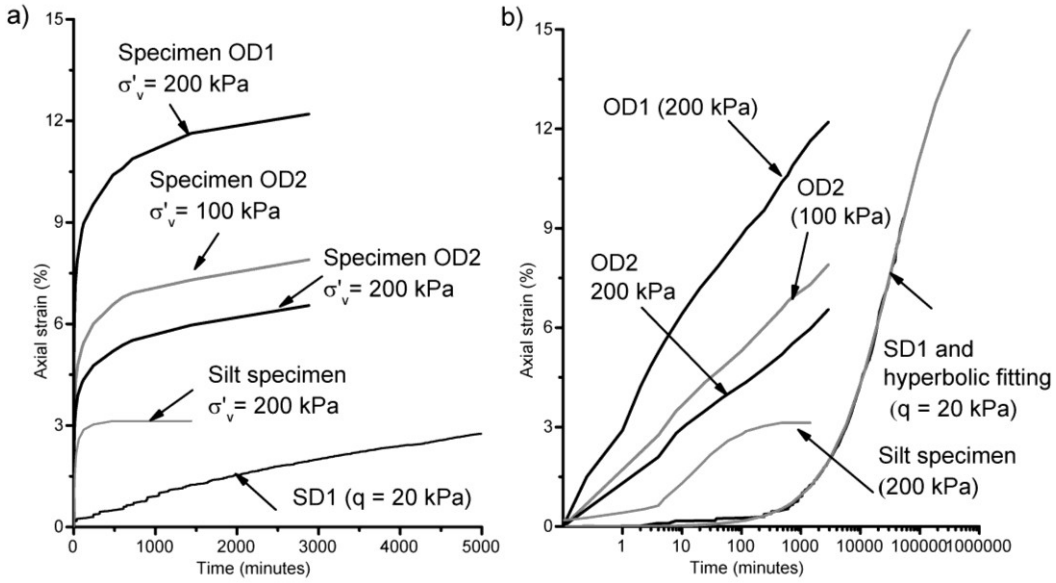

Figure C3. Comparative plot of time settlement curve of peat and clay under vertical stress (σ'v) and triaxial deviatoric stress (q) during consolidation, and triaxial drained compression tests. This figure is provided for comparison purpose. Silt specimen tested is remoulded Devon silt specimen.

C4: Hyperbolic models for peat compression

Fig. C4 presents the plot of cumulative ε_a and ε_v developed under deviatroic and isotropic stress increments with time. Depending on the magnitude of stress (q or p') and SIR used, each of the $\varepsilon_v - t$ or $\varepsilon_a - t$ plots had a unique shape and size (Fig. C4a). Under each stress (q or p') increment, the initial slope of $\varepsilon_v - t$ or $\varepsilon_a - t$ plots and the final magnitude of strain depended on the size of the stress (q or σ'_3) increment or the SIR used. Each of these $\varepsilon_v - t$ or $\varepsilon_a - t$ plots can be represented by a single hyperbolic function of the form:

——— ----- [C.1]

Where, ε_f is the final strain that can be developed under the applied stress increments, k is time to develop half of the final strain, and n is the initial slope of the $log\ \varepsilon_v - log\ t$ or $log\ \varepsilon_a - log\ t$ plots. The uniqueness of the p'-ε_v - expressed by Eq. [6.2] and presented in Figs. 6.8a, 6.8b, 6.13b showed that irrespective of the SIR and the number of stress increments applied, the final strain that can be developed under a unique stress increment (q or σ'_3) at a unique strain rate will be same. This uniqueness also supports the principle of superposition. This implies that if $\varepsilon_v - t$ *or* $\varepsilon_a - t$ plot under the first stress increment is known, it is possible to predict the strain and strain rate at any time under the subsequent stress increments. This implication can be used to estimate the viscous deformation of peat foundations under small load increments, which resemble the field conditions that exist during the re-levelling of a road embankment or surfacing of a railway embankment after the primary and secondary settlement of subgrades.

Fig. C4b presents the plot of measured cumulative ε_v with time. The lines joining the constant strain rates developed under subsequent stress increments (q or p') as presented in Figs. 6.8, 6.13b are linearly plotted on top of the $\varepsilon_v - t$ plots. This linearity makes it possible to predict the time needed and the magnitude of strain to be developed to attain a particular strain rate under the subsequent stress increments (q or p') relative to the time and magnitude of strain under the first

stress increment. The ε_f under the first stress increment can be considered as the volumetric or axial strain at a time equal to 100 years. The fitting parameters k, ε_f, and n can be determined from laboratory test results. The final strain and time to reach the final strain under the subsequent stress increments will be the linear multiplication of the final strain and the corresponding time under the first stress increment. Because of the similarity of the shape of $\varepsilon_v - t$ *or* $\varepsilon_a - t$ plots for different stress increments, the parameter n can be assumed constant. For specimen SD1, this value was 0.85. With the computed parameters ε_f, k, and n, the $\varepsilon_v - t$ *or* $\varepsilon_a - t$ plots under each q or p' can be traced as shown in Fig. C4b. Each of these lines represents the hyperbolic fitting of strain developed under constant q from the beginning of loading.

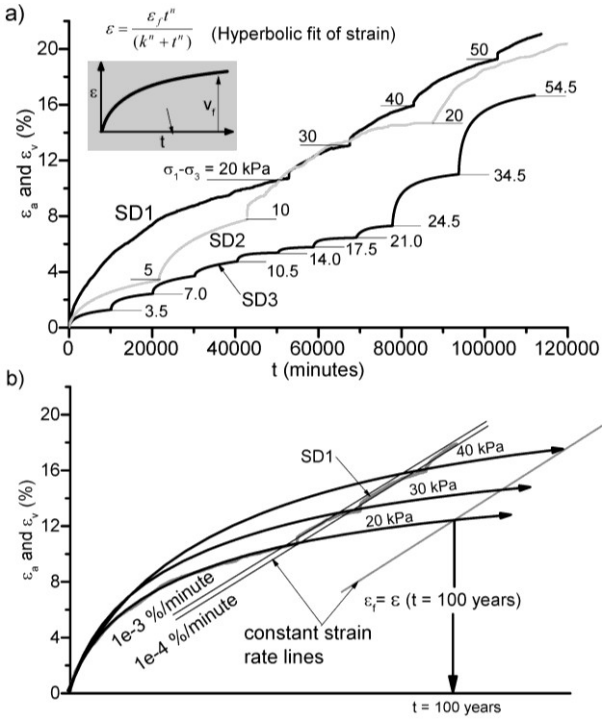

Figure C4. Plot of development of cumulative volumetric and axial strains on Shelby tube specimens under multiple stress increments, and b) hyperbolic fitting for cumulative strain.

Fig. C4b presents the plot of measured cumulative ε_v with time. The lines joining the constant strain rates developed under subsequent stress increments (q or p') as

presented in Figs. 6.8, 6.13b are linearly plotted on top of the $\varepsilon_v - t$ plots. This linearity makes it possible to predict the time needed and the magnitude of strain to be developed to attain a particular strain rate under the subsequent stress increments (q or p') relative to the time and magnitude of strain under the first stress increment. The ε_f under the first stress increment can be considered as the volumetric or axial strain at a time equal to 100 years. The fitting parameters k, ε_f, and n can be determined from laboratory test results. The final strain and time to reach the final strain under the subsequent stress increments will be the linear multiplication of the final strain and the corresponding time under the first stress increment. Because of the similarity of the shape of $\varepsilon_v - t$ *or* $\varepsilon_a - t$ plots for different stress increments, the parameter n can be assumed constant. For specimen SD1, this value was 0.85. With the computed parameters ε_f, k, and n, the $\varepsilon_v - t$ *or* $\varepsilon_a - t$ plots under each q or p' can be traced as shown in Fig. C4b. Each of these lines represents the hyperbolic fitting of strain developed under constant q from the beginning of loading.

Appendix D: Conference paper: A case study of the long-term deformation of peat beneath an embankment structure

Citation: Acharya, M.P. and Hendry, M. T. 2015. A case study of the long term deformation of peat beneath an embankment structure, To be presented in XV Pan-American conference on Soil Mechanics and Geotechnical Conference, Buenos Aires November 15 to 18, 2015

D A Case Study of the Long-Term Deformation of Peat beneath an Embankment Structure

Mohan ACHARYA[a,2], Michael HENDRY[a], and Tom EDWARDS[b]

[a] *University of Alberta, Edmonton, Canada*
[b] *Canadian National Railway, Edmonton, Alberta, Canada*

Abstract. Vast areas of northern Canada are covered by peat and wetlands. The number of engineering project built within peat-covered areas is increasing as resource and infrastructure development continues to expand in northern Canada. The prediction of settlements and deformations of structures built upon peat is notoriously difficult. This is further complicated as there are only a few well documented and published case studies on which to base judgment and performance predictions; and of those available, few have used contemporary instrumentation and data recording systems. This paper presents the results of an ongoing study of the long-term deformation of peat after the completion of embankment construction. The study site consists of an embankment bridge approach recently constructed upon peat. This embankment was instrumented to measure the pore pressures, settlement and horizontal deformation occurring within the embankment and the peat foundation. The analysis of three years of measured deformations and pore pressure showed that the long-term deformation is influenced by the generation and the seasonal temperature driven, expansion, and expulsion of gases.

Keywords. Peat, embankment, settlement, and lesson learning

---

[2] *Corresponding Author.*

D 1.0 Introduction

Peat and highly organic soils are common throughout the world, from tropical regions to cold climates. These soils consist primarily of the fragmental remains of vegetation in various stages of decomposition in the presence of excessive moisture [1, 2]. Peat deposits are noted as having highly variable physical and engineering properties including very high water content, and high compressibility [3]. These characteristics of highly organic soils have posed challenges for engineers around the world.

Vast portions of northern Canada are covered by peatland with depths ranging up to several meters. The number of engineering project built within peat-covered areas is increasing as resource and infrastructure development continues to expand in northern Canada. Long stretches of roads and railways have been constructed over these peat deposits. In Alberta, a 440 km long railway line between Edmonton and Fort McMurray, known as the Canada National (CN)'s Lac-la-Biche subdivision (LLBS) is estimated to have more than 120 km of embankment constructed over peat formations. These embankments have been characterized by excessive settlements requiring frequent maintenance to maintain the serviceability of the track.

This paper presents the results of an ongoing study of the long-term deformation of peat after the completion of embankment construction. This study site consists of an embankment bridge approach recently built upon previously undisturbed peat. This embankment was instrumented to measure the pore pressures, settlement and horizontal deformation occurring within the embankment and the peat foundation. An analysis of three years of measured deformations and the replication of these behaviours in the laboratory showed that there is a strong influence of the gases within the peat to the long-term deformation and settlement of the subgrade an overlying structure.

D 2.0 Description of site

The study site is located in Northern Alberta on CN's line at mile 263.5 on the LLBS Subdivision near the town of Anzac, Alberta (Fig. D1) where the railroad crosses a large expanse of peat bog (Fig. D1). The alignment of this track section was shifted westward in 2008 due to the construction of a new bridge. Additional granular fill (0.5 m) was added to the west side of the embankment in late 2010 (Fig. D2a).

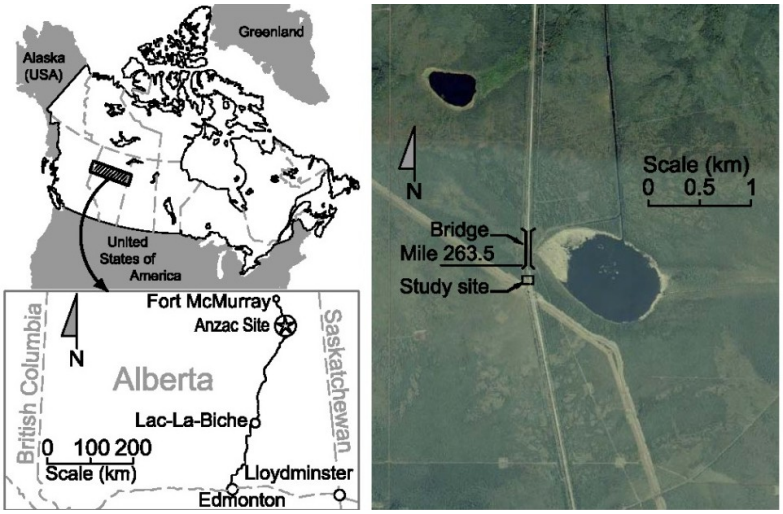

Figure D1. Locations of the Lac-la-Biche subdivision and the Anzac Site near MP 236.5.

A ground investigation was conducted at this site in May 2011. The site investigation showed that the embankment consisting of 2 to 3 m of granular fill (including ballast and subballast) overlying an undisturbed peat layer that is approximately 3 to 4 m thick (Fig. D2). Underlying the peat is an unoxidized medium plastic silt containing traces of sand and gravel. The silt layer extends below the depth of investigation (deeper than 11.0 m from the top of the embankment).

The samples retrieved from the site investigations were tested to quantify the water content and the fibre content as per the American Society for Testing Materials (ASTM) standards D2974 (ASTM 2007) and D1997 (ASTM 2008).

The water content and fibre content within the peat were found to decrease with depth, with mean values of 580% and 67%, respectively. The peat was found to have a coarse fibrous texture and a yellow-brown colour. The degree of humification was determined to be insignificant, with the plant structures within the peat appearing to be intact. The peat was observed to have finer fibres and a more homogeneous consistency with increasing depth.

D 3.0 Instrumentation

The instrumentation installed consisted of five strain-gauge piezometers (SGP), one extensometer, four vibrating wire piezometers (VWP) and five vibrating wire settlement gauges (VWSG) (Figs. D4a, D4b). All of the sensors were supplied by RST Instruments Ltd. These types of piezometers and extensometers have been successfully used to monitor pore pressures and the vertical deformation of peat at previous sites [4]. The data logger recorded measurements from the instruments every two hours. All of the piezometers were push-in type piezometers, and during installation these were pushed approximately 0.5 m beyond the base of the borehole. The elevations for the top of all of the boreholes were measured relative to a common datum, on the bridge just north of the site, using a total station.

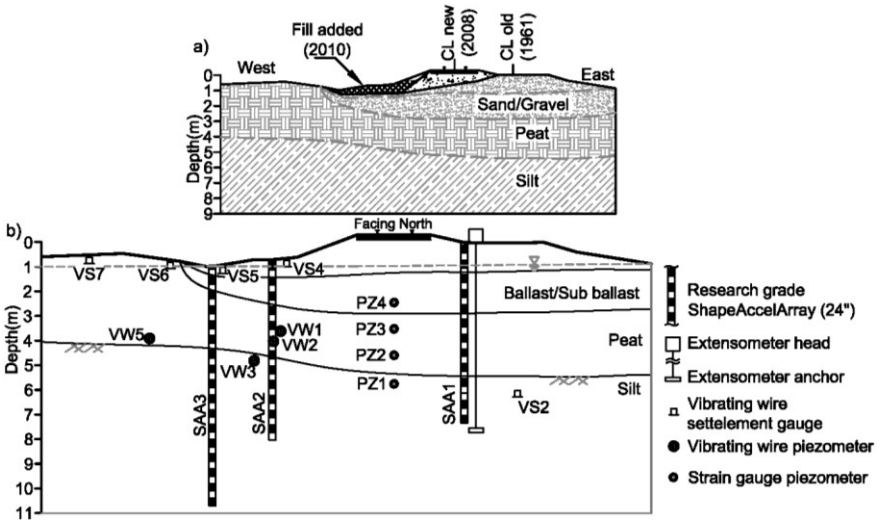

Figure D2. Summary of a) the stratigraphy and history of construction at the field site, and b) the instrumentation installed at the field site.

Four SGPs were installed under the centreline of the track at depths of 2.7 m, 3.85 m, 4.80 m; and 5.9 m. The SGPs (model SGP-730-PI) installed at MP 263.5 have a working range of up to 350 kPa and an accuracy of ±0.1% of the measured pressure. Three of the VWPs were installed at depths of 2.9 m 3.5 m and 4.1 m below the granular fill, and the two VWPs were installed below the unloaded peat at depths of 1.45 m and 3.2 m on the west side of the granular fill. The VWPs (model VW2100-0.35-DPC) have a working range of up to 350 kPa and an accuracy of ±0.1% of the measured pressure.

Two of the VWSGs (VS4 and VS5) are installed at 0.5 m below the top of fill. Two VWSGs (VS6 and VS7) are at 0.5 m from the top of unloaded peat at 0.5 m and 3 m west of the western edge of the granular fill. The fifth VWSG (VS2) was installed to the deep silt layer at a depth of 7.0 m as a reference point to correct for settlement of the reservoir and changes in barometric pressure. The VWSGs (model SSVW105) have a maximum depth of 7 m of hydrostatic head and an accuracy of ±0.1% of the measured depth below the reservoir.

One extensometer was installed on the east side of the rail track and anchored at the depth of 8.5 m below the track in thick silt strata. The linear variable differential transducer (LVDT) sensor used in the extensometer has an accuracy of ±0.1% of the measured displacements. Two SAAs (SAA1 and SAA2) are 7.3 m long arrays installed vertically at the two sides 1 and 2 m away from the end of the ties; and, finally, one SAA (SAA3) is a 9.75 m long array installed vertically at the boundary of the granular fill and the unloaded peat 6 m west of the westernmost rails. These arrays consist of 305 mm long segments with sensors at two ends to record the position, tilt and angle of that segment relative to the base of the array. The short-term and long-term accuracy of measurement relative to the starting shape is ±0.5 and ±1.5 mm respectively.

Figure D3. (Left to right): the strain gauge piezometer, vibrating wire piezometer, vibrating wire settlement gauge, and ShapeAccelArrays which were installed near MP 263.5.

D 4.0 Field measurements

The following is a presentation of the measured pore pressure response and deformation of the peat strata, followed by a discussion of the resulting data sets.

D 4.1 Measurement of pore pressure

Fig. E4a presents the pore pressures measured at MP 263.5 by the strain gauge piezometers (PZ), and Fig. D4b presents the pore pressure measured by the vibrating wire piezometers (VW). The piezometer installed in the silt (PZ1 and VW3) measured a relatively constant pore pressure with some slight seasonal variations. Both types of piezometers installed within the peat layer show annual increases in pore pressure. These increases were highest for the piezometers near or beneath the embankment structures. The maximum measured rise in pore pressure above hydrostatic pressure was reached during the late summer and autumn of 2011, and reached pressures of 14 and 15 kPa above hydrostatic pressure by VW2 and PZ3, respectively. Similar seasonal rises in pore pressure occurred, to a lesser degree, during the warmer months of 2012 and 2013.

The piezometers installed at top peat layer (PZ3 and VW1) measured significant increases in pore pressure during the summer and autumn months and this rise was accompanied by sharp decreases in pore pressure (Figs. D4a, D4b). The magnitude of the rise in pore pressure prior to the drop, measured below the centre

of track, was nearly constant for three successive summers of 2011 to 2013. But the rise in pore pressure below the fill is slightly smaller during summer of 2012 and 2013. Piezometers installed at the bottom of the sub ballast below the centre of the track (PZ4), at the top peat level below the old track (PZ5), and at 1.5m below the unloaded peat surface (VW4) recorded constant pore pressure throughout the year with some gradual increases during summer months (Figs. D4a and D4b).

The piezometer installed at 3.2 m below the unloaded peat surface (VW5); parallel to the piezometer at mid peat level below the embankment showed a significant increase in pore pressure during summer and autumn of 2013 (Fig. D4b).

D 4.2 Measurement of vertical settlement

The extensometer and the VWSGs recorded a gradual settlement of the embankment and foundation throughout the study period (Fig. D4c). The extensometer did not function reliably after the first winter. The total settlement recorded by the extensometer between May and September of 2011 was 28 mm. During the study period, the average cumulative settlement recorded by VWSGs installed on top of granular fill (VS4 and VS5) was 138 and 131 mm, respectively. The average annual settlements recorded by these VWSGs (VS4 and VS5) were 35, 86, and 14 mm, for 2011, 2012, and 2013, respectively.

The settlement recorded by VWSG installed at the boundary between the granular fill and unloaded peat (VS6) was -230 mm (*heaving upwards*) and deformation recorded by VWSG 3 m west of the western edge of the granular fill (VS7) was 30 mm.

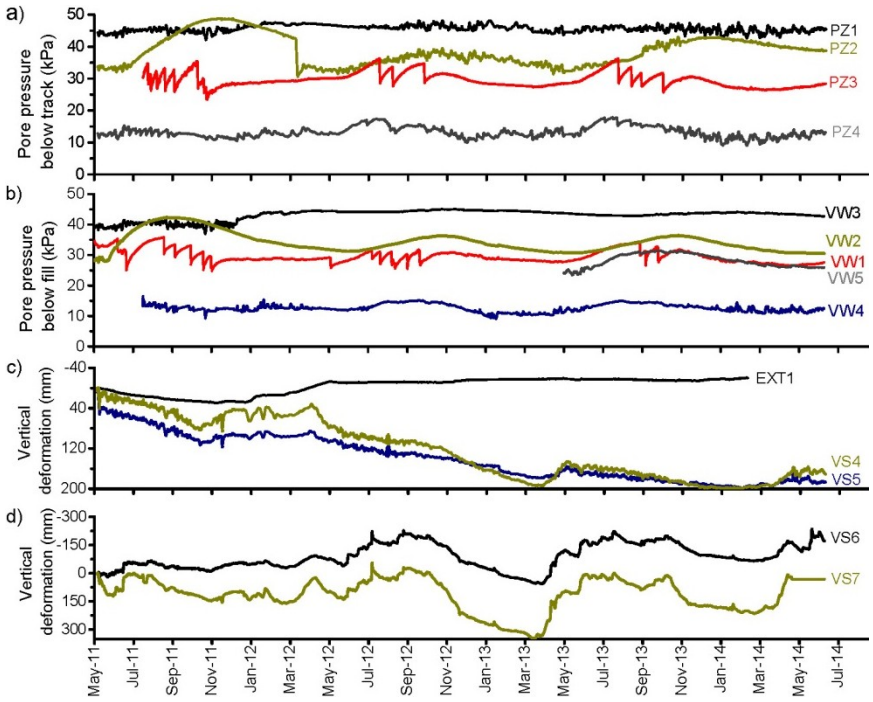

Figure D4. a) The pore pressure measured below the centre of the track, b) the pore pressures measured below the fill, c) the settlement measured below the embankment, and d) the settlement at unloaded peat.

D 4.3 Measurement of horizontal deformations

Fig. D5 presents the horizontal deformation recorded by the vertically installed SAAs. The cumulative horizontal deformation recorded by the array at the boundary between the old and existing track (SAA1) was less than 6 and 8 mm towards the track at the mid peat level and at the ground surface respectively. The SAA between the fill and the existing track (SAA2) recorded a small deformation for the first and second years after the installation of instruments. Similarly, the array at the boundary between the fill and unloaded peat (SAA3) recorded seasonal deformation towards and away from the track for the first and second years after the installation of instruments. Both SAA2 and SAA3 recorded significant horizontal deformation during the summer and autumn of 2013, the third year of installation. The cumulative horizontal deformation recoded by SAA2 was 48 and 33 mm towards the centre of the track at the ground surface and at the mid-peat level respectively. The cumulative horizontal deformation

recorded by SAA3 was 18 and 40 mm away from the centre of the track at the ground surface and at the mid-peat level, respectively.

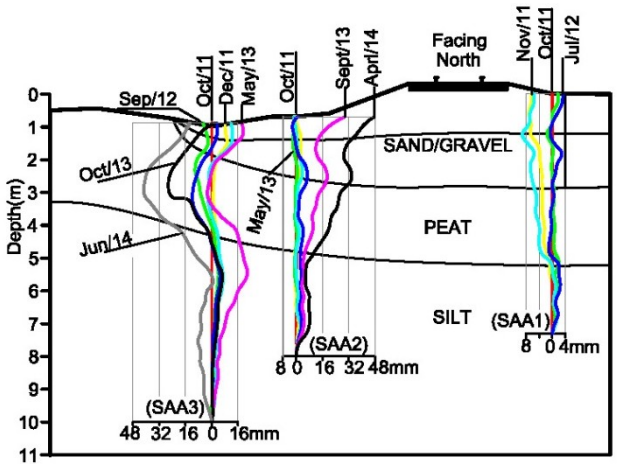

Figure D5. The horizontal deformation recorded by three vertically installed SAA's.

D 4.4 Measurement temperature

Fig. D6 presents the temperatures and the corresponding pressures measured, at MP 263.5, below the embankment and fill at different depths as measured by the VWPs and VWSGs. The measured temperature just below the surface of the embankment (Fig. D6a) ranged from 30°C, during the summer, to -20°C during the winter. Within the sub ballast, the temperature ranged from a high of 20°C in mid-July to a low of -3°C in mid-February. The response to the changes in the surface temperature is greatly reduced with increasing depth within the peat layer. The temperatures ranged from 2 to 8°C near the surface of the peat layer, from 2.7 to 6.5°C, at the mid peat layer (3.5 m depth). Deeper within the silt layer, at a depth of 7.0 m, the temperature variation was 0.7°C, ranging between 3.5 and 4.2°C.

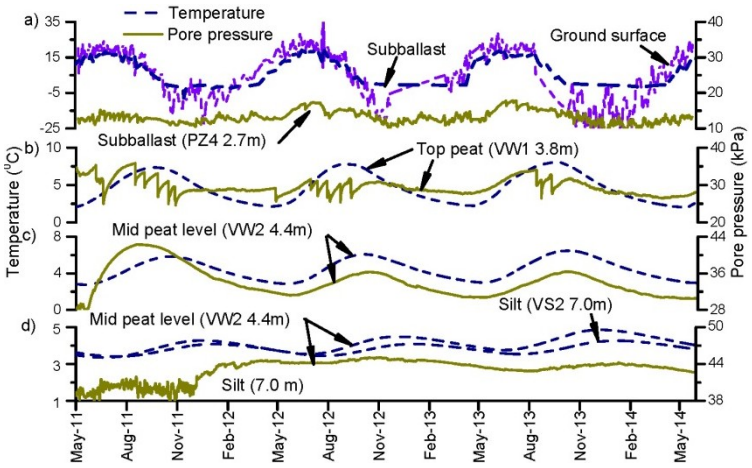

Figure D6. The measured temperature and pore pressure at a) the ground and sub ballast layer, b) top peat, c) mid peat, and d) bottom peat and silt layers.

D 5.0 Discussion

The field measurements showed that the pore pressures beneath the embankment, within peat layer follows the cyclic rise and fall in temperature with increase in pore pressure during the summer and autumn (Figs. D6a, D6b). This pore pressure increases was, hypothesised, and through laboratory testing, shown to be the result of the thermal expansion of gas within the peat [5]. This laboratory testing consisted of the placement of peat specimen within a triaxial cell at constant confining pressure, while the temperature was incrementally increased. The result of this testing showed that 10°C increase in temperature results in a 30 kPa increases in pore pressure.

The pore pressure drops measured by VW1 and PZ3 were hypothesised to be a result of the movement of gas bubbles within peat and expulsion of gas bubbles from the drainage boundary [6]. Laboratory isotropic consolidation tests conducted on peat specimens and cylindrical cellulose foam specimens replicated this field behaviour. The peak pore pressures before pressure drops were found to be the pressure necessary to expel the gas bubbles from the voids within the peat structure. The laboratory tests also showed the immediate volume change due to expulsion of gas bubbles. Based on the laboratory isotropic consolidation tests a

correlation between the volumetric strain and amount of pore pressure drops is derived [7].

The presence of gas bubbles in the peat subgrade and its effect on the movement of the track surface can be seen by the cyclic movement of track surface (Fig. D7). This movement is due to the thermal expansion and contraction of gas bubbles. The vertical movement of track is correlated to the subsurface temperature (Fig. D7b) with upward movement of track when the subsurface temperature is higher. The presence and effect of gas bubbles (Figs. D4a, D4b, D7a, D7b) shows multiple mechanisms in the long-term deformation of peat foundation. Horizontal deformation at peat was 20 to 25% of vertical deformation measured below the granular fill (Figs. D4c, D5). The vertical deformation below the fill slowed noticeably two years after the placement of fill material. The long term deformation which is essentially volumetric was found to be strongly influenced by the generation and the seasonal temperature driven, expansion, movement and expulsion of gases. This implies peat foundation cannot be treated in the same manners as inorganic clay foundation. The prediction of long-term settlement with conventional approach underestimates the total settlement.

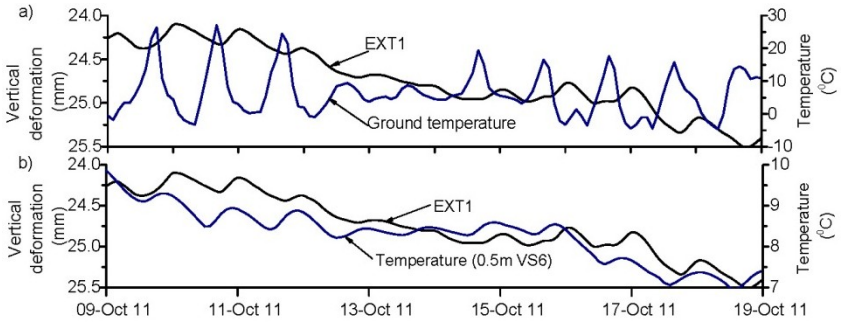

Figure D7. The measured day night variation of temperature and movement of track surface at the field site.

D 5.0 Conclusion

The field measurement of deformation temperature and pore pressure on a peat subgrade of a railway embankment has provided new insight into the mechanism

of long-term deformation of peat foundations. The field measurements also provided comprehensive dataset of vertical settlement, horizontal deformation and pore pressure in peat foundation. The results showed that multiple mechanisms are involved in the compression of peaty foundation; and the deformation is predominantly volumetric with lateral deformation less than 25% of vertical deformation. The long-term deformation was found to be partially driven by the generation and the seasonal temperature driven, expansion, and expulsion of gases.

D 6.0 Acknowledgements

The authors would like to acknowledge Canadian National Railway (CN) for providing both the project and funding. This research was made possible through the Railway Ground Hazard Research Program, which is funded by the Natural Sciences and Engineering Research Council of Canada, Canadian Pacific Railway, and CN.

D 7.0 References

[1] MacFarlane, I.C. 1969. Muskeg Engineering Handbook. University of Toronto Press, Toronto.

[2] Hobbs, N.B. Mire morphology and the properties and behaviour of some British and foreign peats, Quarterly Journal of Engineering Geology and Hydrogeology, 19(1986), 7-80

[3] Landva, A.O. Characterization of Escuminac peat and construction on peatland, In Proceedings of the 2nd international workshop on Characterisation and Engineering Properties of Natural Soils, Singapore, (2007), 2135-2191.

[4] Hendry M.T, Martin C.D and Barbour S.L. The measurement and analysis of the cyclic response of railway embankments and underlying soft peat foundations to heavy axle loads. Canadian Geotechnical Journal 50(2013): 467-415.

[5] Acharya, M.P. Hendry, M.T. and Martin, C.D. Thermally induced pore pressure response in peat beneath a railway embankment, International Journal of Geotechnical Engineering. In press, 2015a

[6] Acharya, M.P. Hendry, M.T. and Martin, C.D. Effect of the presence and movement of gas bubbles on pore pressure behaviours observed in peat, Canadian geotechnical Journal, In press, 2015b

[7] Acharya, M.P. Hendry, M.T. and Martin, C.D. Quantification of settlement of peat subgrade underlying railway embankment due to expulsion of gas out of peat subgrades. Submitted for review in ICE proceeding Geotechnical Engineering, 2015c.

Appendix E: Poster: Growing lateral support for railway embankment in peatlands

Citation: Acharya, M.P., Hendry, M. T. and Martin, C. D. 2014. Growing lateral support for railway embankment in peatlands, presented in CaRRLs workshop April 24, 2015.

E Growing lateral support for railway embankments in peatlands

E 1.0 Introduction

Peat contains the fragmental remains of dead vegetation in various stages of decomposition (Muskeg engineering hand book, 1969). Peat accumulates due to the addition of dry matter in the presence of excessive moisture (Hobbs, 1986). The accumulation process is extremely slow and common only at comparatively cold and wet climates. Together with the accumulation peat undergoes aerobic and anaerobic decomposition and consolidation during drying of peat. As a result peat accumulates at somewhat slower rate than the rate of addition (Hobbs, 1986). As different plant and parts of plants decomposes in a different rate peat land evolves at diverse conditions.

Considerable portion of northern Canada and more than 50% of northern Alberta is covered by the peatland with thickness extending from few to several meters. The number of engineering project built within peat-covered areas is increasing as resource and infrastructure development continues to expand in northern Canada. As peat is characterized with very high water content, and high compressibility embankments constructed over peat subgrade have been characterized by instability, and continuing long term settlements. Effort to reinforce the embankments laterally with the provision of berms are not stabilising the embankment but rather sinking together with the embankment.

Through the observation of peatland surrounding railway embankments in northern Alberta and a review of ecological evolution of peatlands, this study presents the process of ecological evolution, the change in the state of peatlands and application of this natural process in geotechnical engineering to reinforce the embankment constructed on peat lands.

E 2.0 Evolution of peatland and peatland ecology

The evolution of peat land is complex with geological, biological and ecological process that takes thousands of years. There are two basic stages on the formation of peat in peatland. First, the ecological stage consists “plants growing near the

low land where water is accumulated and in long run gradually engulfing the water body". The whole water body consists of plants remains which grew and died on the time being. The second, "biological stage is retardation of microbial activity than the high productivity of plants" (Moore 1988). This retarded biological activity is due to the formation of acidic environment formed under the low aeration condition beneath the plants grown at the surface. Fig. E1 presents the pictures of chronological evolution of peatland in northern Canada. It takes a long time and biological and ecological effort to change a hostile acidic environment to plant-friendly environment where all type of plants can grow.

Figure E1. Typical chronological evolution of peat land in northern wetlands.

Evolution of peat land involves the chemical and biological, and environmental changes. Depending on the chemical environment, the availability of minerals, nutrients, and water, different plants grows and disappears at different phases of peat land evolution (Fig. E2). Some plants evolve helps to reduce the hostile environment absorbing toxic materials. Different plant species grows at acidic and basic peatland.

Fig. E3 presents the vegetation at different stage of peat succession around the lake bogs. Plants of different species and sizes grow corresponding to the distance from the water level. Near the water shoreline plants are smaller (including reeds and swamp reeds) and away from the water shoreline, plants are bigger and stronger (including cotton grass and Fen wood. This diversity is related to the water level away from the water shore line. The drop in water table provide air and temperature, increasing the soil mineralization and nutrients from the oxidation of metals absorbed by peat.

Sphagnum and water lettuce: grows in water and acidic environments.

Pitcher plant, Orchid grows in less acidic environments.

Cotton and Reed grass and trees grows in less acidic and basic environments.

Figure E2. Ecological diversity of peatland based on the chemical and biological environment of peatland.

E 3.0 Observation at field site in northern Alberta

Fig. E4 presents location of site where large change in vegetation system is observed near MP 263.5 of CN Lac La Biche subdivision, connecting Edmonton and Fort McMurray. An Oil pipe line was constructed during the winter of 2013-14. The pipeline obstructed the south to north flow of water to the lake on the east side of the track. This cut off of water flow changed the peatland to relatively stiff enough to walk through. A dense layer of cotton grass grew, making the surface further drier and stronger. Small trees grew beside the track, and water body near the track is covered by vegetation. This is a process of ecological evolution in peatland and can have geotechnical significance in the development of lateral support to the existing embankments passing through the peat lands.

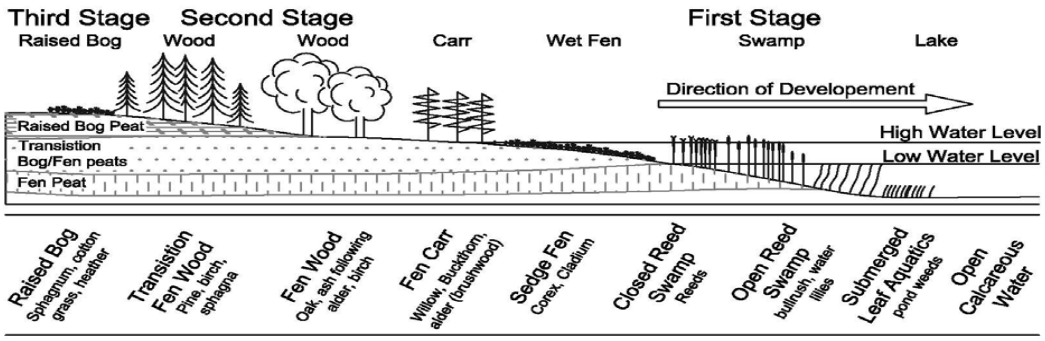

Figure E3. Vegetation and peat succession in the filling of a lake (after Hobbs, 1986 and reproduced from Hendry, 2012).

Fig. E5 presents a typical section, where the ground surface between the water ditch and embankment is elevated to provide a better environment for plant growth. The addition of mineral soil on top of the peat and plantation of suitable plants that can grow in hostile environment can make this part of section strong and can provide lateral support to the railway embankment.

E 4.0 Conclusion

From field observations and review of literature on ecological evolution of peatland, it is concluded that plants can be grown beside the railway track to

provide the lateral support for the railway embankments constructed on peat lands. The existing cross-section of railway embankments can be modified to include elevated surface where plants with capability of reinforcing soil can grow.

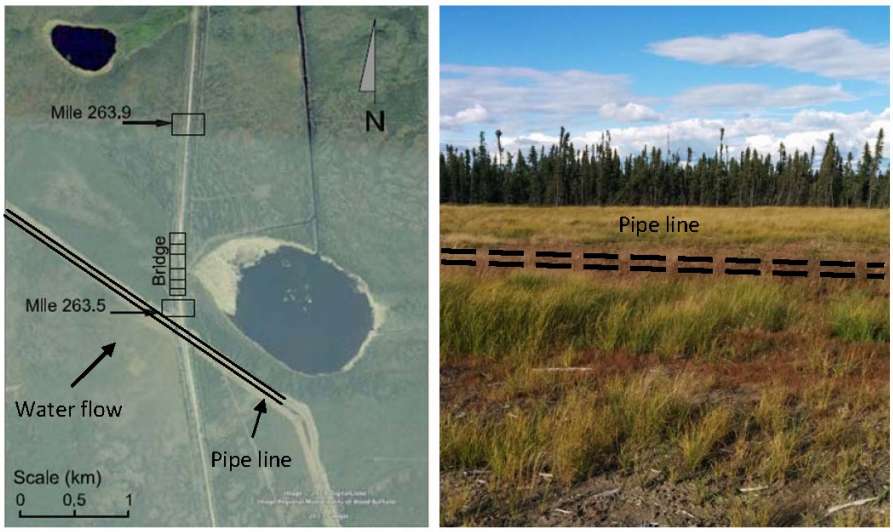

Figure E4. (Left) Location of site observation site used to study the ecological changes along CN railway line joining Edmonton and FortMcMurray near MP 263.5. (Right) Changes in vegetation one year after the cut off of water flow to the lake on the east side of the track.

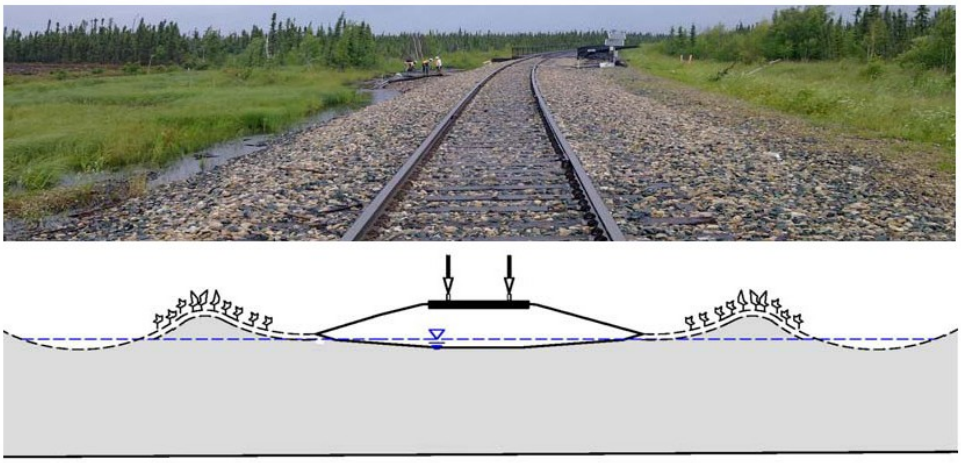

Figure E5. (Top) Section of existing railway embankment near Anzac, Alberta, Canada, (Bottom) proposed section for the construction of new railway embankment or to reinforce the existing embankment in peat lands.

E 5.0 References

Hendry, M. T. 2011. The geomechanical behaviour of peat foundations below rail-track structures. PhD Thesis, University of Saskatchewan, Saskatoon, Canada.

Hobbs, N. B. 1986. Mire morphology and the properties and behaviour of some British and foreign peats. Quarterly Journal of Engineering Geology and Hydrogeology, 19, (1), 7-80.

MacFarlane, I. C. 1969. Engineering characteristics of peat, Muskeg engineering handbook, I. C. McFarlane, ed., Univ. of Toronto Press, Canada, 78-126.

Moore, P. D. 1989. The ecology of peat-forming processes: a review. International Journal of Coal Geology, 12, (1), 89-103.